DEVELOPMENT OF ENZYME ELECTRODES

by

Yogeshvar Nath Kalia

A thesis submitted in partial fulfilment of the degree of
Doctor of Philosophy of the University of London
and for
the Diploma of Membership of Imperial College

Physical Chemistry Section
Department of Chemistry
Imperial College of Science, Technology and Medicine
London

October 1990

ABSTRACT

Conducting organic salt electrodes have been shown to oxidise both flavin-linked oxidoreductases and NAD-dependent dehydrogenases. However the precise nature of the mechanism involved is controversial. Three alternative mechanisms have been proposed: homogeneous mediation, heterogeneous redox catalysis and a modified enzyme process. This thesis is concerned with the elucidation of the mechanism by which these enzyme electrodes operate.

A variety of electroanalytical techniques were employed including a.c. impedance spectroscopy and rotating disk and ring-disk methods. The a.c. studies showed that TTF-TCNQ electrodes fabricated using silicone oil followed a homogeneous pathway whilst those made with polystyrene as a binder primarily operated via a heterogeneous mechanism. The experiments using a rotating Pt-ring TTF-TCNQ disk suggested that pressed pellet electrodes also follow a homogeneous mechanism. Due to some anomalous results seen in these experiments, an investigation of the nucleation properties of various flavoenzymes was undertaken.

A conducting organic salt enzyme electrode using invertase, mutarotase and glucose oxidase trapped behind a cellulose acetate membrane was developed and was shown to be capable of determining sucrose in soft drinks. The sensor had a linear response from 25 μM up to 11 mM sucrose. A kinetic model for this three enzyme system was devised using the theory for membrane electrodes developed by Albery and Bartlett (J. Electroanal. Chem., 194, 211, (1985)). By varying the ratio of the respective enzymes, the rate determining step was shown to be the hydrolysis of sucrose by invertase.

A preliminary investigation into developing a sensor to monitor creatine levels in urine using creatinase and sarcosine oxidase was undertaken. In-vitro studies showed that the sensor had a linear range from 25 to 400 μM creatine. A nitrate sensor using NAD-linked nitrate reductase was also developed. It gave a linear response from 30 μM up to 3mM nitrate. Kinetic models were designed and used to analyse the experimental data.

For my parents

The woods are lovely, dark, and deep,

But I have promises to keep,

And miles to go before I sleep,

And miles to go before I sleep.

Stopping by Woods on a Snowy Evening

Robert Frost

ACKNOWLEDGEMENTS

I would like to thank:

John Albery for his supervision (!). I also wish to thank "The Ultimate Wolfson Wally" for providing, along with a certain postdoc, a shoulder to lean on as I attempted to cross the Quad back to Derby Hall, one fair autumn evening last September. The Master also deserves credit for accepting a wandering Bear in the first place and making all that was to follow possible.

At this point, I feel it would not go amiss to acknowledge the inventor of the fax machine, without whom Chapter 5 would have been rather different.

Mike Pritchard and John Hooper for their excellent technical assistance.

Returning to UG days, they were joyfully misspent in the company of the GBY crew and our honorary members - Jim "Dylan" Anderson, Phil "The Beast" Clapp, Martin "Beaker" Davies, Suki "Wuki" Klair, Andy "Urko" Pennell, Girish "The Rat" Rao, Mike "Babyface" Shipman, Dilip "The Rockstar" Shukla and last, but not least, Fran Daniel.

The current members of the WJA group: Arshad, Bill, George, Gamini, Imran, Jinhai, Lindy, Ying, ...er Simon, Mark A, Andrew Raymond (my infamous dance partner), the man known to the world as SM, Mex, and of course GBM, the scourge of the electrical appliance, Big Bad Ben.

The former members of the WJA army, Anne, Bernard my favourite management consultant, Nick the man from RS and the one and only Ged O'Shea.

Our academic visitors: Richard Guy of the inimitable entrance and Mike Elliott who survived despite Ged's best efforts.

The denizens of the ESCA lab, Simon and "Kasparov" Cummins, deserve a mention. Special thanks must go to Mark "The Professor" Golden with whom I have

shared many an enjoyable evening in various parts of the capital. He also deserves praise for a certain act of bravery above and beyond the call of duty.

The members of the Fifth and Sixth floors. In particular: that ever present pair of postdocs, the Tweedledum and Tweedledee of inorganic chemistry - Drs. Dengel and Kelly. I've spent many a horrible evening - in the nicest possible sense, but the worst possible taste - in Stan's with Andy. As for Paul "The Chuckie Egg Hero" Kelly, after the Hanky Trick, the Mars Bar Debacle and the sordid Newcastle Brown Affair, what can one say .... so I leave it to the man himself, "... just possibly the greatest human being I have ever met. " (P. F. Kelly, 1990). I would also like to thank Andy B., Chris, Fitzy, Paul W., Victor, Jenny and Vanessa.

I thank Phil for putting up with me for six years. I bet it felt like at least ten. Thanks for catching me when I fell.

I wish to thank Jon Parr and I would like to extend a special thanks to Bryan Driscoll for keeping in touch.

My deepest thanks go to my fellow Wolfson Wallies for sharing the lab with me for two years: Peter Galley, Girish Rao and Edmond Magner or as they will be immortalised: WingCo, Rat and the Monsignor.

A word to the wise :

Mix a little foolishness with your serious plans:

it's lovely to be silly at the right moment

Horace

CONTENTS

LIST OF FIGURES

LIST OF TABLES

CHAPTER 1
INTRODUCTION

This thesis is concerned with the development of electrochemical sensors using conducting organic salt enzyme electrodes. These systems combine the high selectivity of enzymes with the ease of control of electrochemistry. The chapter begins with a brief description of the properties of some of the flavoenzymes used in this work. This is followed by a section on protein electrochemistry. The chapter concludes with an outline of the rest of the thesis.

1.1 FLAVOENZYMES

Many processes of fundamental importance in nature depend on the transfer of electrons between redox proteins and the utilisation of the energy yielded by such a mechanism. Flavoenzymes form an important family of redox proteins whose name derives from their containing either riboflavin (RF), flavin mononucleotide (FMN) or flavin adenine dinucleotide (FAD) as a redox-active prosthetic group. Flavoenzymes can be further subdivided into two categories depending on whether or not they contain a metal centre, usually iron or molybdenum.

The central isoalloxazine system is composed of a fused three-ring structure containing benzene, pyrazine and pyrimidine (Figure 1.1). The tricyclic flavins serve as two-electron oxidants with the final product being a 1,5-dihydroflavin (hydroquinone form). One-electron reduction of flavins yields a radical anion (semiquinone). The electrons accepted by the flavin are rapidly transferred to a more powerful oxidant, usually oxygen.

The equilibrium constant for the dissociation of the holoenzyme into cofactor and apoenzyme is of the order of 10^{-8} or 10^{-9} M. However reduction of the isoalloxazine system results in the loss of aromaticity and is accompanied by a change from a planar to

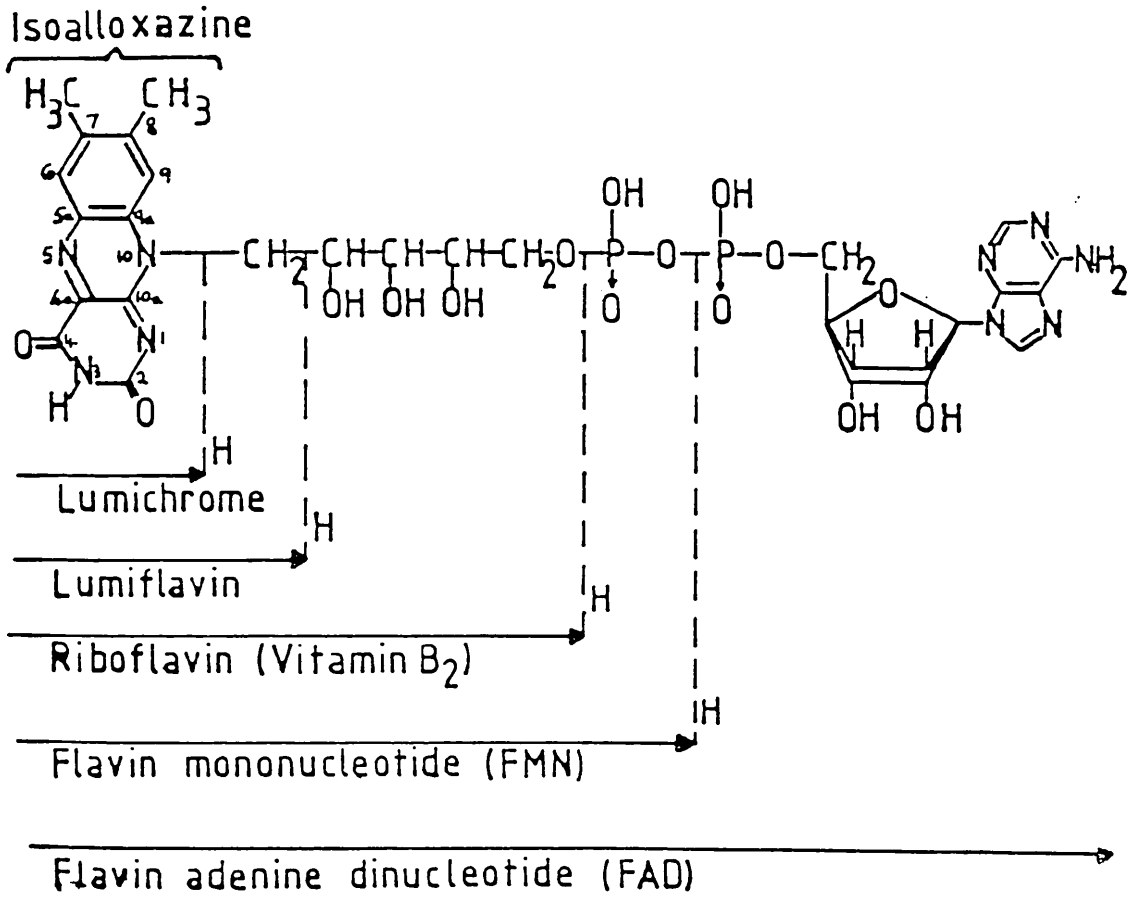

Figure 1.1 Chemical structure of flavin based systems

a puckered geometry. This leads to the apoenzyme having a different affinity for the oxidised and reduced forms of the prosthetic group.

The properties of some of the flavoenzymes used will be outlined in the following sections.

1.1.1 Glucose Oxidase

The enzyme obtained from *Aspergillus niger* is a dimer (M_r=160000) consisting of two monomers (M_r=79000). It has a hydrodynamic radius of 4.3nm (1). The enzyme has a polysaccharide coat which provides rigidity and in addition, serves to increase its solubility. The enzyme catalyses the oxidation of glucose

β-D-glucose + glucose oxidase-FAD $\longrightarrow$

δ-D-gluconolactone + glucose oxidase-$FADH_2$

The reduced enzyme is then reoxidised by molecular oxygen.

glucose oxidase-$FADH_2$ + O_2 $\longrightarrow$

glucose oxidase-FAD + H_2O_2 +$2e^-$

There are two tightly bound FAD groups per dimer. O'Malley and Weaver (2) proposed that the dimer was held together by a disulphide linkage, but Tsuge (3) and Jones (4) have suggested that non covalent interactions are responsible for maintaining structural integrity. Swoboda (5) showed that binding of FAD caused a marked conformational change, the holoenzyme assuming a far more compact rigid structure than the flexible apoenzyme.

Glucose oxidase has been the subject of extensive study and its kinetic parameters have been determined (6,7). The enzyme shows a high specificity for the β-anomer of D-glucose. Apart from the glucose anomers numerous other potential substrates have been tried (8). These results led Keilin and Hartree (9) to suggest that substitution in the 1-, 2- or 3-OH groups of glucose removed glucose oxidase activity entirely whereas substitution in the 4- or 6- positions reduced the activity to 1 or 2% of

that for β-D-glucose. However more recent work (10-12) showed that both D-glucosone and 2-Deoxy-D-glucose showed considerable activity, far more than other possible substrates, indicating that, modification of the C-2 position was permissible.

1.1.2 Xanthine Oxidase

Xanthine oxidase (M_r = 283000) is an example of a flavoenzyme which contains metal atoms in addition to the flavin moiety. It was the first mammalian enzyme found to contain molybdenum (13). Although it is commonly found, its exact function appears to depend on the complexity of the organism. In lower organisms, xanthine may be the sole nitrogen source and thus the conversion of xanthine to uric acid may be the first step in nitrogen uptake. In mammals it catalyses the oxidation of hypoxanthine to xanthine and that of the latter to uric acid, thus playing an integral part in purine catabolism. The reactions it catalyses are of the form

$$RH + OH^- \longrightarrow ROH + H^+ + 2e^-$$

It is now accepted that milk xanthine oxidase contains FAD, molybdenum, iron and acid-labile sulphur in the ratio 1:1:4:4. The subunit structure has not yet been entirely resolved. Denaturation studies using thiols and guanidine (8M) failed to reduce the molecular weight to less than 100000 (14). Thus it appears that there is a stable subunit of approximately half the molecular weight of the native enzyme. Evidence from inhibition studies using alloxanthine indicates that there are two active sites since 1 mole of xanthine oxidase binds 2 moles of alloxanthine, presumably one per molybdenum centre.

1.1.3 D-Sarcosine Oxidase

This enzyme catalyses the oxidative demethylation of sarcosine

$$CH_3NHCH_2COOH + O_2 + H_2O \longrightarrow HCHO + NH_2CH_2COOH + H_2O_2$$

It has been obtained from a variety of sources, namely, *Arthrobacter*, *Pseudomonas and Corynebacterium* species. The enzyme obtained from the latter source has been shown to

contain 1 mole of covalently bound FAD[8α-(N^3-histidyl)-FAD] together with 1 mole of non-covalently bound FAD per mole of enzyme (M_r=174000). The enzyme consists of four non-equivalent subunits: A, M_r=110000; B, M_r=44000; C, M_r=21000; D, M_r=10000. Hayashi (15,16) and Suzuki (17) showed that the covalently bound flavin was attached to subunit B.

Elegant work by Jorns (18) involving a spectrophotometric study of the effect of sulphite on the flavin absorbance at 450nm showed that although only 50% of the flavin was reduced by the sulphite, all catalytic activity was lost. Since the sulphite-unreactive flavin was still able to oxidise sarcosine it was proposed that one flavin moiety accepted reducing equivalents from the substrate and passed the electrons onto the second flavin which reduced oxygen to hydrogen peroxide. The sulphite inhibited the enzyme by reducing the second flavin thus preventing the reoxidation step. The study also showed that on removal of the non-covalently bound FAD, the resulting semiapoprotein lost 98% of its activity towards the substrate. Sarcosine was unable to reduce the covalent FAD whereas sulphite did react with the semiapoprotein. This showed that the substrate was oxidised by the non-covalently bound FAD which was then oxidised by the covalently bound FAD moiety which in turn reduced molecular oxygen.

1.2 ELECTROCHEMISTRY OF PROTEINS

1.2.1 Direct Electron Transfer

Electrochemical techiques should be ideal for examining the properties of flavoenzymes and redox proteins in general. However although proteins are generally charged the problem lies in binding them in an orientation that facilitates electron transfer. The high overpotentials required to drive electron transfer also tend to denature the protein. The strong electrostatic field present near the electrode surface has an adverse effect on the weak electrostatic interactions which maintain the native conformation of

the protein with the net result often being the irreversible adsorption of the protein onto the electrode surface itself.

A second factor is that the active site is usually buried deep within the enzyme, thus the distance between the redox active centre and the electrode may be such that the rate of electron transfer is too slow to be measured (1). The distance dependence and consequently the rate of electron transfer in biological systems follows an exponential relationship, $k \propto \exp(-\alpha d)$. In proteins, doubling the separation from 0.8 to 1.7 nm leads to the transfer rate falling by $\approx 10^4$. A further drawback with these high overpotentials is that any impurity will also be turned over by the electrode.

Thus either the electrode surface has to be modified so as to ensure that the orientation of the protein with respect to the surface is optimised or a mediator is used which can shuttle electrons to the electrode, removing the requirement for close approach.

1.2.2 Mediated Electron Transfer

A mediator serves as a shuttle between the redox centre of the protein and the electrode surface. Its reactions can be summarised

$$E_{ox} + S \longrightarrow E_{red} + P$$

$$E_{red} + M_{ox} \longrightarrow E_{ox} + M_{red}$$

$$M_{red} \longrightarrow M_{ox} + e^-$$

Szentrimay (19) lists the following requirements for an ideal mediator:

1. Well defined electron stoichiometry
2. Known formal electrode potential
3. Both homogeneous and heterogeneous electron transfer need to be fast
4. To study biological systems it must be soluble in aqueous media near pH 7

5. Both oxidised and reduced forms should be stable
6. Interactions with the redox protein should not affect the redox potential of the mediator

Organic molecules commonly used as mediators include viologens, quinones, phenazines and phenylenediamines (20). The most common inorganic mediators are ferrocene derivatives. Substituents can readily be introduced into either or both cyclopentadienyl rings. As this provides a means of modulating the redox potential, these systems possess significant versatility.

1.2.3 Modified Electrodes

A promoter can be used to modify the surface of a metal electrode so as to bind the protein in a more favourable orientation and thus enhance the rate of electron transfer. A promoter is distinguished from a mediator by the fact that it is not electroactive at the electrode potential employed.

Pioneering work in this field was carried out by Kuwana (21) and Hill (22) using tin-doped indium oxide and 4,4-bipyridyl coated gold electrodes respectively. Albery, Hill and co-workers (23) carried out a mechanistic rotating-ring disk study of the bipyridyl modified gold electrode/cytochrome c system. Their results showed that for electrochemistry to be observed the protein must diffuse to the electrode surface and by interacting with the surface modifier attain the most favourable orientation for electron transfer. Following rapid electron transfer, the protein dissociates from the surface and diffuses away into the bulk solution (Figure 1.2). A prerequisite for reversible kinetics was rapid association of the incoming protein and surface modifying group. Since adsorption complicates electroanalytical techniques, for instance cyclic voltammetry, it was advantageous if modifiers prevented irreversible adsorption and subsequent denaturing of reactant protein systems.

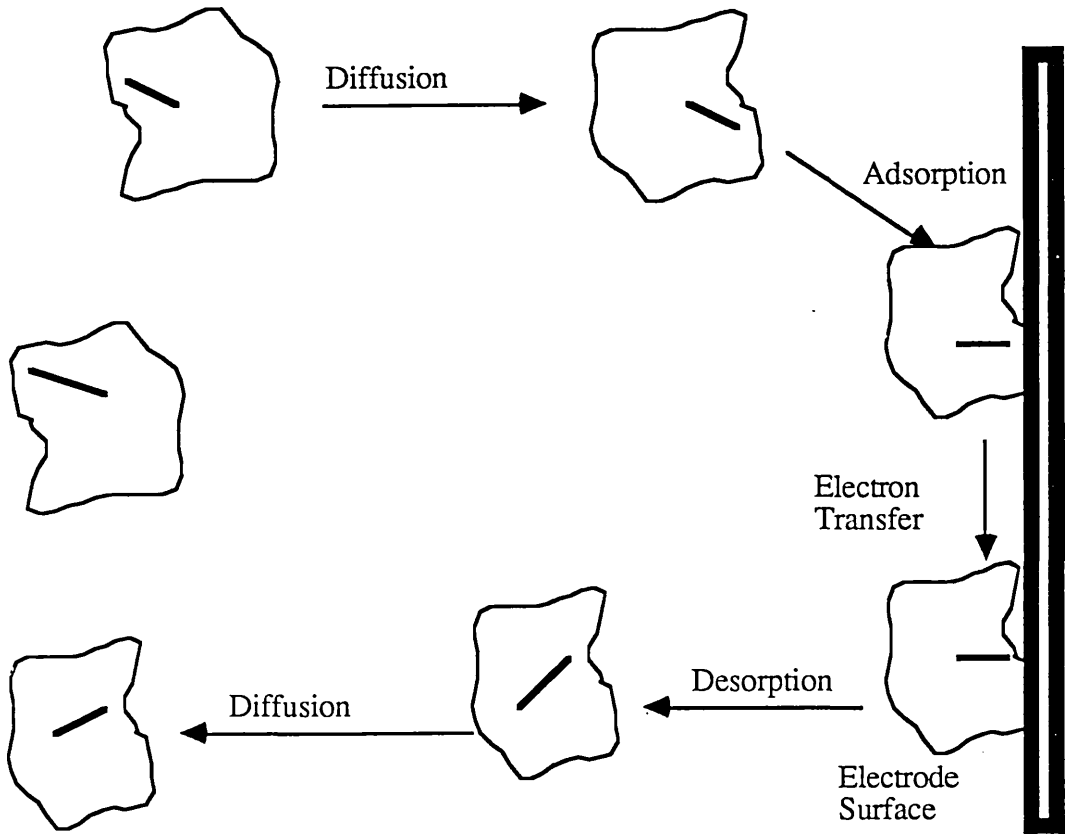

Figure 1.2 Scheme depicting the mechanism of a protein redox reaction at an electrode surface (52)

1.2.4 Chemically Modified Enzymes

Instead of creating a more amenable electrode surface an alternative approach was to modify the enzyme: if the mountain will not come to Mohammed then Mohammed must go to the mountain. It was known that redox enzymes could transfer electrons to small ions or molecules which served as homogeneous mediators shuttling between the enzyme and a metal electrode but one question remained: could these relays be covalently attached to the enzyme without loss of activity, thus enabling direct electron transfer from the FAD/$FADH_2$ couple to the electrode? The answer came in 1987 when Heller (1) showed that if ferrocenecarboxylic acid was reacted with a carbodiimide, the O-acylisourea product could acetylate available primary amine groups on glucose oxidase to yield a covalently modified enzyme capable of transferring electrons to a metal electrode (Figure 1.3). Since the relays reduced the effective distance between the FAD units and the electrode, d_{FE}, it followed that by increasing the number of relays, thus reducing the inter-relay, d_{RR}, and relay-electrode, d_{RE}, separations, the rate of electron transfer could be further enhanced.

Bartlett (24) showed that greater stability and longevity were obtained if ferrocenecarboxylic acids with longer sidechains were used, namely, the acetic and butanoic acid derivatives. More recently Bartlett (25) has shown that glucose oxidase can be modified by tetrathiafulvalene (TTF), tetracyanoquinodimethane (TCNQ) or the organic salt TTF-TCNQ. The implications this result has on the mechanism of electron transfer at conducting organic salt electrodes are discussed in later chapters.

1.2.5 Flavoenzyme Electrochemistry

1.2.5.1 Electrochemistry of Glucose Oxidase

Bockris (26) has used differential pulse voltammetry to investigate the electrochemical behaviour of GOD at graphite electrodes. His results showed that a variety of electron transfer reactions were possible depending on the extent of protein

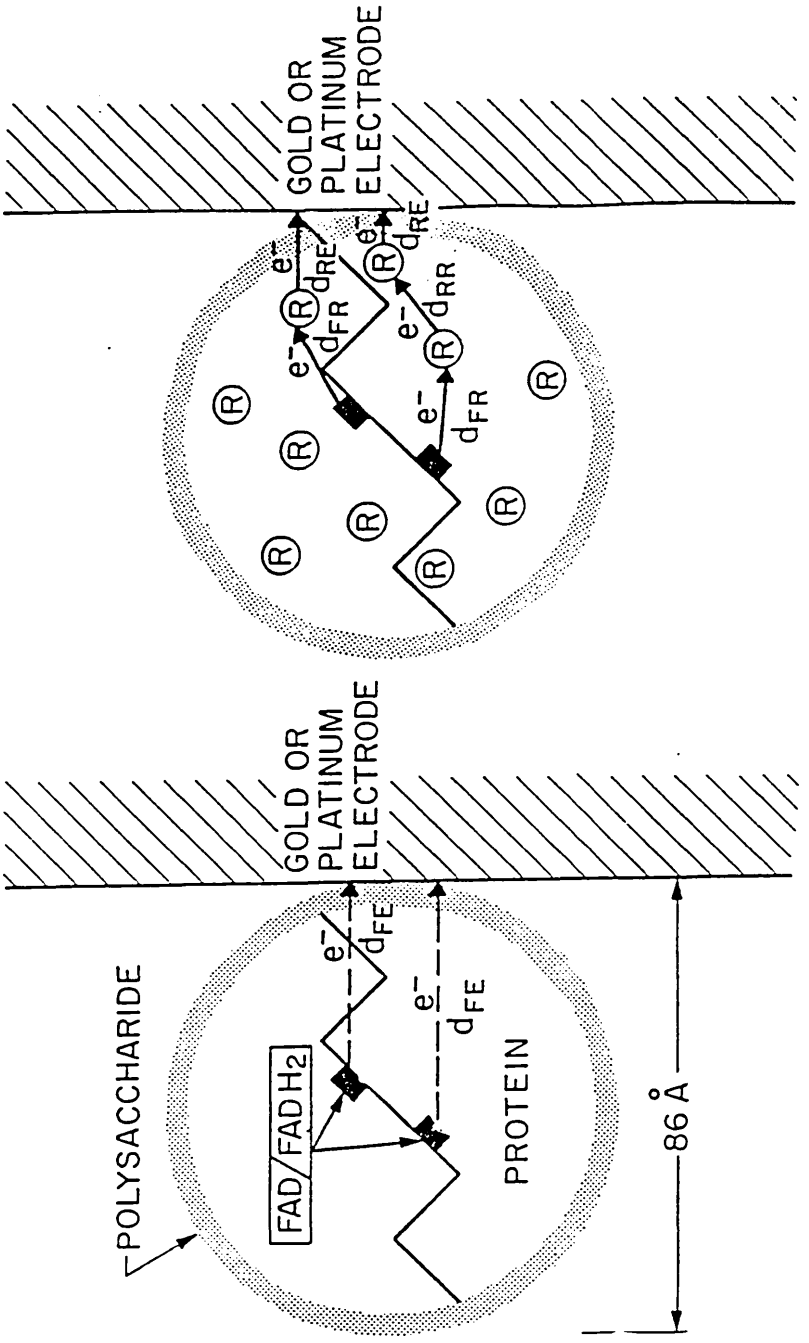

Figure 1.3 Diagram of a glucose oxidase molecule reacting at a metal electrode prior to and after modification by incorporation of electron relays (1)

adsorption and resulting conformational modifications. If extensive protein unfolding occurred then electron transfer from FAD adsorbed directly on the surface was a possibility. The peaks due to these strongly adsorbed moieties were unchanged on addition of glucose.

The redox potential of GOD has been shown using potentiometric titration to lie between -102 mV and -322 mV (vs. SCE pH = 6) (27,28). Bockris observed 3 peaks, at -417, -302 and -222 mV (vs. SCE pH = 6). The first peak was attributed to a strongly adsorbed state whose redox potential was shifted markedly from that of free GOD in solution owing to the strength of the surface interaction. The peaks at -302 and -222 mV were in the potential range expected for native GOD in solution; however this did not preclude weak adsorption since if this were to occur it would do so without pronounced conformational change thus one would not expect to observe a significant shift in redox potential.

Bockris proposed four possible situations which could explain his results (Figure 1.4):

a. Direct through space electron transfer from a native GOD molecule in solution near to the electrode surface.

b. Electron transfer from a weakly adsorbed GOD molecule which has retained much of its conformational integrity.

c. Electron transfer from a strongly adsorbed GOD molecule which has been partially denaturatured.

d. Direct electron transfer from a redox centre which has dissociated completely from the enzyme owing to the severity of the interaction with the electrode surface.

In order to determine which peaks were due to free FAD irreversibly adsorbed on the electrode (26), Bockris recorded the electrochemical response of a 20 μM GOD solution. The electrode was then washed and inserted into fresh enzyme-free buffer

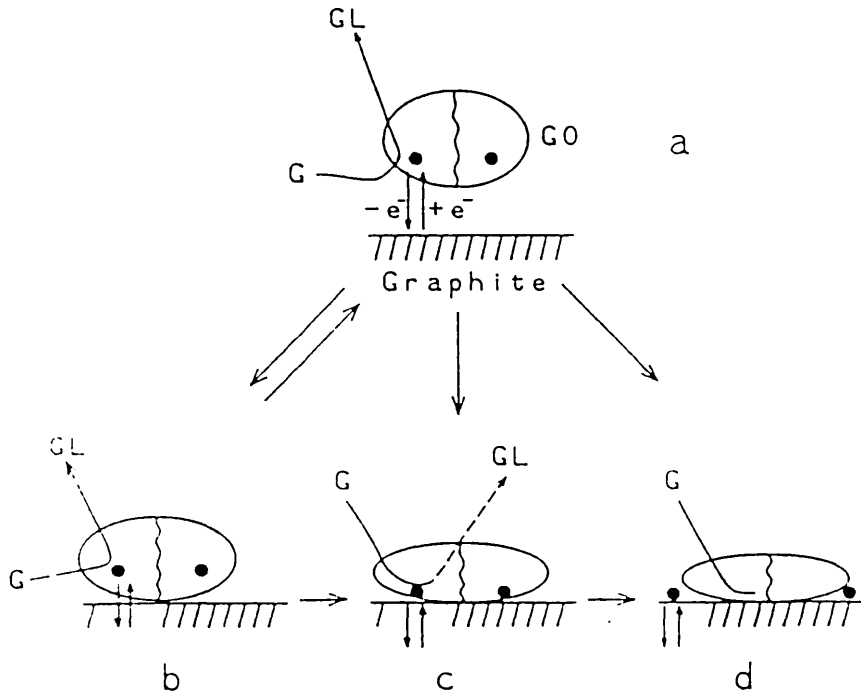

Figure 1.4 Schematic representation of enzyme interactions at a graphite electrode (26)

solution and differential pulse voltammograms of the electrode before and after washing compared. It was found that the peaks at -417 and -222 mV were due to strongly adsorbed species. The former peak was probably due to FAD which had become completely dissociated from the enzyme owing to the extent of protein denaturation. Bockris concluded that since different adsorption states were present, the reduction peaks observed could not all be attributed to dissociated FAD. Moreover, it implied that GOD could assume more than one configuration on the electrode surface.

In 3M urea GOD undergoes partial denaturation whereas in 6M urea the holoenzyme breaks down yielding free FAD and the apoenzyme (1). Bockris found that at the lower urea concentration the peak at -417 mV increased markedly with respect to that at -222 mV, whilst at 6M urea the peak at -222 mV vanished completely and only that at -417 mV remained. It was apparent that the peak observed at -222 mV was due to strongly adsorbed holoenzyme whereas that at -417 mV was caused by free FAD.

Experiments carried out in the presence of glucose revealed that the magnitude of the reduction peaks at -222 and -302 mV was decreased in the presence of substrate: the implication being that these two peaks were from enzyme molecules which had retained their catalytic activity. As the peak observed at -417 mV remained unchanged it was either from dissociated FAD or from a catalyically inactive enzyme molecule. To account for the small change in the size of the reduction peaks Bockris proposed that only a few GOD molecules were of the weakly adsorbed yet catalytically active variety, the majority being strongly adsorbed yet catalytically inactive. Alternatively it was suggested that only one of the two FAD moieties per enzyme was available to interact with the incoming glucose molecule, the other having dissociated, and this semiapoprotein had a reduced catalytic efficiency.

1.2.5.2 Electrochemistry of Xanthine Oxidase

Early workers (30-34) had proposed that the mechanism of action of xanthine oxidase involved intramolecular electron transfer in the sequence Mo → FAD → Fe/S.

However Massey and co-workers (35) showed that the actual electron transfer sequence was FAD → Mo . The Fe/S centres connect the reductive and oxidative pathways of the reaction mechanism. In the reductive cycle they serve as electron sinks oxidising any Mo(IV) and Mo(V) to Mo(VI) thus ensuring a rapid rate of reaction with an incoming xanthine molecule. In the oxidative process where the final reaction step involved oxidation of $FADH_2$ by molecular oxygen they regenerate reduced flavin. In later work, Bray (36) determined the absolute values of the reduction potentials using potentiometric titration and these showed good agreement with those found by Massey who had given the reduction potentials of the various couples relative to that of Fe/S(II) (35).

1.3 CONDUCTING ORGANIC SALTS

The search for electronic devices with ever-faster response times led workers to investigate the possibilities of creating synthetic or organic metals whose properties could be modified by altering specific substituent groups present in the constituent molecules. Several comprehensive reviews are available in the literature (37 and references therein).

1.3.1 Structural and Physical Properties

Tetrathiafulvalinium tetracyanodiquinomethanide TTF-TCNQ (38,39) is a molecular solid whose structure consists of discrete stacks of TTF and TCNQ (Figure 1.5). Individual molecules are stacked face-to-face since this facilitates stabilising intermolecular π-π interactions which create a delocalised electronic system. From molecular orbital theory, orbital overlap of N discrete molecules produces a band with N states. The electrical conductivity is influenced by the degree of occupancy of the band, the extent of interstack interactions and the presence of structural defects. In TTF-TCNQ each molecule has a non-integral charge ie. $TTF^{0.59+}TCNQ^{0.59-}$ thus both components contribute to charge-transfer processes which give rise to electrical conductivity.

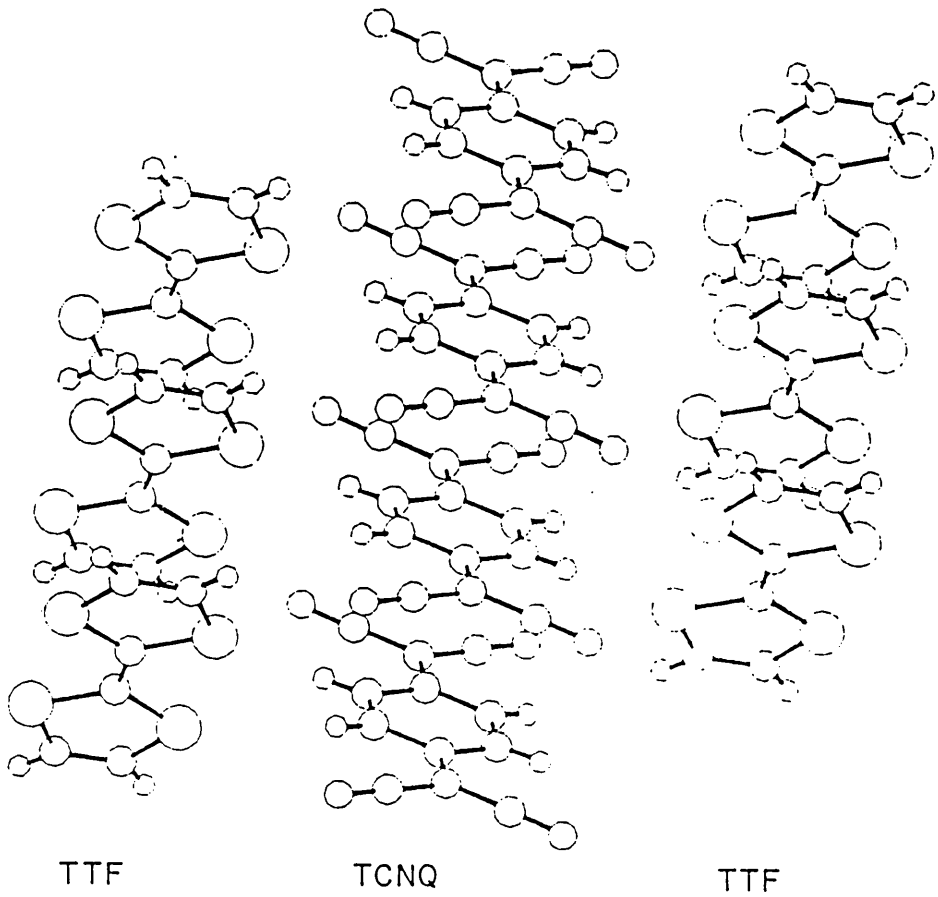

Figure 1.5 Segregated stacks of TTF and TCNQ molecules in TTF-TCNQ viewed normal to the stacking axis (37)

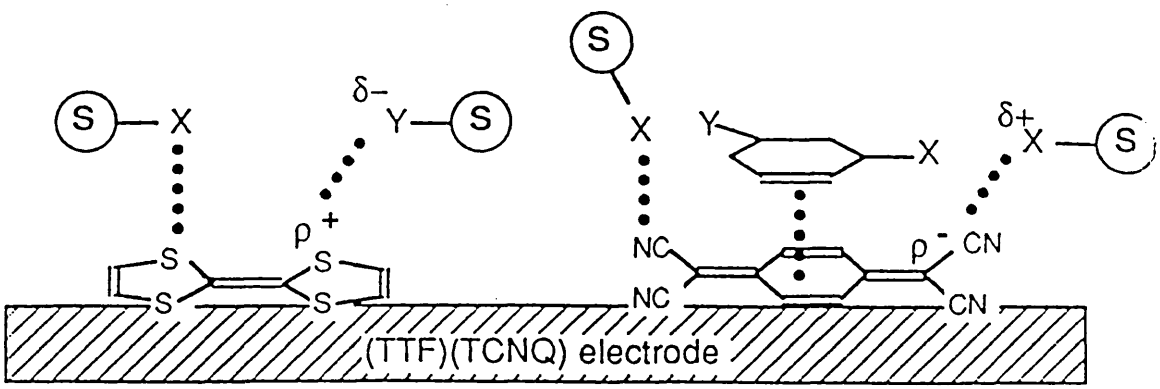

Figure 1.6 Schematic representation of possible substrate-electrode interactions at a TTF-TCNQ electrode (37)

1.3.2 Electrochemical Properties

It is to be expected that rates of electron transfer at conducting organic salt electrodes are different from those at, say, a platinum electrode, simply because of the drastically different nature of the electrode surfaces. Organic salts could facilitate specific adsorption processes which were not feasible on metallic surfaces. Also, π-π interactions with unsaturated reactants could enhance electron transfer, as could hydrogen-bonding or other polar interactions of a similar nature (Figure 1.6). A detailed study of the electrochemical properties of TTF-TCNQ was carried out by Jaeger and Bard (40). They fabricated pressed-pellet electrodes and examined the effect of background electrolyte on the nature of the cyclic voltammograms yielded by the system. They found that although the electrode could be oxidised or reduced in all electrolytes, the presence of reverse peaks was dependent on the solubility of the ion pairs formed during the forward sweep. Thus in a LiAc solution, if the potential exceeds +0.65V (vs SCE) during the forward sweep then since the acetate salts of TTF^{+} and TTF^{2+} are soluble, their reduction is not observed in the reverse sweep, where the only peak present is due to the reduction of $TCNQ^{\circ}$. Similarly, if the electrode is reduced then the only peak which is observed on the subsequent anodic sweep is due to the oxidation of TTF° since the lithium salts of $TCNQ^{-}$ and $TCNQ^{2-}$ are soluble and consequently lost to the solution.

$$\text{TTF-TCNQ (s)} \longrightarrow \text{TTF}^{+}\text{(aq)} + \text{TTF}^{2+}\text{ (aq)} + \text{TCNQ}^{\circ}\text{ (s)}$$

$$\text{TTF-TCNQ (s)} \longrightarrow \text{TTF}^{\circ}\text{ (s)} + \text{TCNQ}^{-}\text{ (aq)} + \text{TCNQ}^{2-}\text{ (aq)}$$

However in a KBr solution where salts of both TTF and TCNQ are insoluble, return peaks for all products are observable.

The stable range in lithium acetate observed by Jaeger and Bard surpassed that predicted from inspection of the redox potentials of the individual constituents TTF°/TTF^{+} (+0.30V) and $TCNQ^{\circ}/TCNQ^{-}$ (+0.19V), by an amount corresponding to the enthalpy of formation of the crystal lattice, which is reported as being 0.39eV (41).

1.3.3 Redox Processes at TTF-TCNQ Electrodes

Three mechanistic routes are possible. First, the conducting salt can adopt true metallic behaviour, in which case electron transfer between reactant and electrode proceeds via states close to the Fermi level of the electrode. In TTF-TCNQ these states are associated with the TCNQ constituent (Figure 1.7). Since the conduction band associated with the TCNQ stacks is only partially full it can accept as well as donate electrons thus facilitating redox processes. For direct electron transfer the evidence points to a role for TCNQ, however this does not preclude the involvement of a lower TTF subband.

Alternatively, if different oxidation states of TTF and TCNQ are present on the electrode surface then pathways involving mediated electron transfer are possible (Figure 1.8). However since no lattice redox reactions are observed in the ideally polarisable region this implies that the mediator concentrations must be small.

A third route involves, what has been termed, "retro charge-transfer" (37). This involves electron transfer by reaction with neutral TTF° or $TCNQ^{\circ}$ present on the electrode surface (Figure 1.9). These species may be created either by initial dissolution of the TTF-TCNQ complex followed by precipitation of TTF° and $TCNQ^{\circ}$ or more simply by direct formation on the electrode surface itself. This process would only be energetically favourable if the solvation energy of the neutral species compensated for the electrostatic lattice energy lost by their formation. In an oxidative process, the incoming substrate molecule is oxidised by one of the neutral electrode species; this is followed by oxidation of the other neutral species by the electrode, since both ionic forms have been regenerated they can now recombine. Thus "retro-charge transfer" is synonymous with the theory of heterogeneous redox catalysis, as proposed by Albery (42), concerning the mechanism of electron transfer at these electrodes.

TCNQ subband

$$\{(TTF^{0.59+})(TCNQ^{0.59-})\}_n + D \longrightarrow D^+ + \{(TTF^{0.59+})(TCNQ^{(0.59+1/n)-})\}_n$$

$$\{(TTF^{0.59+})(TCNQ^{0.59-})\}_n + A \longrightarrow A^- + \{(TTF^{0.59+})(TCNQ^{(0.59-1/n)-})\}_n$$

TTF subband

$$\{(TTF^{0.59+})(TCNQ^{0.59-})\}_n + D \longrightarrow D^+ + \{(TTF^{(0.59-1/n)+})(TCNQ^{0.59-})\}_n$$

$$\{(TTF^{0.59+})(TCNQ^{0.59-})\}_n + A \longrightarrow A^- + \{(TTF^{(0.59+1/n)+})(TCNQ^{0.59-})\}_n$$

Figure 1.7 Mechanism of direct electron transfer at a TTF-TCNQ electrode (37)

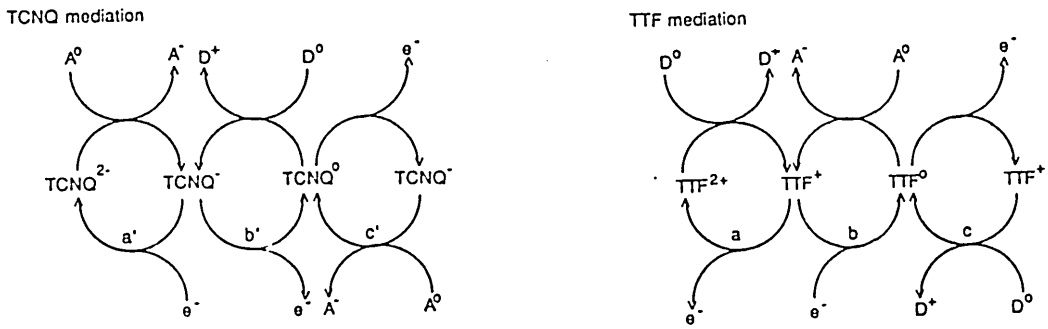

Figure 1.8 Mechanism for mediated electron transfer at a TTF-TCNQ electrode (37)

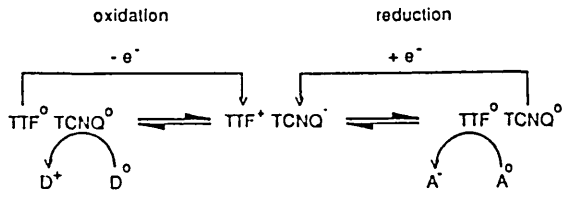

Figure 1.9 Mechanism for retro-charge transfer prior to electron transfer at a TTF-TCNQ electrode

1.3.4 Amperometric Enzyme Electrodes Using TTF-TCNQ

Biosensors (43) aim to measure the concentration of the desired metabolyte or foodstuff in its natural environment with a minimum perturbation of the system. An enzyme electrode is a biosensor which functions by using a redox enzyme to turn over the substrate and then electrochemically reoxidises the reduced enzyme/cofactor thus using the substrate-dependent biochemical reaction to produce a measurable current. Glucose oxidase is the most comprehensively studied enzyme using this technique due in no small part to its exceptional stability (44-46). The heterogeneous electrochemical rate constant has been evaluated (46) and kinetic analysis of the experimental data has shown the rate determining step to be transport of glucose through a dialysis membrane (Figure 1.10). This property is a prerequisite for use of the electrode as a biosensor since its response will be unaffected by changes in enzyme activity.

Other enzymes investigated using TTF-TCNQ electrodes include choline oxidase (47) which oxidises choline and the subsequent reaction product betaine aldehyde and xanthine oxidase which sequentially oxidises hypoxanthine and xanthine (48).

In-vivo studies using GOD adsorbed on TTF-TCNQ microelectrodes have been used to measure glucose levels in the brains of live freely moving rats (47,49). A linear response was obtained with only a marginal loss of enzyme activity over a period of 10 days. After 28 days the electrode response had fallen to half of its original value.

The mechanism of electron transfer at these electrodes has been the centre of much debate. Initially it was proposed that glucose oxidase reacted by homogeneous mediation (49,50). As mentioned above, Albery has suggested the reaction proceeds via heterogeneous redox catalysis (42). Recent work in the laboratories of Bartlett (25) has suggested that a modified enzyme might be involved though it is unclear whether the enzyme would remain on the electrode surface in its modified state or would return to the bulk solution.

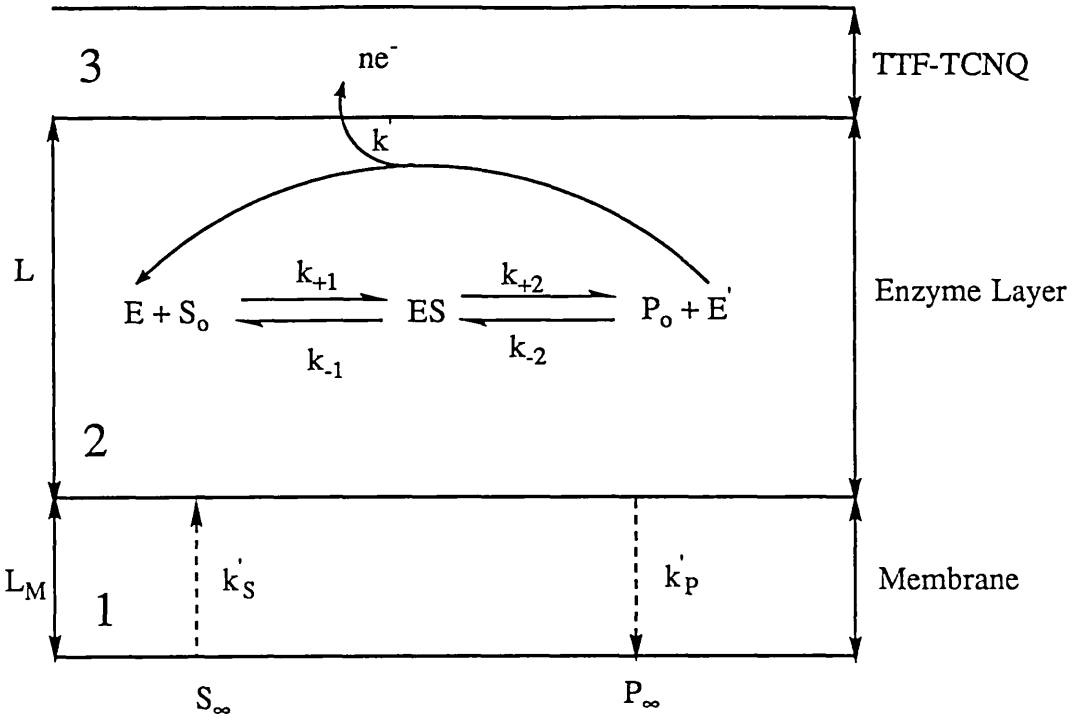

S = substrate

P = product

E = enzyme

Rate determined by either **1.** transport of substrate across the membrane

or **2.** enzyme kinetics

or **3.** electrode kinetics

Figure 1.10 Scheme depicting the action of a simple enzyme electrode

1.4 ORGANISATION OF THESIS

The next two chapters deal with the development of a series of electrochemical sensors using enzyme electrodes. Chapter 2 deals mainly with preliminary investigations of sensors for determining nitrate and creatine and an analysis of the xanthine/hypoxanthine system. Kinetic models for each system are devised using the theory developed by Albery and Bartlett (51). Chapter 3 is concerned with the development of a sucrose sensor using invertase, mutarotase and GOD. A kinetic model is used to explain the behaviour of this three enzyme system. Chapter 4 details the results of pressed pellet rotating TTF-TCNQ disk Pt-ring experiments including an investigation of nucleation phenomena observed on the Pt-ring. It also includes use of Nicholson/Shain (52) analysis to determine the second order rate constant for the oxidation of reduced glucose oxidase by TTF^+. Chapter 5 is concerned with the use of a.c. impedance spectroscopy to elucidate the mechanism operating at these electrodes.

REFERENCES

1. Y. Degani and A. Heller, J. Phys. Chem., 11, 1285, (1987)

2. J. J. O'Malley and J. L. Weaver, Biochemistry, 11, 3527, (1972)

3. H. Tsuge, O. Natsuakai and K. Ohashi, J. Biochem., 78, 835, (1975)

4. M. N. Jones, P. Manley and A. Wilkinson, Biochem. J., 203, 285, (1982)

5. B. E. P. Swoboda, Biochem.Biophys.Acta., 175, 365 and 380, (1969)

6. Q. H. Gibson, B. E. P. Swoboda and V. Massey, J. Biol. Chem., 239, 3927, (1964)

7. H. J. Bright and M. Appleby, J. Biol. Chem., 244, 3625, (1969)

8. M. Dixon and E. C. Webb, Enzymes, 3rd ed., Longman, New York, (1979)

9. D. Keilen and E. F. Hartree, The Enzymes 2nd ed. , Ed. Boyer, Academic Press, New York, p. 576, (1963)

10. R. B. McCamb, W. D. Yushok and W. G. Batt, J. Franklin. Inst., 263, 161, (1957)

11. A. Sols and G. de la Fuente, Rev. espan. fisiol., 13, 231, (1957)

12. A. Sols and G. de la Fuente, Biochem. Biophys. Acta., 24, 206, (1957)

13. D. E. Green and H. Beinert, Biochem. Biophys. Acta, 11, 599, (1953)

14. R. C. Bray, The Enzymes, 3rd. Edn., Academic Press, New York, (1975)

15. S. Hayashi, S. Nakamurai and M. Suzuki, Biochem. Biophys. Res. Commun., 96, 924, (1980)

16. S. Hayashi, S. Nakamurai and M. Suzuki, Biochem. Int., 4, 617, (1982)

17. M. Suzuki, J.Biochem (Tokyo), 89, 599, (1981)

18. M.S. Jorns, Biochemistry, 24, 3189, (1985)

19. R. Szentrimay, P. Yeh and T. Kuwana, Electrochemical Studies of Biological Systems, Ed. D. Sawyer, ACS, Washington DC (1977)

20. M. L. Fultz and R. A. Durst, Anal. Chim. Acta., 140, 1, (1982)

21. P. Yeh and T. Kuwana, Chem. Lett., 1145-48, (1977)

22. M.J. Eddowes, H.A.O. Hill, J.Chem. Soc. Chem. Commun., 771, (1977)

23. W.J. Albery, M.J. Eddowes, H.A.O. Hill and A.R. Hillman, J. Amer. Chem. Soc., 103, 3904, (1981)

24. P.N. Bartlett, R.G. Whittaker, M.J. Green and J. Frew, J. Chem. Soc. Chem. Commun., 1603, (1987)

25. P. N. Bartlett, personal communication

26. A. Szucs, G. D. Hitchens and J. O'M. Bockris, Bioelectrochem. Bioenerg., 21, 133, (1989)

27. F. Duke, R. Kust and L. King, J. Electrochem. Soc., 116, 32, (1969)

28. M. Stankovich, L. Schopfer and V. Massey, J. Biol. Chem., 253, 4971, (1978)

29. L. Gorton and G. Johansson, J. Electroanal. Chem., 113, 151, (1980)

30. D.Edmondson, D. Ballou, A. Van Heuvelen, G. Palmer and V. Massey, J. Biol. Chem., 248, 6135, (1973)

31. V. Massey, V. Komai, G. Palmer and G.B. Elion, J. Biol. Chem., 245, 2837, (1970)

32. R. C. Bray, G. Palmer and H. Beinert, J. Biol. Chem., 239, 2667, (1964)

33. R. C. Bray and T. Vanngard, Biochem. J., 114, 725, (1969)

34. E. I. Stiefel, Proc. Nat. Acad. Sci. U.S.A., 70, 988, (1973)

35. J. S. Olson, D. P. Ballou, G. Palmer and V. Massey, J. Biol. Chem., 249, 4363, (1974)

36. R. Cammack, M. J. Barber and R. C. Bray, Biochem. J., 157, 469, (1976)

37. M. D. Ward, Electroanalytical Chemistry Vol.16 Ed. A.J. Bard, Marcel Dekker, New York

38. J. Ferraris, D. O.Cowan, V. Walatka and J. H. Perlstein, J. Amer. Chem. Soc., 95, 948, (1973)

39. E. Ehrenfreund, E. F. Rybaczewski, A. F. Garito and A. J. Heeger, Phys. Rev. Lett., 28, 873, (1982)

40. C. D. Jaeger and A. J. Bard, J. Am. Chem. Soc., 101, 1690, (1980)

41. R. Metzger, J. Chem. Phys. , 66, 2525, (1977)

42. W. J. Albery, P. N. Bartlett, D. H. Craston and B. J. Driscoll, to be published

43. A. P. F. Turner, I. Karube and G. S. Wilson, Biosensors - Fundamentals and Applications, Oxford University Press 1987.

44. J. J. Kulys, M. N. Pesliakiene and A. S. Samalius, Bioelectrochem. Bioenerg., 8, 81,(1981)

45. N. K. Cenas and J. J. Kulys, Bioelectrochem. Bioenerg., 8, 103, (1981)

46. W. J. Albery, P. N. Bartlett and D. H. Craston, J. Electroanal. Chem, 194, 223, (1985)

47. W. J. Albery, P. N. Bartlett and A. E. G. Cass, Phil. Trans. R. Soc. Lond. B, 316, 107, (1987)

48. K. McKenna and A. Brajter-Toth, Anal. Chem., 59, 954, (1987)

49. M. G. Boutelle, C. Stanford, M. Fillenz, W. J. Albery and P. N. Bartlett, Neurosci. Lett., 72, 283, (1986)

50. J. J. Kulys, Biosensors, 2, 3, (1986)

51. W. J. Albery and P. N. Bartlett, J. Electroanal. Chem., 194, 211, (1985)

52. R. S. Nicholson and I. Shain, Anal. Chem., 36, 706, (1964)

CHAPTER 2
KINETIC MODELLING OF ENYZME ELECTRODES

This chapter details the initial development of enzyme electrodes for monitoring creatine and nitrate together with an investigation of the mechanism of the hypoxanthine/xanthine system (1,2). The kinetics of the three systems are different and theoretical models are proposed to explain the action of each sensor. The creatine sensor uses a two enzyme system in which only the second enzyme, sarcosine oxidase, is electroactive. In the case of hypoxanthine/xanthine a single electroactive flavoenzyme, xanthine oxidase, turns over the substrate, hypoxanthine, and the primary product xanthine. The nitrate sensor utilises a NADH-dependent enzyme, nitrate reductase.

Although the kinetics of the three systems are different, the underlying principles for the operation of each sensor are the same. The enzyme is trapped near to the electrode surface behind a semi-permeable cellulose acetate membrane. The substrate diffuses through the membrane and is turned over by the enzyme which is reduced. The reduced enzyme, or cofactor, is then oxidised by the electrode producing a current which is related to the substrate concentration.

The electrode response is governed by one of three processes: transport of substrate across the membrane, the kinetics of the enzyme reaction, or if electron transfer between the reduced enzyme and the electrode is slow the electrode kinetics. Complex behaviour where the response depends on the interplay between different factors is also possible. In order to use an enzyme electrode as a sensor it is desirable for the response to be governed solely by transport kinetics.

2.1 EXPERIMENTAL

2.1.1 Chemicals and Solutions

TTF-TCNQ was prepared according to the method of Ferraris (3). All solutions were freshly made up each day using a stock pH 7.4 buffer containing 0.1M Na_2HPO_4 and 0.15M NaCl, the pH of the buffer having been adjusted to 7.4 using conc. HCl. All solutions were made using doubly deionised water (DDW) which had been purified by passage through an ion-exchange resin (Houseman) followed by circulation through a Milli-Q system (Millipore). All solutions were degassed using argon prior to and during electrochemical measurements. Creatinase [E.C. 3.5.3.3], sarcosine oxidase [E.C. 1.5.3.1], xanthine oxidase [E.C. 1.1.3.22] and nitrate reductase [E.C. 1.9.6.1] were obtained from Sigma and used as supplied (Table 2.1). The enzyme concentrations used were as follows : 1000 U/ml creatinase and 7 U/ml sarcosine oxidase, 4.5 U/ml xanthine oxidase and 3 U/ml nitrate reductase.

2.1.2 Membranes

Spectra/Por 2 dialysis membrane with a molecular weight cut-off (MWCO) of 12000-14000 was used for the creatine and nitrate sensors. Spectra/Por 4, which has the same molecular cutoff as Spectra/Por 2, but is thicker and thus has a longer dialysis time was used for the xanthine/hypoxanthine system. The membranes were pretreated to remove impurities by soaking in a 10g dm^{-3} aqueous solution of Na_2CO_3 for 10 minutes. Membranes were stored in 10 mmol dm^{-3} Tris solution containing 1 mmol dm^{-3} EDTA at 4°C.

2.1.3 Electrodes

Working electrodes were fabricated in-house by Mr. M. Pritchard. A platinum disk connected to a brass contact was press-fitted into teflon with a recess (depth 1mm) to produce a cavity electrode. A 9:1 (w/w) mixture of TTF-TCNQ and polystyrene, acting as a binder, was packed into the cavity and left to air dry. The area of the

TABLE 2.1

Commercially avaliable enzyme preparations

ENZYME	EC NUMBER	SIGMA	SOURCE
Creatinase	3.5.3.3	C 7024	*Flavobacterium*
Sarcosine Oxidase	1.5.3.1	S 8764	*Arthobacter species*
Xanthine Oxidase	1.1.3.22	X 4500	*Buttermilk suspension*
Nitrate Reductase	1.9.6.1	N 7265	*Aspergillus species*

electrode used for the creatine and nitrate sensors was 0.0314 cm^2. A larger electrode of area 0.3848 cm^2 was used for the xanthine/hypoxanthine system. The electrode was pretreated by cycling overnight between -150 and +350 mV (vs. SCE). Saturated calomel electrodes made in-house were used as reference electrodes. Counter electrodes were made of platinum gauze.

2.1.4 Apparatus

Experiments were carried out using a modular electronics system designed in-house by Mr. J. Hooper. Bryans 60000 or Gould 273 chart recorders were used to record experimental results.

2.1.5 Experimental Procedures

A drop of enzyme solution was placed on the electrode and trapped behind a membrane which was secured by an "o"-ring (Figure 2.1). Care was taken to avoid trapping air bubbles. Excess enzyme was removed by copious washing with DDW. The electrode was poised at +250 mV for creatine and nitrate and +300 mV for xanthine / hypoxanthine and allowed to settle until a steady backgound current was reached before any substrate was added.

Experiments were performed using standard procedures (4,5).

2.2 CREATINE ELECTRODE

Creatine and phosphocreatine play significant roles in the storage and transport of phospate-bond energy (6). Phosphocreatine has a regulatory role as it maintains a steady ATP/ADP ratio, fluctuations of which would be harmful to the functioning of myofibrils, cation pumps and other ATP-dependent systems. Creatine is synthesised from arginine, glycine and methionine (7). It is eliminated from the kidneys in the glomerular filtrate but is reabsorbed in the renal tubules. Healthy individuals excrete very little creatine in their urine; creatinuria being indicative of kidney dysfunction and certain

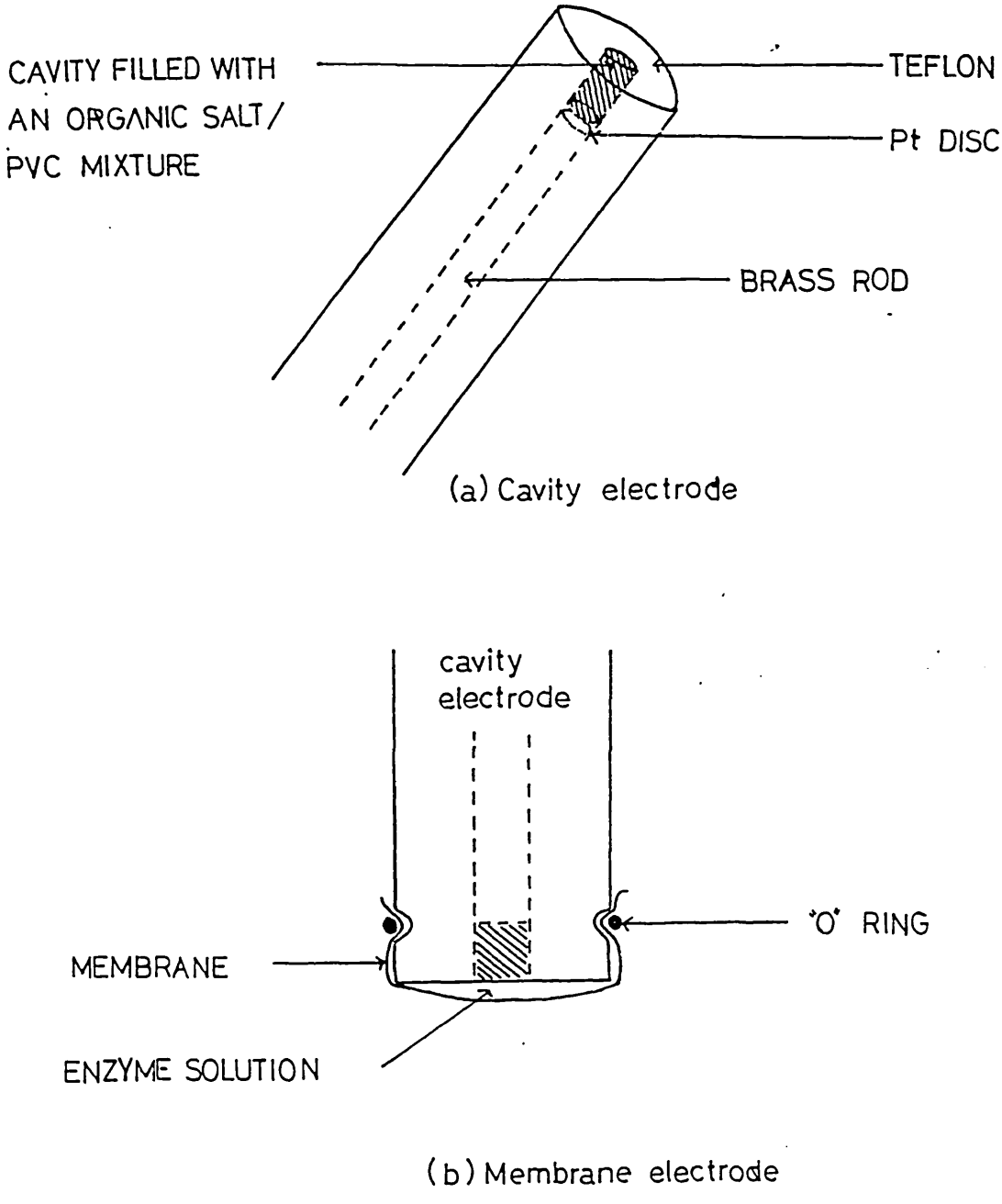

Figure 2.1 Diagram of a cavity electrode

muscle disorders (7,8). If an individual is suffering from such a condition the plasma creatine level exceeds that which can be reabsorbed by the kidneys.

The food industry is also interested in determining creatine levels since results appear to show that its concentration is directly related to the muscle protein content (8).

Two methods of analysis are currently in use. The first entails conversion of creatine to creatinine which is determined by the Jaffe reaction using sodium picrate (9). This has been criticised on the grounds that it lacks specificity. The second method is based on the reaction of creatine and 1-napthol and diacetyl (10,11).

Here a two-enzyme system was used in which creatinase (E.C. 3.5.3.3) hydrolysed creatine, producing sarcosine which was oxidised by sarcosine oxidase (E.C. 1.5.3.1), an electroactive flavoenzyme (5). The overall process can be summarised as follows:

$$\text{creatine} + H_2O \longrightarrow \text{sarcosine} + \text{urea}$$

$$\text{sarcosine} + H_2O + O_2 \longrightarrow \text{glycine} + \text{formaldehyde} + H_2O_2$$

This system, in conjunction with creatininase (E.C. 3.5.2.10), has been used in the diagnostic analysis of serum and urine creatinine levels (12).

2.2.1 Theory

The kinetic model (Figure 2.2) used is based on the theory of the steady state operation of an amperometric enzyme electrode as derived by Albery and Bartlett (13).

In analysing the enzyme kinetics it is assumed that a one substrate one product enzyme, E_1, in this case creatinase, converts the first substrate creatine, P, to the intermediate product sarcosine, Q. This is oxidised to R by the second enzyme, sarcosine oxidase E_2, which is simultaneously reduced to E_2'. The overall reaction scheme is given by

$$P + E_1 \underset{}{\overset{K_1}{\rightleftharpoons}} E_1P \overset{K_2}{\rightleftharpoons} E_1Q \overset{K_3}{\rightleftharpoons} E_1 + Q$$

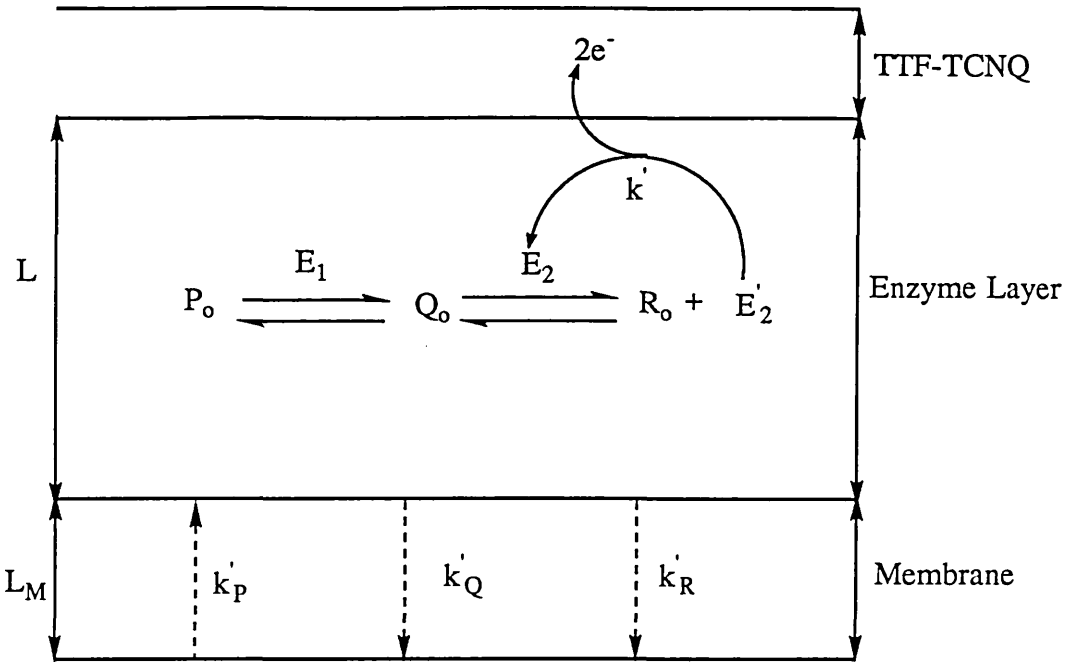

P = creatine

Q = sarcosine

R = formaldehyde + glycine

E_1 = creatinase

E_2 = sarcosine oxidase

Figure 2.2 Kinetic scheme for the creatine electrode

$$Q + E_2 \underset{\longleftarrow}{\xrightarrow{K_4}} E_2Q \underset{\longleftarrow}{\xrightarrow{K_5}} E_2R \underset{\longleftarrow}{\xrightarrow{K_6}} E_2' + R$$

$$E_2' \longrightarrow E_2$$

For each step it is possible to write an equilibrium constant of the form

$$K_n = k_n \backslash k_{-n} \qquad 2.1$$

and the overall equilibrium between a given reactant and product can be described by K_{TDn} where

$$K_{TD1} = K_1K_2K_3 \qquad 2.2$$

and $$K_{TD2} = K_4K_5K_6 \qquad 2.3$$

The transport of molecules through the membrane is governed by the mass transfer rate constants k_P', k_Q' and k_R' where

$$k_X' = D_X K_X / L_M \qquad 2.4$$

D_X = diffusion coefficient of P, Q or R

K_X = partition coefficient of P, Q or R

L_M = thickness of the membrane

The reduced enzyme E_2' is oxidised on the electrode at a heterogeneous rate constant k'. The subscripts ∞ and o are used to denote the concentrations of the various species outside and inside the membrane respectively. The electrolyte layer is assumed to have a thickness of the order of a few μm, thus there is no concentration polarisation.

In the steady state the flux j can be written as

$$j = k_P' (P_\infty - P_o) \qquad 2.5$$

$$= L (k_{+1} P_o . E_1 - k_{-1}E_1P) \qquad 2.6$$

$$= L (k_{+2} E_1P - k_{-2}E_1Q) \qquad 2.7$$

$$= L (k_{+3} E_1Q - k_{-3}Q_o.E_1) \qquad 2.8$$

Since $E_1^T = E_1 + E_1P + E_1Q$, then following substitution and rearrangement,

$$\frac{E_1^T}{j} = \frac{1}{L}\left\{\frac{K_M}{k_{cat}}\right\}_1 \left(P_o - Q\,(K_{TD1})^{-1}\right)\left[1 + Q(K_3)^{-1} + Q(K_2K_3)^{-1}\right] + (Lk_{cat1})^{-1} \qquad 2.9$$

where $$\left\{\frac{K_M}{k_{cat}}\right\}_1 = \frac{1}{k_{+1}} + \frac{1}{K_1k_{+2}} + \frac{1}{K_1K_2k_{+3}} \qquad 2.10$$

and $$\frac{1}{k_{cat1}} = \frac{1}{k_{+2}} + \frac{1}{K_2k_{+3}} + \frac{1}{k_{+3}} \qquad 2.11$$

Using a similar treatment for E_2

$$j = L\,(k_{+4}\,Q_o.E_2 - k_{-4}\,E_2Q) \qquad 2.12$$

$$= L\,(k_{+5}\,E_2Q - k_{-5}\,E_2R) \qquad 2.13$$

$$= L\,(k_{+6}\,E_2R - k_{-6}\,R_o.E_2') \qquad 2.14$$

$$= k'(E_2')^{1/2} \qquad 2.15$$

$$= k_R'(R_o - R_\infty) \qquad 2.16$$

As above, $E_2^T = E_2 + E_2Q + E_2R + E_2'$, then following rearrangement

$$\frac{E_2^T}{j} = \frac{1}{LQ}\left\{\frac{K_M}{k_{cat}}\right\}_2 + \frac{j}{K_{TD2}\,(k')^2}\left[R_\infty + j/(k_R')\right] + j\,/(k')^2$$

$$+ \frac{j}{K_6(k')^2}\left(1 + \frac{1}{K_5}\right)\left[R_\infty + j/(k'_R)\right] \qquad 2.17$$

with $$\left\{\frac{K_M}{k_{cat}}\right\}_2 = \frac{1}{k_{+4}} + \frac{1}{K_4k_{+5}} + \frac{1}{K_4K_5k_{+6}} \qquad 2.18$$

and $$\frac{1}{k_{cat2}} = \frac{1}{k_{+5}} + \frac{1}{K_5k_{+6}} + \frac{1}{k_{+6}} \qquad 2.19$$

Now assuming there is no product inhibition, then,

$$\frac{E_1^T + E_2^T}{j} = \frac{1}{L}\left\{\frac{K_M}{k_{cat}}\right\}_1 \left(P_o - Q_o\,(K_{TD1})^{-1}\right)\left[1 + Q_o(K_3)^{-1} + Q_o(K_2K_3)^{-1}\right]$$

$$+ (Lk_{cat})^{-1} + \frac{1}{LQ_o}\left\{\frac{K_M}{k_{cat}}\right\}_2 + (Lk_{cat2})^{-1} + \frac{j}{(k')^2} \qquad 2.20$$

However the probability that a molecule of Q on completion of reaction 1 will proceed into phase 2 of the reaction scheme is given by

$$\text{Prob}\ (\ Q \longrightarrow R\ ) = \frac{Lk_{+4}E_2}{Lk_{-3}E_1 + k'_Q + Lk_{+4}E_2} = k_f \qquad 2.21$$

where $0 \leq k_f \leq 1$

Therefore substitution of eqn. 2.21 into eqn. 2.20 gives

$$\frac{E_1^T + E_2^T}{j} = \frac{(k_{cat1})^{-1} + (k_{cat2})^{-1}}{L} + \frac{j}{(k')^2} + \qquad 2.22$$

$$\frac{1}{L}\left[\left\{\frac{K_M}{k_{cat}}\right\}_1\left(P_o(1 - k_f(K_{TD1})^{-1})\right)^{-1}\left(1 + \frac{k_f P_o}{K_3}\left(1 + \frac{1}{K_2}\right)\right) + \frac{1}{k_f P_o}\left\{\frac{K_M}{k_{cat}}\right\}_2\right]$$

If $E_\Sigma = E_1^T + E_2^T$ then following more manipulation and substitution for P_o,

$$\frac{E_\Sigma}{j} = \left[\frac{(k_{cat1})^{-1} + (k_{cat2})^{-1}}{L} + \frac{j}{(k')^2}\right]\left(1 - \frac{j}{k'_P P_\infty}\right)$$

$$+ \frac{1}{LP_\infty}\left[\frac{1}{(1 - k_f(K_{TD1})^{-1})}\left\{\frac{K_M}{k_{cat}}\right\}_1 + \frac{1}{k_f}\left\{\frac{K_M}{k_{cat}}\right\}_2\right]$$

$$+ \left(1 - \frac{j}{k'_P P_\infty}\right)\frac{k_f}{LK_3(1 - k_f(K_{TD1})^{-1})}\left\{\frac{K_M}{k_{cat}}\right\}_1\left(1 + \frac{1}{K_2}\right) + \frac{E_\Sigma}{k'_P P_\infty} \qquad 2.23$$

This can be rearranged to give a Hanes-type equation of the form

$$\frac{P_\infty}{j} = \frac{1}{k'_{ME}}\left[1 + \frac{P_\infty}{K_{ME}}\left(1 - \frac{j}{k'_P P_\infty}\right)\right] \qquad 2.24$$

where k'_{ME} is a second order electrochemical rate constant for the enzyme electrode at low substrate concentrations and is given by

$$\frac{1}{k'_{ME}} = \frac{1}{LE_{\Sigma}}\left[\frac{1}{(1 - k_f(K_{TD1})^{-1})}\left\{\frac{K_M}{k_{cat}}\right\}_1 + \frac{1}{k_f}\left\{\frac{K_M}{k_{cat}}\right\}_2\right] + \frac{1}{k'_P} \qquad 2.25$$

The constant K_{ME} is the electrochemical equivalent of the Michaelis constant used in homogeneous enzyme kinetics. At substrate concentrations smaller than K_{ME} the enzyme electrode exhibits unsaturated kinetics with the current being determined by k'_{ME} For concentrations greater than K_{ME} the electrode is described as being saturated, its response being governed by $k'_{cat;E}$ the electrochemical equivalent of k_{cat}.

$$K_{ME} = \frac{\frac{A}{L}\left(\left\{\frac{K_M}{k_{cat}}\right\}_1 + \frac{1}{k_f}\left\{\frac{K_M}{k_{cat}}\right\}_2\right) + \frac{E_{\Sigma}}{k'_P}}{\frac{B}{L} + \frac{Ak_f}{LK_3}\left\{\frac{K_M}{k_{cat}}\right\}_1\left(1 + \frac{1}{K_2}\right) + \frac{j}{(k')^2}} \qquad 2.26$$

where $A = \dfrac{1}{1 - k_f(K_{TD1})^{-1}}$ and $B = (k_{cat1})^{-1} + (k_{cat2})^{-1}$

The second term in the denominator is a measure of the forward driving force or irreversibility of the first enzymatic reaction. Hence if K_2, K_3 and by implication K_{TD1} are large, then K_{ME} reduces to

$$K_{ME} = \frac{\frac{1}{L}\left(\left\{\frac{K_M}{k_{cat}}\right\}_1 + \frac{1}{k_f}\left\{\frac{K_M}{k_{cat}}\right\}_2\right) + \frac{E_{\Sigma}}{k'_P}}{\frac{(k_{cat1})^{-1} + (k_{cat2})^{-1}}{L} + \frac{j}{(k')^2}} \qquad 2.27$$

Similarly, $1/k'_{ME}$ is simplified to

$$\frac{1}{k'_{ME}} = \frac{1}{LE_{\Sigma}}\left[\left\{\frac{K_M}{k_{cat}}\right\}_1 + \frac{1}{k_f}\left\{\frac{K_M}{k_{cat}}\right\}_2\right] + \frac{1}{k'_P} \qquad 2.28$$

These kinetics are equivalent to a reaction mechanism in which the breakdown of

the enzyme-substrate complex is sufficiently fast and energetically favourable so as to be essentially irreversible. Thus the reaction scheme will be of the form

$$E_1 + P \underset{\longleftarrow}{\xrightarrow{K_1}} E_1P \xrightarrow{k_2} E_1 + Q$$

$$E_2 + Q \underset{\longleftarrow}{\xrightarrow{K_3}} E_2Q \xrightarrow{k_4} E_2' + R$$

In this system

$$\text{Prob}\ (\ Q \longrightarrow R\ ) = \frac{Lk_{+3}E_2}{Lk_{+3}E_2 + k_Q'} = k_f \qquad 2.29$$

Equation 2.24 can be further simplified by considering the limiting forms at high and low substrate concentrations.

At low substrate concentrations since P_∞ tends to zero,

$$j = k_{ME}'P_\infty = \frac{P_\infty}{\frac{1}{LE_\Sigma}\left[\frac{1}{1 - k_f(K_{TD1})^{-1}}\left\{\frac{K_M}{k_{cat}}\right\}_1 + \frac{1}{k_f}\left\{\frac{K_M}{k_{cat}}\right\}_2\right] + \frac{1}{k_P'}} \qquad 2.30$$

Now the flux will depend on either the transport of substrate through the membrane or on the unsaturated enzyme kinetics. If mass transfer through the membrane is slow,

$$j = k_P'P_\infty \qquad 2.31$$

However if the converse is true and enzyme kinetics are rate limiting then since at low substrate $k_f \simeq 1$

$$j = \frac{LE_\Sigma P_\infty}{\left\{\frac{K_M}{k_{cat}}\right\}_1 + \left\{\frac{K_M}{k_{cat}}\right\}_2} \qquad 2.32$$

At high substrate concentrations as P_∞ becomes large the flux tends to a limiting value.

$$\frac{1}{j_{max}} = \frac{1}{LE_{\Sigma}k_{cat1}} + \frac{1}{LE_{\Sigma}k_{cat2}} + \frac{j}{(k')^2E_{\Sigma}} \qquad 2.33$$

$$+ \frac{k_f}{LK_3E_{\Sigma}(1 - k_f(K_{TD1})^{-1})}\left\{\frac{K_M}{k_{cat}}\right\}_1\left(1+ \frac{1}{K_2}\right)$$

However as substrate concentration increases k_f becomes smaller since as E_2 is saturated k'_Q becomes dominant and eqn. 2.33 reduces to

$$\frac{1}{j_{max}} = \frac{1}{LE_{\Sigma}k_{cat1}} + \frac{1}{LE_{\Sigma}k_{cat2}} + \frac{j}{(k')^2E_{\Sigma}} = \frac{1}{E_{\Sigma}k'_{cat.E}} \qquad 2.34$$

Returning to eqn. 2.24 and introducing a new parameter ρ where

$$\rho = \frac{[j/P_{\infty}]}{k'_{ME}} \qquad 2.35$$

substitution of this into eqn. 2.24 gives

$$y = \frac{\rho^{-1}-1}{P_{\infty}} = \frac{1}{K_{ME}}\left[1 - \frac{\rho k'_{ME}}{k'_P}\right] \qquad 2.36$$

From a plot of y against ρ, the intercept at $\rho=0$ gives k'_{ME} whilst the intercept at $y=0$ is a measure of the relative contributions of the transport and unsaturated enzyme kinetic terms to the heterogeneous rate constant, k'_{ME}.

2.2.2 Results

The response of the electrode to aliquots of creatine is shown in Figure 2.3. In the first experiment the ratio of creatinase to sarcosine oxidase was 295:41 whilst in the second it was increased to 1000:6.6. The most striking feature in these plots is the sigmoidal behaviour which is clearly seen in Figure 2.3. As the concentration of creatinase relative to sarcosine oxidase is increased this is reduced and the response at low substrate concentration tends towards linearity.

Two factors that might reduce the observed current are the

Figure 2.3 The effect of varying the enzyme concentrations on the electrode response to creatine.

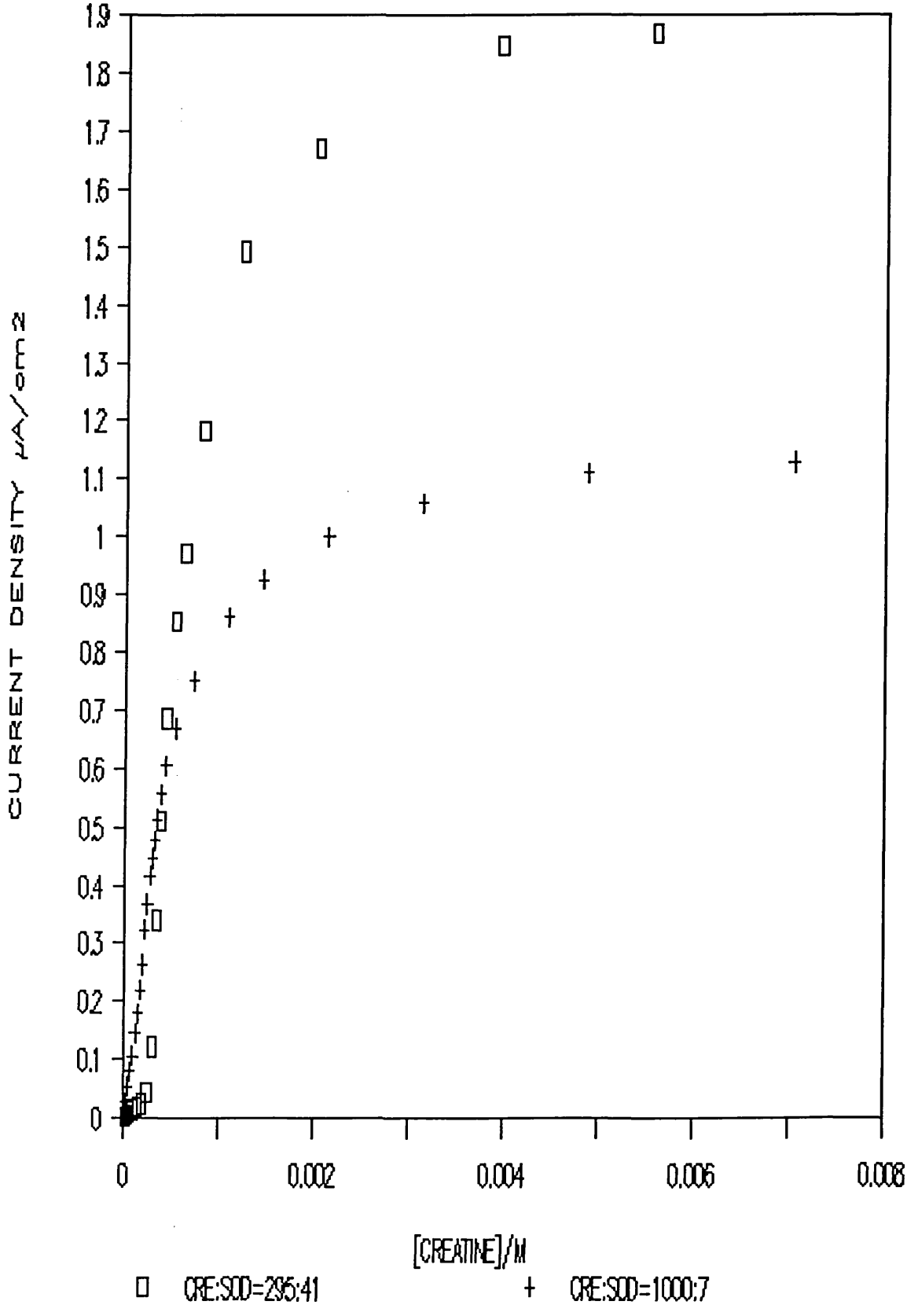

oxygen effect (5) and product inhibition by formaldehyde (14). However neither of these can satisfactorily explain the experimental results. Firstly, an explanation based on the oxygen effect, in which dissolved oxygen competes with the electrode to reoxidise reduced enzyme, can be ruled out since if this were the cause of the anomalous behaviour it would have a more significant effect at lower sarcosine oxidase concentrations whereas the converse is true. Secondly, although formaldehyde inhibits the action of sarcosine oxidase, its effect is only significant at high concentrations.

The sigmoidal nature of the electrode response at low creatine concentrations can be accounted for if the sarcosine oxidase preparation is assumed to contain an impurity, I, which binds to the creatinase rendering it inactive (15). Consider the following equilibrium

$$EI \rightleftharpoons E \rightleftharpoons EP \rightleftharpoons EQ \rightleftharpoons E + Q$$

At low substrate concentrations the equilibrium lies to the left with creatinase being predominantly in the EI form. However as the substrate concentration is increased the equilibrium is shifted to the right as more creatine is now avalable and displaces the inhibitor.

Hoeffken and coworkers (16) determined the crystal structure of creatinase and have studied the nature of the binding site using the competitive inhibitor carbamoyl sarcosine which is a close analogue of the substrate creatine. The preparation of sarcosine oxidase contains EDTA and potassium gluconate. The former is known not to inhibit creatinase (12). However gluconate might have an adverse effect on the enzyme since its carboxylate and hydroxyl groups could enable it to bind at the active site (Figure 2.4).

In order to examine whether gluconate acted as an inhibitor a typical calibration plot was compared to a run in the presence of 8mM gluconate. From the results in Figure 2.5 it is apparent that lower currents are obtained in the presence of gluconate and the system tends to saturate earlier.

Figure 2.4 Schematic representation of the carbamoyl sarcosine binding geometry

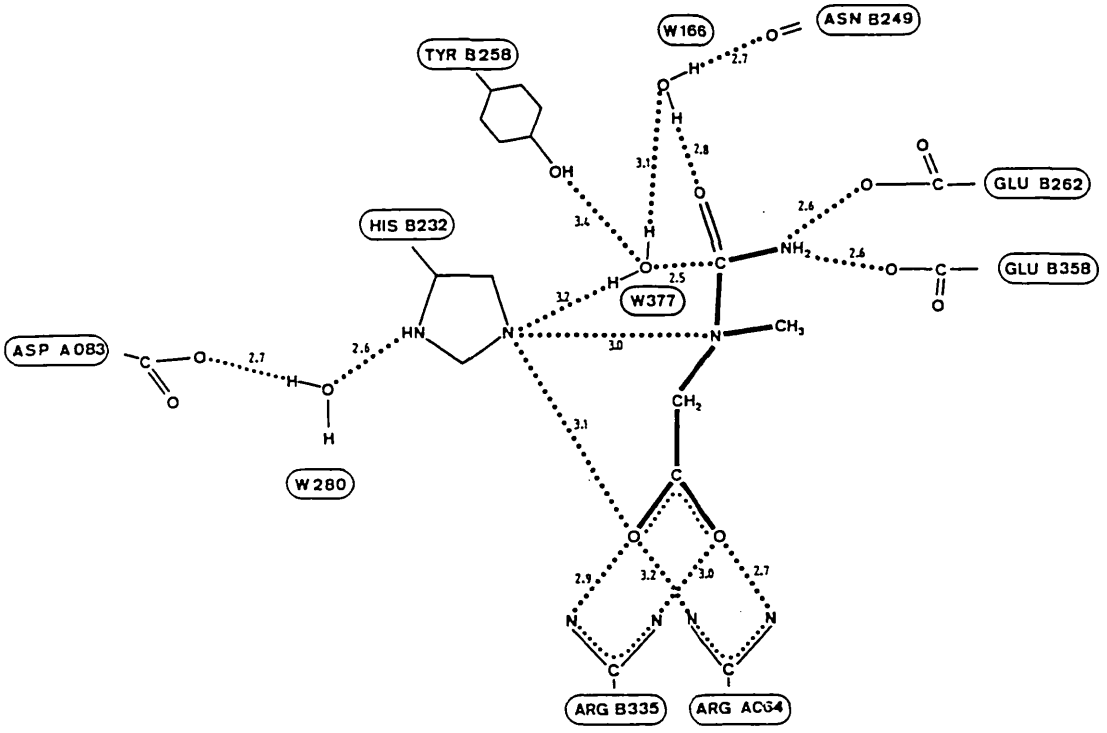

Figure 2.5 Inhibitory effect of gluconate on the electrode response to creatine. Creatinase : sarcosine oxidase = 1000 : 7 U/ml.

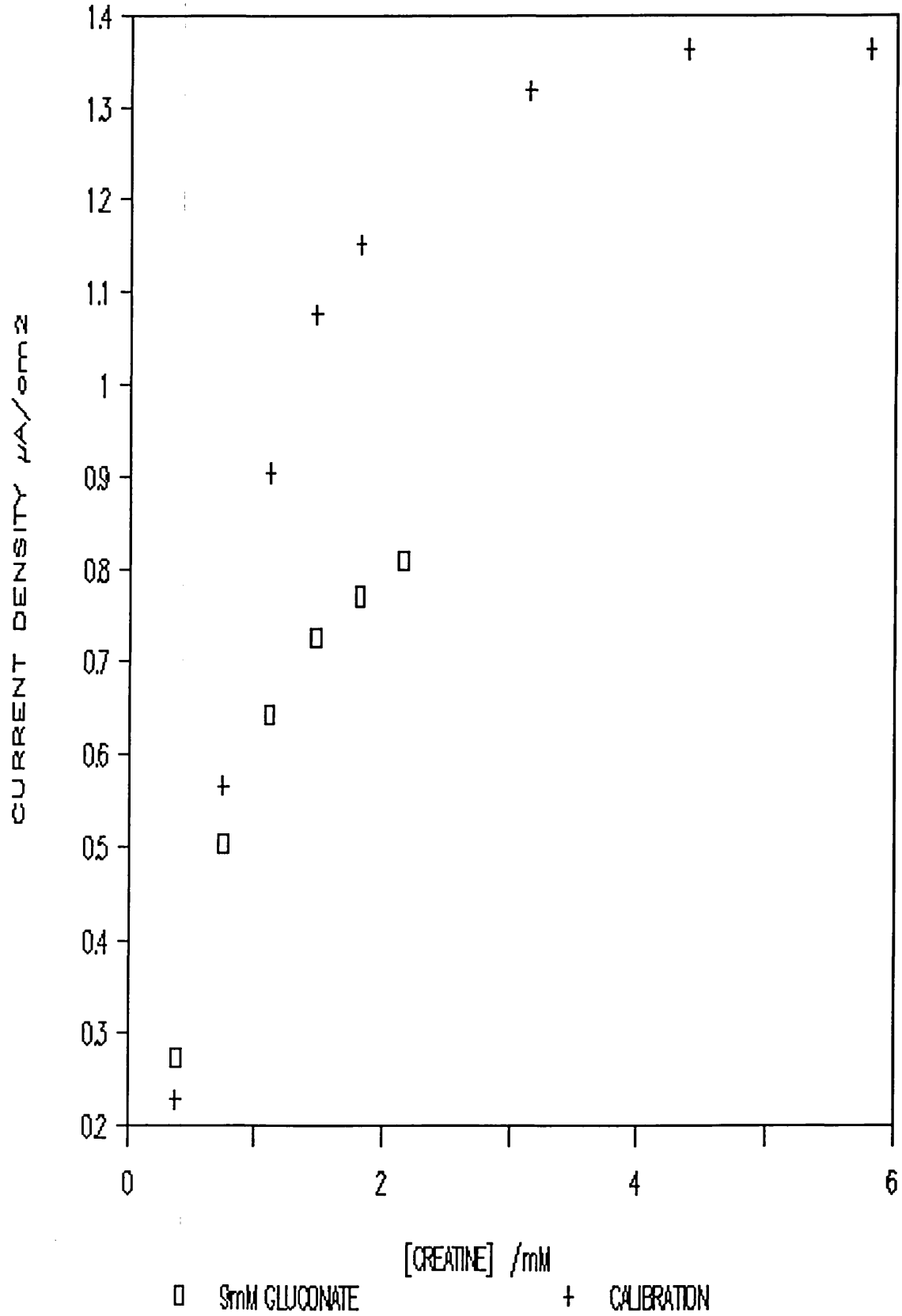

Instead of showing a characteristic plateau at low creatine concentrations, the Hanes plot (Figure 2.6) initially decreases then increases again. This indicates that the electrode response is not governed solely by transport of substrate through the membrane. This result is not in disagreement with the hypothesis that enzyme inhibition is operating at low substrate levels. From the intercept at $P_{\infty}=0$ it is possible to determine the heterogeneous electrochemical rate constant, k'_{ME}, for the unsaturated electrode. This is found to be $1.1x10^{-5}$cm s^{-1}. The mass transfer rate constant, k'_{P}, can be calculated from the intercept at y=0 from a plot of y against ρ (Figure 2.7). Since the intercept is approximately 1 this implies that mass transport is the dominant rate limiting factor at low substrate concentrations. The results are shown in Table 2.2. In order to use this system as a sensor for determining higher levels of creatine it would be advisable to have a higher concentration of better purity enzyme behind the membrane to ensure transport control.

An attempt was made to use the sensor to determine creatine levels in human urine. Although ascorbate was prevented from interfering with the electrode by adding ascorbate oxidase to the bulk solution outside the membrane, enough electroactive species were still present so as to mask the response due to creatine. Thus urine must be purified chromatographically using standard ion exchange columns before it can be analysed using this sensor (7).

Figure 2.6 The Hanes plot for the creatine electrode using data in Figure 2.3. Creatinase : sarcosine oxidase = 1000 : 7 U/ml

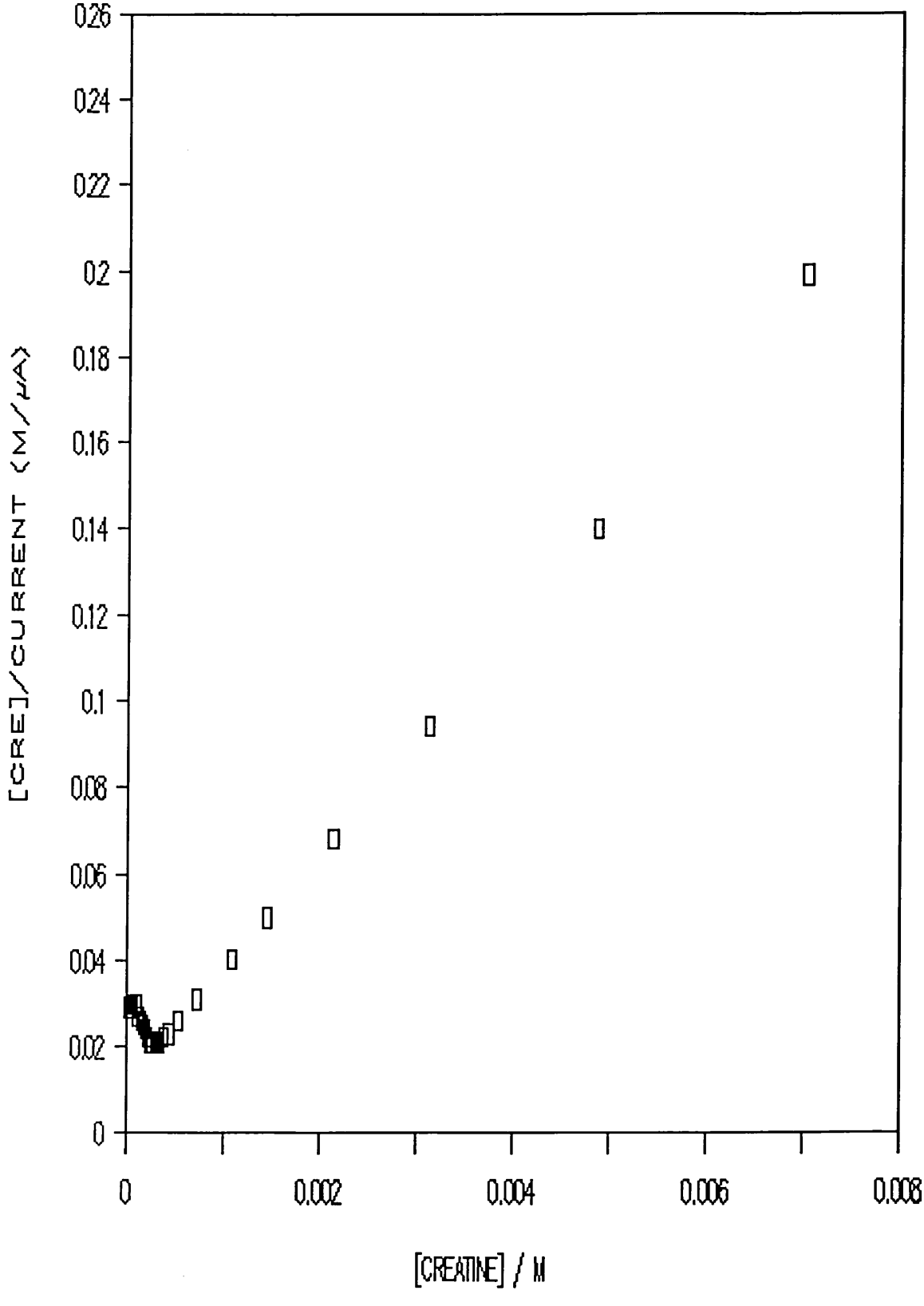

Figure 2.7 The rho plot for the creatine electrode using the data in Figure 2.3. Creatinase : sarcosine oxidase=1000 : 7 U/ml

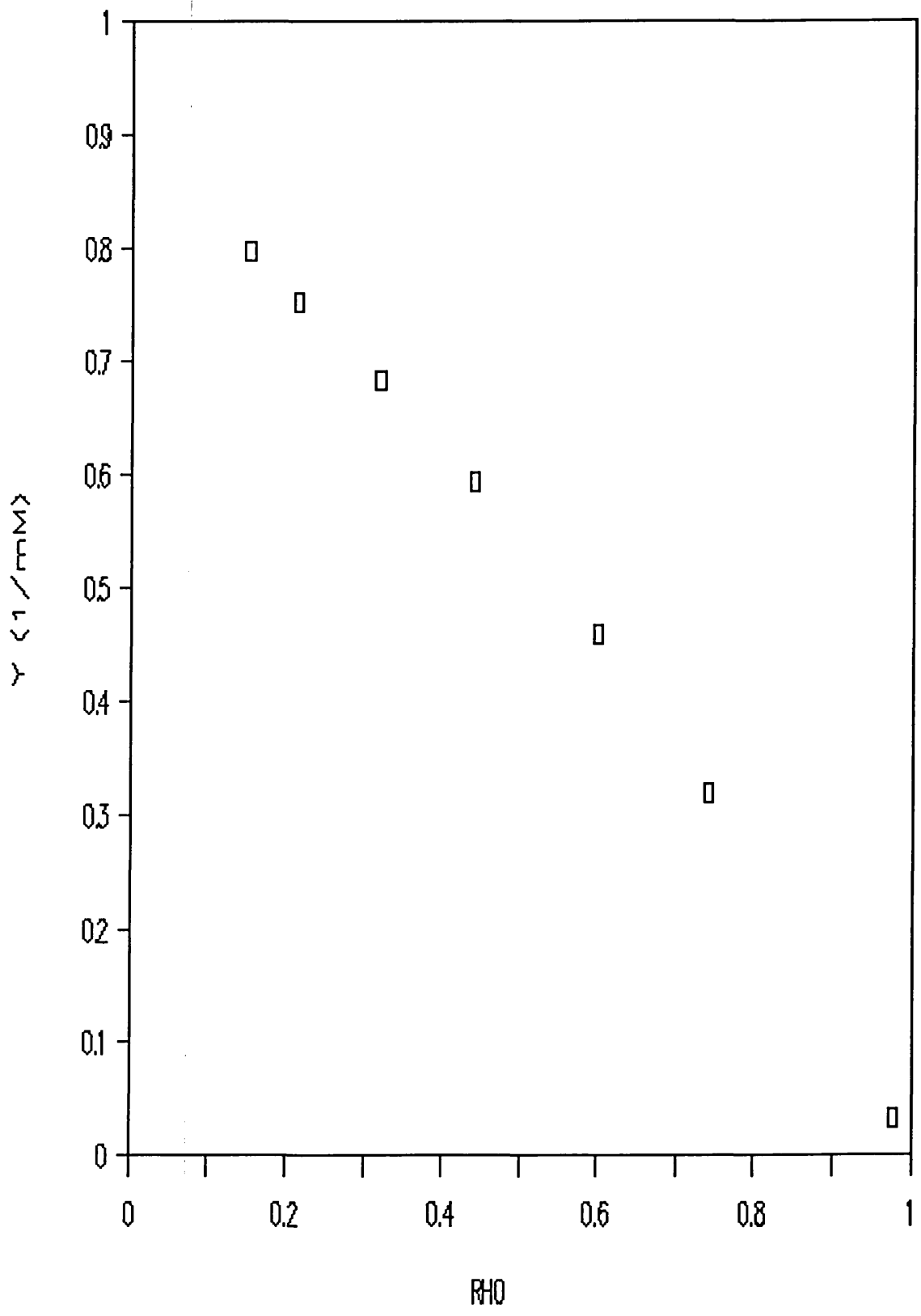

TABLE 2.2

Kinetic parameters for the creatine sensor

Heterogeneous Rate Constant, k'_{ME}	1.1×10^{-5} cm s^{-1}
Intercept at y=0 in the ρ-plot	$1 \Rightarrow k'_{ME} = k'_S$
Intercept at $\rho = 0$ in the ρ−plot, (mM^{-1})	$0.95 \Rightarrow K_{ME} = 1.1$ mM

2.3 XANTHINE / HYPOXANTHINE ELECTRODE

As previously described in §1.2 xanthine oxidase plays an important role in purine catabolism. The commonest purines in the body are adenine and guanine and these undergo initial deamination to produce hypoxanthine and xanthine respectively. Then hypoxanthine (via xanthine) and xanthine itself are oxidised to produce uric acid see Figure 2.8 (17). Excessive xanthine oxidase activity results in overproduction of urate which because of its relative insolublity can precipitate out in the kidneys leading to the formation of kidney stones. It can also crystallize out in cartilaginous tissue in which case it causes gout. The aim of this section was to use a kinetic model to explain and compare the reponse to hypoxanthine and xanthine (1,2).

2.3.1 Theory

2.3.1.1 Response to Xanthine

To create a kinetic model (Figure 2.9) for the system it is convenient to first analyse the electrode response to the second substrate xanthine. Using a simple one-intermediate equilibrium model

$$X + E \underset{k_{-1}}{\overset{k_{+1}}{\rightleftharpoons}} EX \underset{k_{-2}}{\overset{k_{+2}}{\rightleftharpoons}} E' + U$$

$$E' \xrightarrow{k'} E$$

the flux, j, can be written as

$$j = k'_X(X_\infty - X_o) \tag{2.37}$$

$$= L\,(k_{+1}X_o.E - k_{-1}EX) \tag{2.38}$$

$$= L\,(k_{+2}EX - k_{-2}U_o.E') \tag{2.39}$$

$$= k'(E')^{1/2} \tag{2.40}$$

$$= k'_U(U_o - U_\infty) \tag{2.41}$$

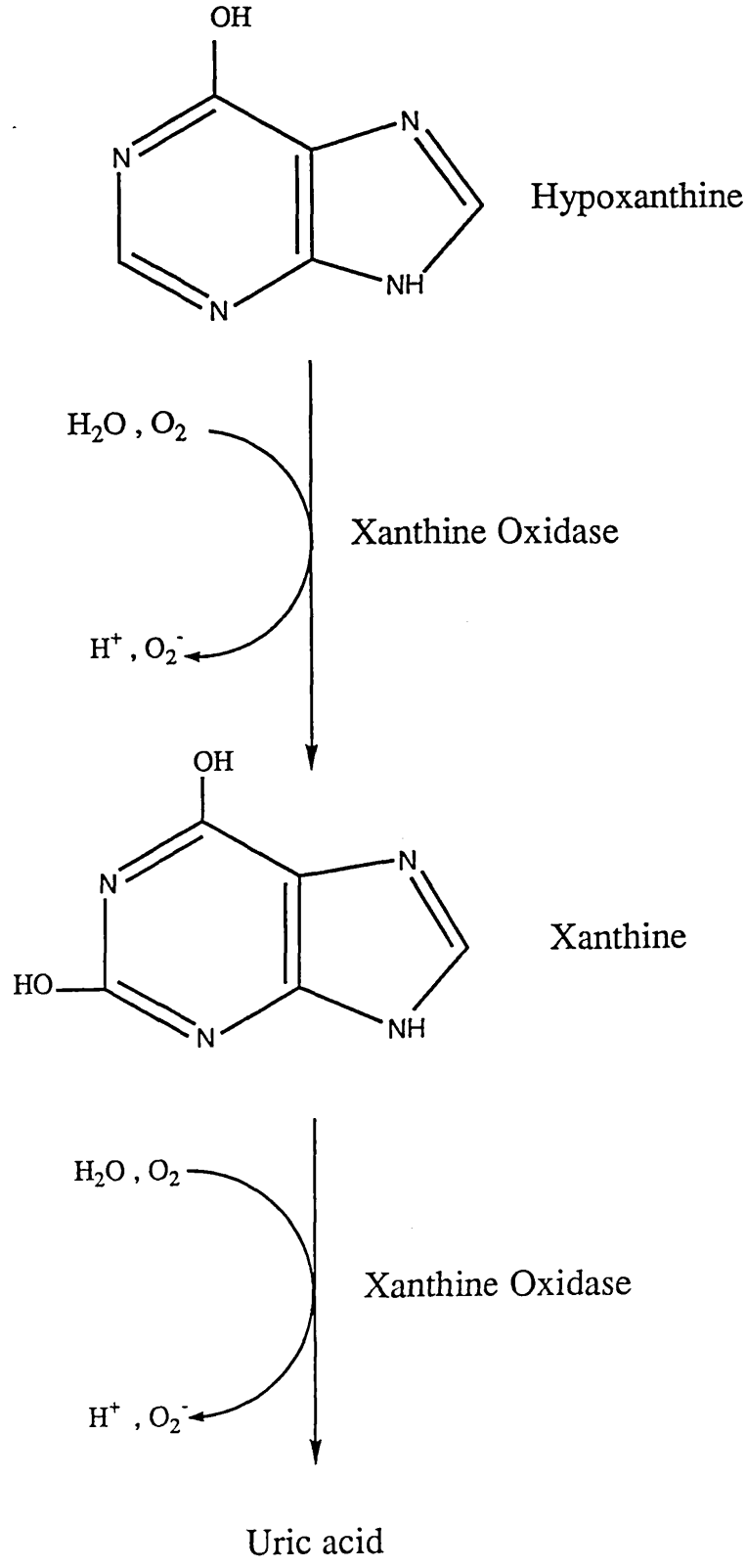

Figure 2.8 The final stage of purine catabolism involves hypoxanthine and xanthine intermediates

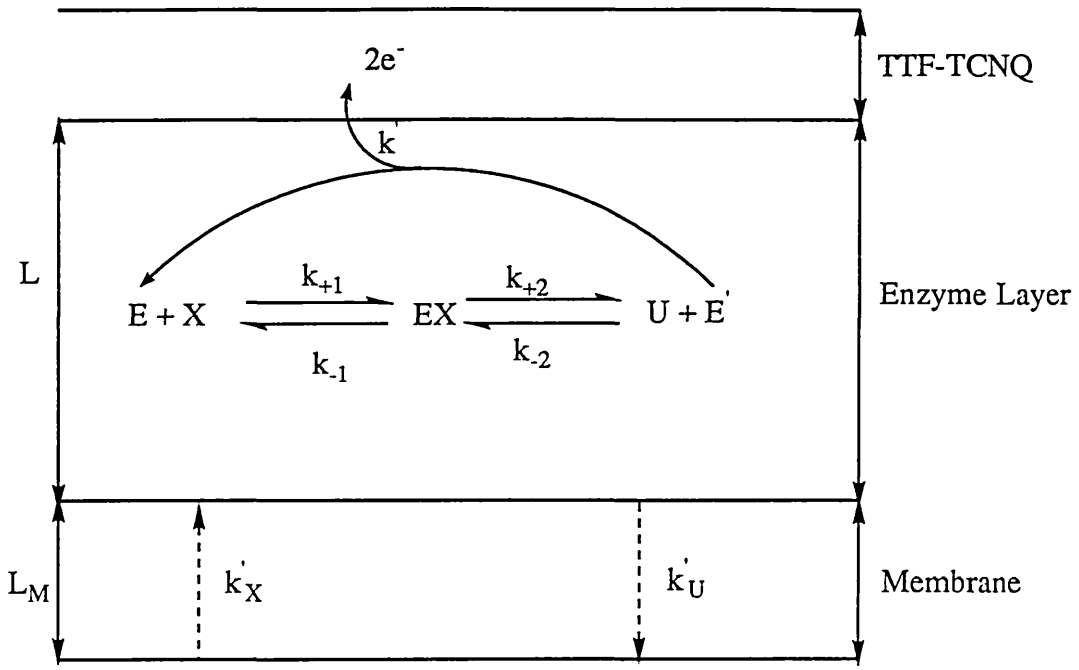

X = xanthine

U = urate

E = xanthine oxidase

Figure 2.9 Kinetic scheme for the xanthine electrode

and since $E_\Sigma = E + EX + E'$ then following substitution and rearrangement

$$\frac{E_\Sigma}{j} = \frac{1}{LX_\infty}\left[\left\{\frac{K_M}{k_{cat}}\right\} + \frac{j}{(k')^2K_{TD}}\left(U_\infty + \frac{j}{k'_U}\right)\right] + \frac{E_\Sigma}{k'_X X_\infty}$$

$$+ \left[\frac{1}{Lk_{cat}} + \frac{j}{(k')^2} + \frac{j}{(k')^2K_2}\left(U_\infty + \frac{j}{k'_U}\right)\right]\left(1 - \frac{j}{k'_X X_\infty}\right) \qquad 2.42$$

If there is no product inhibition then

$$\frac{X_\infty}{j} = \frac{1}{k'_{ME}} + X_\infty\left[\frac{1}{Lk_{cat}E_\Sigma} + \frac{j}{(k')^2E_\Sigma}\right]\left(1 - \frac{j}{k'_X X_\infty}\right) \qquad 2.43$$

with $$\frac{1}{k'_{ME}} = \frac{K_M}{Lk_{cat}E_\Sigma} + \frac{1}{k'_X} \qquad 2.44$$

As in §2.2.1, the response at low substrate is governed by the rate constant k'_{ME}, whereas, at high substrate concentrations it depends on either electrode or enzyme kinetics.

If the enzyme-substrate complex EX is the predominant enzyme form ie. $EX \gg E'$, implying that $1/Lk_{cat} \gg j/(k')^2$ then the saturated enzyme kinetics are rate-limiting,

$$\frac{X_\infty}{j} = \frac{1}{k'_{ME}} + \frac{X_\infty}{Lk_{cat}E_\Sigma}\left(1 - \frac{j}{k'_X X_\infty}\right) \qquad 2.45$$

Rewriting this in terms of the kinetic parameter ρ where

$$\rho = \frac{[j/X_\infty]}{k'_{ME}} \qquad 2.46$$

and substituting eqn. 2.46 into eqn. 2.45 gives

$$y = \frac{\rho^{-1} - 1}{X_\infty} = \frac{k'_{ME}}{Lk_{cat}E_\Sigma}\left[1 - \frac{\rho k'_{ME}}{k'_X}\right] \qquad 2.47$$

From a plot of y against ρ the intercept at $\rho=0$ gives $k'_{ME}/Lk_{cat}E_\Sigma$ whilst the intercept at $y= 0$ compares k'_{ME} and k'_X.

However if $E' \gg EX$, implying $j/(k')^2 \gg 1/Lk_{cat}$, then the response is governed by the electrode kinetics and

$$\frac{X_\infty}{j} = \frac{1}{k'_{ME}} + \frac{X_\infty j}{(k')^2 E_\Sigma}\left(1 - \frac{j}{k'_X X_\infty}\right) \qquad 2.48$$

Now,

$$y' = \frac{\rho^{-1} - 1}{jX_\infty} = \frac{k'_{ME}}{(k')^2 E_\Sigma}\left(1 - \frac{\rho k'_{ME}}{k'_X}\right) \qquad 2.49$$

Now the intercept at $\rho = 0$ gives $k'_{ME}/(k')^2 E_\Sigma$. The intercept at $y' = 0$ remains unchanged.

2.3.1.2 Response to Hypoxanthine

To simplify the treatment it is convenient to consider the behaviour of the electrode at the extremes of (i) low and (ii) high substrate concentration separately.

2.3.1.2.1 Unsaturated Conditions

Under these conditons the enzyme is predominantly in the free or E form. The factors governing the kinetics of the system in this model are the unsaturated enzyme kinetics, transport of hypoxanthine from the bulk solution through the membrane and loss of the primary reaction product, xanthine, through the membrane before it can be turned over by the enzyme. The kinetic scheme for this system is shown in Figure 2.10.

The probability that a molecule of xanthine reacts with the enzyme rather than diffusing out through the membrane is given by

$$\Pi_X = \frac{L\left\{\frac{K_M}{k_{cat}}\right\}_X E_\Sigma}{L\left\{\frac{K_M}{k_{cat}}\right\}_X E_\Sigma + k'_X} = \frac{k'_{ME,X}}{k'_X} \qquad 2.50$$

Therefore the overall flux is given by

$$j = (1 + \Pi_X)\, L\left\{\frac{K_M}{k_{cat}}\right\}_H E_\Sigma H_o \qquad 2.51$$

Now if the concentration of hypoxanthine in the bulk is H_∞ then,

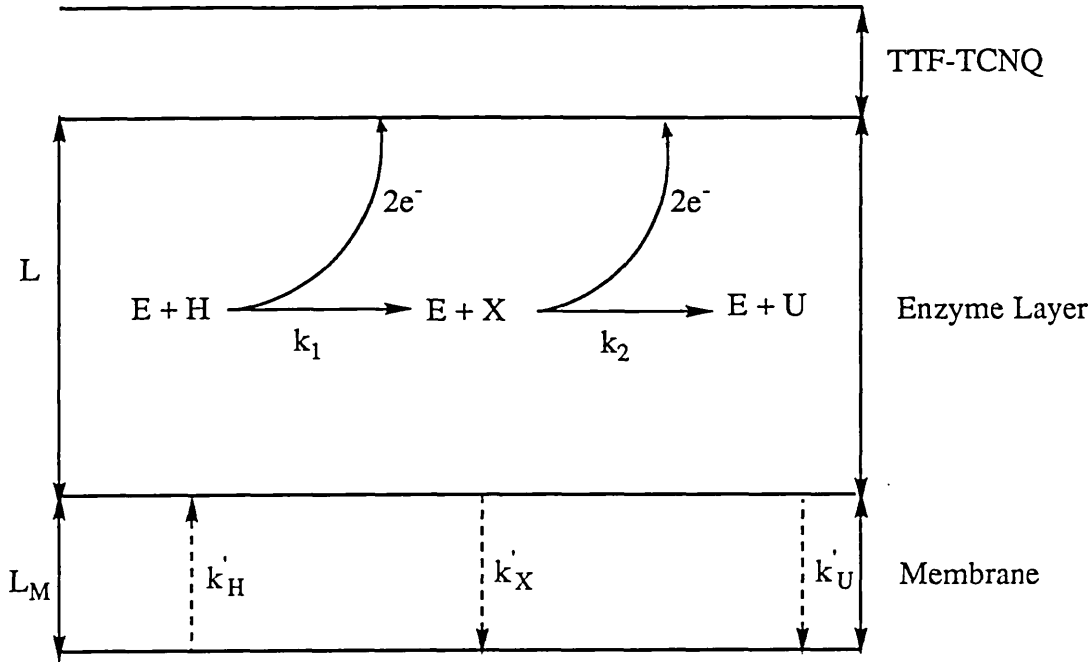

H = hypoxanthine

X = xanthine

U = urate

E = xanthine oxidase

Figure 2.10 Kinetic scheme for the hypoxanthine system under unsaturated conditions

$$L\left\{\frac{K_M}{k_{cat}}\right\}E_\Sigma H_o = k'_H(H_\infty - H_o) \qquad 2.52$$

Thus eqn. 2.51 becomes

$$j = \frac{(1+ \Pi_X)\left\{\frac{K_M}{k_{cat}}\right\}_H LE_\Sigma k'_H H_\infty}{L\left\{\frac{K_M}{k_{cat}}\right\}_H E_\Sigma + k'_H} \qquad 2.53$$

If $k_1 = \left\{\frac{K_M}{k_{cat}}\right\}_H E_\Sigma$ and $k_2 = \left\{\frac{K_M}{k_{cat}}\right\}_X E_\Sigma$ then,

$$\frac{1}{1+\Pi_X}\left(\frac{1}{k'_H} + \frac{1}{Lk_1} \right) = \frac{H_\infty}{j} = \frac{1}{(1+\Pi_X)k'_{ME,H}} \qquad 2.54$$

2.3.1.2.2 Saturated Conditions

Under these conditions since the free enzyme concentration, E, will be negligible the enzyme will be present either in its reduced form E' or in a complex with either hypoxanthine or xanthine, EH or EX respectively. At high substrate concentrations the rate of loss of xanthine through the membrane to the bulk becomes more significant. The kinetic scheme representing this case is shown in Figure 2.11.

Now if the overall flux, j, is given by

$$j = j_H + j_X \qquad 2.55$$

j_H = flux due to hypoxanthine

j_X = flux due to xanthine

then since the system is following saturated kinetics, we have the following

$$E_\Sigma = EH + EX + E' \qquad E \simeq 0$$

$$E_\Sigma = \frac{j_H}{Lk_{cat,H}} + \frac{j_X}{Lk_{cat,X}} + \frac{j}{(k')^2} \qquad 2.56$$

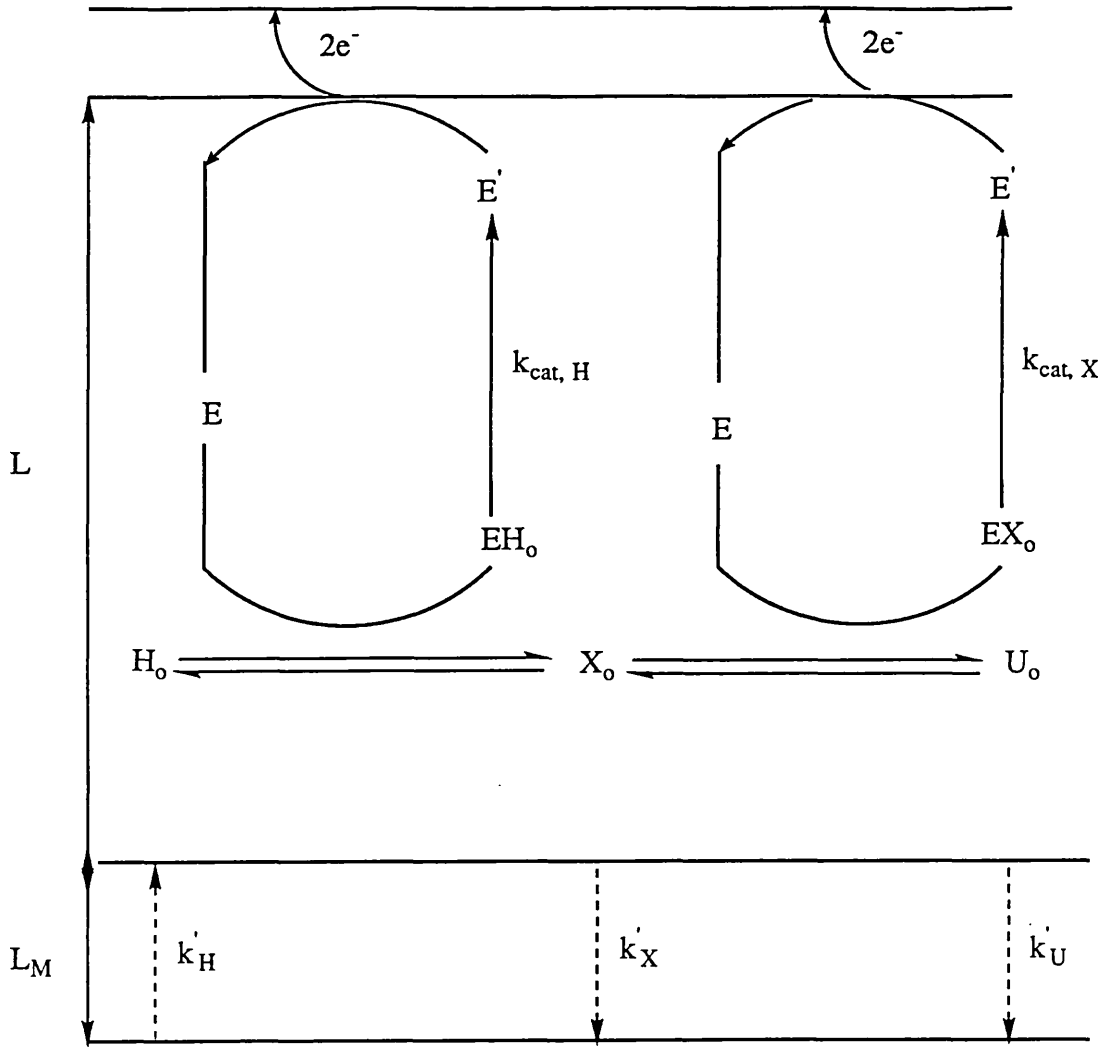

E = xanthine oxidase

H = hypoxanthine

X = xanthine

U = urate

Figure 2.11 Kinetic scheme for the hypoxanthine system under saturated conditions

As xanthine is a reaction product of the oxidation of the primary substrate, hypoxanthine, $j_H > j_X$. If a new parameter Λ is introduced where,

$$\Lambda = \frac{j_H}{j} \qquad 2.57$$

Λ is a measure of whether the enzyme kinetics are sufficiently fast so as to be capable of oxidising xanthine before it can escape through the membrane to the bulk. Therefore, as $j_H \rightarrow j$ the greater the likelihood that a molecule of xanthine will escape before it can be turned over by the enzyme.

Substituting for Λ and remembering that $j_X = j - j_H$, eqn. 2.56 becomes

$$\frac{E_\Sigma}{j} = \Lambda \left\{ \frac{1}{Lk_{cat,H}} - \frac{1}{Lk_{cat,X}} \right\} + \frac{1}{Lk_{cat,X}} + \frac{j}{(k')^2} \qquad 2.58$$

If the enzyme kinetics are fast then $j_H \simeq j_X$ and $\Lambda \simeq 1/2$ whereas if transport through the membrane is fast then $j_H \simeq j$ and $\Lambda \simeq 1$.

2.3.2 Results

The response of the electrode to xanthine is shown in Figure 2.12. As outlined in the above theory the intercept at $X_\infty = 0$ in the Hanes plot (Figure 2.13) enables the electrochemical rate constant k'_{ME} to be found. This has a value of 4.5×10^{-5}cm s^{-1}. The normal rho plot (Figure 2.14) is a straight line with a negative gradient indicating that at high xanthine concentrations the electrode response is governed by the saturated kinetics of the enzyme. The intercept at y=0, $k'_X/k'_{ME,X}$, shows that both enzyme kinetics and transport of substrate across the membrane play a role in determining the electrode response at low xanthine concentrations. It also enables Π_X to be calculated. From Π_X one can determine a value for the rate constant, Lk_1. The modified rho plot is essentially linear with a slight positive gradient (Figure 2.15), thus showing that electrode kinetics do not of themselves control the response at high xanthine concentrations. If the converse was true then a straight line with a negative gradient would be observed. The results are

Figure 2.12 Electrode response to xanthine. 4.5 U/ml xanthine oxidase

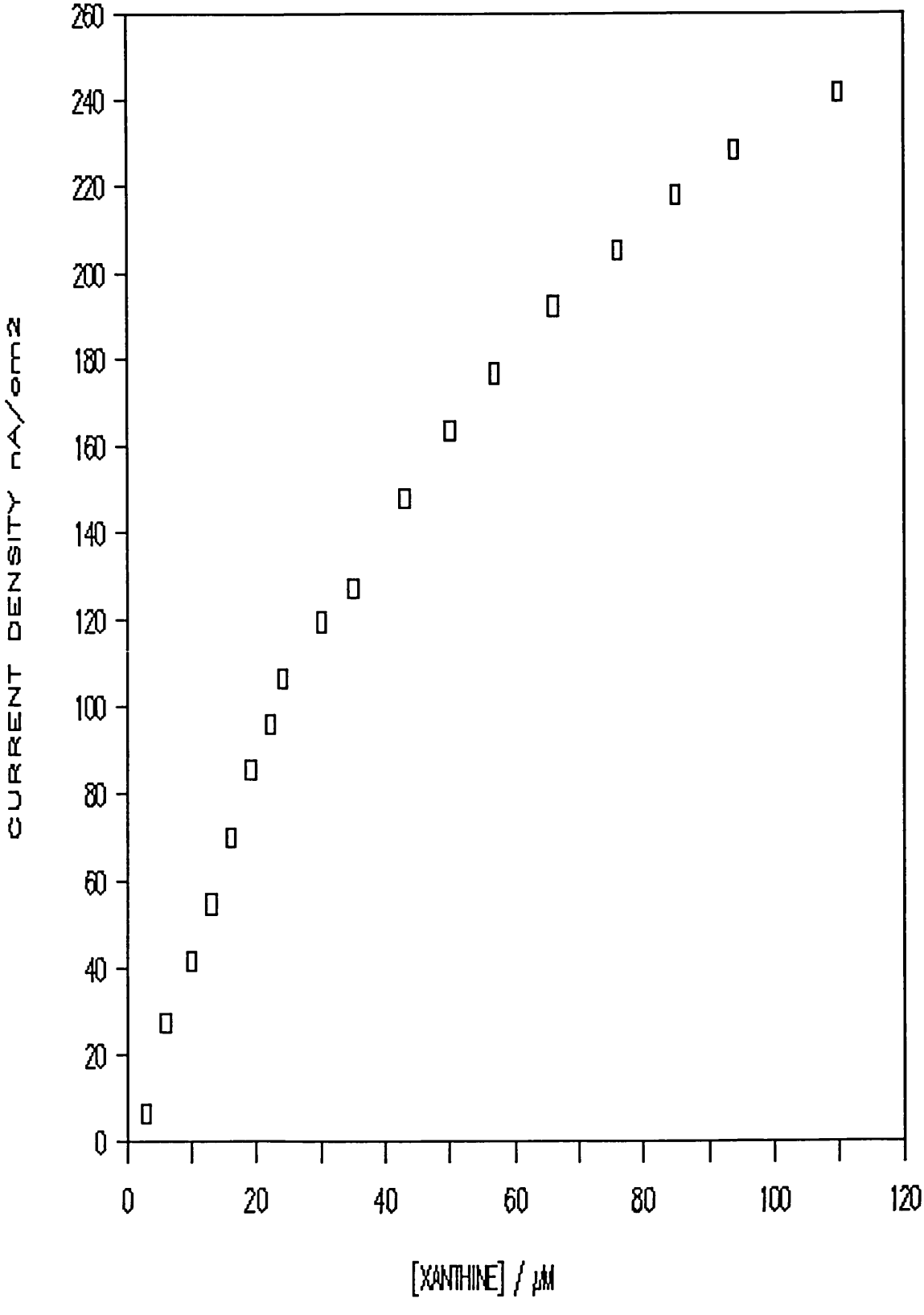

Figure 2.13 The Hanes plot for the xanthine electrode using the data in Figure 2.12

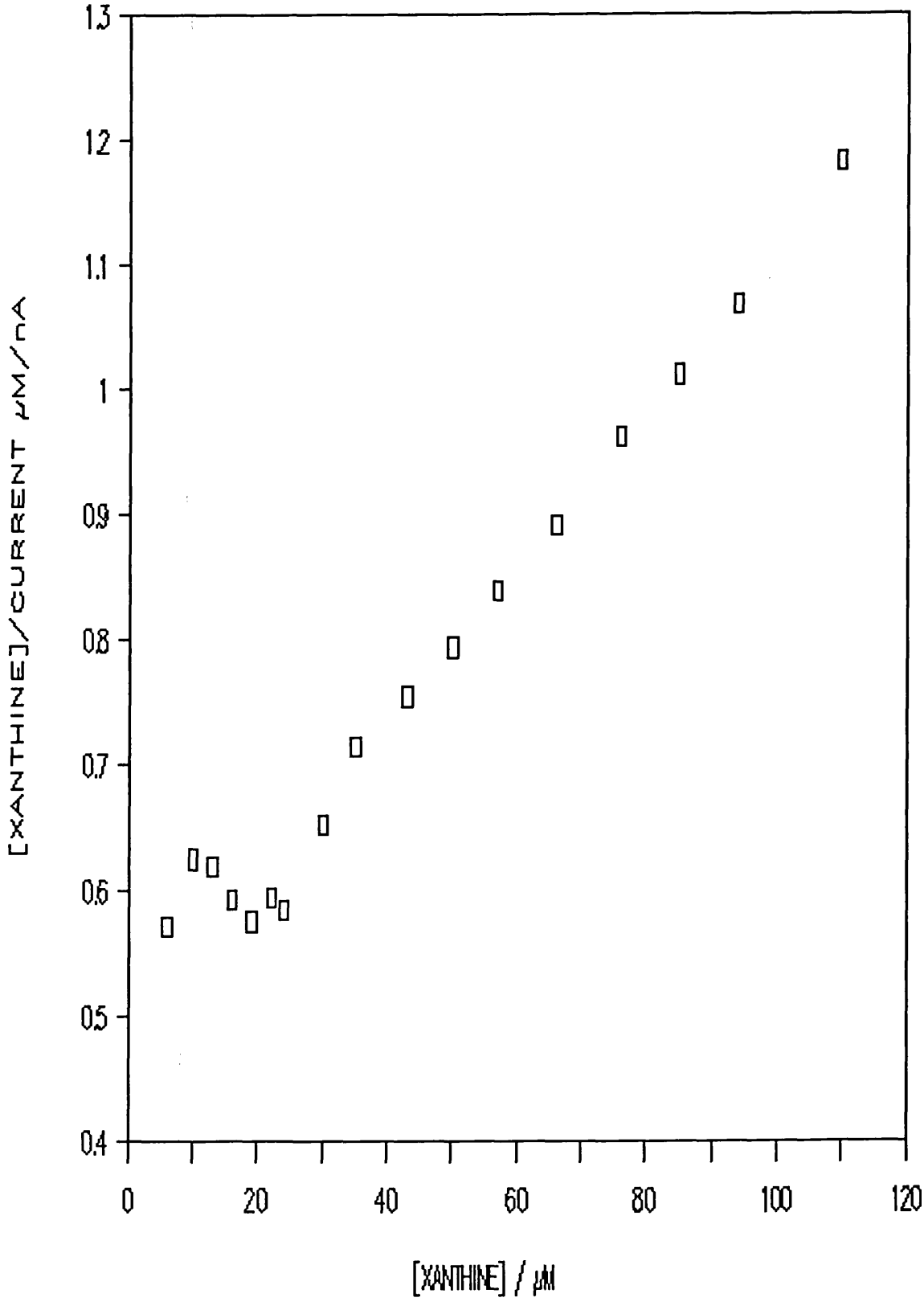

Figure 2.14 The rho plot for the xanthine electrode using data from Figure 2.12

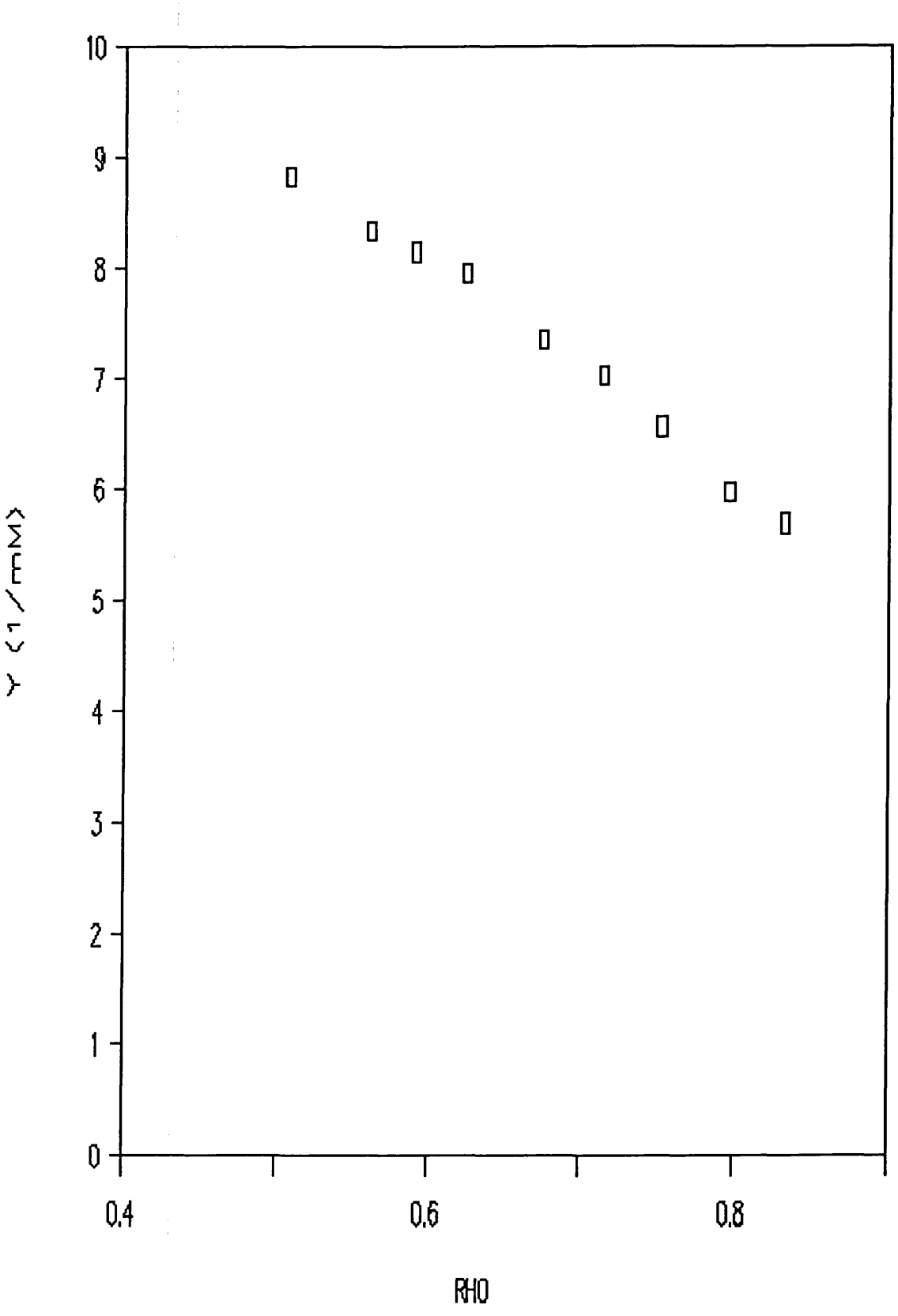

Figure 2.15 The modified rho plot for the xanthine electrode using the data from Figure 2.12

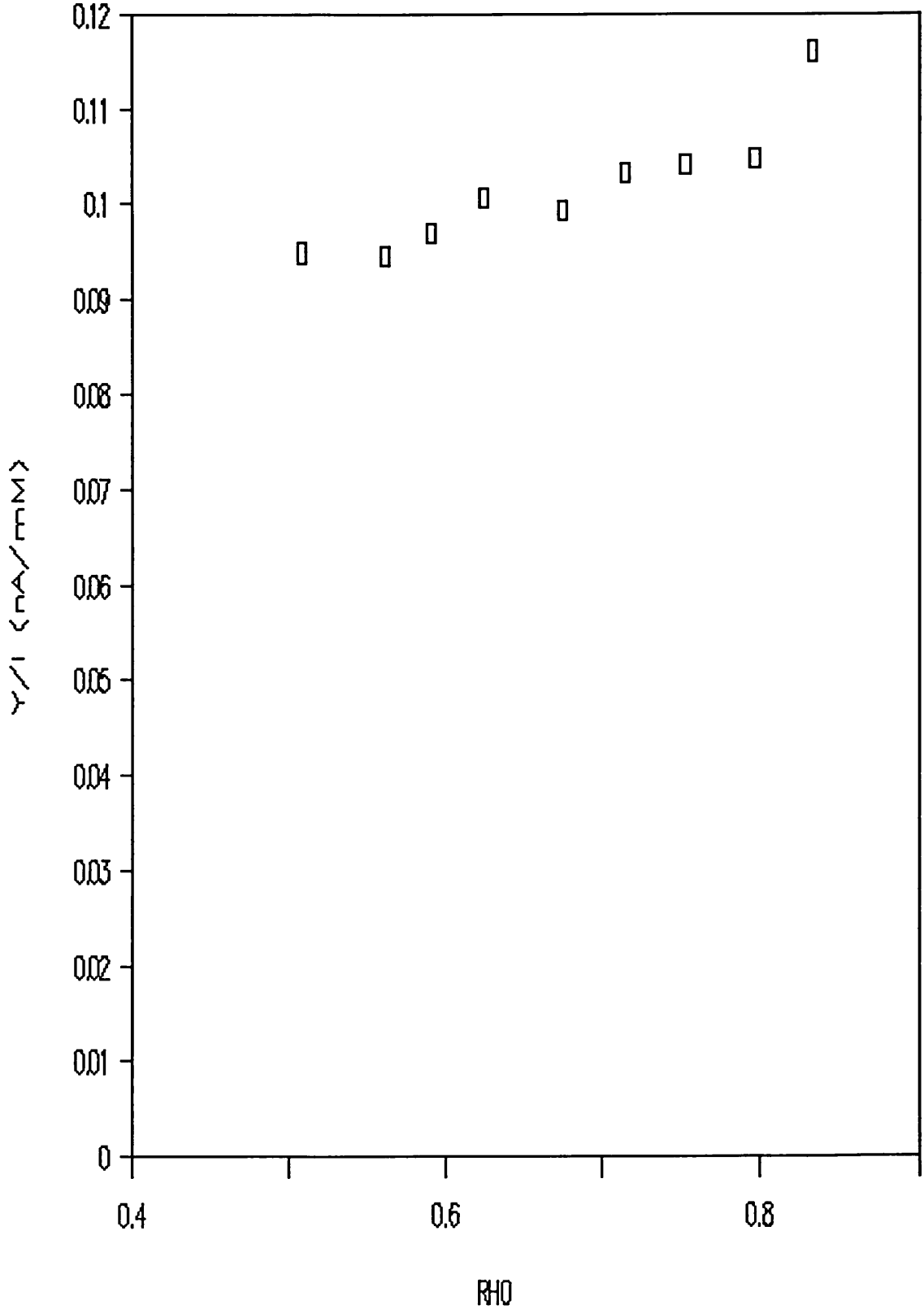

presented in Table 2.3.

Krenitsky (18) has shown that xanthine is turned over more rapidly by the enzyme than hypoxanthine, the relative rates being 170:130, ie. $Lk_1 = 0.76\ Lk_2$. Hence the rate constant for reaction between hypoxanthine and xanthine oxidase can be found. Figure 2.16 shows a plot of the electrode response to successive aliquots of hypoxanthine. Since $k_{ME,H}$ is known from the Hanes plot (Figure 2.17), k_H' can be evaluated and is found to be 3.6×10^{-4}cm s^{-1}. This is almost six times as large as the mass transfer rate constant for xanthine, k_X'. Since the only structural difference between the two molecules is a single hydroxyl group it is unlikely this would have such a marked effect. On analysing possible errors in the experiment, assuming an error factor of 20 %, then errors in evaluating the mass transfer rate constants can introduce a factor of 3 into the calculation. By comparing the respective values of the unsaturated enzymatic and mass transfer rate constants it is apparent that the response at low substrate concentrations, for both xanthine and hypoxanthine, is determined by a combination of these processes and cannot be attributed solely to either enzyme kinetics or to transport across the membrane alone.

Figure 2.16 Electrode response to hypoxanthine. 4.5 U/ml xanthine oxidase

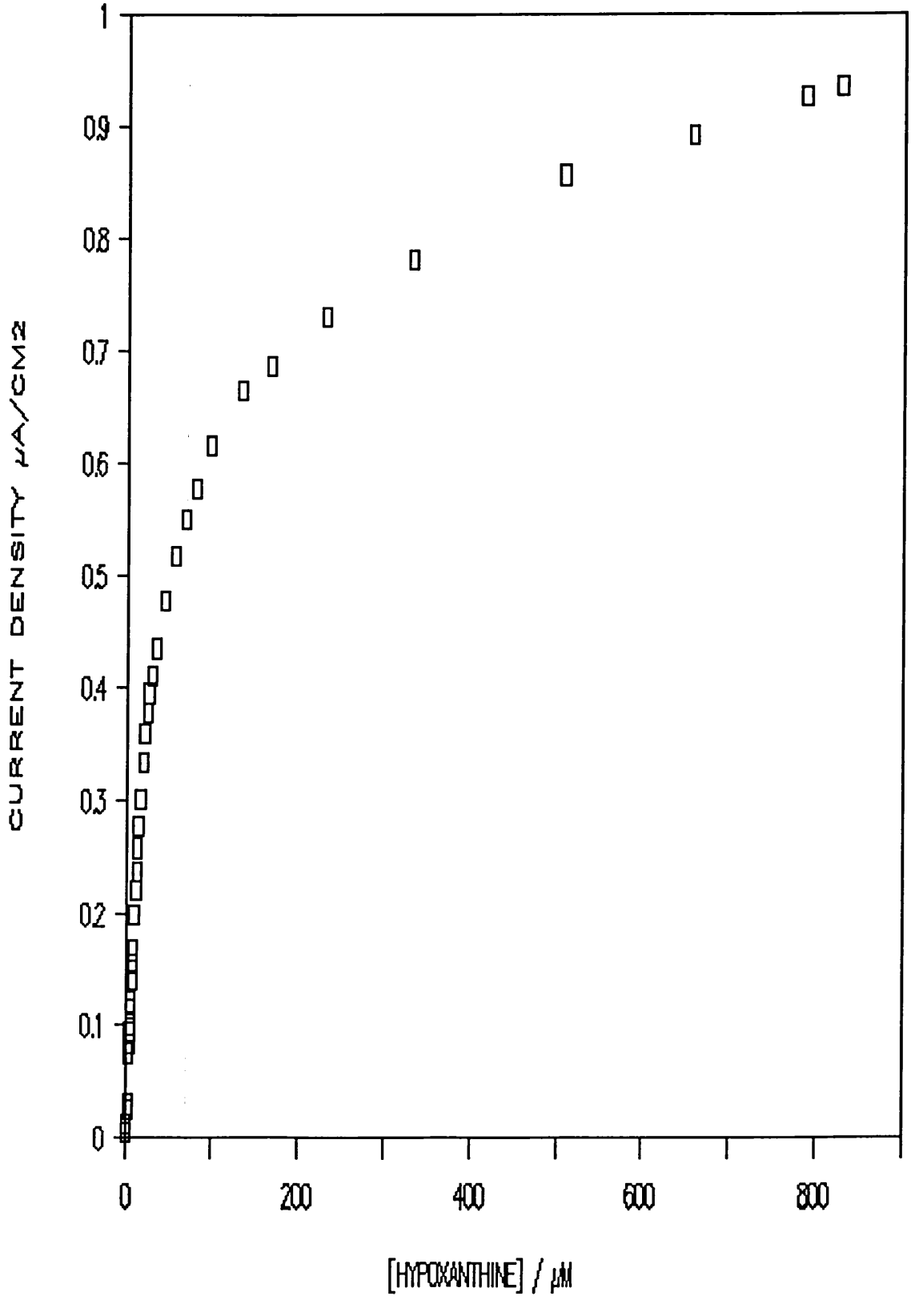

Figure 2.17 The Hanes plot for the hypoxanthine electrode using data from Figure 2.16

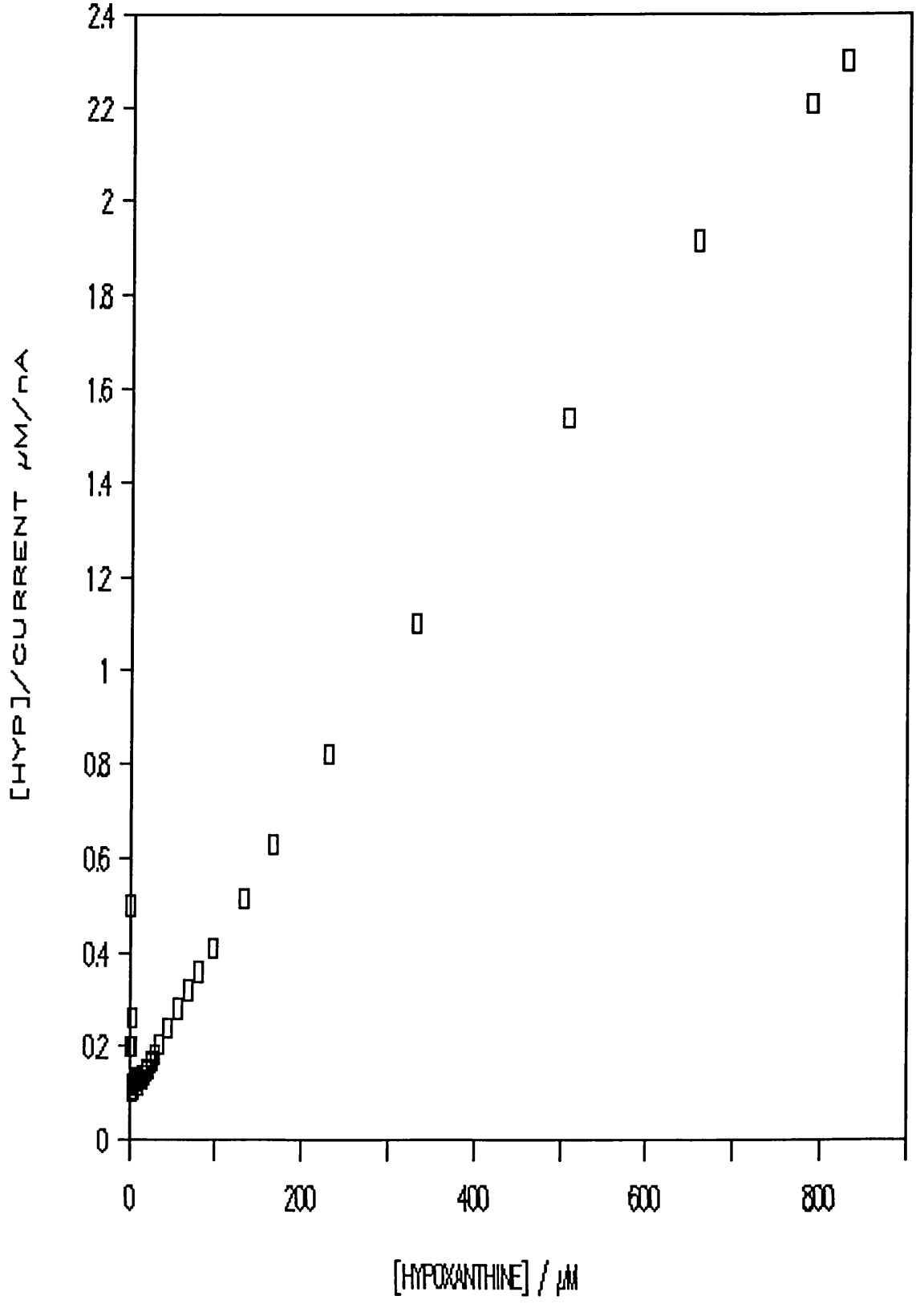

TABLE 2.3

Kinetic parameters for the xanthine/hypoxanthine system

	Hypoxanthine	Xanthine
Heterogeneous Rate Constant, k'_{ME}, cm s^{-1}	8.9×10^{-5}	4.5×10^{-5}
Mass Transfer Rate Constant, k'_S, cm s^{-1}	3.6×10^{-4}	6.3×10^{-5}
Π_X		0.7
Intercept at $\rho=0$ in the $\rho-$plot		$15 mM^{-1}$ $\Rightarrow K_{ME} = 70\ \mu M$

2.4 NITRATE SENSOR

Vasodilators are molecules which affect the flow of blood by controlling the degree of blood vessel dilation. A common vasodilator is acetylcholine. Endothelium-derived relaxing factor (EDRF) is produced by the vascular endothelium and mediates the action of various vasodilators (19). As an example, a vessel from which the endothelium has been removed will fail to respond to the vasorelaxant action of acetylcholine. A similar result is observed in patients who suffer from diseases which have a deleterious effect on the endothelium such as artherosclerosis.

Furchgott (20) proposed that EDRF was itself NO since it was known that nitrovasodilators such as glyceryl trinitrate, which function by releasing NO, mimicked the behaviour of EDRF. Evidence supporting this theory came from a study using chemiluminescence techniques (20) which showed that EDRF and NO had similar properties: for example haemoglobin was known to be capable of binding both EDRF and NO and it also inhibited tissue relaxation. The investigation also showed that superoxide dismutase reduced the decay of both NO and EDRF indicating that O_2^- inactived both compounds. Thus the body could inhibit the action of EDRF via uptake by haemoglobin or enhance its action by using SOD to mop up any superoxide anions present which could react with NO to produce NO_3^-.

Moncada et al (21) used N^G-monomethyl-L-arginine (L-NMMA), a specific inhibitor of EDRF synthesis to confirm that EDRF was in fact NO. They monitored the basal forearm blood flow in a series of volunteers and observed the effect upon it of infusing L-NMMA. They found that the inhibitor caused a 50% reduction in basal blood flow and from their results suggested that endothelium-derived NO was continuously released in the forearm arterial bed where it attenuated basal blood flow and mediated the action of acetylcholine.

In neutral aqueous solution NO reacts with dissolved oxygen to produce NO_2 which then forms NO_2^- and NO_3^- according to the reactions shown below

$$2NO + O_2 \longrightarrow 2NO_2$$

$$2NO_2 + H_2O \longrightarrow NO_2^- + NO_3^- + 2H^+$$

thus rather than trying to monitor the shortlived NO species it was more convenient to follow the nitrate concentration (19). This section deals with the preliminary development of an enzyme electrode to measure nitrate.

2.4.1 Theory

The theory used is essentially that derived by Albery and Bartlett (22). The key difference being that nitrate reductase reacts by using NADH to catalyse the reduction of nitrate thereby producing NAD^+, as opposed to yeast alcohol dehydrogenase which uses NAD^+ to oxidise ethanol creating electroactive NADH. Thus the present reaction is followed by monitoring the decrease in current as aliquots of nitrate are added to the bulk solution. The model assumes that excess NADH is present thus ensuring that the concentration of free enzyme, E, is negligible compared to the enzyme-cofactor complex E.NADH . It is also assumed that complex formation is sufficiently rapid to enable an equilibrium to be established between E and E.NADH (Figure 2.18).

If one assumes the presence of the following equilibria

$$E.NADH + S \underset{k_{-1}}{\overset{k_{+1}}{\rightleftharpoons}} E.NADH.S \underset{k_{-2}}{\overset{k_{+2}}{\rightleftharpoons}} E.NADH.P \xrightarrow{k_{+3}} E + NAD + P$$

then the following series of equations can be written for the flux, j_E,

$$j_E = k_S'(S_\infty - S_o) \qquad 2.59$$

$$= L (k_{+1}EH.S_o - k_{-1}ES) \qquad 2.60$$

$$= L (k_{+2}ES - k_{-2}EP) \qquad 2.61$$

$$= Lk_{+3}EP \qquad 2.62$$

Substitution followed by rearrangement gives

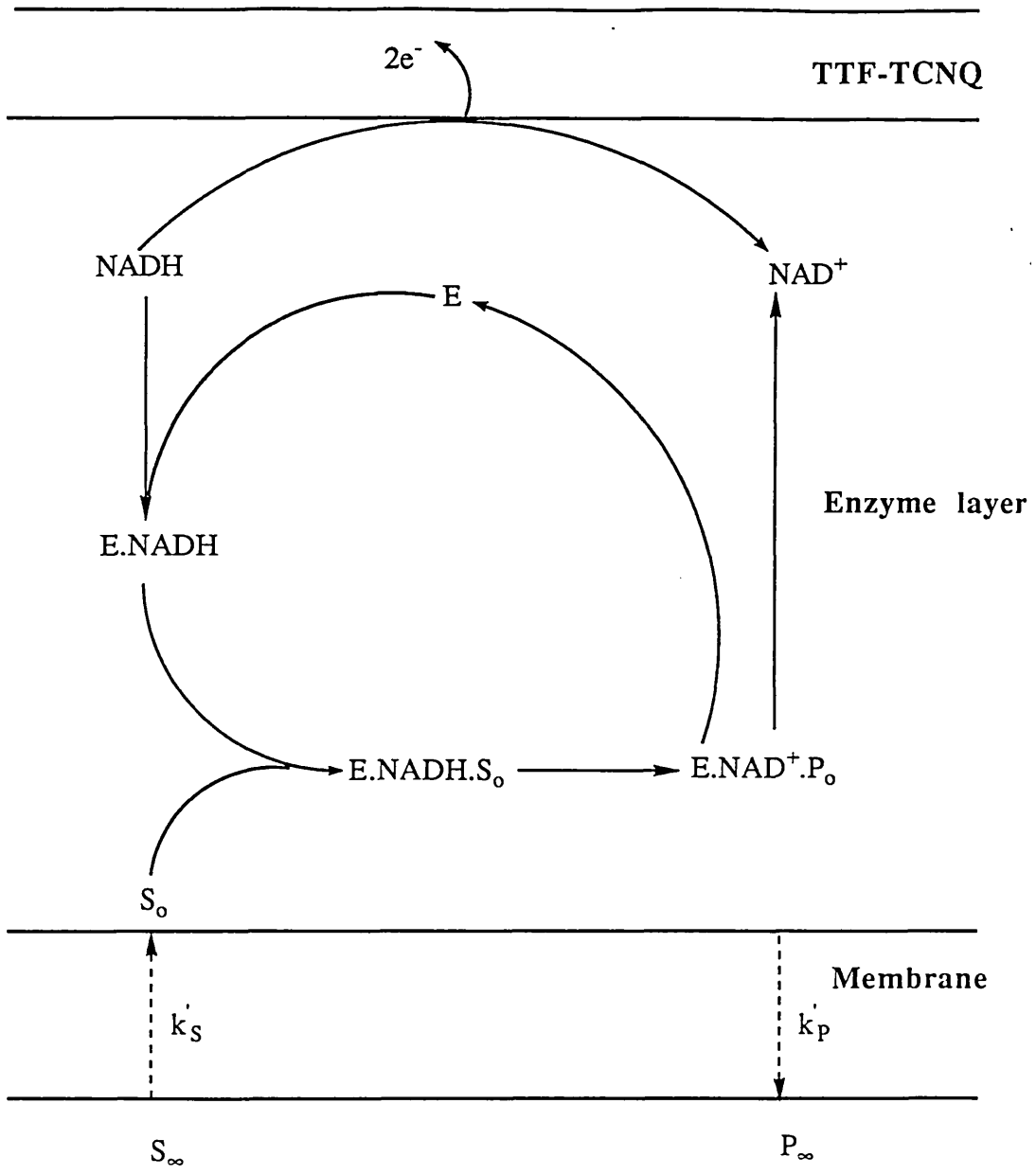

E = Nitrate Reductase

$S = NO_3^-$

$P = NO_2^-$

Figure 2.18 Kinetic scheme for the nitrate sensor

Figure 2.19 Electrode reponse to nitrate. 3 U/ml nitrate reductase

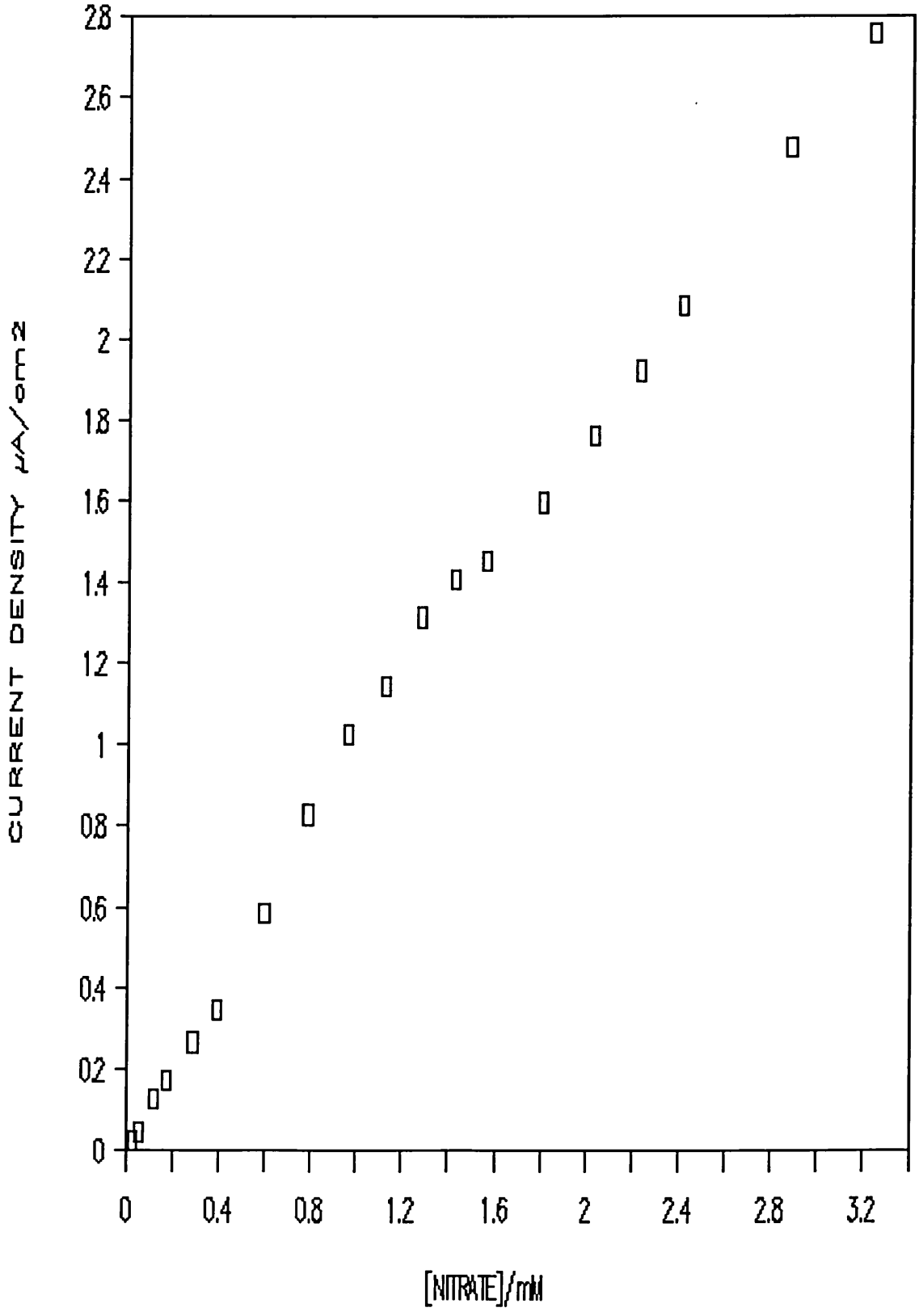

Figure 2.20 The Hanes plot for the nitrate electrode using data from Figure 2.19

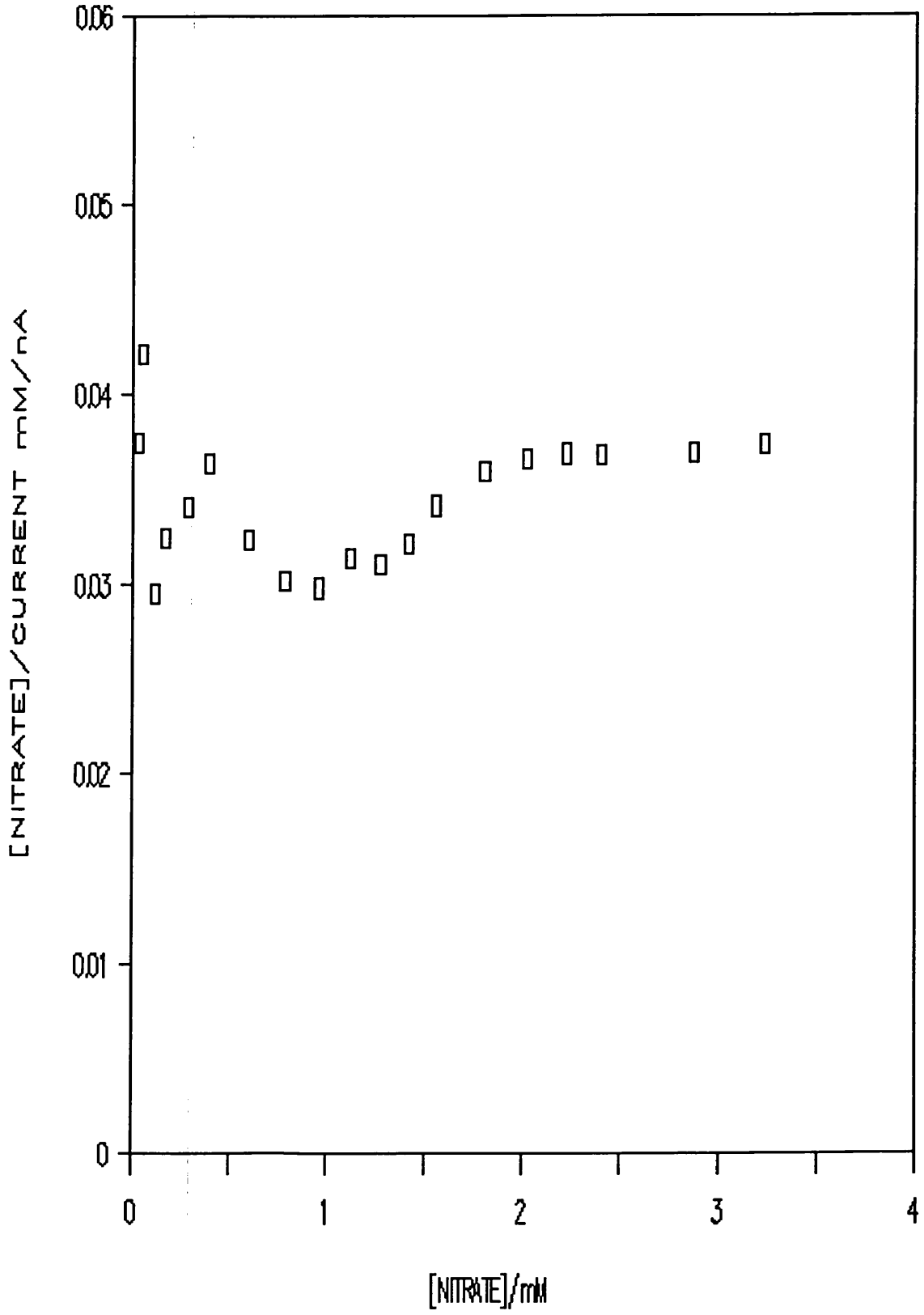

Figure 2.21 The rho plot for the nitrate electrode using data from Figure 2.19

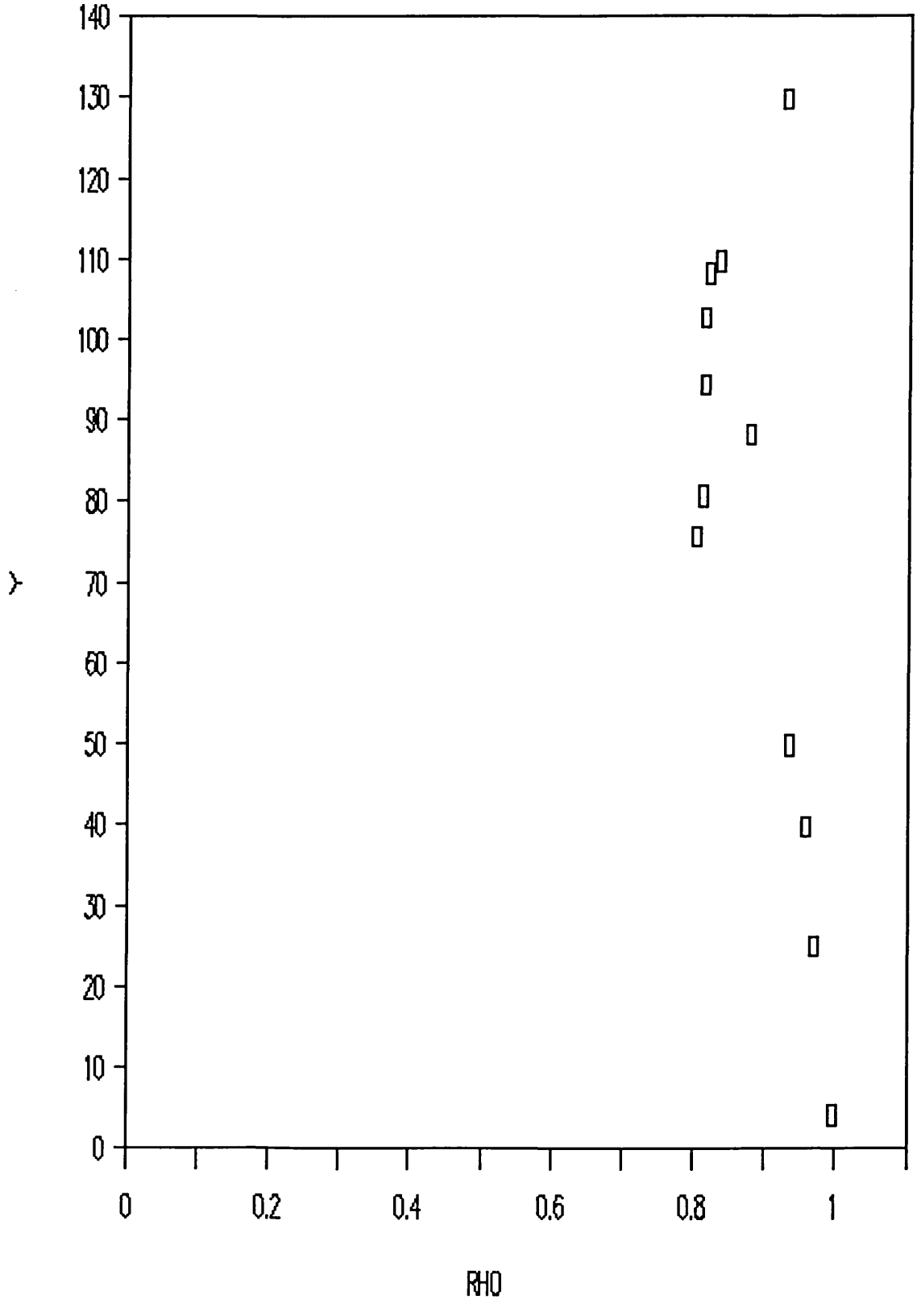

$$\frac{E_\Sigma}{j_E} = \frac{1}{LS_\infty}\left\{\frac{K_M}{k_{cat}}\right\} + \frac{1}{Lk_{cat}}\left(1 - \frac{j_E}{k'_S S_\infty}\right) + \frac{E_\Sigma}{k'_S S_\infty} \qquad 2.63$$

This can be converted to a Hanes-type equation of the form

$$\frac{S_\infty}{j_E} = \frac{1}{k'_{ME}} + \frac{S_\infty}{Lk_{cat}E_\Sigma}\left(1 - \frac{j_E}{k'_S S_\infty}\right) \qquad 2.64$$

where $$\frac{1}{k'_{ME}} = \frac{1}{LE_\Sigma}\left\{\frac{K_M}{k_{cat}}\right\} + \frac{1}{k'_S} \qquad 2.65$$

As shown in previous sections this can be rearranged to give a characteristic ρ-plot of the form

$$y = \frac{\rho^{-1} - 1}{X_\infty} = \frac{k'_{ME}}{Lk_{cat}E_\Sigma}\left(1 - \frac{\rho k'_{ME}}{k'_S}\right) \qquad 2.66$$

with $$\rho = \frac{[j_E/S_\infty]}{k'_{ME}} \qquad 2.67$$

2.4.2 Results

The response of the electrode to additions of nitrate is shown in Figure 2.19. As can be seen it is essentially linear over a concentration range of three orders of magnitude, hence it is not surprising that the Hanes plot (Figure 2.20) shows that transport of substrate across the membrane is the rate-limiting process and governs the response at all substrate concentrations. From the intercept at $S_\infty=0$ a value of $9.2\text{x}10^{-6}$cm s^{-1} is obtained for k'_{ME}. The ρ-plot (Figure 2.21) shows that the intercept at $y=0$ passes through $\rho=1$ confirming that membrane kinetics govern the electrode response.

2.5 CONCLUSIONS

The results presented in this chapter show that diverse enzyme systems, including coupled enzymes, can be used as sensors at TTF-TCNQ electrodes and their behaviour described adequately by modifications to the theory developed by Albery and Bartlett (13).

REFERENCES

1. K. Mckenna and A. Brajter-Toth, Anal. Chem., 59, 954, (1987)

2. D. H. Craston, Ph. D. Thesis, Univ. of London, (1986)

3. J. Ferraris, D. O. Cowan, V. Walatka and J. H. Perlstein, J. Amer. Chem. Soc., 95, 948, (1973)

4. B. J. Driscoll, Ph. D. Thesis, Univ. of London, (1988)

5. L. J. Murphy, Ph. D. Thesis, Univ. of London, (1989)

6. J. B. Walker, Adv. in Enzymology, 50, 177, (1979)

7. E. Mussini, L. Colombo, G. De Ponte and F. Marcucci., J. Chromat., 305, 450, (1984)

8. Z. Dvorak, Anal. Chim. Acta, 208, 307, (1988)

9. J. W. Dubnoff, in S. P. Colwick and N. O. Kaplan (Eds) Methods in Enzymology, 3, 637, Academic Press, New York (1957)

10. D. R. Anderson, C. M. Williams, G. M. Krise and R. M. Dowben, Biochem J., 67, 258, (1957)

11. A. H. Ennor and L. A. Stocken, Biochem J., 310, (1953)

12. Y. Matsuda, N. Wakamatsu, Y. Inouye, S. Uede, Y. Hashimoto, K. Asano and S. Nakamura, Chem. Pharm. Bull., 34, 2155, (1986)

13. W. J. Albery and P. N. Bartlett, J. Electroanal. Chem, 194, 211, (1985)

14. M. Suzuki, J. Biochem. (Tokyo), 89, 599, (1981)

15. K. J. Laidler and P. S. Bunting, The Chemical Kinetics of Enzyme Action, Clarendon Press, Oxford, (1973)

16. H. W. Hoeffken, S. H. Knof, P. A. Bartlett, R. Huber, H. Moellering and G. Schumacher, J. Mol. Biol., 204, 417, (1988)

17. A.L. Lehninger, Biochemistry, Worth Pub., New York, (1981)

18. R. C. Bray, The Enzymes 3rd Edn, Ed P.D. Boyer, Academic Press New York (1975)

19. R. J. Palmer, A. G. Ferrige and S. Moncada, Nature, 327, 524, (1987)

20. R.F. Furchgott, in Mechanisms of Vasodilation vol IV, Ed. P. M. Vanhoutte, Raven New York, (1987)

21. P. Vallance, J. Collier and S. Moncada, Lancet, 28/9/89, 997

22. W. J. Albery, P. N. Bartlett, A. E. G. Cass and K. W. Sim, J. Electroanal. Chem., 218, 127, (1987)

CHAPTER 3
DEVELOPMENT OF A SUCROSE SENSOR

This chapter describes the development of an amperometric sensor to measure sucrose using a conducting organic salt enzyme electrode. The same methodology is employed as for the sensors described in the previous chapter, with the substrate diffusing through a semi-permeable membrane and undergoing a series of reactions. Three enzyme catalysed processes occur in the electrolyte layer trapped behind the membrane. First the sucrose is hydrolysed by invertase to yield α-D-glucose and β-fructose. Then the α-D-glucose is isomerised to β-D-glucose in a reaction catalysed by mutarotase. Finally β-D-glucose is oxidised to β-D-glucono-δ-lactone. The reactions are summarised in the following equations

$$\text{sucrose} + H_2O \longrightarrow \alpha\text{-D-glucose} + \beta\text{-fructose}$$

$$\alpha\text{-D-glucose} \longrightarrow \beta\text{-D-glucose}$$

$$\beta\text{-D-glucose} + O_2 \longrightarrow \beta\text{-D-glucono-}\delta\text{-lactone}$$

To date the majority of methods used to detect sucrose have involved using either a Clarke type electrode to monitor O_2 consumption or a platinum anode to detect H_2O_2 formation (1-5). Coulet et al (2) adopted the latter approach and immobilised the enzymes on activated collagen membranes. Their work indicated that asymmetric coupling in which invertase and mutarotase were co-immobilised on one face and glucose oxidase on the other permitted better sensitivity than random co-immobilisation.

Scheller and Renneberg (4) used a platinum electrode to design an enzyme electrode which detected sucrose in the presence of glucose. They employed a multilayer system in which any incoming hydrogen peroxide or glucose was enzymatically converted to non-electroactive products by an anti-interference layer consisting of glucose oxidase and catalase. Sucrose molecules passed unscathed through this layer and entered a second enzymatic layer containing invertase and glucose oxidase where the eventual reaction

product H_2O_2 was oxidised by the platinum electrode. Although they found that the response to sucrose was slow they failed to use mutarotase, relying solely on spontaneous mutarotation to produce the β-glucose anomer.

Matsumoto et al (6) used flow injection analysis to design an enzyme reactor to simultaneously determine glucose, fructose and sucrose. A non-electrochemical approach was used by Nieman and Swindlehurst (7). They determined the concentration of any H_2O_2 produced via a chemiluminescence reaction with luminol.

3.1 EXPERIMENTAL

3.1.1 Chemicals and Solutions

The conducting organic salt and all solutions were prepared as in §2.1.1. Invertase [E.C. 3..2.1.26] was obtained from Sigma (TypeX I 4753) as were mutarotase [E.C. 5.1.3.3] (M 5526) and glucose oxidase [E.C. 1.1.3.4] (Type VII G 2133).

3.1.2 Membranes

Spectra/Por 2 membranes obtained from Pierce were used in all experiments unless otherwise indicated.

3.1.3 Electrodes

All electrodes and other equipment were the same as in the last chapter. The TTF-TCNQ electrode was poised at +300 mV (vs. S.C.E.). Experiments were performed following standard procedures(9).

3.2. THEORY

In creating a kinetic model for this system it is convenient to consider the action of invertase separately from that of mutarotase and glucose oxidase.

3.2.1. Mechanism of Invertase Action

A study of sucrose hydrolysis has shown that the products, D-fructose and D-glucose, inhibit the action of invertase (8). D-fructose was shown to be a competitive inhibitor and D-glucose a partial non-competitive inhibitor. Assuming that all equilibria are fast, then the reaction scheme shown in Figure 3.1 applies.

The subcripts o and ∞ are again used to denote concentrations inside and outside the membrane respectively. As glucose, P, is a non-competitive inhibitor it does not affect binding of sucrose, S, then since

$$EP = \frac{E.P_o}{K_P} \qquad 3.1$$

and $$ES = \frac{E.S_o}{K_S} \qquad 3.2$$

it follows that $$EPS = \frac{EP.S_o}{K_S} = \frac{E.P_o.S_o}{K_S K_P} \qquad 3.3$$

Similarly for fructose, F,

$$EF = \frac{E.F_o}{K_F} \qquad 3.4$$

The flux, j, is given

$$j = k_a ES + k_b EPS \qquad 3.5$$

$$= \frac{E.S_o}{K_S}\left\{k_a + \frac{k_b P_o}{K_P}\right\} \qquad 3.6$$

Since the total enzyme concentration E_1 is given by

$$E_1 = E + ES + EF + E + EPS \qquad 3.7$$

Therefore substituting for the various enzyme complexes,

$$E = \frac{E_1}{1 + \frac{S_o}{K_S} + \frac{F_o}{K_F} + \frac{P_o}{K_P} + \frac{P_o.S_o}{K_P K_S}} \qquad 3.8$$

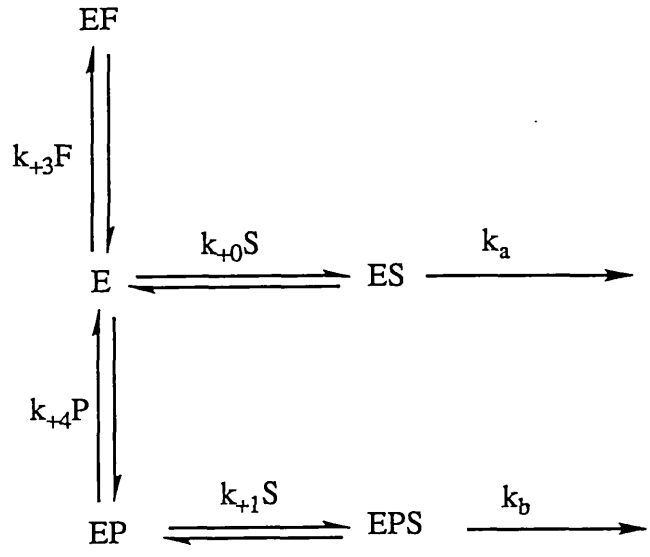

E = Invertase

F = Fructose

P = Glucose

S = Sucrose

Figure 3.1 Kinetic scheme for the action of invertase

Substituting eqn. 3.8 into eqn. 3.6 gives

$$j = \frac{E_1\left\{ k_a + \frac{k_b P_o}{K_P} \right\}}{\frac{K_S}{S_o}\left\{1 + \frac{S_o}{K_S} + \frac{F_o}{K_F} + \frac{P_o}{K_P} + \frac{P_o.S_o}{K_P K_S}\right\}} \qquad 3.9$$

Rearranging this expression

$$\frac{S_o}{j} = \frac{\frac{F_o}{K_F\left(1 + \frac{P_o}{K_P}\right)} + 1}{\frac{1}{K_S}\left\{ \frac{\left(k_a + \frac{k_b P_o}{K_P}\right) E_1}{\left(1 + \frac{P_o}{K_P}\right)} - 1 \right\}} \qquad 3.10$$

This expression can be simplified by considering the relative magnitude of the terms in the denominator.

First assuming that,

$$\frac{\left(k_a + \frac{k_b P_o}{K_P}\right) E_1}{\left(1 + \frac{P_o}{K_P}\right)} \gg 1 \qquad 3.11$$

then it follows that

$$\frac{S_o}{j} = \frac{K_S}{\left(k_a + \frac{k_b P_o}{K_P}\right) E_1} \left\{ \frac{F_o}{K_F} + \left(1 + \frac{P_o}{K_P}\right) \right\} \qquad 3.12$$

Case 1

$$\text{If } \frac{F_o}{K_F} \gg \left(1 + \frac{P_o}{K_P}\right) \text{ then } j = \frac{K_F}{F_o K_S}\left(k_a + \frac{k_b P_o}{K_P}\right) E_1 S_o \qquad 3.13$$

Case 2

$$\text{However when } \frac{F_o}{K_F} \ll \left(1 + \frac{P_o}{K_P}\right) \text{ then } j = \frac{\left(k_a + \frac{k_b P_o}{K_P}\right) E_1 S_o}{\left(1 + \frac{P_o}{K_P}\right) K_S} \qquad 3.14$$

Case 2 can be further simplified as follows :

$$\text{Case 2a: if } \frac{P_o}{K_P} \ll 1 \qquad \text{then } j = \left(k_a + \frac{k_b P_o}{K_P}\right) \frac{E_1 S_o}{K_S} \qquad 3.15$$

$$\text{Case 2b: alternatively if } \frac{P_o}{K_P} \gg 1 \text{ then } j = \left(\frac{k_a K_P}{P_o} + k_b\right) \frac{E_1 S_o}{K_S} \qquad 3.16$$

The extent of the inhibition due to fructose determines which case predominates.

3.2.2 Mutarotase/Glucose Oxidase System

Considering this two enzyme system separately (Figure 3.2) and applying the same analysis as used in the previous chapter, a series of simultaneous equations involving the flux, j, can be written

$$j = L(k_{+4} P_o . E_2 - k_{-4} E_2 P) \qquad 3.17$$

$$= L(k_{+5} E_2 P - k_{-5} E_2 Q) \qquad 3.18$$

$$= L(k_{+6} E_2 Q - k_{-6} Q_o . E_2) \qquad 3.19$$

$$= L(k_{+7} Q_o . E_3 - k_{-7} E_3 Q) \qquad 3.20$$

$$= L(k_{+8} E_3 Q - k_{-8} E_3 R) \qquad 3.21$$

$$= L(k_{+9} E_3 R - k_{-9} R_o . E_3') \qquad 3.22$$

$$= k'(E_3')^{1/2} \qquad 3.23$$

$$= k_R'(R_o - R_\infty) \qquad 3.24$$

Introducing a probability factor, k_f

$$\text{Prob } (Q \longrightarrow R) = k_f = \frac{L k_{+7} E_3}{L k_{+7} E_3 + k_Q' + L k_{-6} E_2} \qquad 3.25$$

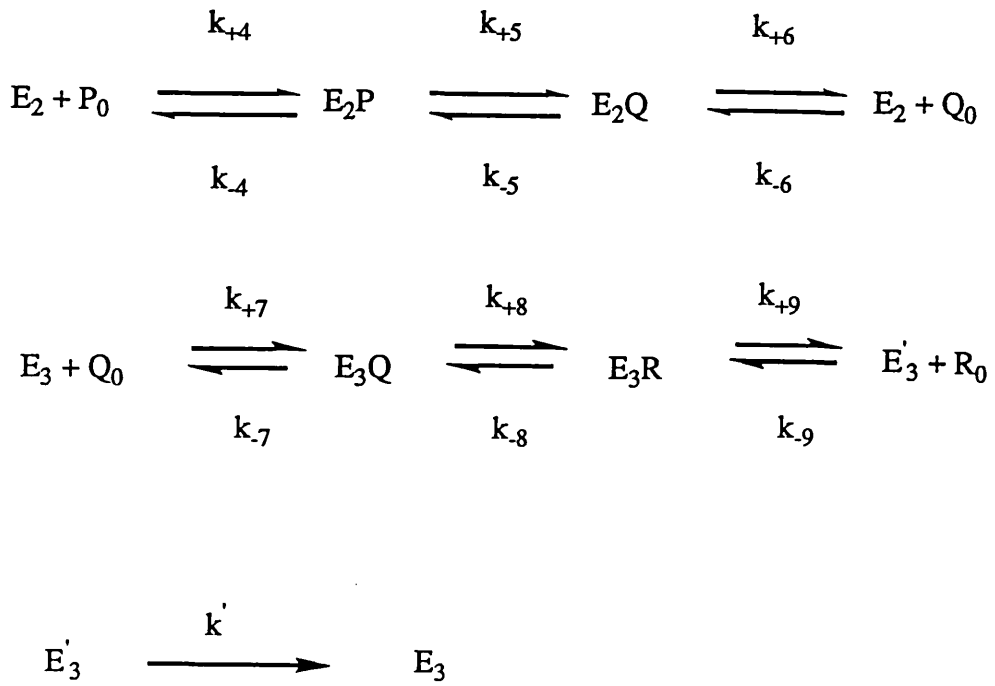

E_2 = mutarotase

E_3 = glucose oxidase (oxidised)

E'_3 = glucose oxidase (reduced)

P_0 = alpha glucose Q_0 = beta glucose

R_0 = gluconolactone

Figure 3.2 Kinetic scheme for the mutarotase / glucose oxidase system

to describe the probability of a newly formed Q molecule reacting with E_3 and rearranging eqns. 3.17-3.25 the following expression for Q_o is obtained

$$Q_o = \frac{j}{LE_3k_f}\left\{\frac{K_M}{k_{cat}}\right\}_3 + \frac{1}{K_{TD3}\,E_3k_f}\left(\frac{j}{k'}\right)^2\left(R_\infty + \frac{j}{k'_R}\right) \qquad 3.26$$

where $$\left\{\frac{K_M}{k_{cat}}\right\}_3 = \frac{1}{k_{+7}} + \frac{1}{K_7k_{+8}} + \frac{1}{K_7K_8k_{+9}} \qquad 3.27$$

and $$K_{TD3} = K_7K_8K_9 \qquad 3.28$$

Similarly, introducing a probability factor for P

$$\text{Prob}\,(\,P \longrightarrow Q\,) = k_g = \frac{Lk_{+4}E_2}{Lk_{+4}E_2 + k'_P} \qquad 3.29$$

therefore,

$$P_o = \frac{j}{LE_2k_g}\left\{\frac{K_M}{k_{cat}}\right\}_2 + \frac{j}{LK_{TD2}E_3k_fk_g}\left\{\frac{K_M}{k_{cat}}\right\}_3 + \frac{1}{K_{TD2}K_{TD3}E_3k_fk_g}\left(\frac{j}{k'}\right)^2\left(R_\infty + \frac{j}{k'_R}\right) \qquad 3.30$$

where $$\left\{\frac{K_M}{k_{cat}}\right\}_2 = \frac{1}{k_{+4}} + \frac{1}{K_4k_{+5}} + \frac{1}{K_4K_5k_{+6}} \qquad 3.31$$

and $$K_{TD2} = K_4K_5K_6 \qquad 3.32$$

Since the final product D-glucono-δ-lactone does not inhibit the action of glucose oxidase eqn. 3.30 reduces to

$$P_o = \frac{j}{LE_2k_g}\left\{\frac{K_M}{k_{cat}}\right\}_2 + \frac{j}{LK_{TD2}E_3k_fk_g}\left\{\frac{K_M}{k_{cat}}\right\}_3 \qquad 3.33$$

3.2.3 Overall Model for Sucrose

The equations derived in §3.2.1 and §3.2.2. can be combined to obtain an overall picture of the sucrose system (Figure 3.3).

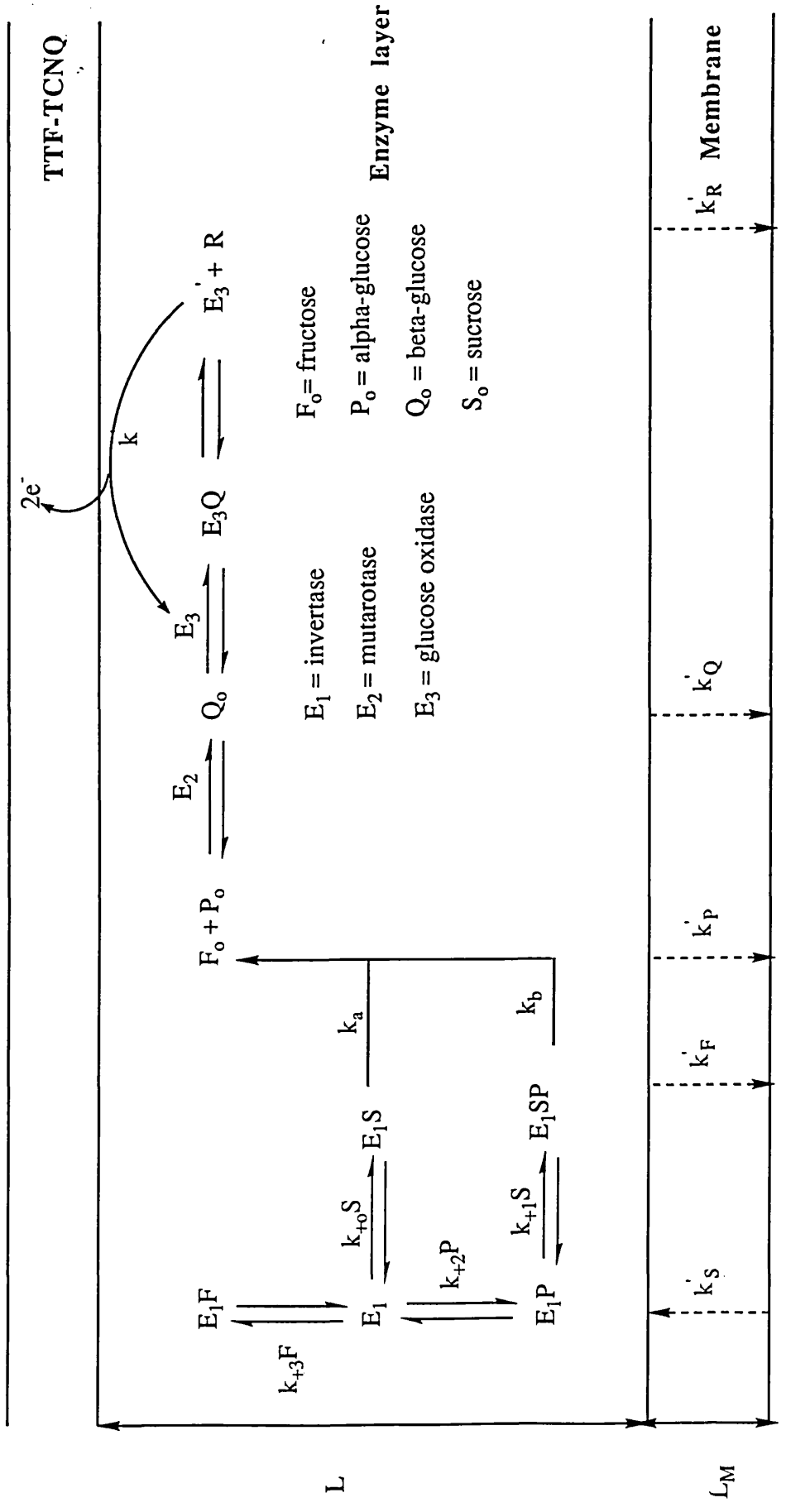

Figure 3.3 Overall kinetic scheme for the sucrose sensor

3.2.3.1 Case 1

Rearranging eqn. 3.13 and substituting for P_o using eqn. 3.33

$$\frac{1}{j}=\frac{K_F F}{K_F E_1 k_a S_o}-\frac{k_b}{LK_P k_a}\left[\frac{1}{E_2 k_g}\left\{\frac{K_M}{k_{cat}}\right\}_2+\frac{1}{K_{TD2}E_3 k_f k_g}\left\{\frac{K_M}{k_{cat}}\right\}_3\right] \qquad 3.34$$

since $j=k_S'(S_\infty - S_o)$, then

$$\frac{1}{j}=\left(\frac{K_S F}{K_F E_1 k_a}+\frac{1}{k_S'}\right)\frac{1}{S_\infty}-$$

$$\frac{k_b}{LK_P k_a}\left[\frac{1}{E_2 k_g}\left\{\frac{K_M}{k_{cat}}\right\}_2+\frac{1}{K_{TD2}E_3 k_f k_g}\left\{\frac{K_M}{k_{cat}}\right\}_3\right]\left(1-\frac{j}{k_S' S_\infty}\right) \qquad 3.35$$

Since mutarotase and glucose oxidase exhibit much faster kinetics than invertase

$$\frac{1}{j}=\left(\frac{K_S F_o}{K_F E_1 k_a}+\frac{1}{k_S'}\right)\frac{1}{S_\infty} \qquad 3.36$$

3.2.3.2 Case 2

Case 2a: Substituting for P_o in eqn. 3.15 and assuming that mutarotase and glucose oxidase act far more rapidly than invertase then,

$$j=\frac{k_a E_1 S_o}{K_S}=\frac{k_a E_1 S_\infty}{K_S}\left(1-\frac{j}{k_S' S_\infty}\right) \qquad 3.37$$

$$j=\frac{S_\infty}{\frac{K_S k_a}{E_1}-\frac{1}{k_S'}} \qquad 3.38$$

Case 2b: In this case a nonsense solution was obtained with j tending to infinity.

Inspection of eqns. 3.36 and 3.38 shows that Case 1 incorporates a fructose dependent term whilst Case 2a does not. Thus an investigation of the variation of flux as a function of fructose concentration can be used to distinguish between the two cases.

3.3. RESULTS

3.3.1 Adsorbed Enzyme Electrodes

In order to investigate the contribution of adsorbed species to the overall electrode response 20μl of enzyme solution containing invertase, mutarotase and glucose oxidase in the ratio 140:140:14 was left to air-dry on the electrode surface. Excess material was washed from the surface using DDW. The response was compared to that from a membrane electrode using the same enzyme system. The results are shown in Figures 3.4 and 3.5. It is clear that the enzymes in the electrolyte layer play an important role in determining the electrode response, however the contribution to the overall flux from adsorbed species is also significant. Although the limiting current, i_{max}, differs by a factor of two in favour of the membrane electrode, the current at low substrate concentrations is more comparable, suggesting that at these concentrations transport of substrate is at least partially responsible for determining the electrode response.

The transients shown in Figure 3.6 reveal an interesting phenomenon, namely, at high concentrations there is an initial drop in the electrode response on addition of substrate. This was previously observed by B. J. Driscoll in relation to a choline electrode (9). The effect is present regardless of whether or not a membrane is used.

The following conclusions can be made from the above results. First, the enzymes must adsorb strongly otherwise they would either be washed off by DDW prior to the experiment or would desorb during the experiment itself causing a downward drift in the observed current. Second, the enzymes are sufficiently robust to be able to withstand air-drying on the electrode surface without significant loss of activity.

It is worth noting that although the three enzymes are randomly adsorbed, the substrate can diffuse from one active site to another quite rapidly since the transients in the absence of the membrane were quicker than when a membrane was used. A possible explanation is that in the adsorbed system α-glucose, released by hydrolysis of sucrose,

Figure 3.4 Comparing the response of membrane and adsorbed enzyme electrodes

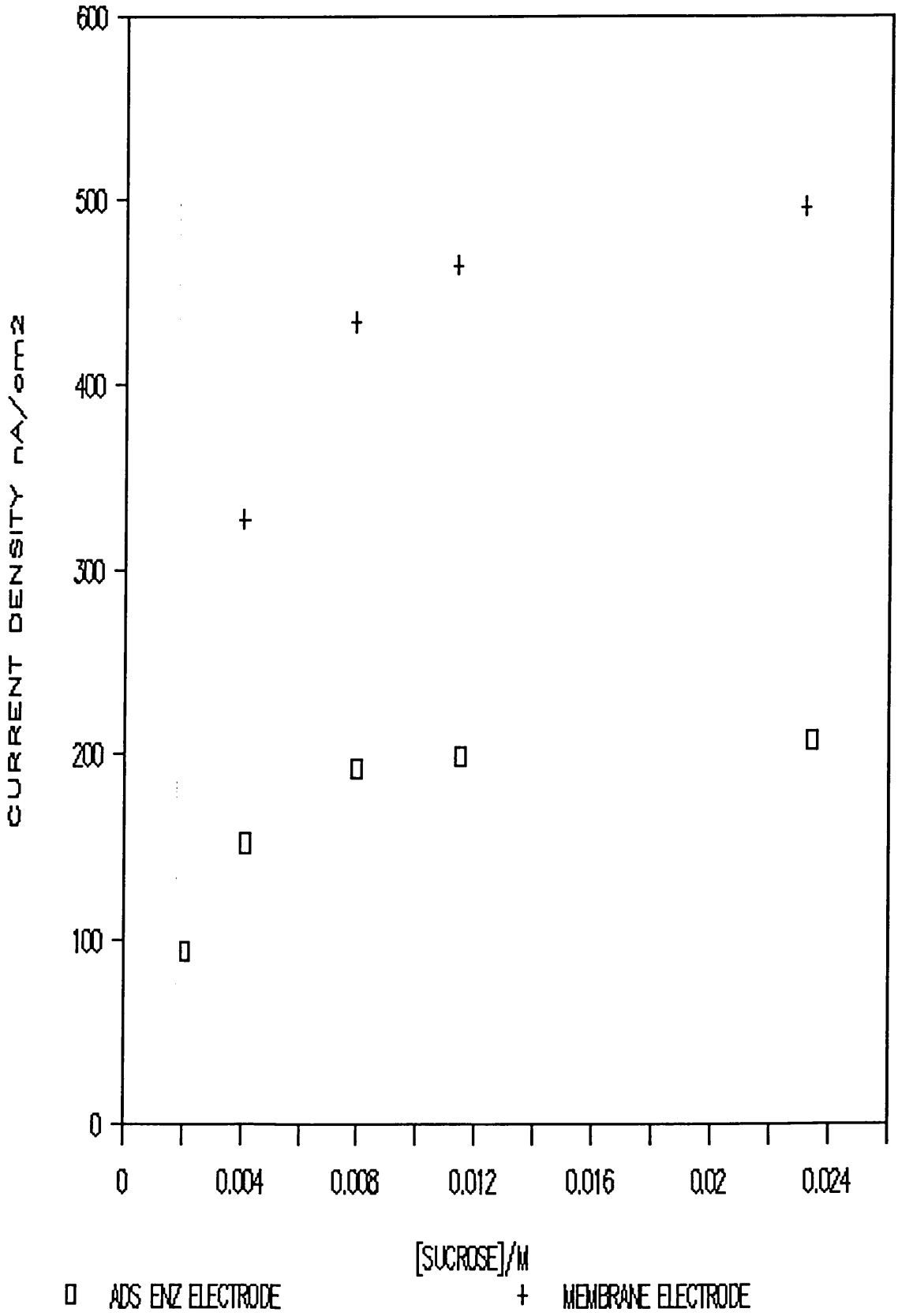

Figure 3.5 Investigating the lifetime of adsorbed enzyme electrodes

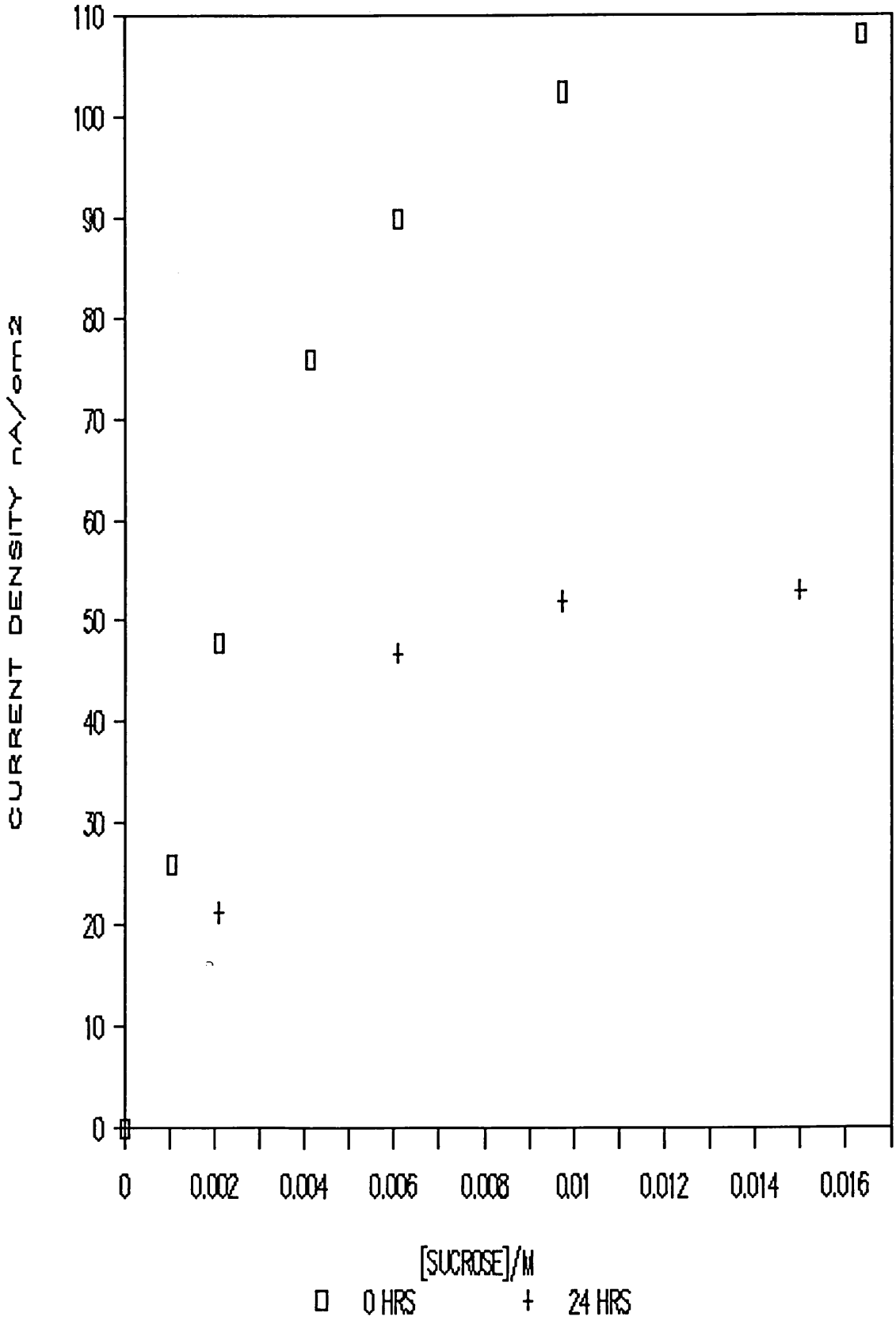

Figure 3.6 Transients for the addition of sucrose to the system at high substrate concentrations

Adsorbed Enzyme

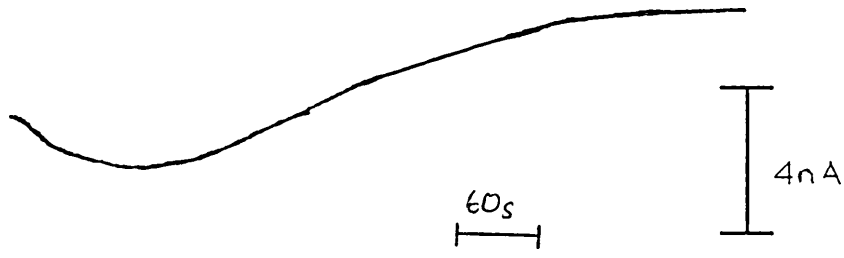

Membrane

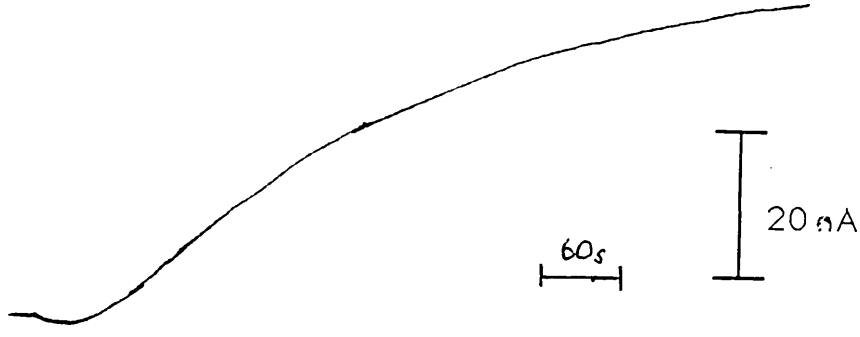

has a shorter distance to diffuse to mutarotase, the next enzyme in the sequence, than in the soluble enzyme system. Similarly for β-glucose and glucose oxidase. This result also supports the suggestion above that transport of substrate through the membrane is rate-determining.

In order to investigate its long term response an adsorbed enzyme electrode was stored overnight in buffer solution under ambient laboratory conditions and its response measured after an interval of 24 hours. The results are shown in Figure 3.5. A fall-off in response of approximately 50% was observed.

3.3.2. Reproducibility and Lifetime of Electrodes

The reproduciblity of enzyme electrodes is determined by two factors. First the ability of the organic salt to oxidise reduced enzyme depends on the nature of electrode surface and can vary by upto 50% depending on the surface roughness of different electrodes. Thus all experiments investigating reproduciblity were carried out with the same electrode. The second factor is the stability of the enzymes used.

The data shown in Figure 3.7 was collected from two experiments using the same enzyme solution on consecutive days with the electrode having been left overnight in buffer solution under ambient laboratory conditions. Figure 3.8 shows the response at low sucrose concentrations. The enzyme mixture consisted of invertase, mutarotase and glucose oxidase in the ratio 145:1419:71. Excellent reproducibility, in excess of 90% was obtained. The electrode response was shown to be effectively linear over a range of three orders of magnitude, from 25μM to 11mM.

3.3.3. Effect of Membrane Thickness

In order to investigate whether membrane kinetics determined the electrode response at low substrate concentrations, results obtained using Spectra/Por 2 and Gallenkamp membranes were compared (Figure 3.9). Both membranes have the same molecular weight cut-off. Since the membrane supplied by Gallenkamp is approximately

Figure 3.7 Reproducibility of the sucrose membrane electrode

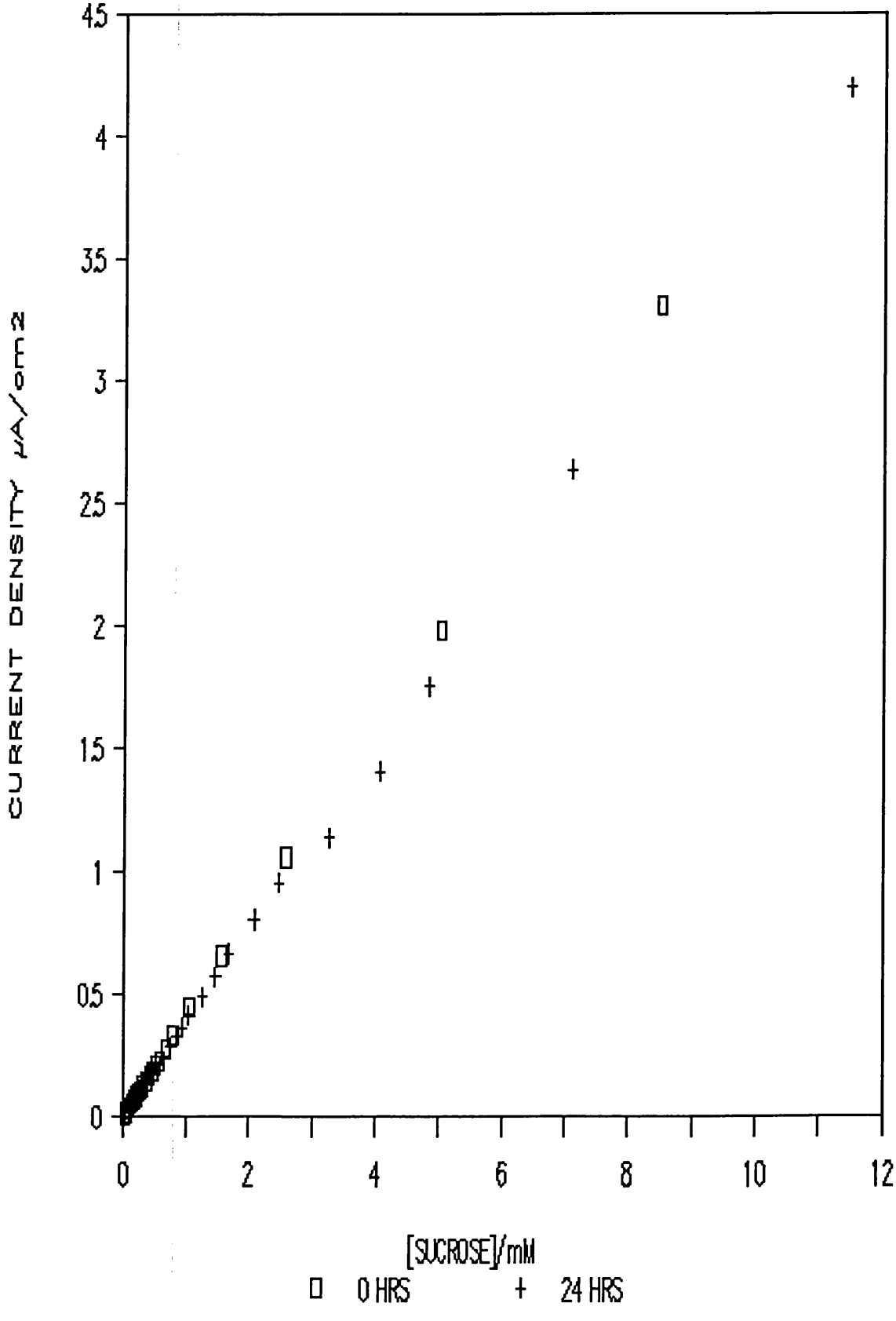

Figure 3.8 Reproducibility of the sucrose sensor at low sucrose concentrations

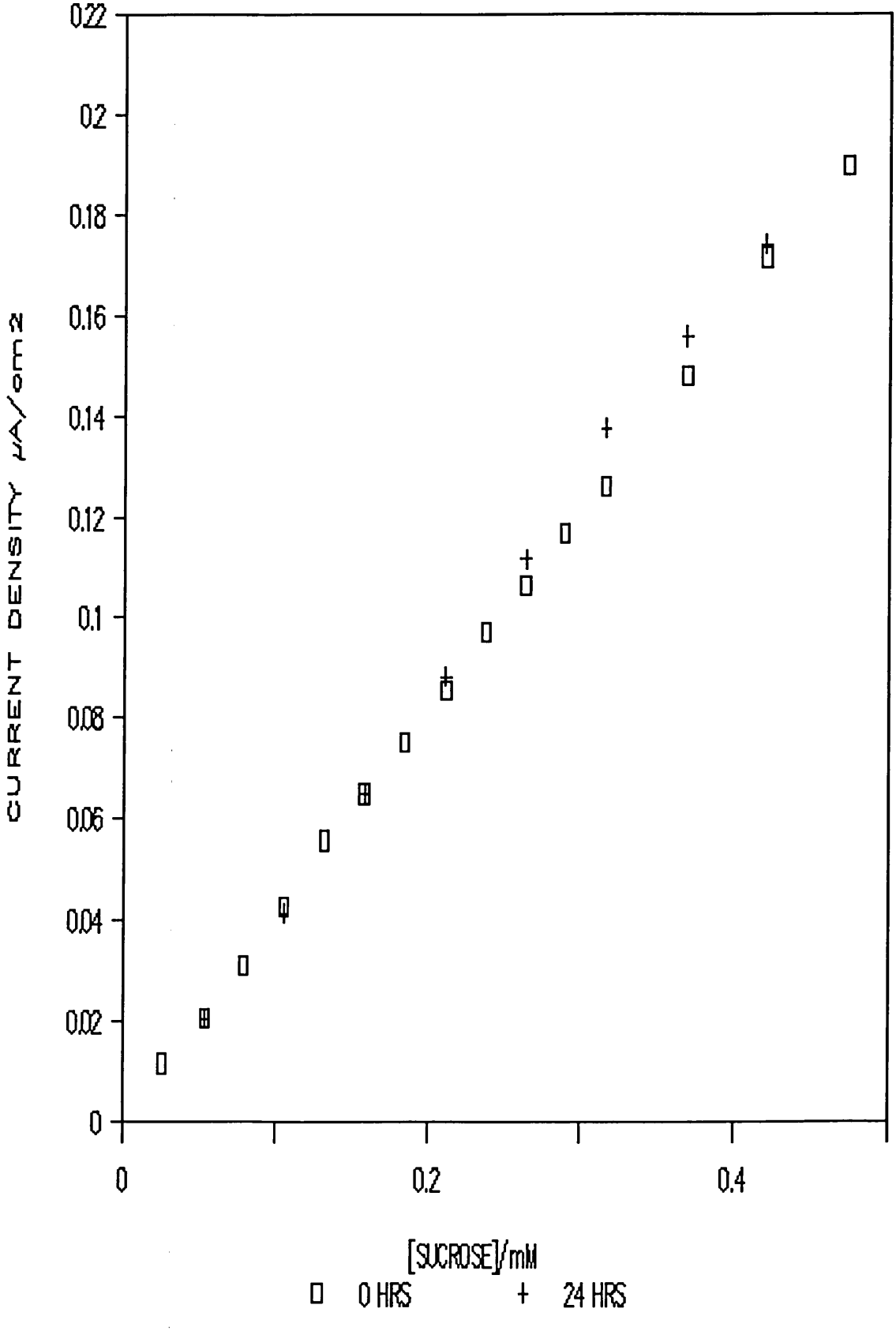

Figure 3.9 Effect on the electrode response of increasing the membrane thickness

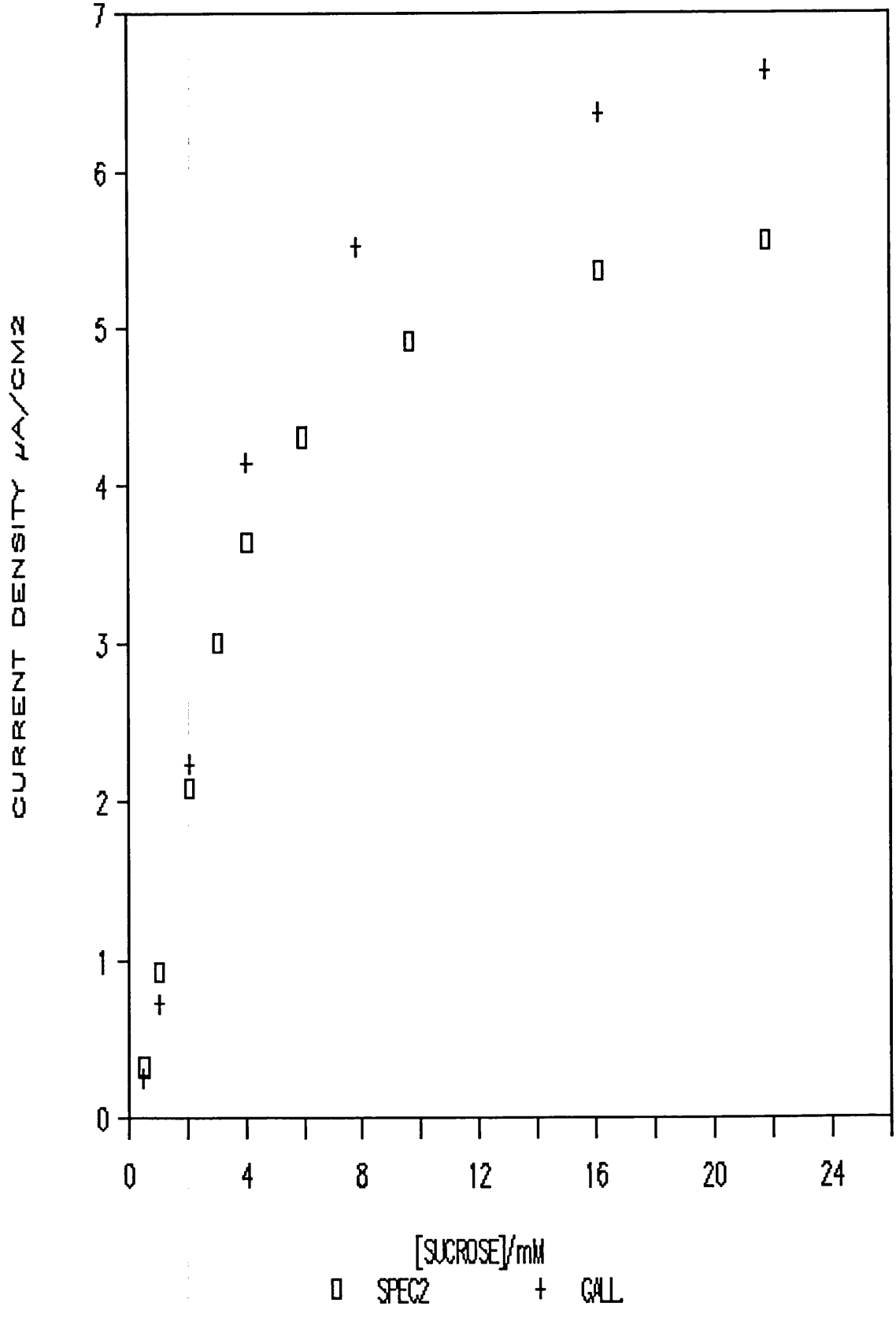

25 times thicker than that obtained from Spectra/Por, the mass transfer rate constant k'_S for sucrose should be decreased by a factor of 25. Thus if the response at low substrate concentrations was indeed determined by transport kinetics then the transients should be significantly slower in the experiment using Gallenkamp membrane. However as can be seen in Figure 3.10 there was no significant change in the transients obtained when Gallenkamp membrane was used. This suggests that the electrode response is governed primarily by enzyme kinetics, even at low sucrose concentrations.

Although the maximum current was greater using the Gallenkamp membrane the difference was only 15% and this lay within the bounds of experimental error since it was a one-off experiment.

3.3.4. Investigation of the Rate Determining Step

The preliminary experiments mentioned above used an excess of mutarotase to ensure that any α-glucose was rapidly converted to the β-anomer. In order to determine which of the enzymatic processes was rate-limiting a series of experiments was performed in which the ratio of the enzymic activities was varied and the results compared with calibration plots using glucose oxidase (Figures 3.11 and 3.12).

The results show that hydrolysis of sucrose by invertase is the slowest enzymatic process. At first sight this appears to contradict the result expected from inspection of the kinetic parameters given in Table 3.1. These would suggest that the action of glucose oxidase would govern the overall rate. However the results become explicable if one considers the nature of the pH profiles of invertase, mutarotase and glucose oxidase.

The optimum pH for glucose oxidase action is 6.5 but the enzyme retains >95% of its maximal activity at pH 6.0 and 7.0 and possesses approximately 75% maximal activity at pH 8.0 (10). Thus at the pH used in this investigation, 7.4, glucose oxidase is operating at near maximum efficiency. The same is true for mutarotase which is almost pH independent between 6.5 and 7.5 (11).

Figure 3.10 Comparison of the transients obtained using Spec2 and Gallenkamp membranes

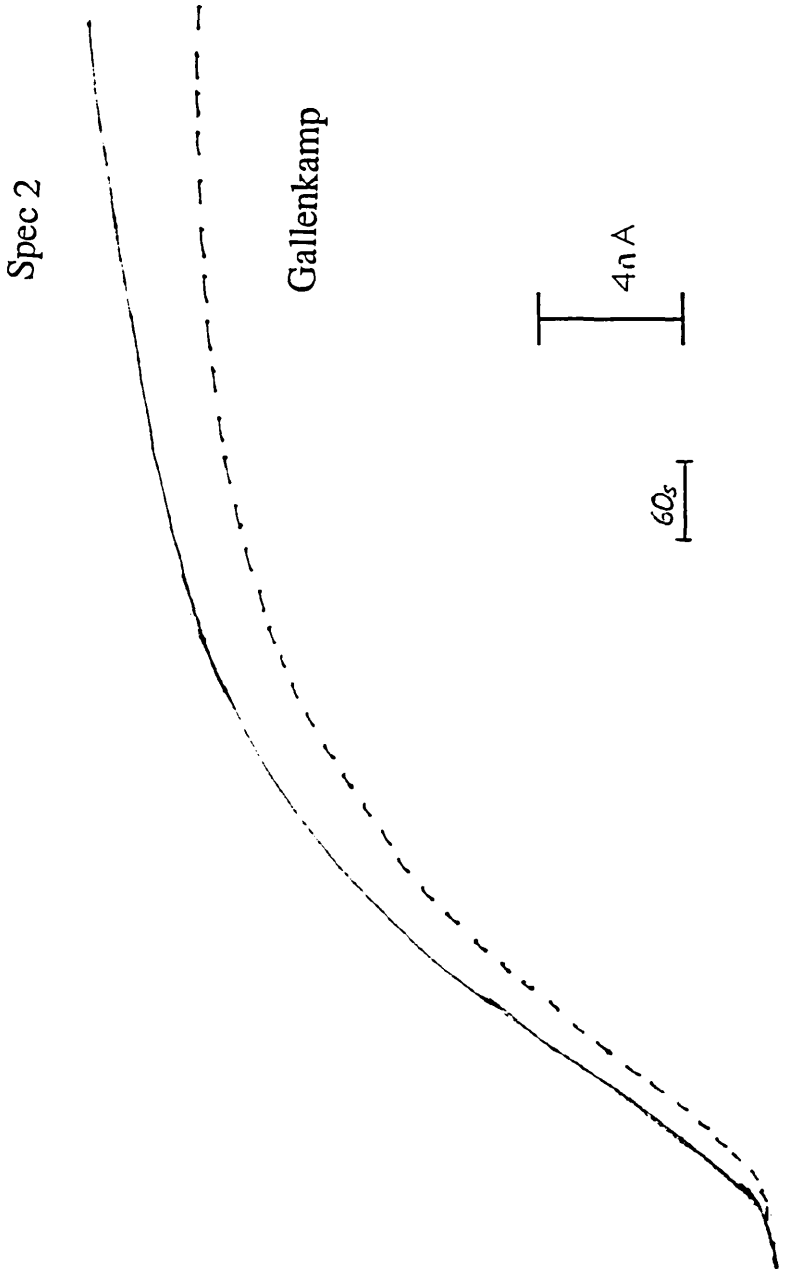

Figure 3.11 Calibration plot using 14 U/ml glucose oxidase

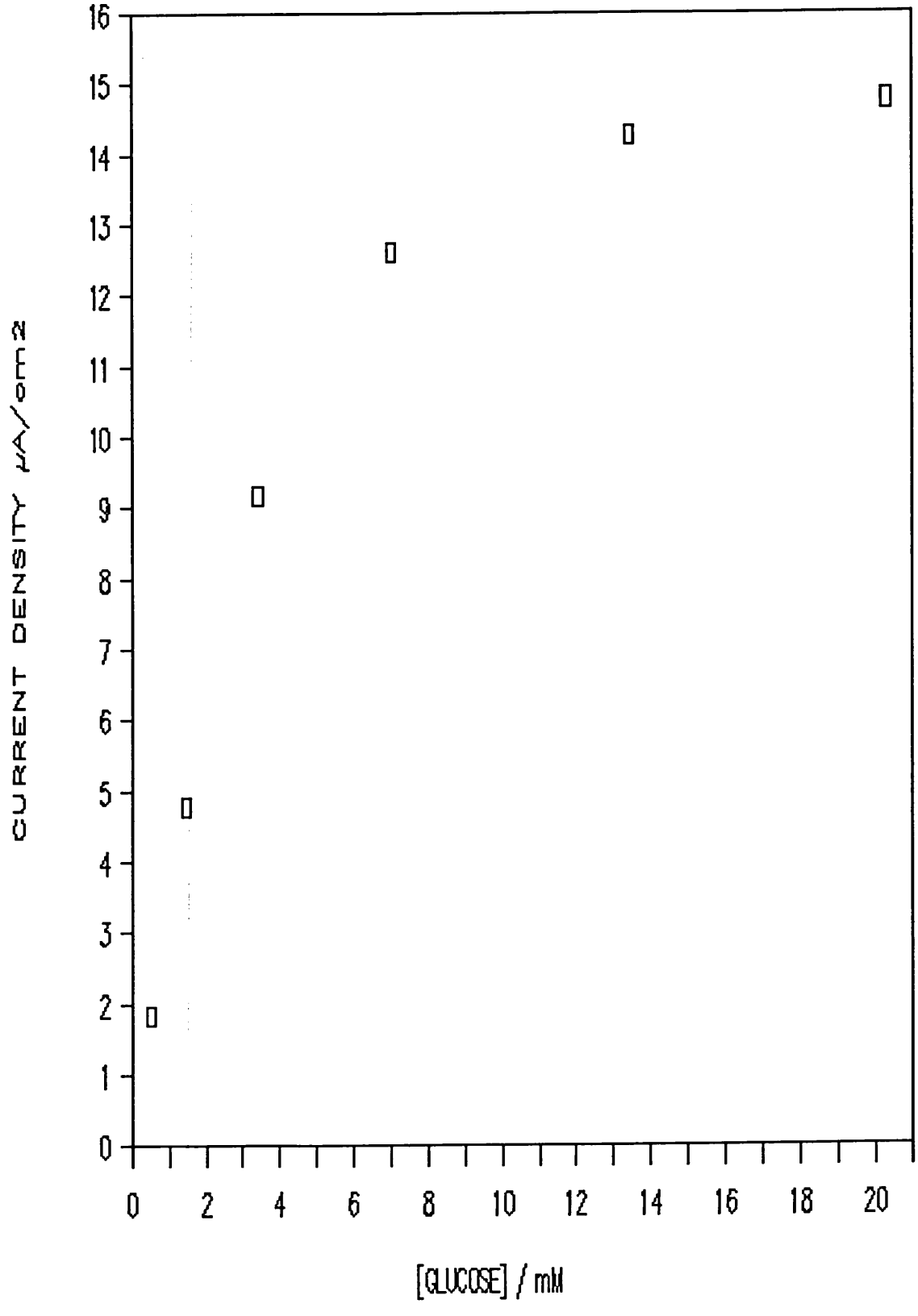

Figure 3.12 Effect on the electrode response of altering the enzyme ratios

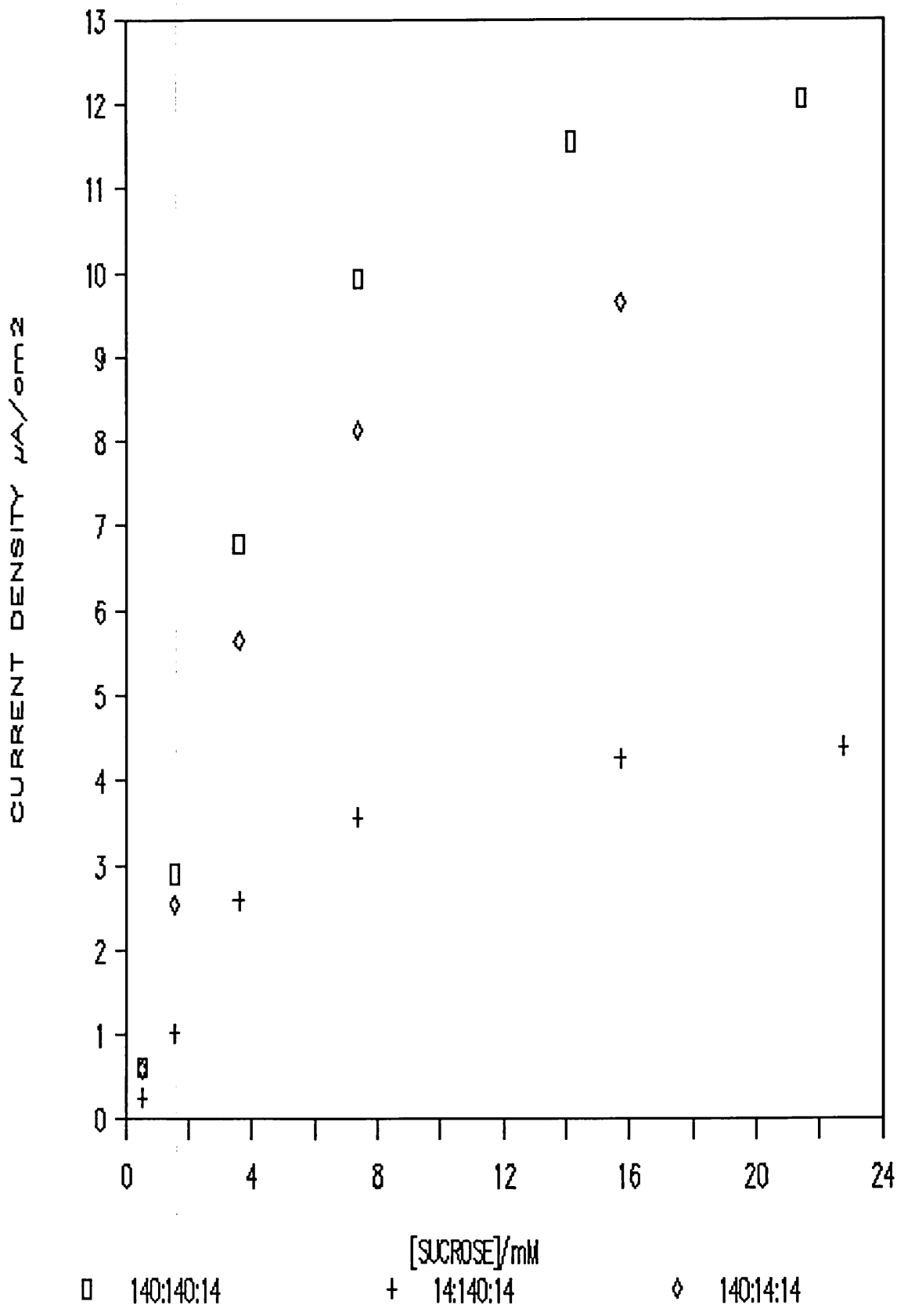

TABLE 3.1

Kinetic parameters for glucose oxidase, mutarotase and invertase

	k_{cat} (s^{-1})	k_{cat}/K_M ($M^{-1}s^{-1}$)
Glucose Oxidase (10)	2.1×10^4	6.4×10^5
Mutarotase (11)	2.5×10^5	1.8×10^7
Inver tase (11)	1.1×10^5	4.3×10^6
Invertase pH=7.4	5.5×10^3	2.1×10^5

The optimum pH for invertase action lies between 3.5 - 5.0 (11). Under more acidic conditions there is a sharp fall-off in enzyme activity whilst on the alkaline side of the optimum range there is a slower decline. Studies of the pH dependence (12-24) have led to the conclusion that the active site contains an unprotonated COO^- group for substrate binding and a protonated histidine residue involved in substrate cleavage. Further work remains to be done to determine the role, if any, of SH- containing cysteine.

Therefore at pH$\simeq$7.4, with the histidine in its unprotonated form, invertase activity is reduced to a mere few per cent, ca.4%, of that seen under optimal conditions (25). Hence the value of the unsaturated rate constant, k_{cat}/K_M , is reduced to $\simeq$ 2 x 10^5 $M^{-1}s^{-1}$ making the hydrolysis of sucrose the rate determining process.

3.3.5. Inhibition by Fructose

Two types of experiments were carried out in order to determine the effect of fructose on the system. The first involved monitoring the response to sucrose in the presence of high ambient fructose concentrations. The second consisted of adding aliquots of fructose to a solution containing a fixed sucrose concentration (8 mM) and observing the decrease in current.

The results (Figures 3.13 and 3.14) clearly illustrate that inhibition by fructose occurs. Thus the system obeys Case 1 rather than Case 2a and exhibits behaviour of the form predicted in eqn. 3.36

$$\frac{1}{j} = \left(\frac{K_S F_o}{K_F E_1 k_a} + \frac{1}{k_S'} \right) \frac{1}{S_\infty}$$

Figure 3.13 Effect on the electrode response of increasing the ambient fructose concentration

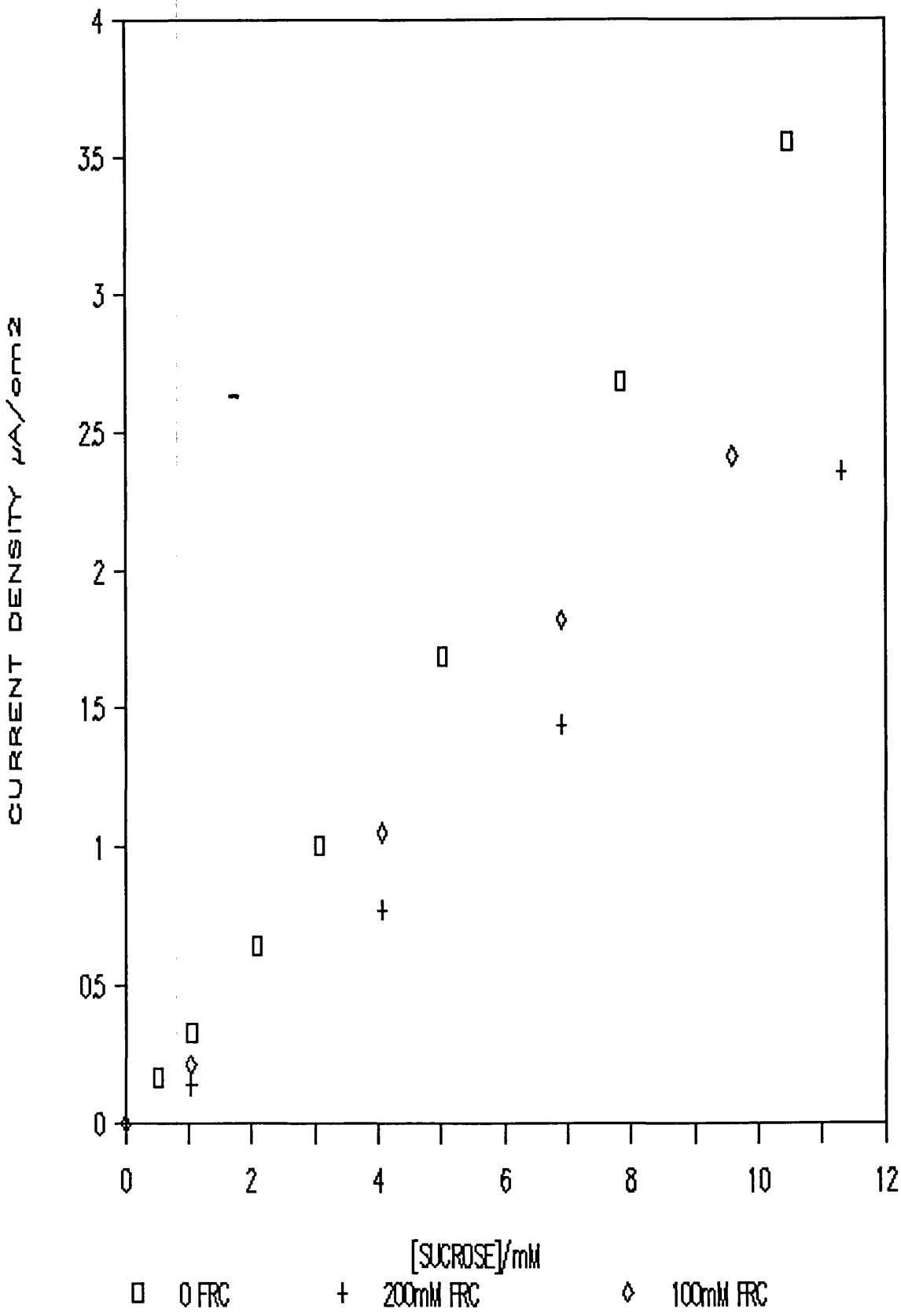

Figure 3.14 Effect of adding fructose to a solution at a fixed sucrose concentration

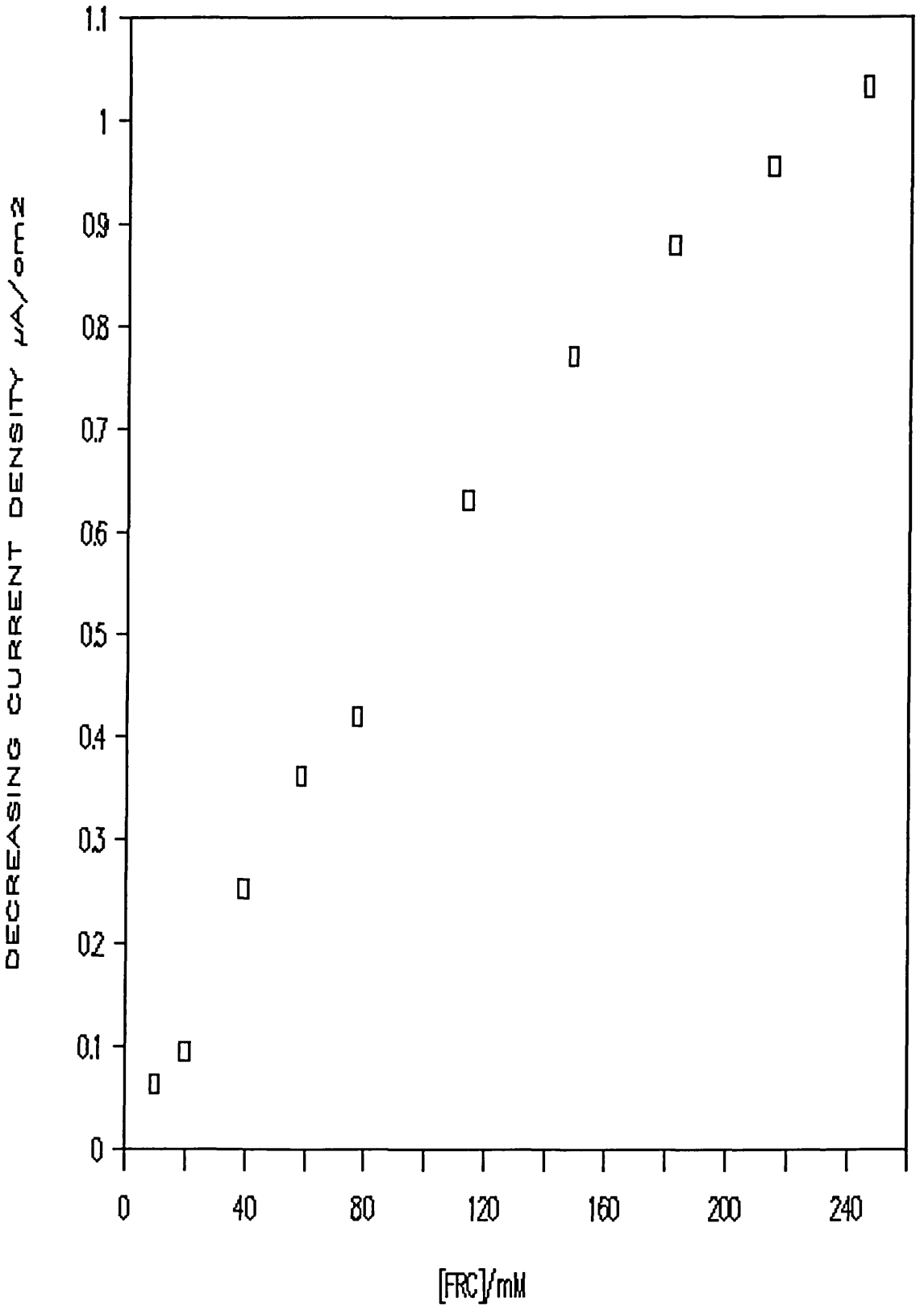

3.3.6. Determining Sucrose Levels in Soft Drinks

Diet Coca-Cola (© Coca Cola Company), which contains an artificial sweetener, aspartame, and purports to contain no sucrose was analysed together with two sucrose containing soft drinks, Pepsi (© Pepsi Inc.) and 7-UP (© Seven-Up International).

A 1971:1987:200 enzyme mixture was used for this series of experiments. In order to investigate whether any poisoning of the electrode occurred, calibration plots (Figure 3.15) were taken before and after the soft drinks had been tested. The response to the respective drinks is shown in Figures 3.16 and 3.17. It is apparent the electrode could distinguish between sucrose and non-sucrose containing soft drinks since the response to Pepsi and Diet Coke differed by over two orders of magnitude. The results showed that Pepsi had a marginally higher sucrose content than 7-Up, 0.5M compared with 0.44M. This corresponds to approximately 160g sucrose per litre of soft drink.

The transients presented in Figure 3.18 show that 90% of the steady state response was reached within 150 s. This compares favourably with the transients obtained in the calibration plot using sucrose.

3.4 DISCUSSION

In summary, the above chapter has detailed the development of an amperometric sensor for measuring sucrose using a TTF-TCNQ electrode. It has been shown that at the pH used in these experiments the electrode response is determined by the kinetics of invertase action. The optimum pH range for invertase lies between 3.5 and 5 but this is precluded from use since the organic salt is unstable below pH 5. A theoretical model has been described which is capable of accounting for the observed inhibition by fructose. The sensor was tested on samples of soft drinks and has shown itself to be capable of distinguishing between those which contain sucrose and those which do not. Exposure to potential contaminants present in these samples did not have a deleterious effect on the

Figure 3.15 Calibration plots showing the electrode response prior to and after testing the soft drink samples

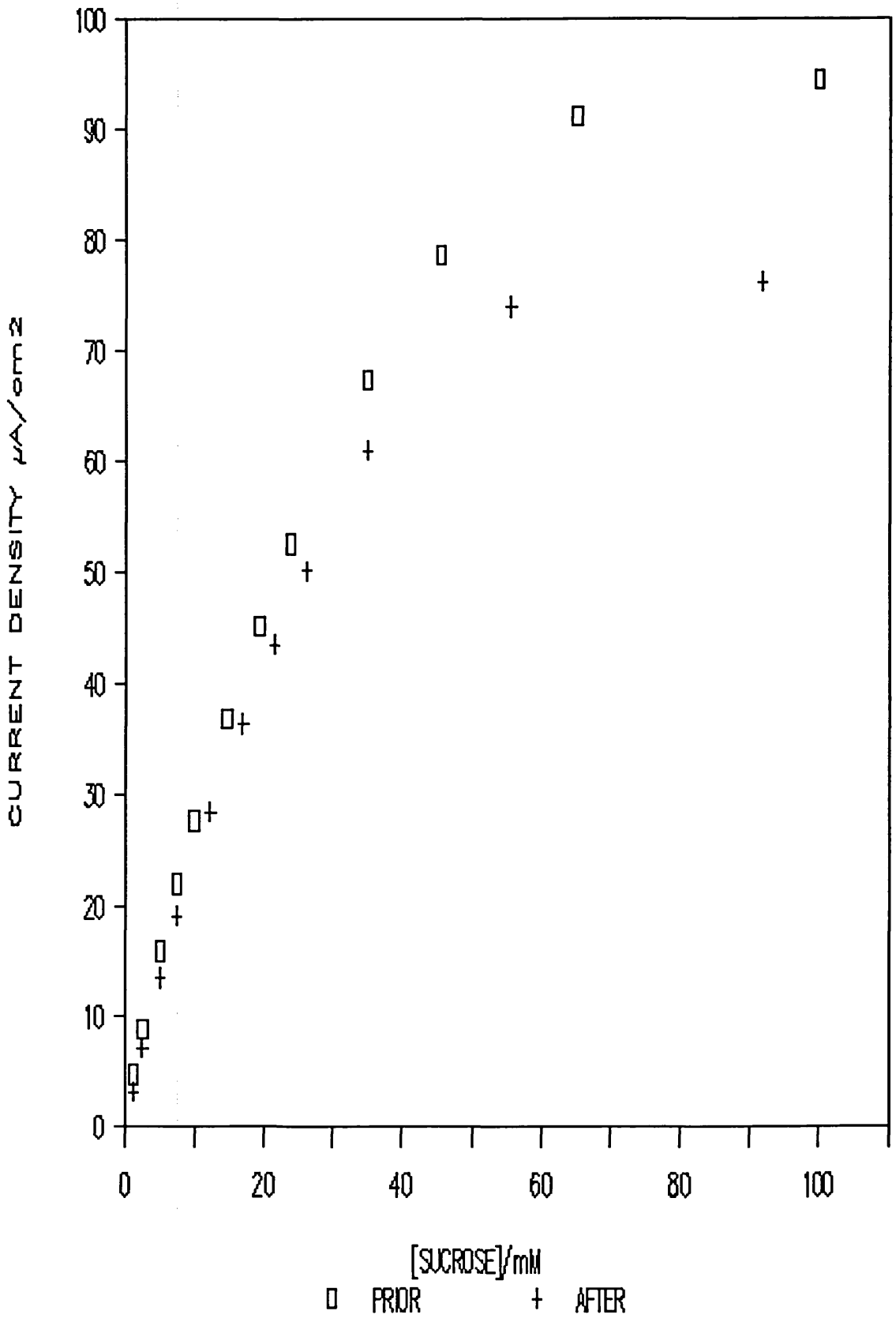

Figure 3.16 Electrode response to aliquots of Pepsi, 7-UP and Diet Coke. Buffer volume = 20 mL.

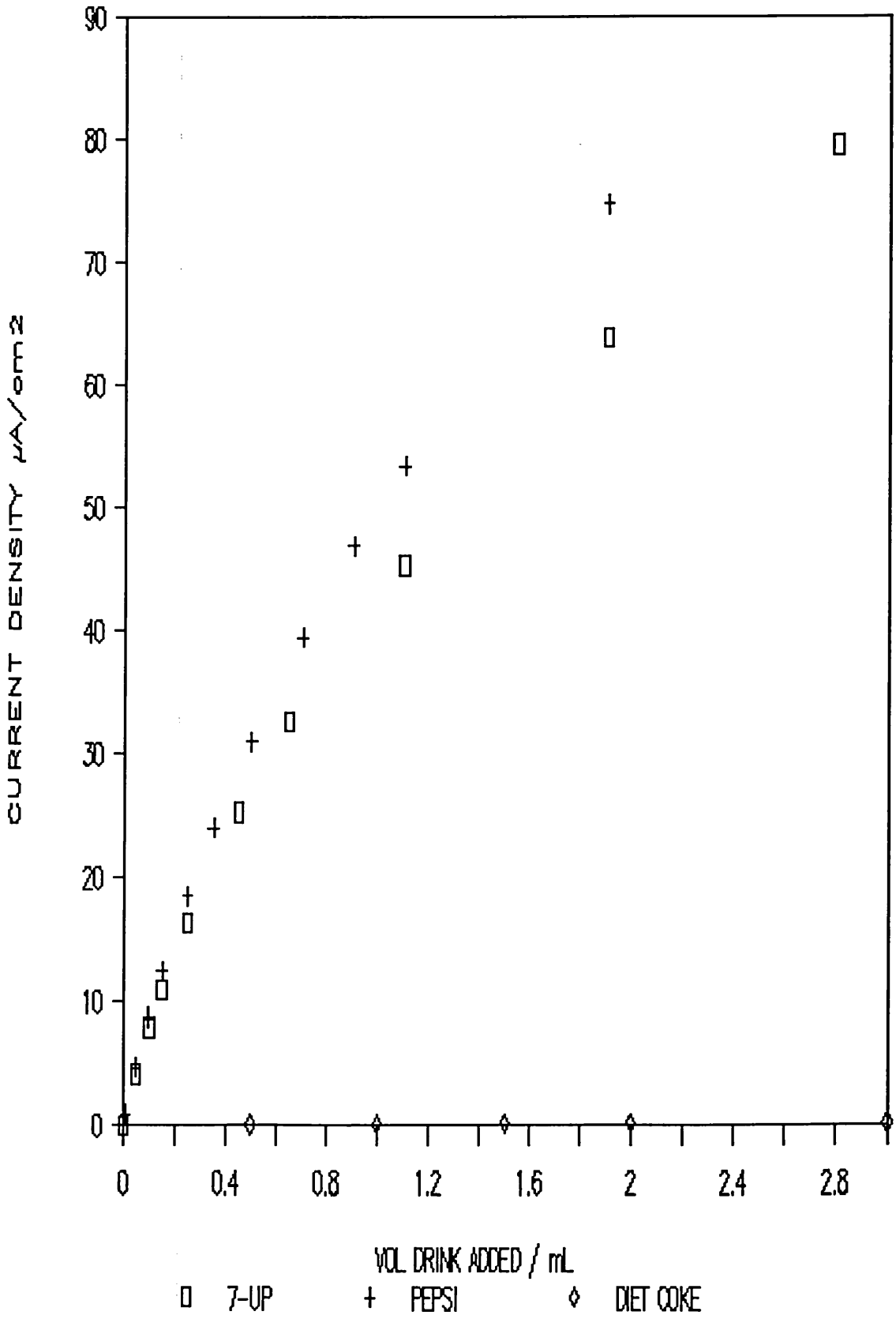

Figure 3.17 Electrode response to Diet Coke

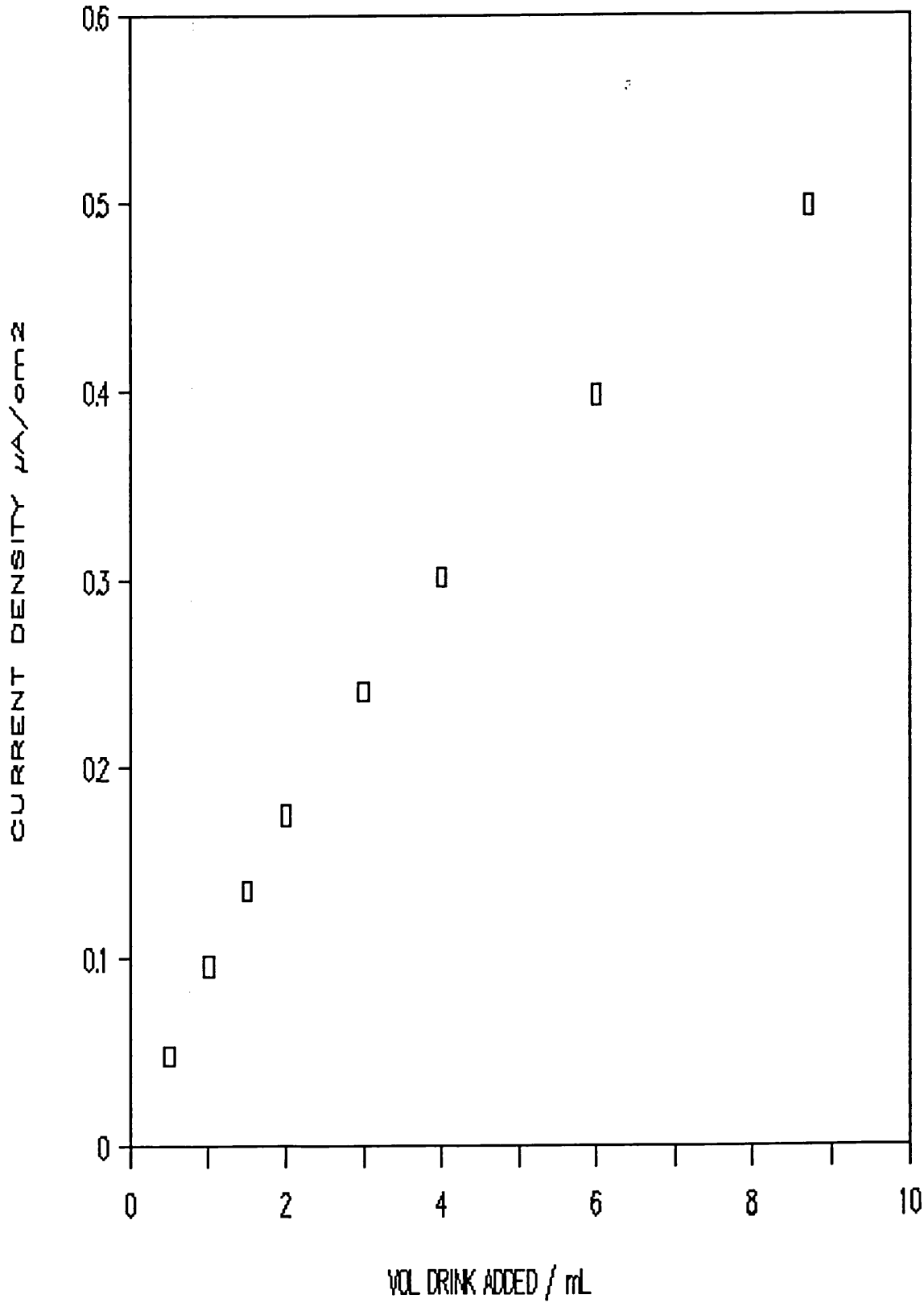

Figure 3.18 Comparing the transient obtained with Pepsi with that from the calibration plot

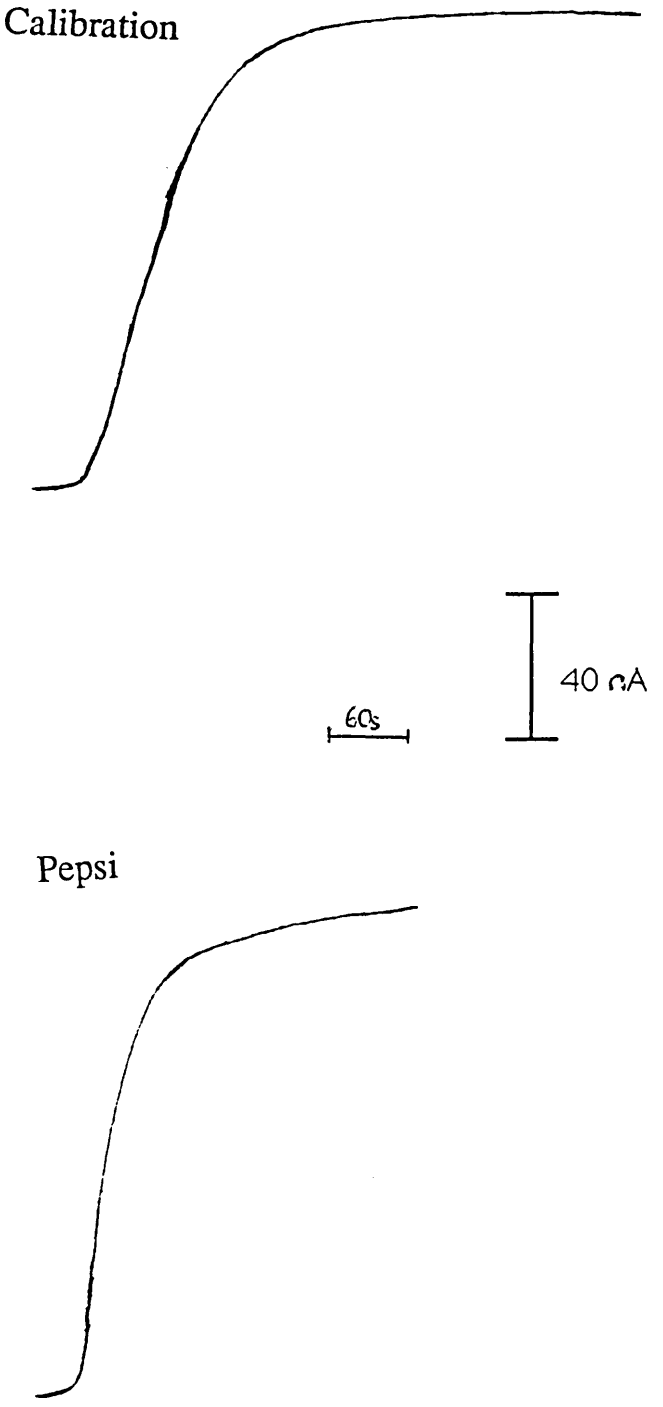

electrode: the response upto 3mM being reproducible to within a few per cent whilst at 9mM the limiting currents differed by approximately 20%. Since none of the enzymes used is prohibitively expensive, it is possible to use high enzyme concentrations behind the membrane and it is suggested that a mixture consisting of invertase, mutarotase and glucose oxidase in the ratio 2000:2000:200U is suitable for detecting sucrose.

REFERENCES

1. L. Macholan and H. Konecna, Collect. Czech. Chem. Commun., 48, 798, (1983)
2. C. Bertrand, P. R. Coulet and D. C. Gautheron, Anal. Chim. Acta., 126, 23, (1981)
3. F. Scheller and Ch. Karsten, Anal. Chim. Acta., 155, 29, (1983)
4. F. Scheller and R. Renneberg, Anal. Chim. Acta., 152, 265, (1983)
5. Y. Xu, G. G. Guilbault and S. S. Kuan, Anal. Chim. Acta., 61, 782, (1989)
6. K. Matsumoto, H. Kamikado, H. Matsubara and Y. Osajima, Anal. Chim. Acta., 60, 147, (1988)
7. C. A. (Koerner) Swindlehurst and T. A. Nieman, Anal. Chim. Acta., 205, 195, (1988)
8. D. Combes and P. Monsan, Carbohydrate Research, 117, 215, (1983)
9. B. J. Driscoll, Ph. D. Thesis, Univ. of Lond., (1988)
10. Biochemica Information, Ed. J. Keesey, Boehringer Mannheim Biochemicals, (1987)
11. H. N. Chang and P. J. Reilly, Biotech. Bioeng., XIX, 923, (1977)
12. C. S. Hudson, J. Amer. Chem. Soc., 32, 1220, (1910)
13. L. Michaelis and H. Davidsohn, Biochem. Z., 35, 386, (1911)
14. R. Kuhn, Z. Physiol. Chem., 125, 28, (1923)
15. K. Myrback, Z. Physiol. Chem., 158, 160, (1926)
16. K. Myrback, Soc. Biol. Chemists, India, Silver Jubilee Souvenir, (1955)
17. K. Myrback and E. Willstaedt, Arkiv Kemi, 15, 379, (1960)
18. K. Myrback, Festschrift Arthur Stoll, p.551, Basel, (1957)
19. K. Myrback, Arkiv. Kemi, 11, 47, (1957)
20. D. Perkins, Biochem. J., 55, 649, (1953)
21. K. Myrback, The Enzymes, 2nd Edn., Vol. 4, p.374, Academic Press, New York, (1960)

22. K. Myrback and E. Willstaedt, Arkiv. Kemi, 13, 179, (1957)

23. S. Shall and A. Waheed, Biochem. J., 111, 33P, (1969)

24. J. O. Lampen, The Enzymes, 3rd Edn., Vol. 5, p.291, Academic Press, New York, (1975)

25. A. Goldstein and J. O. Lampen, Methods Enzymol., 42, 504, (1975)

CHAPTER 4
MECHANISTIC STUDIES USING ROTATING DISK AND RING-DISK TECHNIQUES

This chapter describes an investigation of the mechanism of electron transfer at a TTF-TCNQ electrode using rotating disk and ring-disk techniques. The proposed theories are outlined in the early part of the chapter together with a review of the work done to date on elucidating the nature of the mechanism. A more rigorous mathematical treatment is given in Appendices A, B and C. Initial experiments were done using a pressed pellet TTF-TCNQ disk/Pt-ring electrode. A series of experiments in which the ring potential was swept between +0.8V and −0.5V showed the presence of nucleation phenomena at the Pt-ring electrode. The latter half of the chapter is devoted to examining the nucleation properties of glucose oxidase and other enzyme systems using a Pt-disk electrode.

4.1 AN OVERVIEW

The earliest work was done in the laboratories of J. J. Kulys (1). He determined the second order rate constant for the oxidation of reduced glucose oxidase by NMP, $TCNQ^{\circ}$ and $TCNQ^{-}$ under conditions where the enzyme was saturated. The maximum rate was observed using $TCNQ^{\circ}$ for which a value for the second order rate constant k_m, for oxidation of GOD was $3x10^6$ $M^{-1}s^{-1}$ (2). Kulys proposed that a mediator, M, dissolved from the electrode into the solution and underwent a homogeneous reaction in the solution, with reduced glucose oxidase, $GODH_2$, producing reduced mediator M' which could diffuse away into the bulk or was able to return to the electrode to be reoxidised. In order to account for the currents obtained, Kulys predicted that a mediator concentration of 13.5μM was present. He added that this concentration could be much lower depending on the roughness of the electrode: a rougher electrode implied an increased surface area. An anomaly in Kulys' work was that he used potassium phosphate

buffer and K^+TCNQ^- is virtually insoluble thus making it difficult to justify his result.

In a series of experiments using cytochrome b_2 and peroxidase, Kulys (3) investigated the possible role of adsorption of enzyme on NMP-TCNQ and its effect, if any, on the mechanism. His results showed that the response time of electrodes with preadsorbed enzyme was ten times faster than that of electrodes where adsorption was still an ongoing process. He concluded that an electrocatalytically active complex (EAC) was formed after enzyme adsorption and that its formation was rate limiting.

Craston (4) used rotating Pt-ring/TTF-TCNQ pressed pellet or NMP-TCNQ cavity filled disk electrodes to try and accurately measure the solubility of any TCNQ species present. In each case the surface concentration of the mediator was found to be $< 10^{-7}M^{-1}$. However the solubility experiments were carried out in the absence of enzyme thus ignoring the effects of any solubilisation processes. It was also shown that, assuming the maximum rate for oxidation via $TCNQ^o$ was $3x10^6$ $M^{-1}s^{-1}$ then the predicted limiting current was an order of magnitude less than that actually observed. Thus it was assumed that the mechanism involved direct electron transfer between the enzyme and the electrode.

Experiments by Bartlett (5) using single crystal electrodes gave results which indicated a half-order dependence on enzyme concentration. This could not be explained by a mechanism involving direct electron transfer but was consistent with the Kulys model. However the original objections to that theory remained.

In order to account for the half order behaviour a new theory, heterogeneous redox catalysis, was proposed by Albery and Bartlett (6). This held that there was a surface equilibrium between the organic salt A^+B^- and energetic neutral species A^o and B^o, the former being oxidised by the electrode to A^+ and subsequently recombining with B^-, produced upon oxidation of the reduced enzyme by B^o.

Driscoll (7) studied the dependence of current on enzyme concentration, rotation

speed and electrode potential at high substrate concentrations. He found that the diagnostic plots favoured the homogeneous mediation theory. However the heterogeneous redox model proved superior when it came to accounting for the variation of current with electrode potential. It was capable of providing a qualitative explanation for the observed behaviour but failed when it came to explaining the experimentally determined rate constants. Results obtained using membrane electrodes did not point conclusively to one mechanism or the other. It was concluded that neither theory in its present form could adequately account for the observed behaviour.

Murphy (8) studied the mechanism using a rotating Pt-ring TTF-TCNQ disk electrode. A major flaw in the heterogeneous redox catalysis mechanism was its complete inability to explain the observed first order dependence on substrate. The homogeneous mediation model was also found to give a better explanation of the observed variation of current with electrode potential at all substrate concentrations. The heterogeneous redox model was unable to account for the observed enzyme dependence when this was considered in conjunction with the associated rotation speed behaviour. The potential dependence of the ring current could be accounted for by either model. Qualitatively, the observed collection efficiency followed the homogeneous model but the magnitude was approximately half of the expected value. The results suggested that some form of mediated process was in operation.

Work in the laboratories of Bartlett (9) has shown that glucose oxidase can be modified by the incorporation of electron relays such as TTF-TCNQ, TTF or TCNQ. The modified enzyme was shown to be capable of transferring electrons to a Pt-electrode poised at ca. +400mV (vs. S.C.E.). Modification of the enzyme effectively increases the solubility of neutral mediator species such as $TCNQ^{\circ}$ by providing a hydrophobic environment which enhances the concentration in solution.

4.2 AN INTRODUCTION TO THE THEORIES

The mathematical treatment of both the homogeneous mediation and heterogeneous redox catalysis mechanisms relies on using systems of dimensionless parameters to explain the variation in the flux, j, at an organic salt enzyme electrode. The consistency of case diagrams drawn up using these variables can be tested by deriving expressions for the respective case boundaries and showing that these can be simplified to yield the equations describing the behaviour of the individual cases separated at that particular interface.

4.2.1 Homogeneous Mediation

This can be described by the following equations

$$E + S \longrightarrow E' + P$$

$$E' + M \longrightarrow E + M'$$

$$M' \longrightarrow M$$

The mechanism (Figure 4.1) deals with an enzyme electrode where electron transfer between the reduced enzyme, E', and the electrode is facilitated by a mediator, M, reacting homogeneously in solution. The second order differential equations describing the diffusion and reaction kinetics of the enzyme and the mediator in the electrode diffusion layer are solved in terms of dimensionless variables. The boundary conditions lead to seven different cases with eleven case boundaries. The parameter $(\partial u/\partial \chi)_o$ (eqn. A.21) is found for each case and by substitution of this in eqn. A.20 gives an expression for the flux in that case.

The original model was depicted in a three-dimensional case diagram in which the axes were identified with the probability of E reacting with S in the diffusion layer, $\log \kappa_E$, the probability of E' reacting with M in the diffusion layer, $\log \kappa_M$ and $\log \gamma$, a parameter describing the interplay between κ_E and κ_M

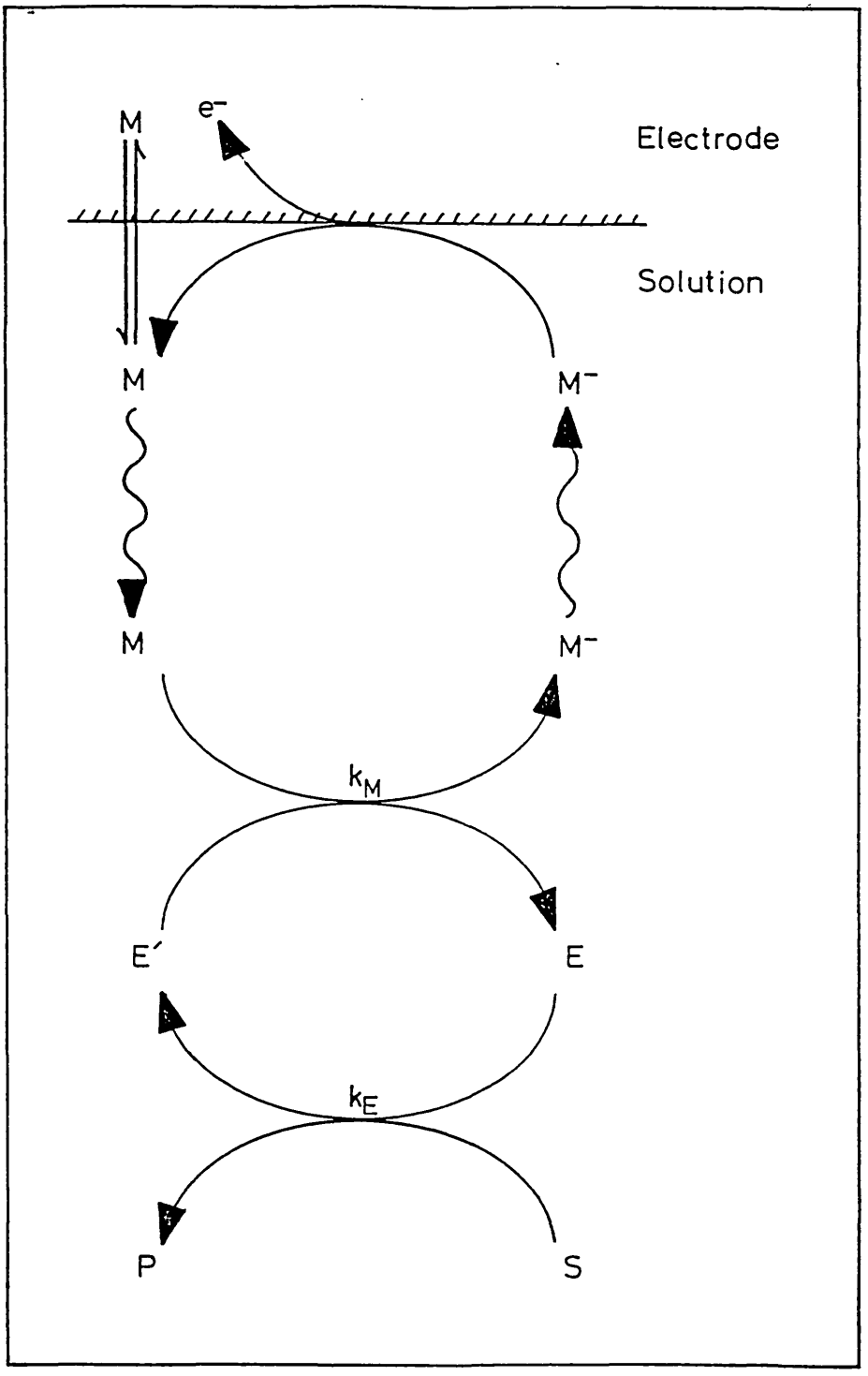

Figure 4.1 The scheme for the homogeneous mediation mechanism

$$\kappa_E = \frac{k_E Z_D^2}{D_E} \qquad 4.1$$

$$\kappa_M = \frac{k_M e_\Sigma Z_D^2}{D_M} \qquad 4.2$$

$$\gamma = \frac{k_M m_o}{k_E} \qquad 4.3$$

In order to ease interpretation, the case diagram was redrawn (Figure 4.2) using a new set of axes, log $(1/\gamma)$, log β and log ϕ, where

$$\frac{1}{\gamma} = \frac{k_E}{k_M m_o} \qquad 4.4$$

$$\beta = \frac{D_E e_\Sigma}{D_M m_o} \qquad 4.5$$

$$\phi = \frac{Z_D^2 k_M m_o}{D_E} \qquad 4.6$$

Now a change in [S], as reflected by a change in k_E, would produce a shift parallel to the $1/\gamma$ axis whereas previously a change in [S] meant a diagonal translation through a series of horizontal planes in the three-dimensional representation. The "new" parameters are related to the old ones as follows

$$\gamma\kappa_E = \phi \quad \text{and} \quad \kappa_M = \phi\beta$$

4.2.2 Heterogeneous Redox Catalysis

This mechanism (Figure 4.3) proposes that the organic salt A^+B^- exists in a labile equilibrium with energetic neutral species A° and B°. The latter oxidises the reduced enzyme E', generating B^- which combines with A^+, formed by oxidation of A° at the electrode, to produce A^+B^-. The behaviour of the system depends on the relative

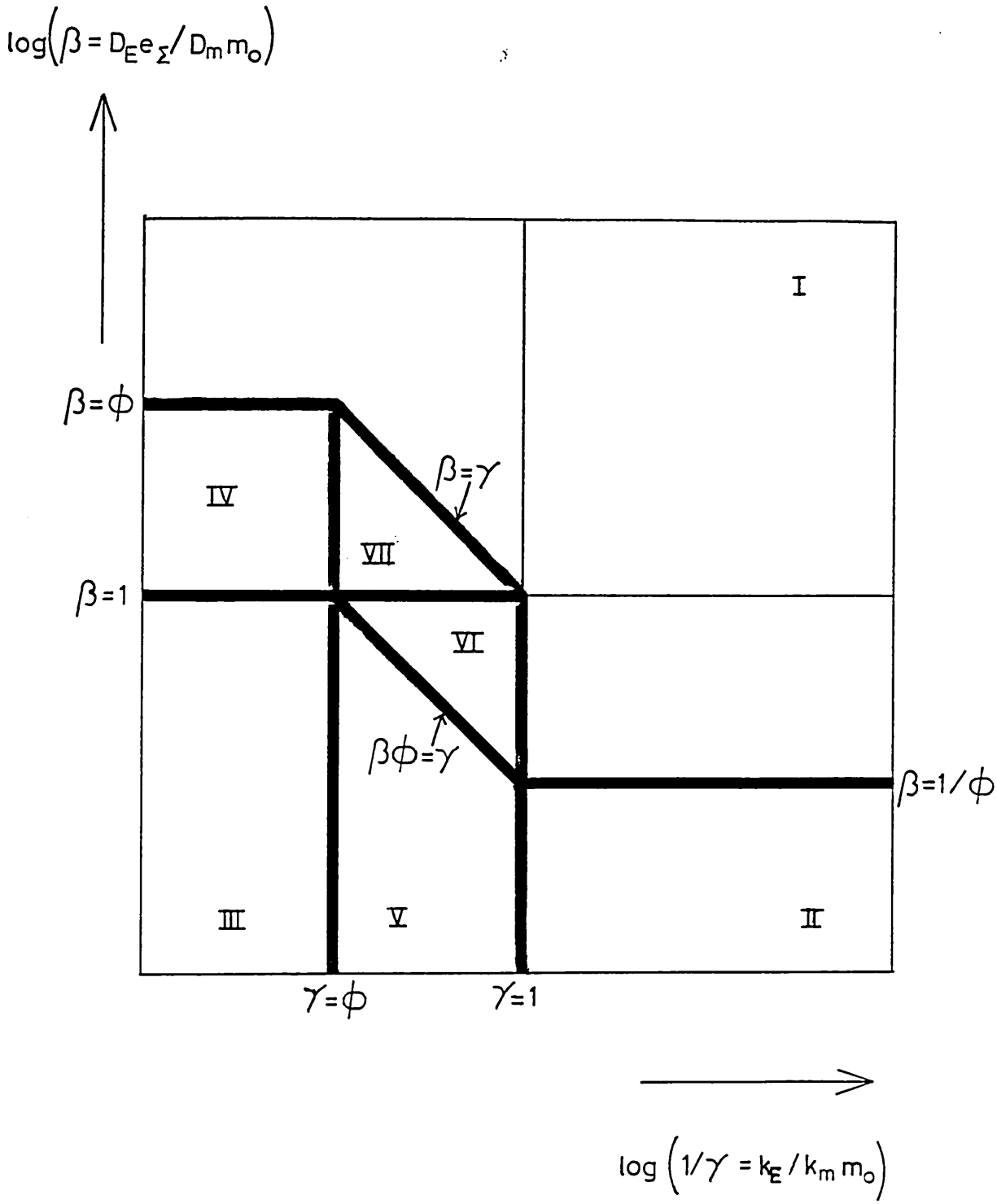

Figure 4.2 The scheme for the 2-D representation of the homogeneous mediation mechanism

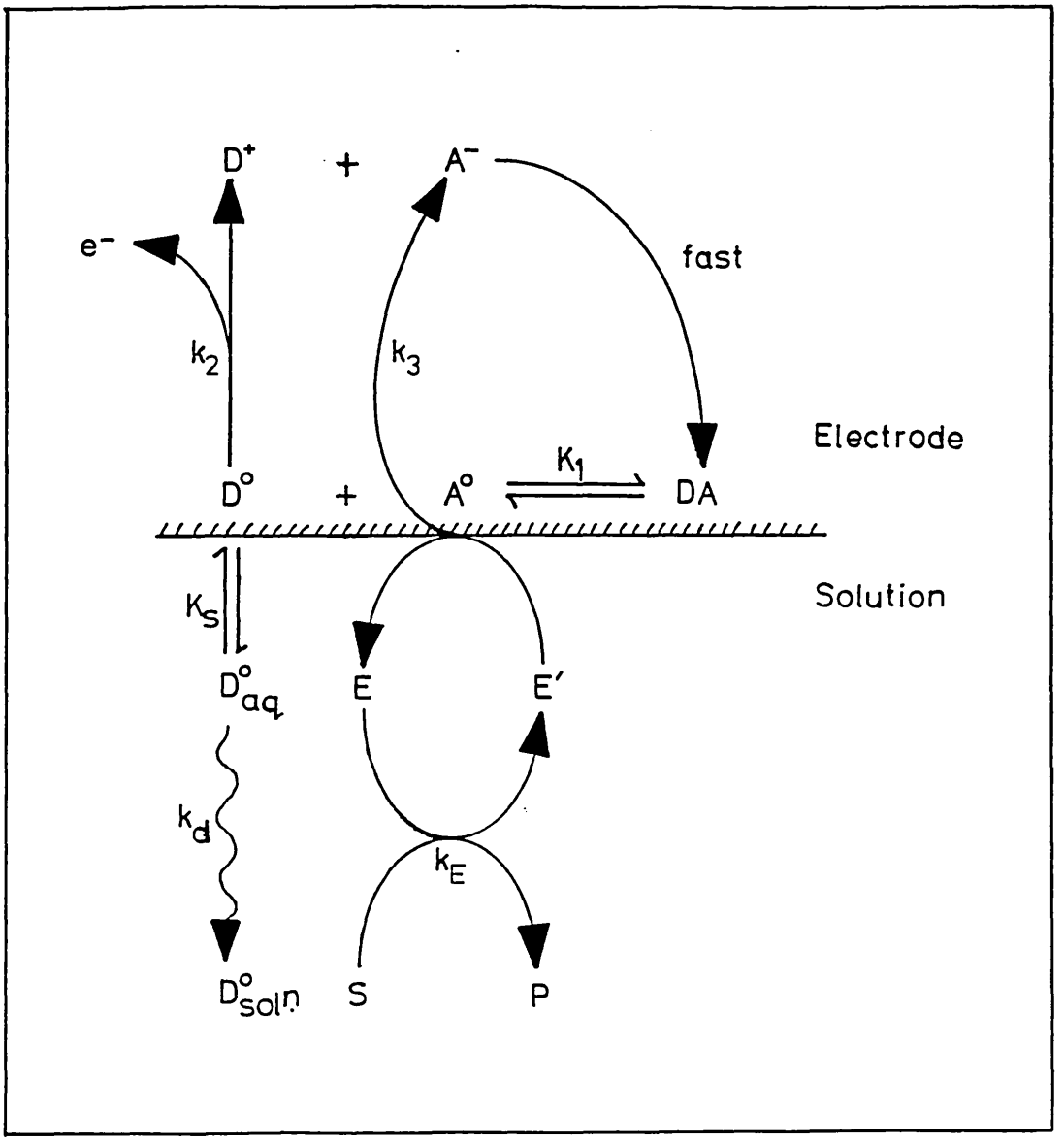

Figure 4.3 The scheme for the heterogeneous redox catalysis mechanism

rates of the surface kinetics, enzyme regeneration and transport of the enzyme to the electrode. On applying the boundary conditions and solving the master equation (eqn. B22) three cases are obtained. Their number increases to six upon considering the effects of θ, a parameter which compares the rate oxidation of A° with its rate of dissolution from the electrode.

4.3 EXPERIMENTAL

4.3.1 Chemicals and Solutions

All solutions were prepared as in §2.1.1

4.3.2 Enzyme Preparations

All enzyme preparations were purchased from Sigma unless otherwise indicated (Table 4.1). Modified enzyme was prepared by stirring a solution of glucose oxidase with one of the mediators TTFTCNQ, TTF or TCNQ for 2-3 hours followed by filtration. The filtrate was left to dialyse for 48 hours using 0.1M phosphate/0.15M NaCl buffer. The solution was changed after 24hrs.

4.3.3 Electrodes

TTF-TCNQ was prepared according to the literature (10). The polystyrene (PST)/salt electrode was prepared according to §2.1.3. The Silicone-oil/salt electrode was prepared by mixing a drop of Si-oil with the salt to obtain a thick almost dry paste which was inserted into the electrode cavity. The pressed pellet electrode consisted of a 7mm diameter TTFTCNQ disk, fabricated using a pressure of 9×10^8 N m^{-2}, surrounded by a Pt-ring with an internal diameter of 7.5 mm and an outer diameter of 8 mm . No binder was used in this electrode. A 5 mm glassy carbon electrode was used for the Nicholson/Shain experiment. Electrodes were poised at +300 mV (S.C.E.) unless indicated otherwise.

TABLE 4.1

Commercially available enzyme preparations

ENZYME	EC NUMBER	SIGMA	SOURCE
Glucose Oxidase	1.1.3.4	G 7016	*Aspergillus niger*
Sarcosine Oxidase	1.5.3.1	S 8764	*Arthrobacter*
Choline Oxidase	1.1.3.17	C 4405	*Arthrobacter globiformis*
Alcohol Oxidase	1.1.3.13	A 2404	*Pichia pastoris*
Xanthine Oxidase	1.1.3.22	X 4500	*Buttermilk suspension*
Sulfite Oxidase	1.8.3.1	S 0263	*Chicken liver*

4.3.4 Electronics

The same apparatus was used as in §2.1.4

4.3.5 Experimental Procedures

Standard techniques were followed. All experiments were carried out in an Atmos bag (Aldrich) using an inert argon atmosphere. Solutions were degassed throughout using either argon or nitrogen. Nucleation experiments were performed at a scan rate of 20 mV/s unless indicated otherwise.

4.4 RESULTS

4.4.1 Nicholson - Shain determination of k_m for TTF^+ / $GODH_2$

The theory of stationary electrode polarography developed by Nicholson and Shain (17) was used to evaluate the second order rate constant k_M for the oxidation of $GODH_2$ by TTF^+. The system was considered as a catalytic reaction with reversible charge transfer Case VII (17) of the form

$$O + ne \rightleftharpoons R$$

$$O + Z \longrightarrow R$$

Nicholson and Shain extended the theory developed by Saveant and Vianello (18). First they solved the differential equations for simple systems in the absence of any chemical reaction. They tabulated their results in the form of a current function in terms of dimensionless variables Table I (17). Next they considered specific types of chemical reaction which could be occurring in solution. Again they created a series of current functions Table XII (17) from which a working curve representing the ratio of the kinetic to the diffusion currents, i_k/i_d, could be constructed. The precise nature of the working curve would vary according to $(E - E_{1/2})n$ where $E_{1/2}$ is the half-wave potential. The diffusion current i_d is given

Figure 4.4 Cyclic voltammograms at 5 mV/s of a) TTF^+Cl^-/GOD and b) on addition of 165 mM glucose . [TTF+Cl] = 50μM.

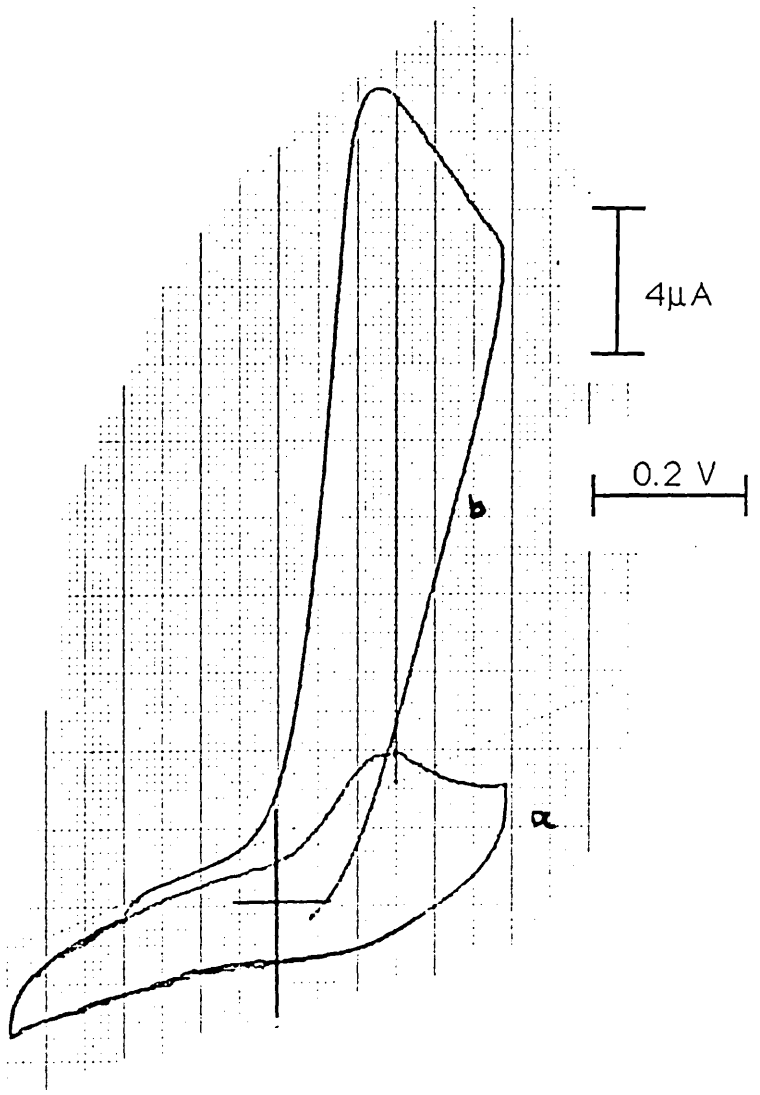

Figure 4.5 Plot of k_f against $1/\nu$

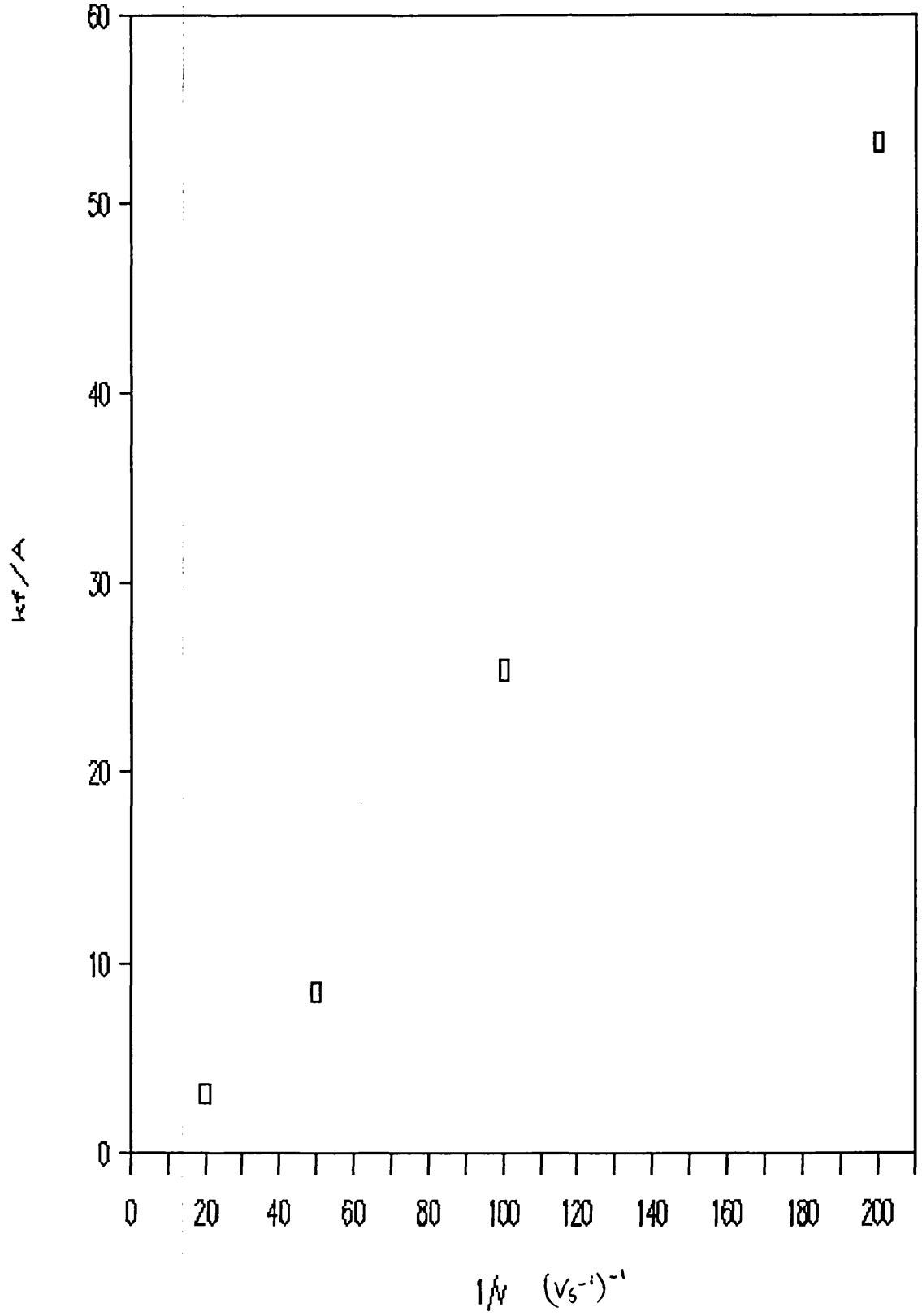

$$i_d = nFAC_o^* \sqrt{\pi D_o a}\ \chi(at) \qquad 6.1$$

where and the kinetic current, i_k, in the case of a catalytic system by

$$i_k = nFAC_o^* \sqrt{\pi D_o k_f}\ \chi'(at) \qquad 6.2$$

Experimentally a series of cyclic voltammograms were taken of TTF^+Cl^- in the presence of GOD but in the absence of the glucose to obtain i_d at a number of different scan rates. The process was then repeated after addition of glucose to evaluate i_k at each scan rate (Figure 4.4). From the working curve values of $(k_f/a)^{1/2}$ are obtained corresponding to the i_k/i_d ratios found by experiment, k_f being a pseudo first order rate constant. From a plot of k_f vs. $1/\nu$ (Figure 4.5) it is possible to evaluate the second order rate constant k_M since

$$k_f = k_M [\ FAD\ ] \qquad 6.3$$

where [FAD] is 2[GOD] since there are two FAD groups per molecule of enzyme. Assuming that the protein was 100% active a value of $3.8 \pm 0.8 \times 10^6\ M^{-1}s^{-1}$ was obtained which is in close accord with that found by Kulys for $TCNQ^\circ$ (2). After obtaining a more accurate measure of the enzyme concentration by spectrophotometric methods this value was amended to give $4.2 \pm 0.8 \times 10^6\ M^{-1}s^{-1}$. Thus both TTF^+ and $TCNQ^\circ$ are capable of oxidising reduced glucose oxidase at relatively fast rates.

4.4.2 Comparison of Rotation Speed Behaviour

4.4.2.1 Unmodified GOD

To date mechanistic studies investigating the rotation speed dependence of the biocatalytic current used either pressed pellet or Si-oil electrodes (4,7,8). In both cases an inverse relationship between the current and the rotation speed was observed. An investigation of the behaviour at PST electrodes was undertaken and the results compared with those from Si-oil and pressed pellet electrodes.

The results are shown in Figures 4.6-4.8. It is apparent that whilst Si-oil and pressed pellet electrodes show an inverse rotation speed dependence the converse is true

Figure 4.6 Rotation speed dependence of a TTF-TCNQ / polystyrene electrode [GOD] ≈ 100 U/ml

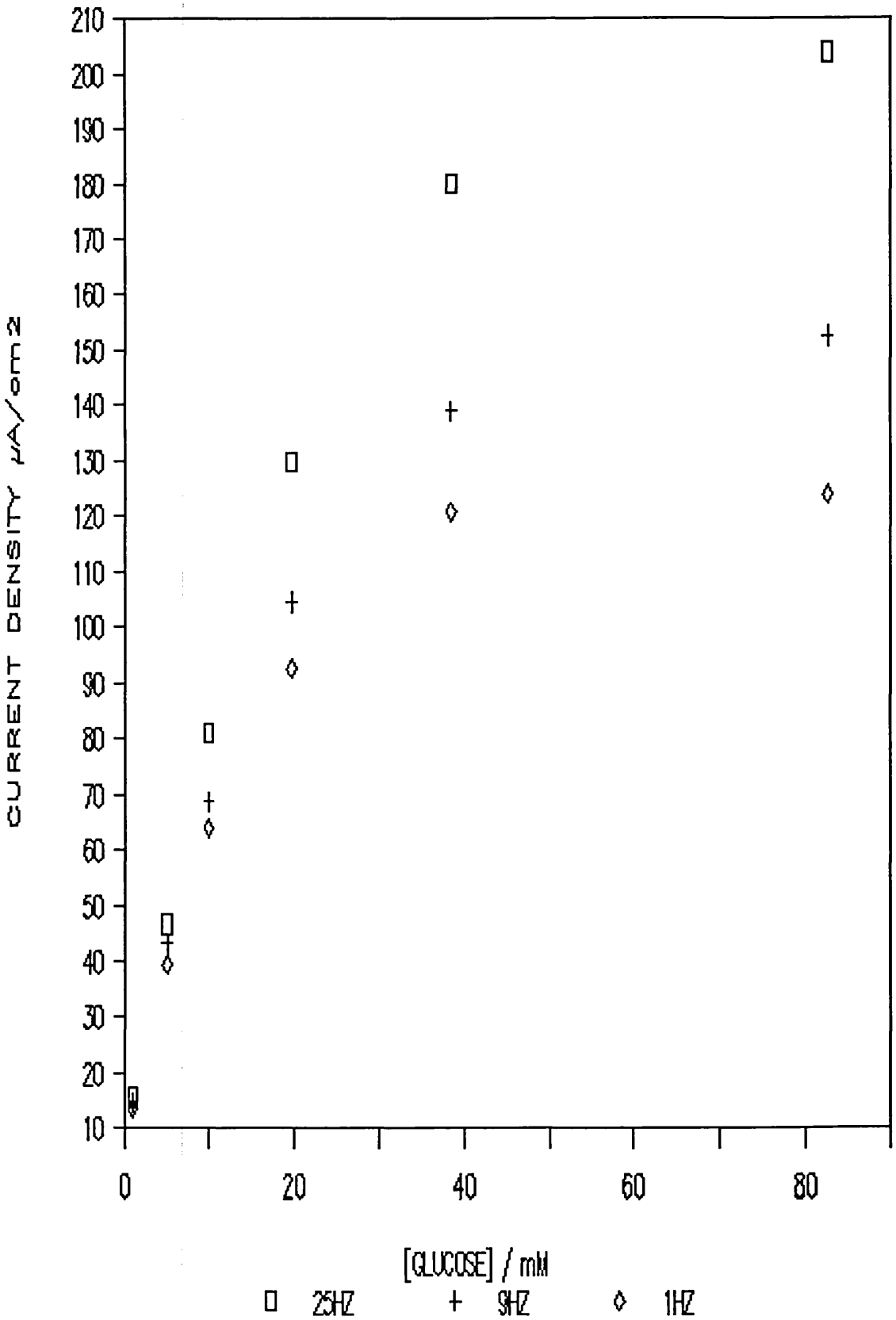

Figure 4.7 Rotation speed dependence of a TTF-TCNQ / silicone oil electrode . [GOD] = 100 U/ml.

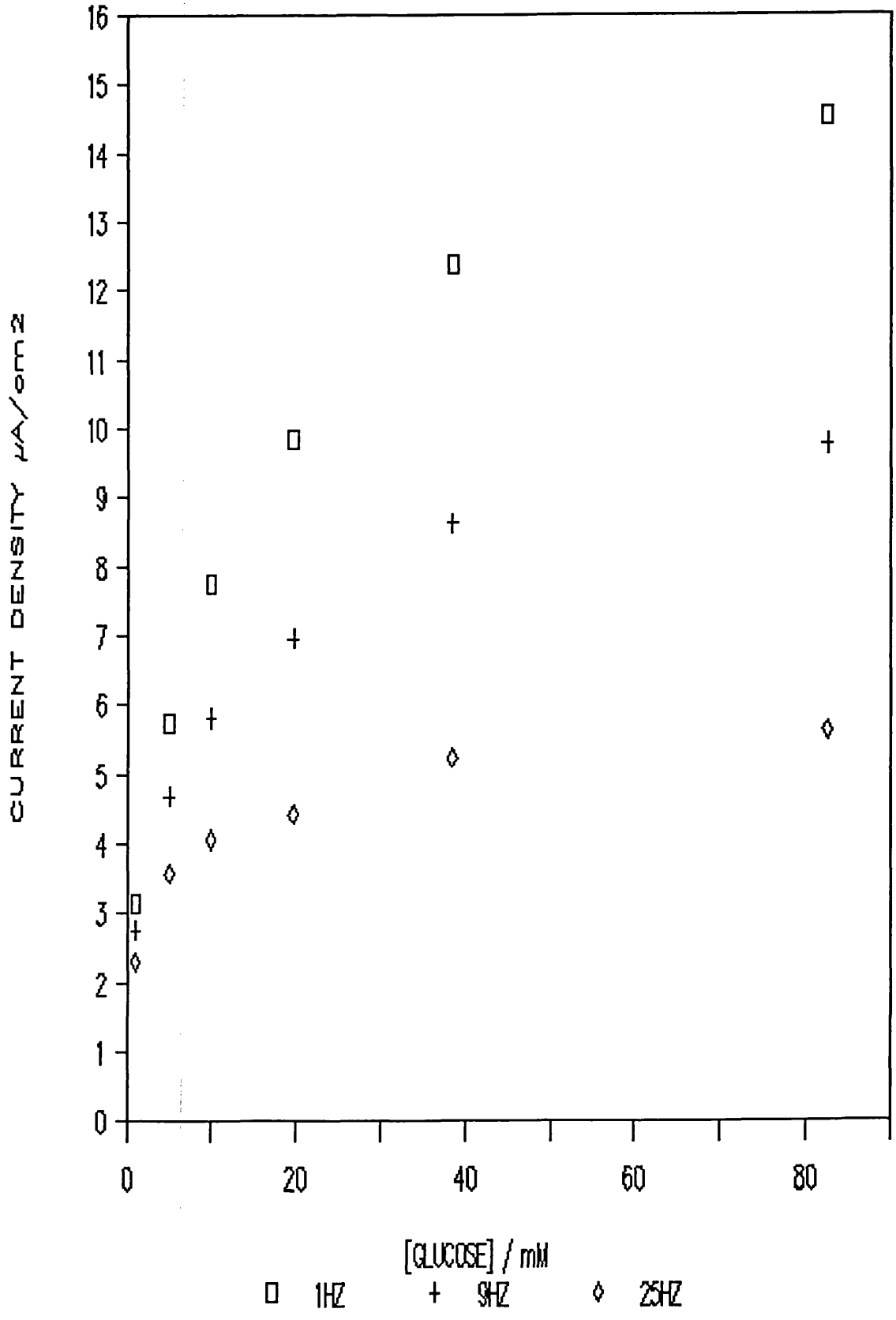

Figure 4.8 Rotation speed dependence of a pressed pellet TTF-TCNQ electrode. [GOD] = 100 U/ml

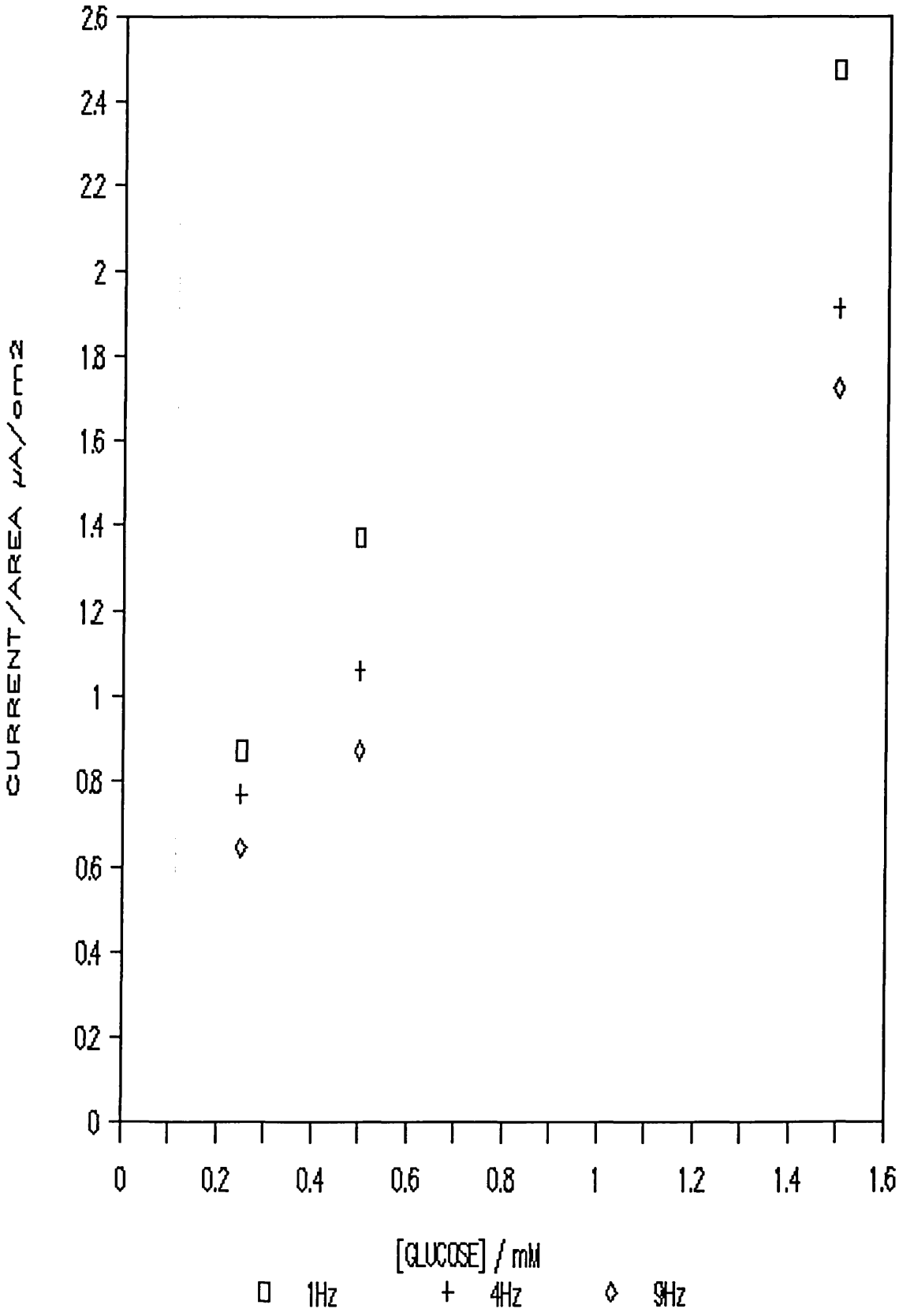

for electrodes made with PST binder. This implies that the method of fabrication might influence the nature of the mechanism.

Murphy (8) examined the electrode surface of polymer (PST and PVC) paste, Si-oil and pressed pellet electrodes using scanning electron microscopy. The results showed that electrodes which gave "good" results had very rough surfaces whilst "poor" electrodes had a preponderance of binder at the surface with far fewer organic salt crystals visible. Both PST and Si-oil electrodes were found to have very rough surfaces as compared to pressed pellet electrodes and gave correspondingly higher saturation currents. At high rotation speeds the lack of a binder meant that Si-oil electrodes started to corrode and eventually disintegrate into the solution. Thus although the chemical potential of a TTF-TCNQ crystal will be the same in both PST and Si-oil electrodes the supporting material may affect the rate with which a mediator can enter the solution to facilitate homogeneous mediation or its rate of reaction with enzyme on the electrode surface. Hence the rate limiting process at polymer paste and Si-oil electrodes might be different owing to the former's more robust nature. As mentioned above pressed pellet electrodes contain no binder but are held together by the pressure used in their fabrication and ring disk studies have shown that they corrode steadily (vide infra).

The results obtained in these laboratories suggesting that the order of increasing saturation current is : pressed pellet < Si-oil < polymer binder appear to contradict those of Brajter-Toth and co-workers (11). They consider organic salt electrodes as systems of ultramicroelectrode crystal arrays and propose that electrodes made using high pressure techniques have a reduced inactive area and hence produce a higher current than either PST or Si-oil electrodes.

The current obtained with the polystyrene electrode was greater than that found with the Si-oil electrode. This is in accord with previous work in these laboratories (4,7,8) and has traditionally been attributed to the greater porosity of the polystyrene electrode with the concomitant increase in surface area.

Under the conditions used in these experiments (assuming a homogeneous mechanism) it has been shown (8) that the system is initially in either Case V or VI at low [glc], crossing into Case II or I as the [glc] is increased. In Case V the rate is determined by the regeneration of E' at the edge of the diffusion layer; in Case VI it is governed by the regeneration of E' in a zero-order reaction layer, again away from the electrode surface. In Case II the rate limiting process is the reaction of E' and M, again in the diffusion layer. Since all possible mediator species are only sparingly soluble, the increased surface area of a PST electrode can have no bearing on reactions occurring in the diffusion layer and the current due to any homogeneous processes should be the same at both electrodes. Hence the mechanism of electron transfer at a PST electrode must be different from that at a Si-oil electrode.

In Case I the reaction between E' and M occurs in a reaction layer close to the electrode surface. The boundary between Case I and II occurs when $\kappa_M=1$, hence

$$\frac{k_M Z_D^2 e_\Sigma}{D_M} = 1$$

thus the reaction layer thickness, χ_M, is equal to the thickness of the diffusion layer, Z_D.

$$\chi_M = \sqrt{\frac{D_M}{k_M e_\Sigma}} \qquad 4.7$$

Murphy (8) showed, using an Si-oil electrode, that this boundary was reached with 5 U/mL GOD. Since the experiments described above used 100 U/mL GOD, thus χ_M is approximately $Z_D/4.5$ and Z_D is given by

$$Z_D = 0.643\, \nu^{1/6} D_M^{1/3} \omega^{-1/2} \qquad 4.8$$

then at 1 Hz, $\chi_M=12\mu$m and at 9Hz, $\chi_M=4\mu$m. This is comparable to the intercrystal spacing (8). However if the homogeneous mechanism was in operation and assuming a surface roughness factor, R, then passing into Case I the current should increase by a factor of R at a PST electrode as compared to that at a Si-oil electrode since the increased surface area extends the "length" of the reaction layer. Since this was not

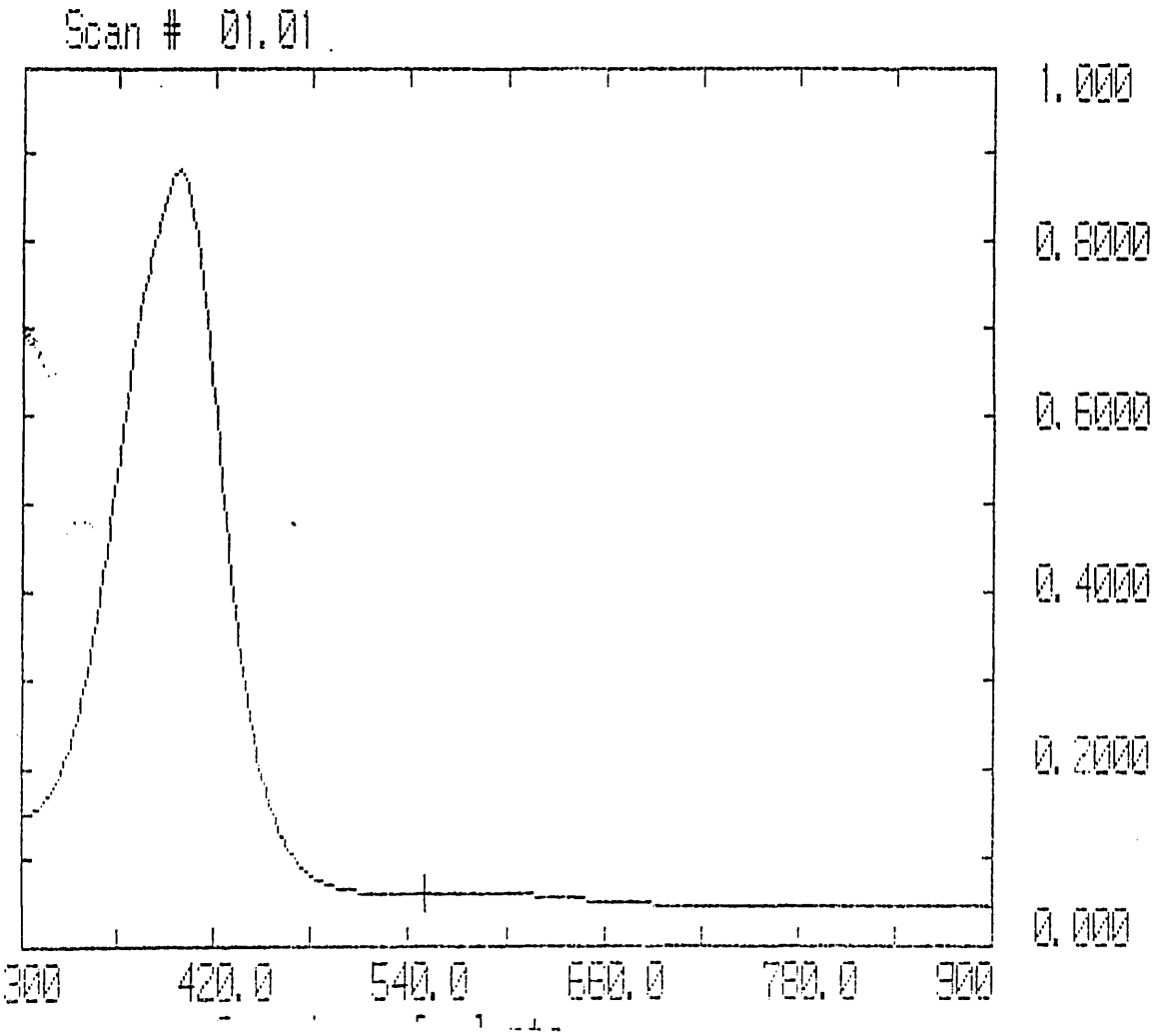

Figure 4.9 UV/Vis spectrum of TTF-TCNQ solubilised in silicone oil

observed it provides further evidence that the homogeneous mechanism does not apply at PST electrodes.

A suspension of TTF-TCNQ in Si-oil was stirred vigorously for 48hrs after which it was centrifuged. The supernatant had a pale green hue. Its UV/Vis spectrum is shown in Figure 4.9, with a peak at 396nm. From a control experiment using a known concentration of TTF-TCNQ in CH_2Cl_2 the extinction coefficient at 399nm, ϵ_{399}, was calculated to be 96000 $M^{-1}cm^{-1}$. Assuming the extinction coefficient has the same value in the two media then approximately 9μM TTF-TCNQ was dissolved in the Si-oil. Thus it is possible that a film of Si-oil at the electrode/solution interface containing dissolved TTF-TCNQ might set up a biphasic system thus complicating electron transfer. The different properties of Si-oil and polystyrene electrodes are explored further in the next chapter using a.c. techniques.

4.4.2.2 Modified Enzyme

Glucose oxidase was modified using TTF in order to investigate the role, if any, of enzyme modification on the observed rotation speed dependence.

The polystyrene paste electrode shows positive rotation speed dependence up to a [glc] of 15mM at which point a switchover to inverse behaviour occurs (Figure 4.10). In the case of the Si-oil electrode, inverse rotation speed behaviour is observed throughout (Figure 4.11). From the Si-oil data it would appear that the modification process is not itself rate limiting.

4.4.3 Rotating Ring-Disk Behaviour

4.4.3.1 Ring Potential at -200 mV

In order to investigate whether species oxidised at the TTF-TCNQ disk could be detected at the Pt-ring the latter was poised at -200 mV.

The homogeneous theory predicts that M can diffuse away from the disk and is capable of being swept out to the ring depending on the particular case in question. For

Figure 4.10 Rotation speed dependence of a TTF-TCNQ / polystyrene electrode using glucose oxidase modified by TTF°. [GOD] ≈ 100 U/ml

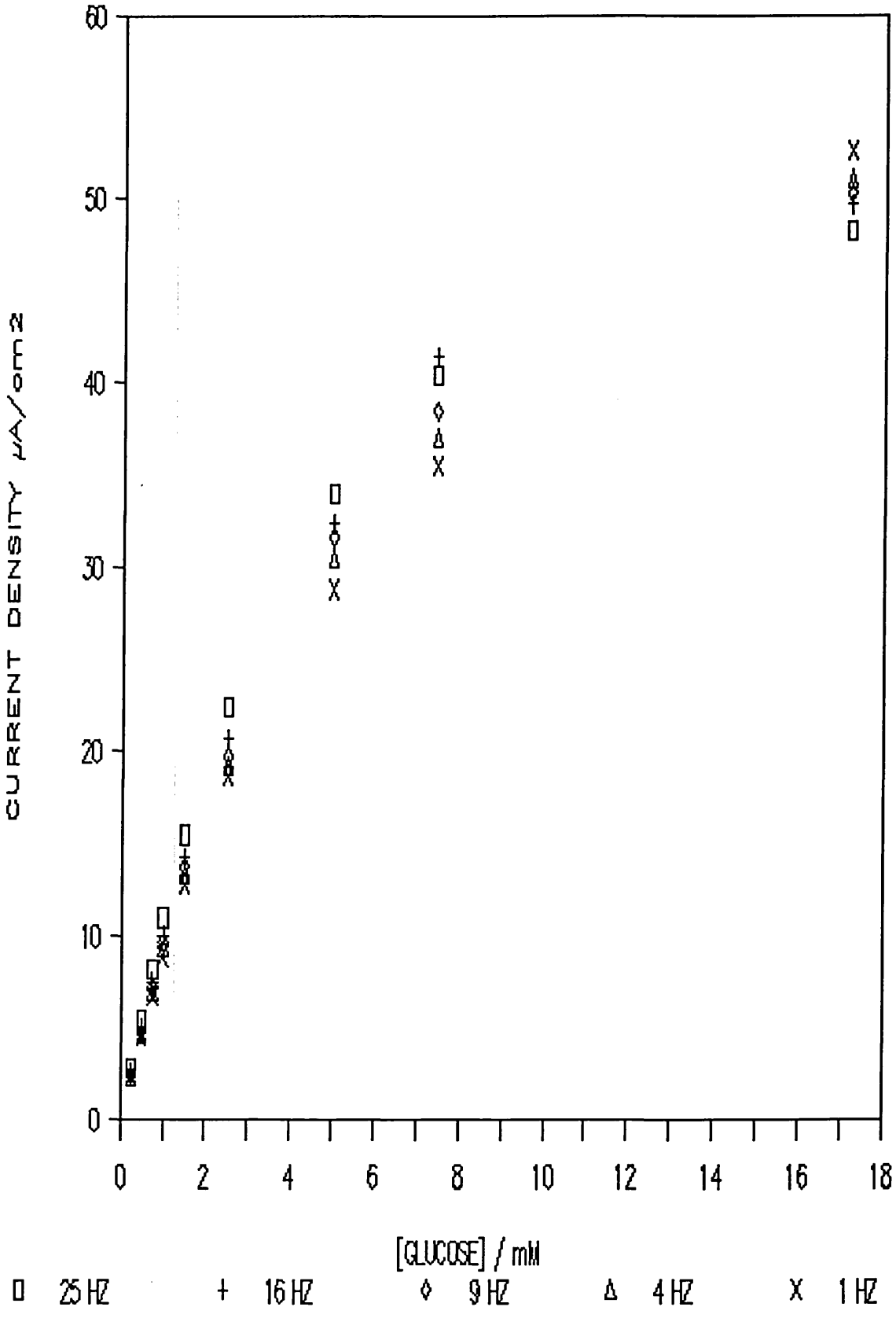

Figure 4.11 Rotation speed dependence of TTF-TCNQ / silicone oil electrode using glucose oxidase modified by TTF°. [GOD] = 100 U/ml.

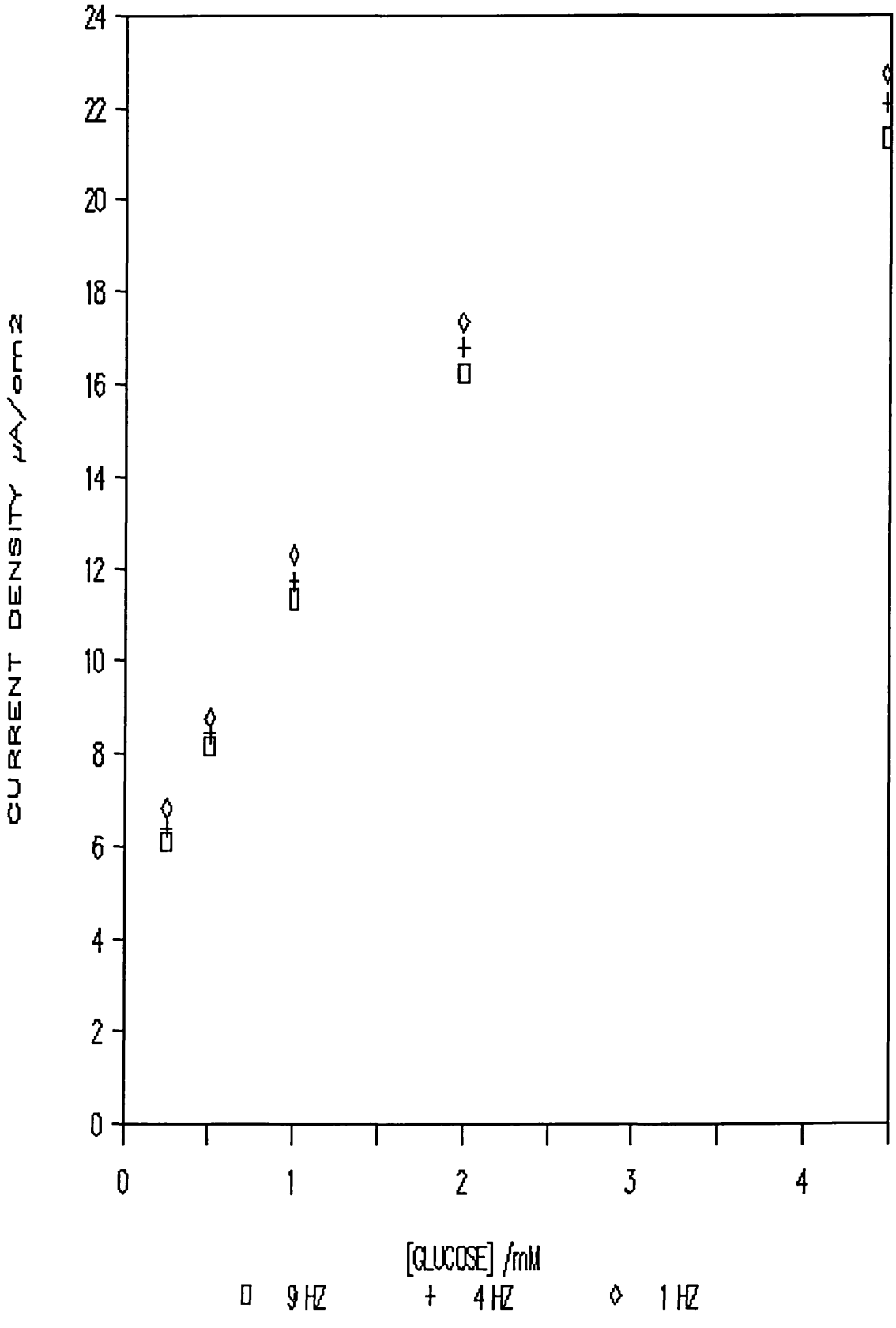

example in Case I all M is consumed in a reaction layer very close to the electrode surface hence only M' is lost to the bulk. Thus in this particular case no reduction current would be seen at the ring. The converse is true in Case V where reaction between E' and M occurs at the edge of the diffusion layer and one would expect a reduction current at the ring. However on approaching the V/VI boundary the reaction between E' and M occurs further inside the diffusion layer, tending to the zero-order reaction layer situation of true Case VI behaviour. Thus the magnitude of the ring current should be small if it is observed at all.

In the heterogeneous redox catalysis theory any ring current is due entirely to dissolution from the electrode of A^{o}, a neutral species corresponding to TTF^{o} or a reduced species if it is $TCNQ^{-}$. Hence this theory predicts that there should be no reduction current at the ring electrode. Turning to the modified enzyme hypothesis there are two possible means of producing a reduction current. First, oxidised modified enzyme swept out from the disk could be reduced directly at the ring. Second, reduction of a charged species, such as TTF^{+}, could form a thin film across the platinum ring producing a modified electrode which was much more amenable to interaction with a biological system thus enhancing the rate of electron transfer and increasing the current due to the process described above.

The results are shown in Figure 4.12. The response at the disk shows the typical current vs. concentration profile whilst a ring current is observed and is proportional to the substrate concentration. This enables the heterogeneous redox catalysis theory to be discarded since it does not predict a reduction current. At [E] = 50 U/mL, with the system in Case V (8), the homogeneous mediation theory predicts that a reduction current should be seen at the ring.

The plots shown in Figure 4.13 illustrate the results of three successive experiments using the same [E]. The disk currents show reasonable reproducibilty but the ring current increases progressively, as does the collection efficiency with each

Figure 4.12 a) Plot of the ring (−200mV) and disk (+300mV) currents vs. [glc] at 9 Hz

b) Collection efficiency vs. [glc]

[GOD] = 100 U/ml

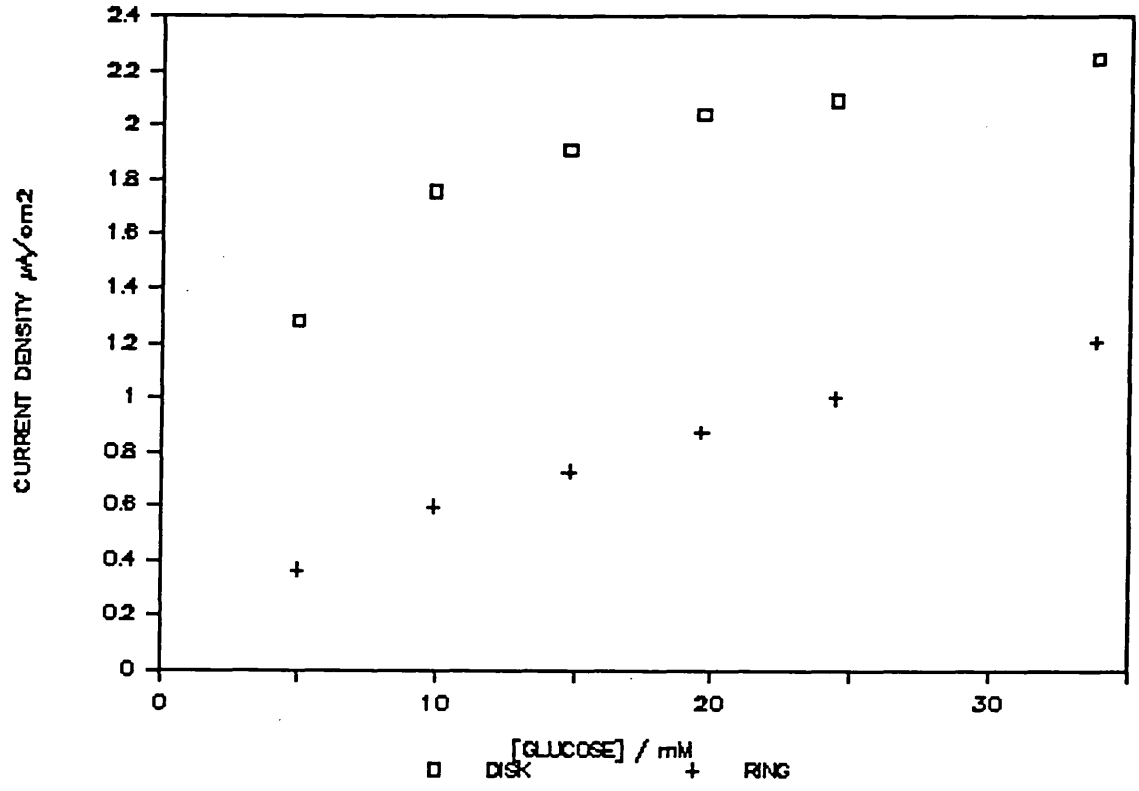

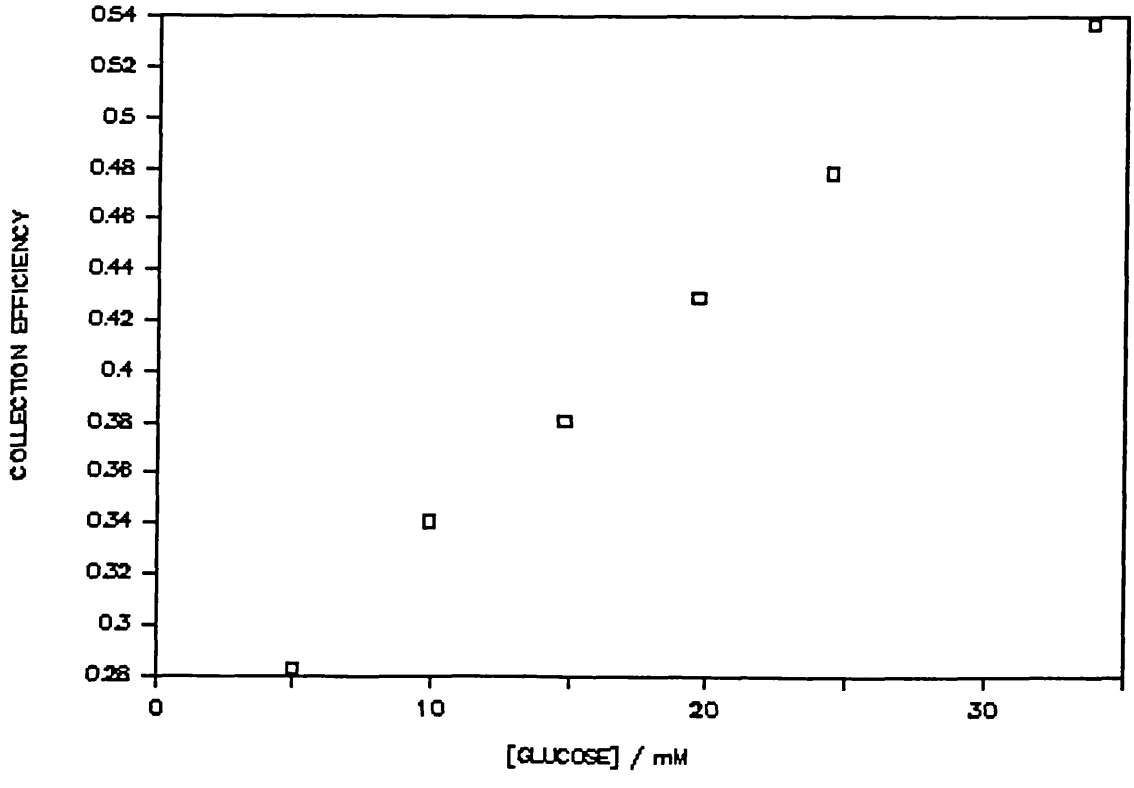

Figure 4.13 a) Plot of the ring (−200mV) and disk (+300mV) currents vs. [glc] at 9Hz for a series of experiments

b) Collection efficiency vs [glc]

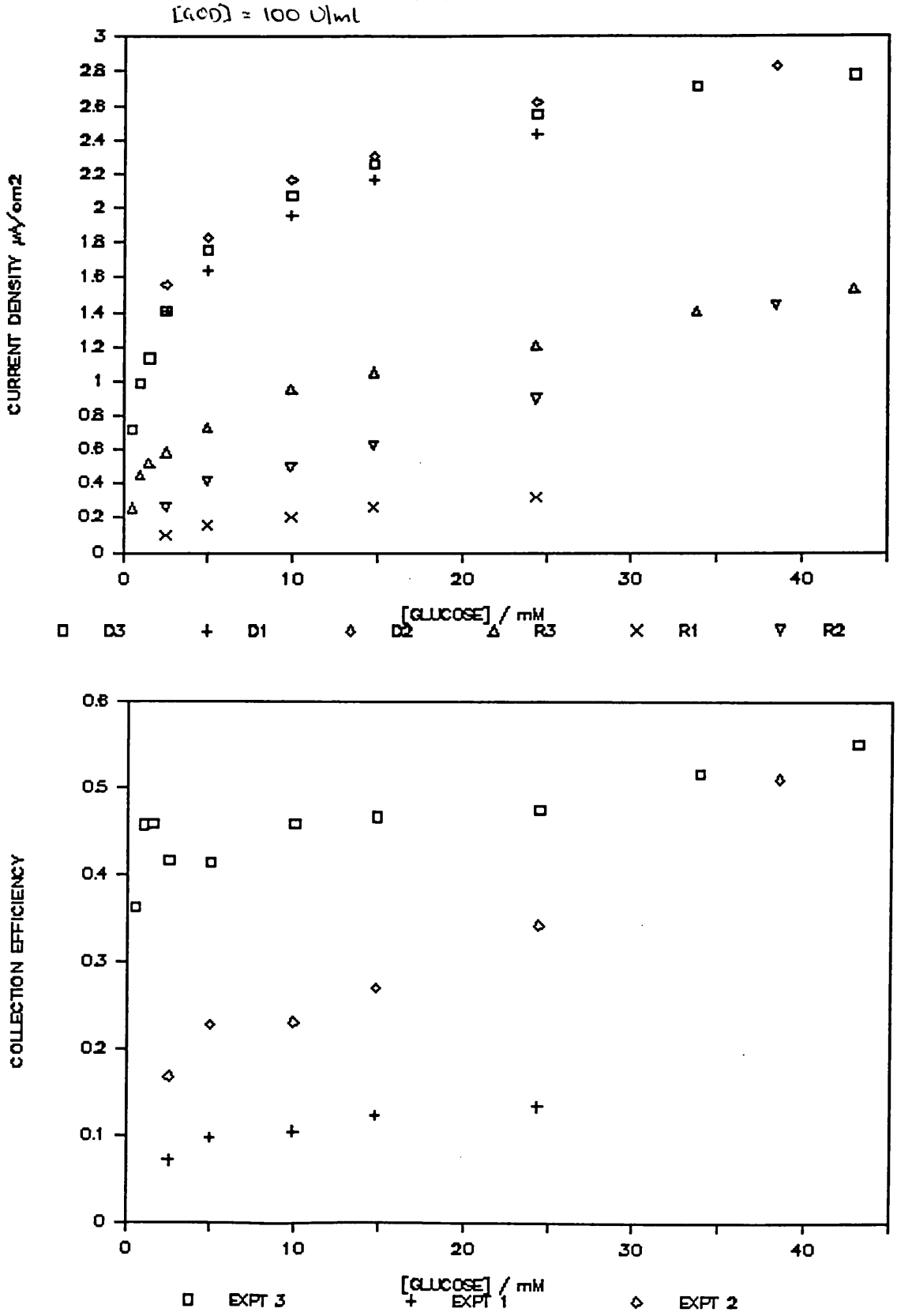

Figure 4.14 a) Plot of the ring (+300mV) and disk (+300mV) currents vs [glc]

b) Collection efficiency vs [glc]

[GOD] = 100 U/ml

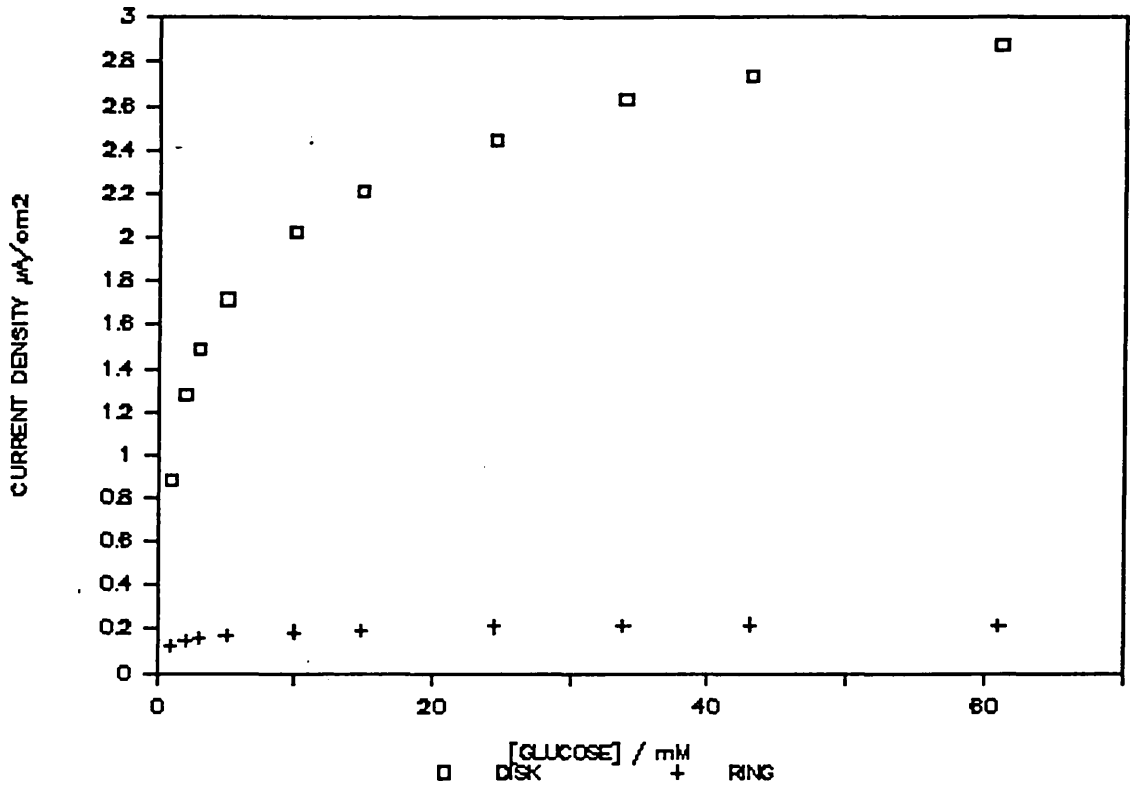

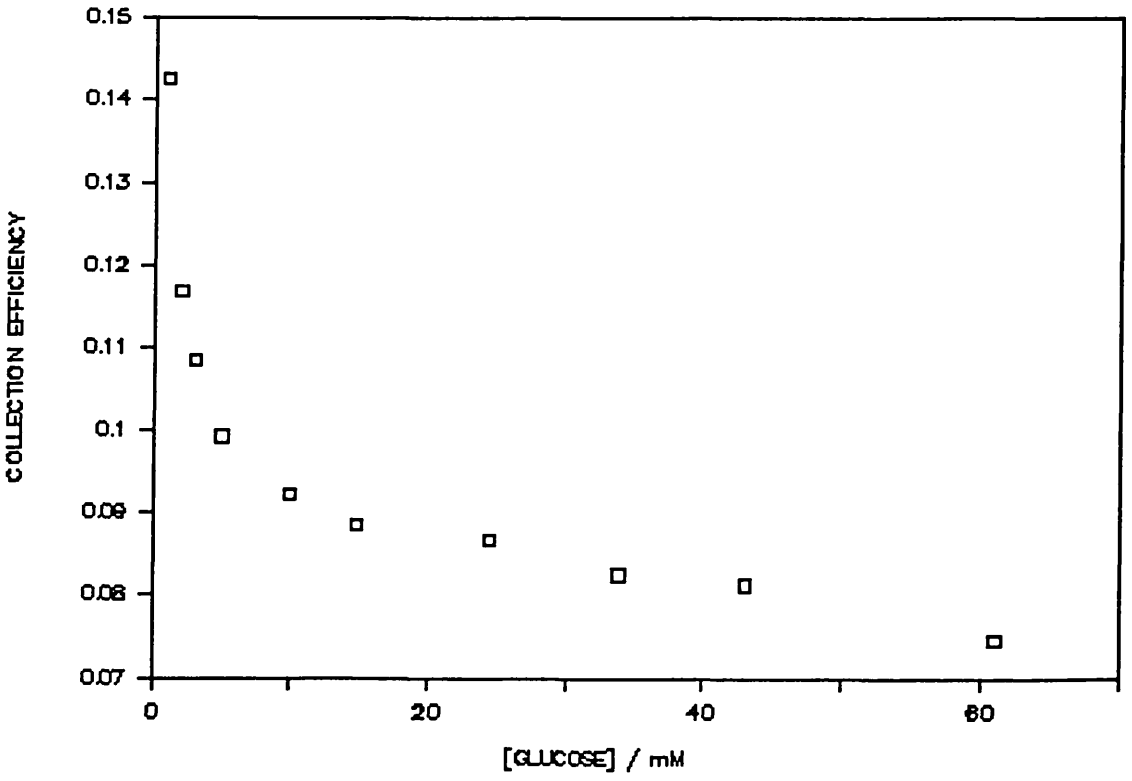

experiment. The ring was not cleaned between experiments and this suggests that a gradual modification of the ring electrode is occurring making electron transfer increasingly facile. This could be attributed to the reduction of either TTF^+ or $TCNQ^\circ$ at the ring.

4.4.3.2 Ring at +300 mV

In this series of experiments the ring was poised at +300 mV. At this potential (8) any M' i.e. TTF° or $TCNQ^-$ should be rapidly oxidised. In the homogeneous theory the magnitude of the ring current would, as mentioned above, depend on the particular case. For the heterogeneous model the ring current would be due to A° diffusing away from the surface with a rate constant k_D, independent of both [E] and [S]. The modified enzyme theory accounts for a ring current by proposing that the ring becomes coated with TTF-TCNQ or $TCNQ^\circ$ and behaves as an ersatz TTF-TCNQ electrode.

The results are shown in Figures 4.14. The ring and disk electrodes behave similarly, with the current seen at the former tending to saturate at a lower [S]. Thus the collection efficiency decreases as [S] increases. These results are in accord with those obtained previously (8). However in a series of subsequent experiments a different pattern of behaviour was observed (Figure 4.15). In these experiments the collection efficiency decreased sharply at first before gradually increasing with each injection of substrate with the final collection efficiency being greater than that observed initially.

The heterogeneous model fails to account for these results since the ring current is shown to vary with [S] and hence can again be discarded. Turning to the homogeneous model, assuming that the system is in Case V, then from Figure A.5, it can be seen that M' has a parabolic concentration profile, the apex of which is given by $\beta\kappa_E/4$. The height of the parabola and hence the observed ring current is proportional to [S]. The parabola reaches a maximum at the V/VI interface. As the case switches to VI the reaction occurs in a zero order reaction layer closer to the electrode producing a skewed profile for M'. Now less M' reaches the ring electrode and the collection efficiency falls. A

decrease in the magnitude of the collection efficiency is also observed for a V/II transition. Although the concentration profile of M^{I} in Case II is still parabolic, the height of the apex being given by $\kappa_M/20$, it is no longer dependent on [S]. Hence although the disk current continues to increase the ring current is constant.

The geometric collection efficiency, $N_o=i_R/i_D$, is an inadequate parameter when dealing with these systems since it assumes that there is a linear concentration profile of the species concerned from the bulk to the disk. However in the homogeneous model several cases predict non linear concentration profiles. As an example, in Case V, M^{I} oxidised to M at the disk can be reduced before it reaches the ring hence adding a catalytic contribution to the ring current. In order to overcome this Albery (12) used the thin gap thin ring (TGTR) approximation to explain the collection efficiency observed at the V/VI interface

$$N_V = 2\left(\frac{r_3 - r_1}{r_1}\right)\left(1 + \frac{r_3 - r_1}{r_1}\right)\left(1 - \frac{r_3 - r_1}{r_1}\right) \qquad 4.9$$

where r_1 = disk radius

and r_3 = outer ring radius

Using the dimensions given in §4.3.3 the calculated collection efficiency for Case V is 0.28 as against the geometric collection efficiency of 0.19. Similarly for Case VI the "true" collection efficiency is given by

$$N_{VI} = \frac{8}{3\sqrt{\pi}}\left[\frac{1}{3}\left\{\left(\frac{r_3}{r_1}\right)^3 - \left(\frac{r_2}{r_1}\right)^3\right\}\right]^{3/2} \qquad 4.10$$

and is calculated to be 0.04.

It is apparent from inspecting Figure 4.14 that the collection efficiency ranges from 0.14 at the lowest substrate concentration, 1mM, to 0.07 at 60mM glucose. Thus qualitatively at least this pattern follows a V → VI or a V → II transition although the magnitude of the experimental collection efficiencies differs from the values predicted by

Figure 4.15 a) Plot of the ring (+300mV) and disk (+300mV) currents vs [glc] at 9 Hz for a series of experiments

b) Collection efficiency vs [glc]

[GOD] = 1000 U/ml

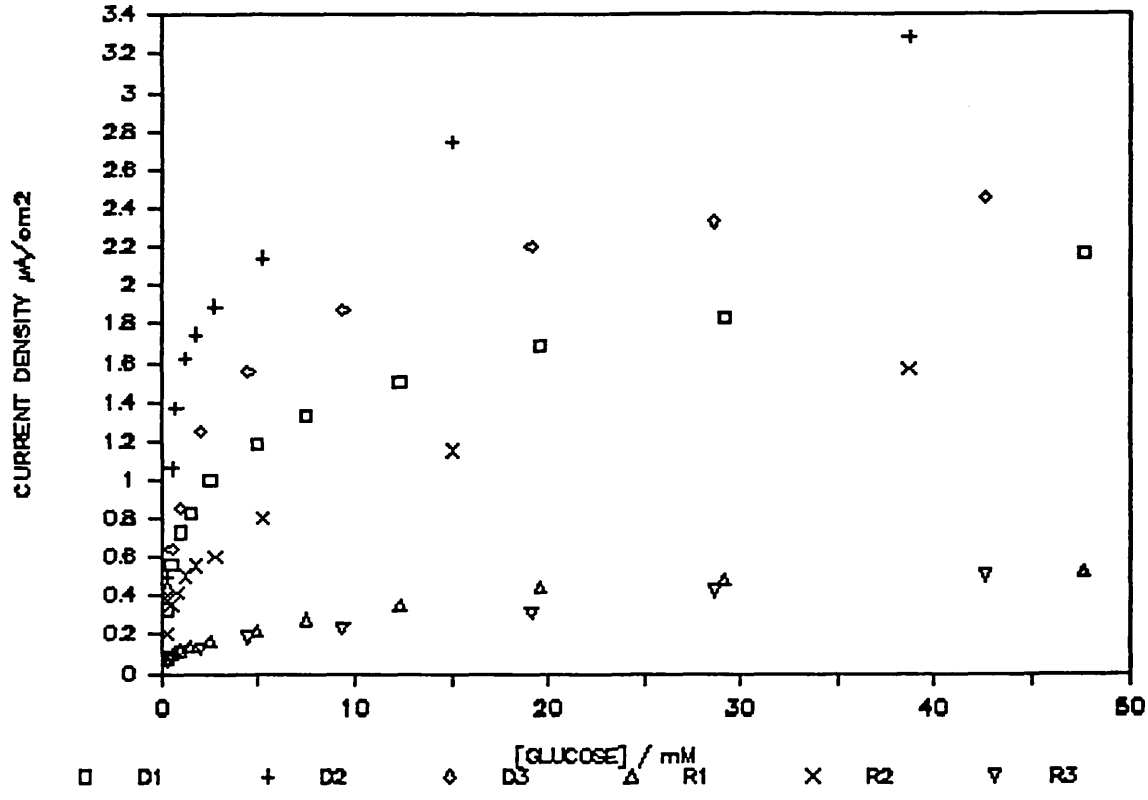

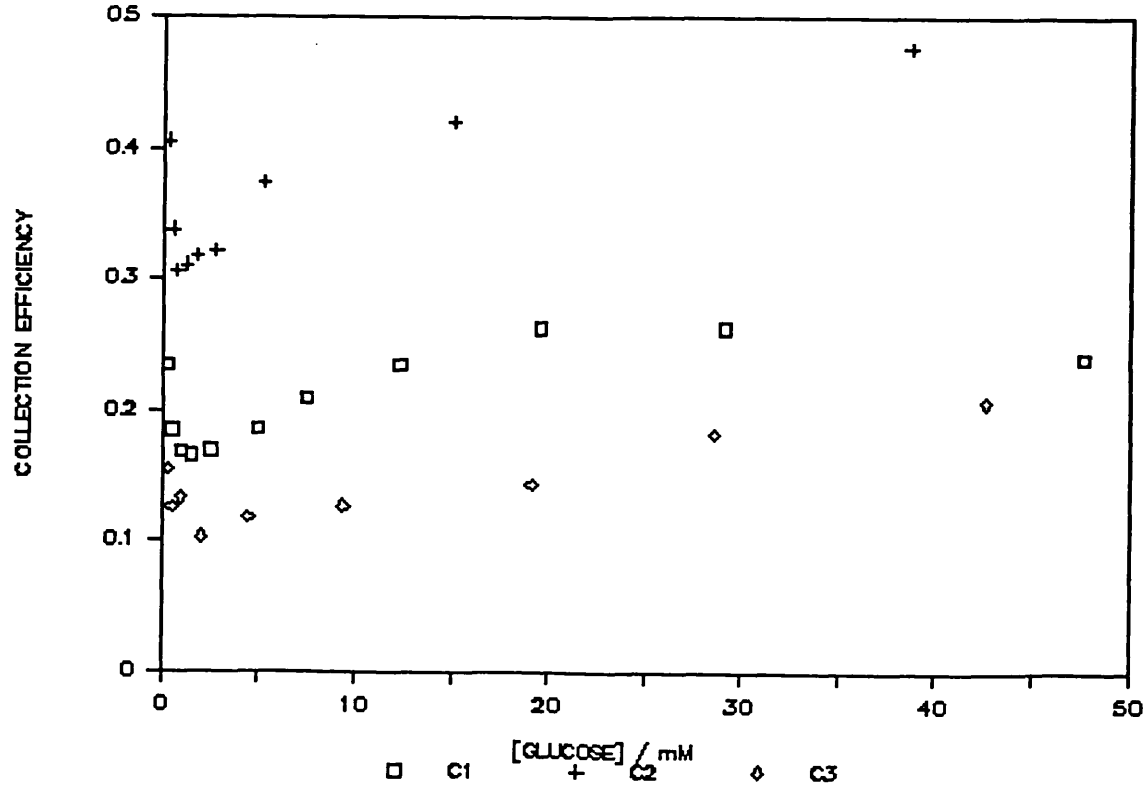

Figure 4.16 a) Plot of the ring (+300mV) and disk (+300mV) currents vs [glc] at 9 Hz

b) Collection efficiency vs [glc]

[GOD] = 100 U/ml

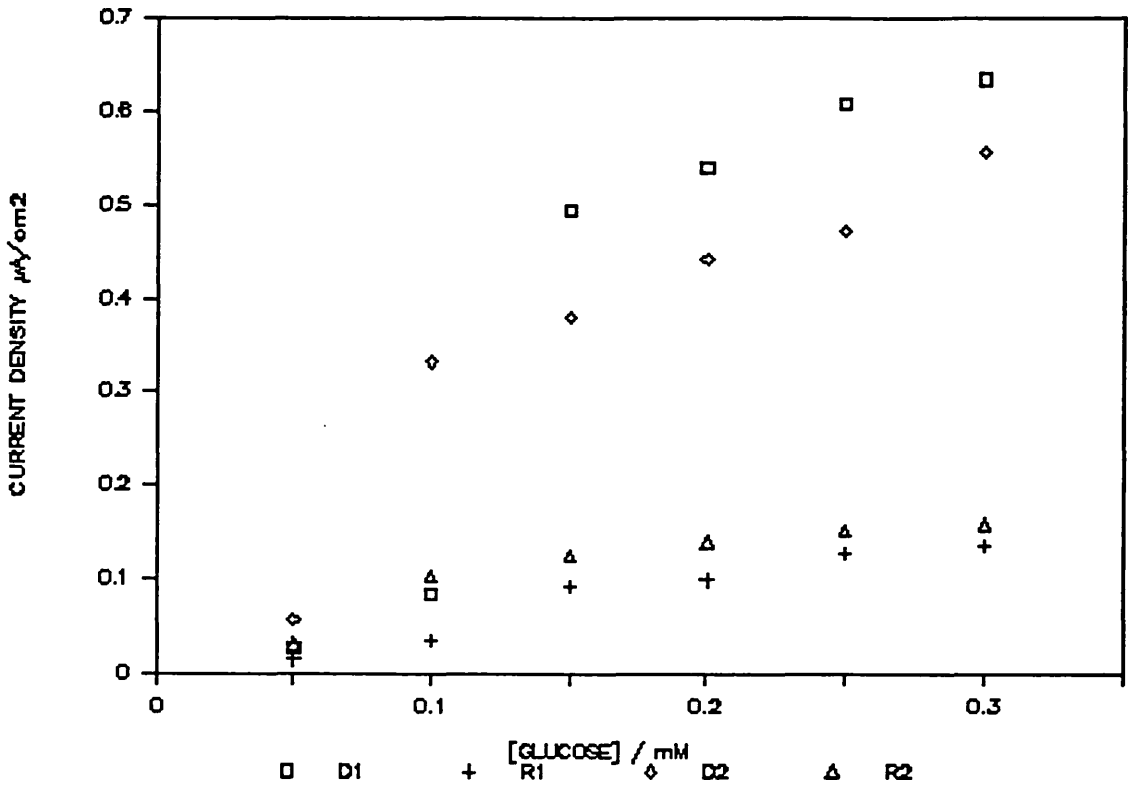

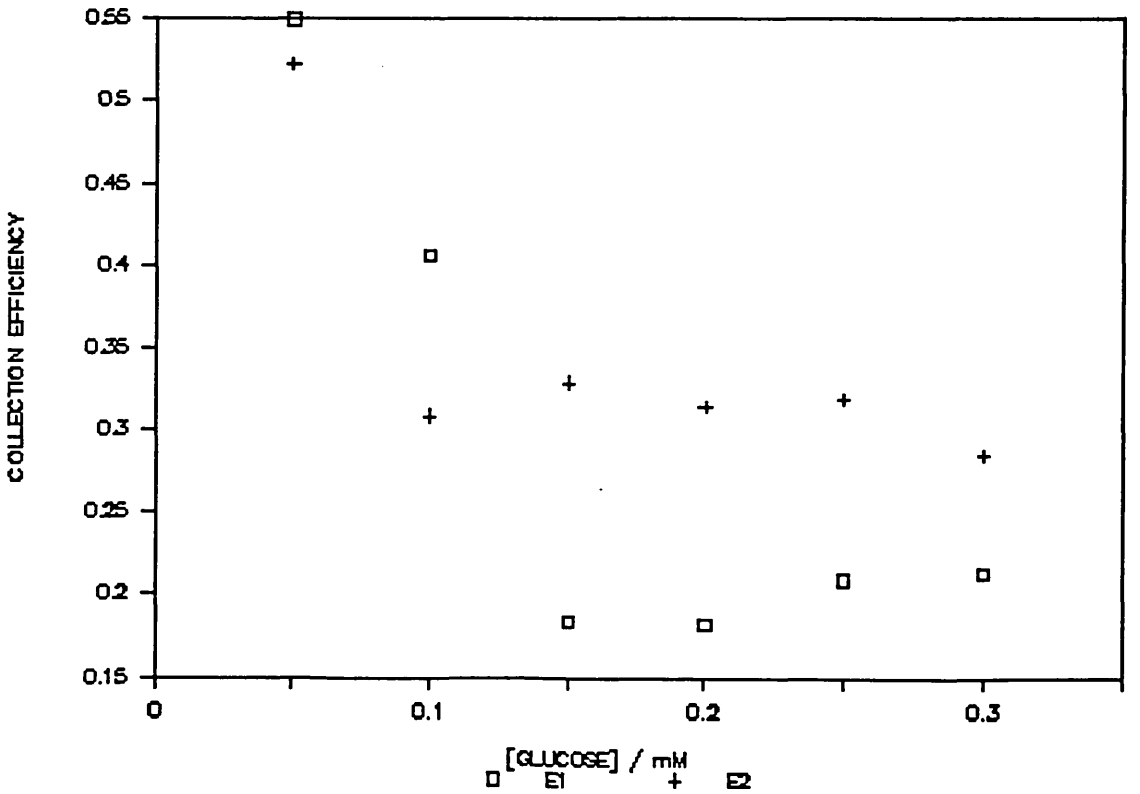

Figure 4.17 Rotation speed dependence of ring (+300mV) and disk (+300mV) currents vs [glc]

[GOD] · 100 U/ml.

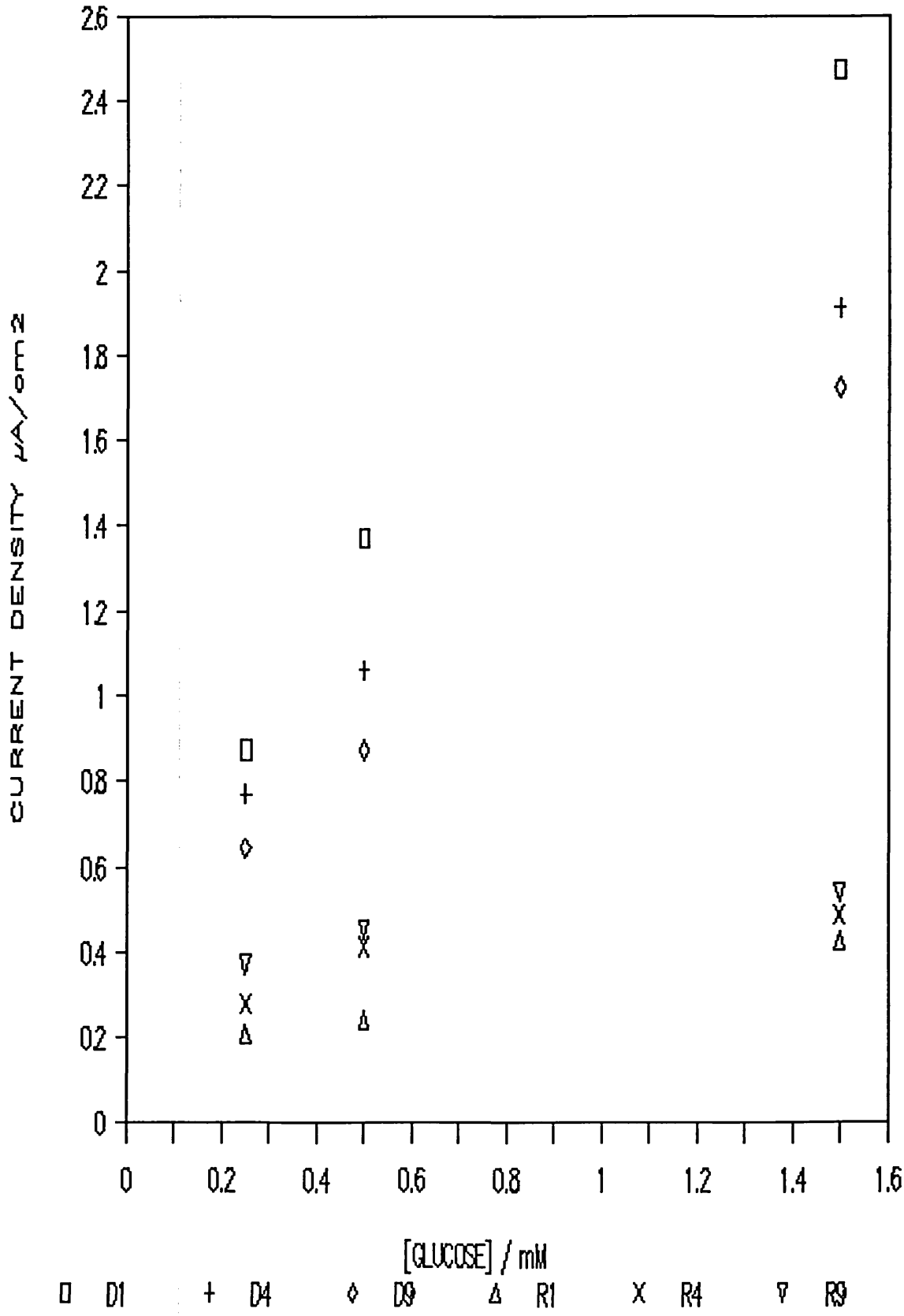

theory.

In the series of experiments shown in Figures 4.15 a lower initial glucose concentration of 250 μM was used. In each case the collection efficiencies follow the same general trend. However the collection efficiencies from the second experiment are a factor of two greater at each substrate concentration. In each experiment an initial decrease was observed, the minimum value occurring between 1-2 mM, followed by a gradual increase.

The variation of collection efficiency at low glucose concentrations was also investigated in two further experiments (Figure 4.16). In the first a high initial collection efficiency of 0.54 was found at 50 μM. This decreased to approximately 0.2 over the range 150 - 300 μM. In the second experiment a high initial collection efficiency of 0.55 was again observed at 50 μM glucose. However it decreased to 0.3 over the range 100 - 300 μM.

The values observed at low substrate concentrations are in accord with those predicted by the homogeneous model for Case V. However it does not explain the initial decrease followed by the gradual increase in collection efficiency observed in the second series of experiments.

The effect of rotation speed on the ring current and hence on the collection efficiency was also investigated (Figures 4.17). It was found that although the current at the TTF-TCNQ disk was inversely proportional to rotation speed, the Pt-ring current increased with rotation speed. Since the Pt-ring is poised at an oxidising potential and the ring current is a measure of the reduced mediator returning to the disk, it follows that the ring current should show the same rotation speed dependence as the disk. These results are qualitatively in accord with the heterogeneous and modified enzyme theories which predict the ring current is due to material swept across to the Pt-ring from a corroding TTF-TCNQ disk. However, as mentioned above, the heterogeneous redox model cannot explain the substrate dependence of the ring current.

4.4.3.3 Effect of Scanning the Ring Potential

In an attempt to identify a possible mediating species the Pt-ring was swept between -170 mV and +420 mV with the TTF-TCNQ disk poised at +300 mV. As the electrode was rotated at 1 Hz the traces shown in (Figures 4.18 and 4.19) are correctly referred to as polarograms. The first polarogram was taken in the absence of enzyme. A slight peak is visible at approximately +220 mV. As a rotating electrode was used it is difficult to determine E° accurately. As Na^{+} was present as the counter ion in both the buffer and the background electrolyte and since NaTCNQ is insoluble this precludes assignment of the peak to oxidation of $TCNQ^{-}$. Bearing this in mind, the potential range suggests the involvement of TTF species, possibly corresponding to $TTF^{\circ} \rightarrow TTF^{+}$. The second polarogram was recorded after the addition of glucose oxidase and the peak appears to have decreased in magnitude. A possible explanation is that the mediator becomes incorporated into the enzyme, in support of the modified enzyme theory. On addition of glucose, no immediate change was observed in the polarograms. However, when the ring was poised at +300 mV for 120 s, the anodic current was reduced on subsequent polarograms whilst an increased cathodic current was observed (Figure 4.20).

4.4.3.4 Effect of Scanning the Disk

The TTF-TCNQ pressed pellet disk was scanned between -160 mV and +420 mV and the Pt-ring poised at +300 mV. The disk polarograms taken before and after addition of glucose are shown in Figure 4.21. As can be seen there is a slight increase in the anodic current.

4.4.3.5 Extending the Sweep Range - Nucleation

In a further attempt to detect any mediator species present the sweep range of the Pt-ring was extended from -0.75 to +1.0V. The scan rate was kept at 20 mV/s. The TTF-TCNQ disk was maintained at +300 mV. The electrode was rotated at a frequency of 1 Hz.

Figure 4.18 Effect of scanning the ring potential in the absence of enzyme and substrate

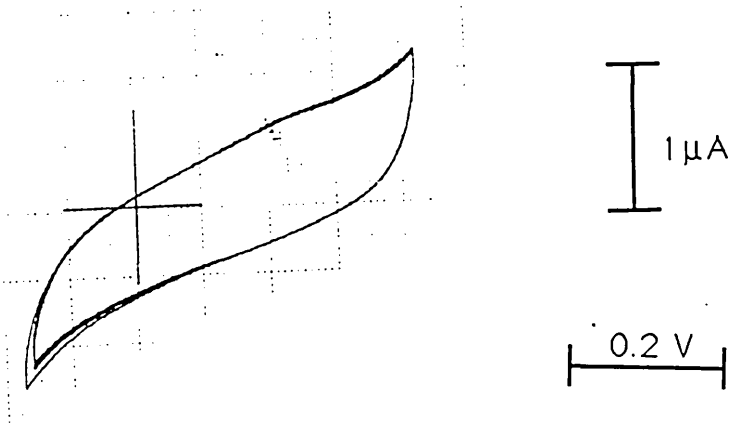

Figure 4.19 Effect of scanning the ring potential in the presence of glucose oxidase (100 U/ml)

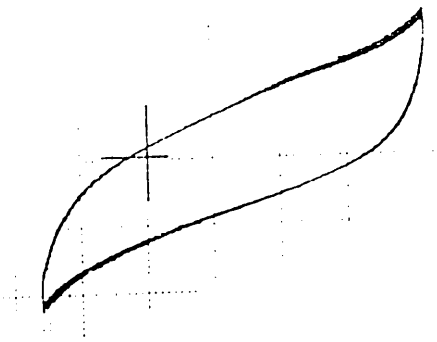

Figure 4.20 Effect of scanning the ring potential in the presence of GOD and glucose. [GOD] = 100 U/ml, [glc] ≈ 20 mM

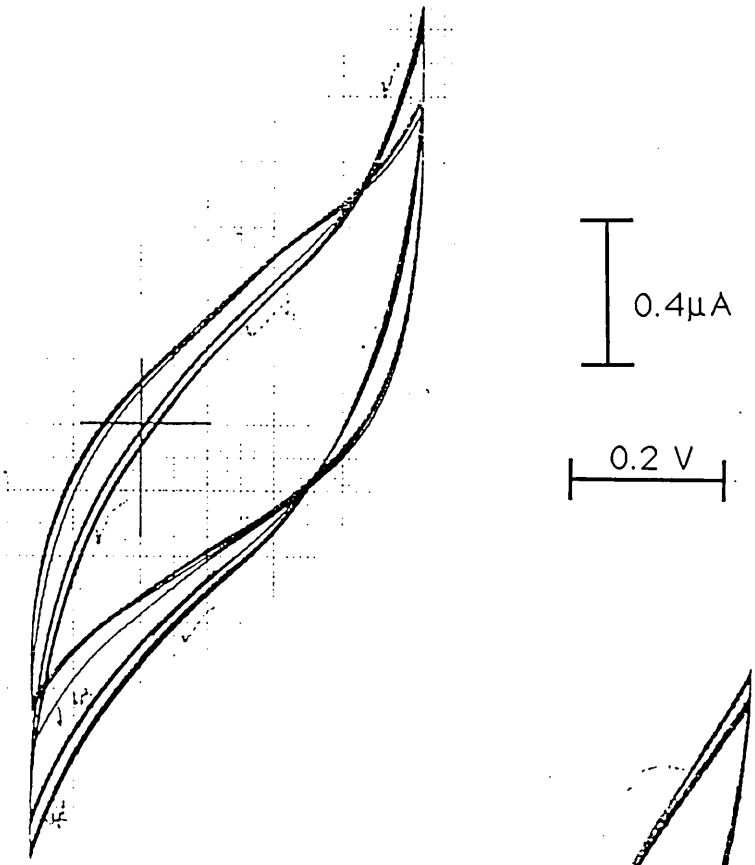

Figure 4.21 Effect of scanning the disk potential

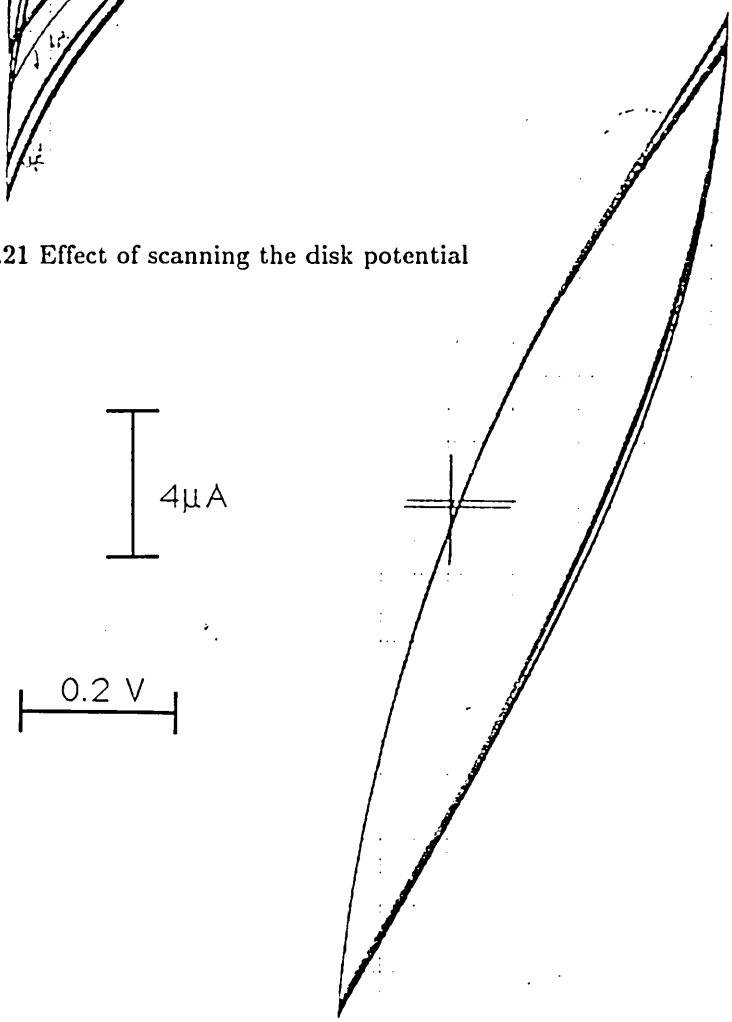

The ring was scanned until a relatively constant polarogram was obtained (Figure 4.22). On adding glucose oxidase, the peak height in the anodic sweep increased slightly. On addition of 2.5 mM glucose the anodic current increased markedly and a peak at + 30 mV appeared in the cathodic direction. The peak heights of both anodic and cathodic peaks increased continuously with each sweep without requiring further addition of substrate. Furthermore, the anodic and cathodic sweeps of the polarogram began to coalesce in the +400 mV region. Eventually the anodic peak height tended toward a constant value. Following addition of a second aliquot of glucose, 5 mM, the peak height rose sharply and the reverse cathodic sweep crossed over the forward anodic sweep: the system was now exhibiting hysteresis, typical of nucleation phenomena. Inspection shows that the area of the hysteresis loop increased with each successive sweep. It is also clear that the cathodic sweeps pass through a point of common potential.

4.4.3.5.1 Steady State Currents

In order to determine the steady state currents, an electrode exhibiting hysteresis was held at fixed potentials on both the forward and reverse sweeps and the direction of current relaxation noted, (Figure 4.23). The polarogram can be divided into 3 regions A, B and C. In segment A the steady state current is equal to or slightly greater than the anodic polarographic current. In zone B the steady state current passes through the middle of the hysteresis loop. In region C the steady state current is less than the cathodic sweep level.

4.4.3.5.2 The Role of the Mediator

In order to ascertain whether TTF species were involved, TTF^+Cl^- was added to a solution containing glucose oxidase and polarograms taken at the Pt-ring of a TTF-TCNQ disk/Pt-ring electrode. A peak due to the oxidation of TTF^+ was clearly apparent (Figure 4.24). On adding glucose, 5 mM, the anodic and cathodic peaks increased in magnitude, the former more markedly than the latter. This suggested a catalytic role for TTF^+.

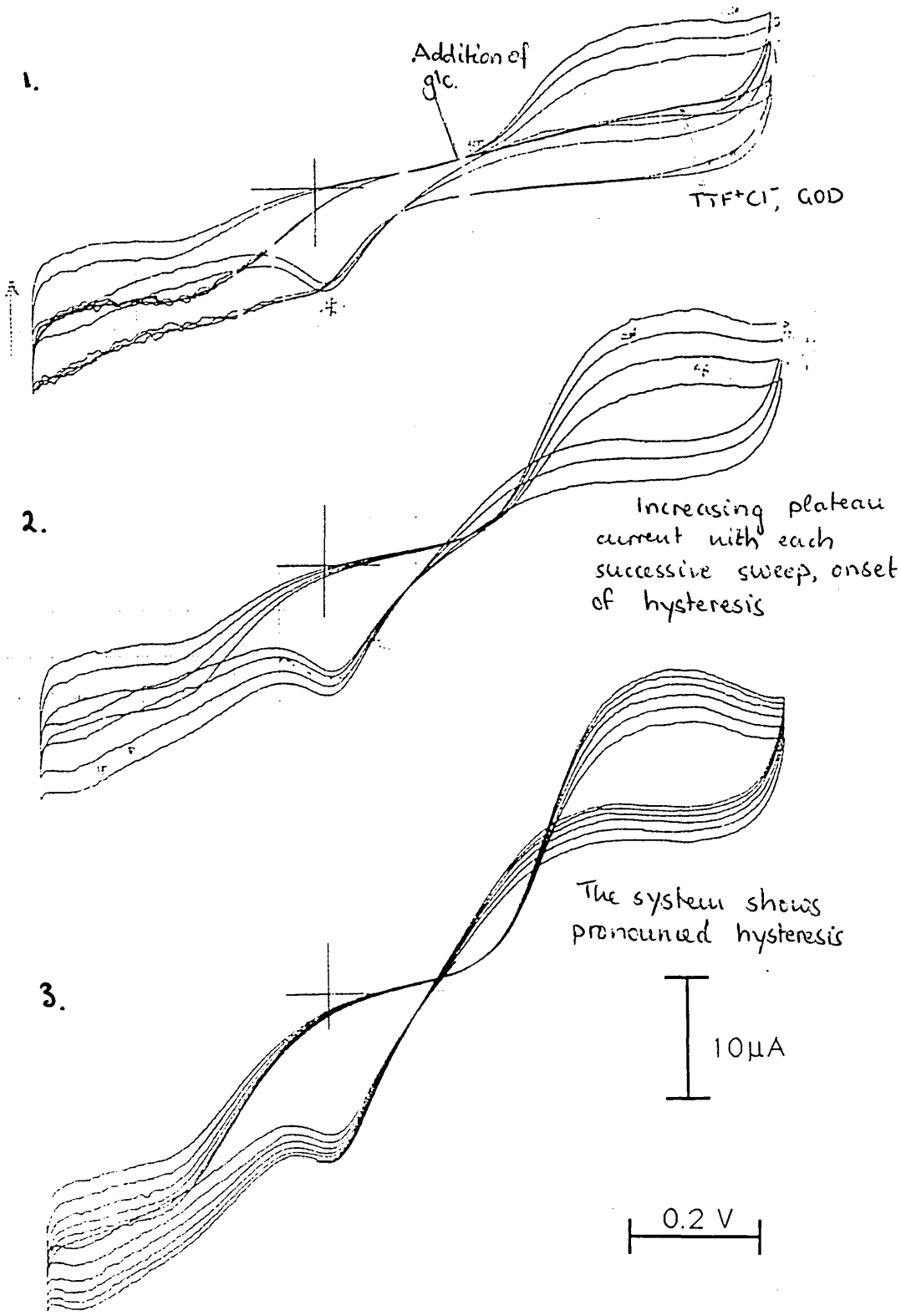

Figure 4.22 Effect of extending the sweep limits : nucleation . [GOD] = 100 U/ml
[Glc] = 20 mM

1. INITIAL EFFECT OF GLUCOSE ADDITION.

2, 3 TIME DEPENDENT HYSTERESIS DEVELOPMENT.

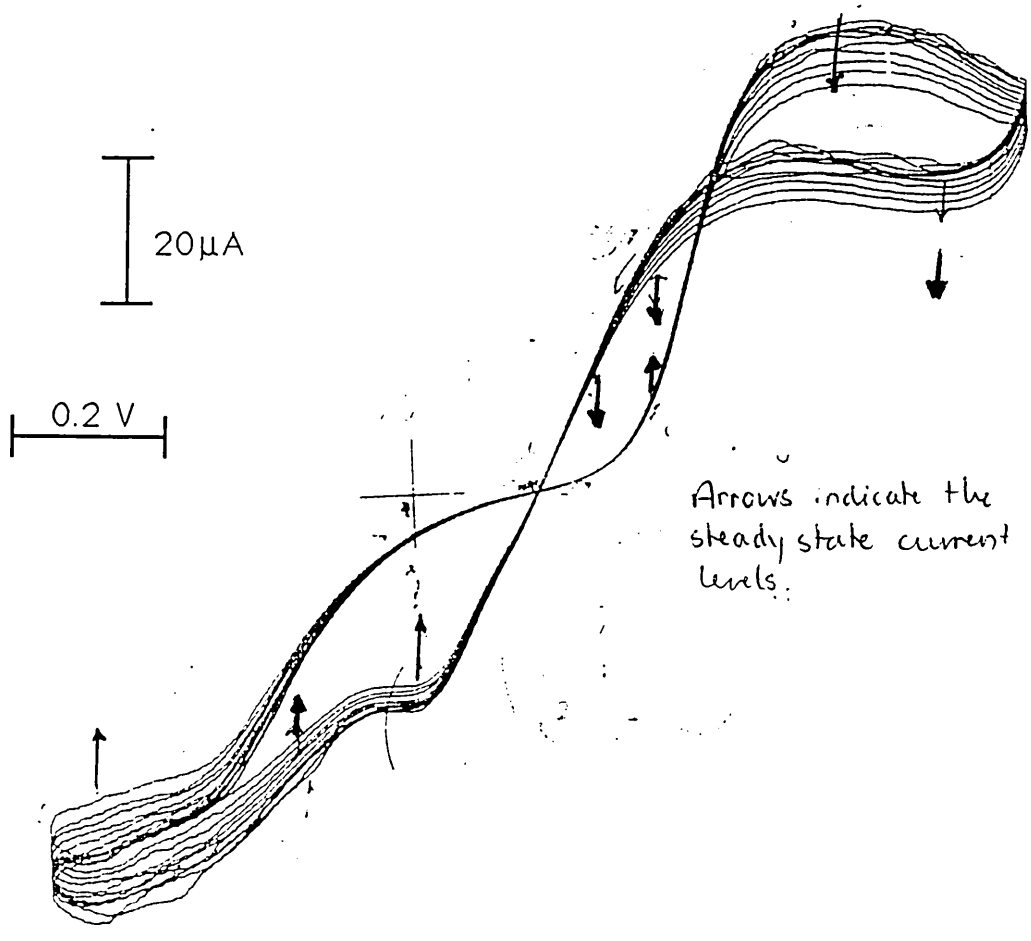

Figure 4.23 Steady state currents for the nucleation process. [GOD] = 100 U/ml
[Gl] = 20 mM

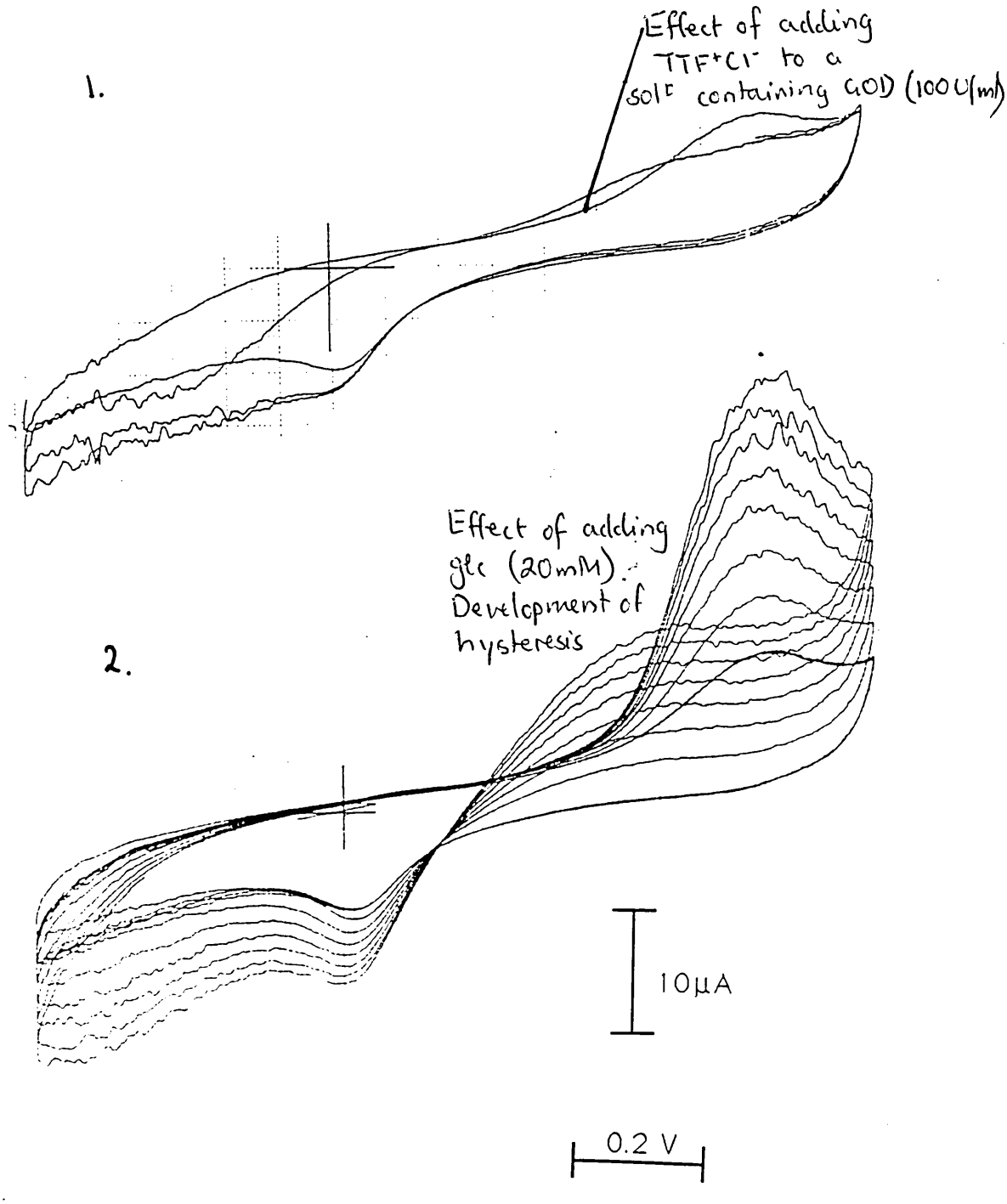

Figure 4.24 Effect of added TTF^+Cl^- on the nucleation process

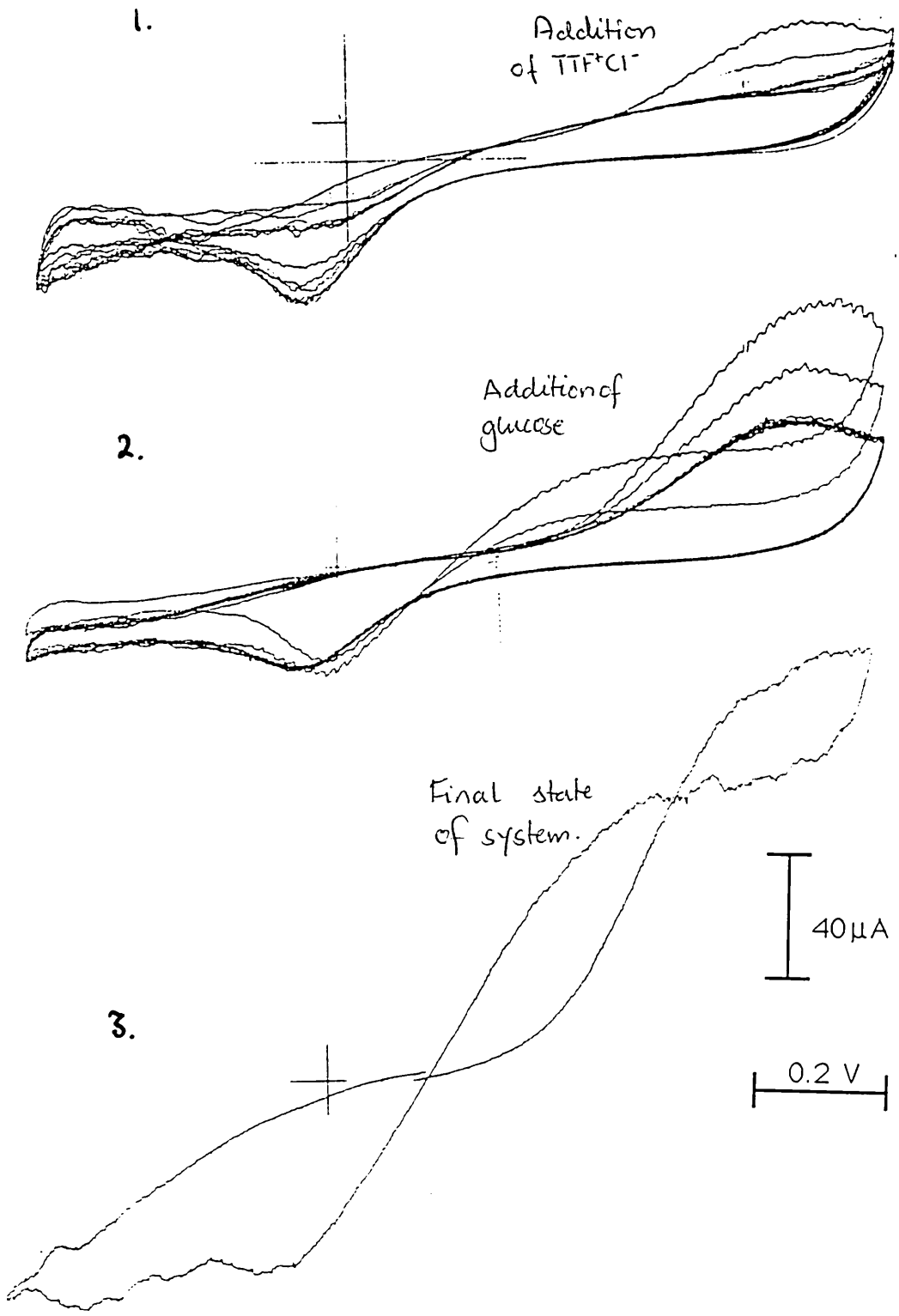

Figure 4.25 Nucleation at a Pt-electrode using TTF^+Cl^- (sat).
[GOD] - 100 U/ml , [glc]: 20 mM

A Pt disk electrode was used to preclude participation of TCNQ in the nucleation. It was pretreated by cleaning with alumina and cycling in 0.2M H_2SO_4. Glucose, 5 mM, was added to a solution containing glucose oxidase and TTF^+Cl^- and nucleation was again observed (Figure 4.25).

A Pt-disk electrode was poised at a series of potentials from +300 mV to −300 mV via 100 mV steps. The Pt-ring was swept between +1V and −0.6V in a solution containing TTF^+Cl^- in buffer solution. Although polarograms were obtained, hysteresis was not observed. The ring current obtained depended on the magnitude and polarity of the disk potential in accord with the theory proposed by Albery and Bruckenstein (13). For example the peak anodic ring current observed when the disk was poised at -300 mV was greater than that seen when the disk was held at 0 V. This is in accord with theory since more TTF^o is generated when the disk is poised at the former potential than at the latter hence producing a greater ring current (Figure 4.26).

4.4.3.5.3 Significance of the Cathodic Peak

In order to investigate the importance of the cathodic peak, a GOD/glucose/TTF^+Cl^- system exhibiting hysteresis at a Pt-disk electrode had its sweep direction reversed at four potentials along the cathodic sweep. The aim of the experiment was to determine how far the cathodic sweep had to progress before reversal of sweep direction caused the subsequent forward scan to follow the anodic pathway (Figure 4.27). At points 1,2 and 3 the anodic sweep followed the cathodic pathway and the anodic peak current was lower than before. No hysteresis loop was observed. Only on reversal at point 4, did the subsequent anodic sweep follow the original anodic pathway. A hysteresis loop was apparent and the anodic current had increased in magnitude. Thus, the cathodic peak had to be reached before the system could revert to its original state.

4.4.3.5.4 Effect of Electrode/Electrolyte

In order to examine whether nucleation was peculiar to platinum surfaces an

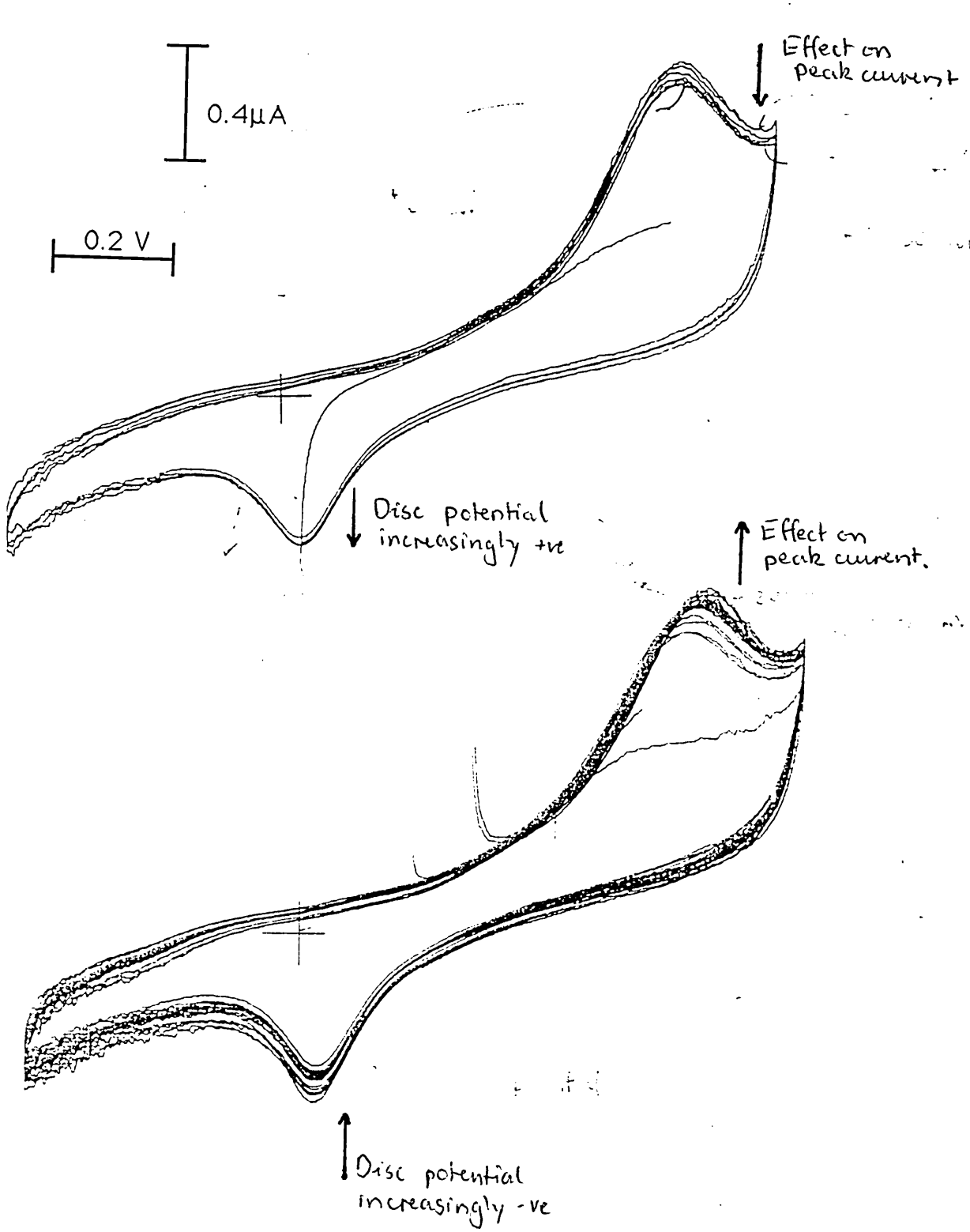

Figure 4.26 Effect of varying the disk potential on the ring polarogram

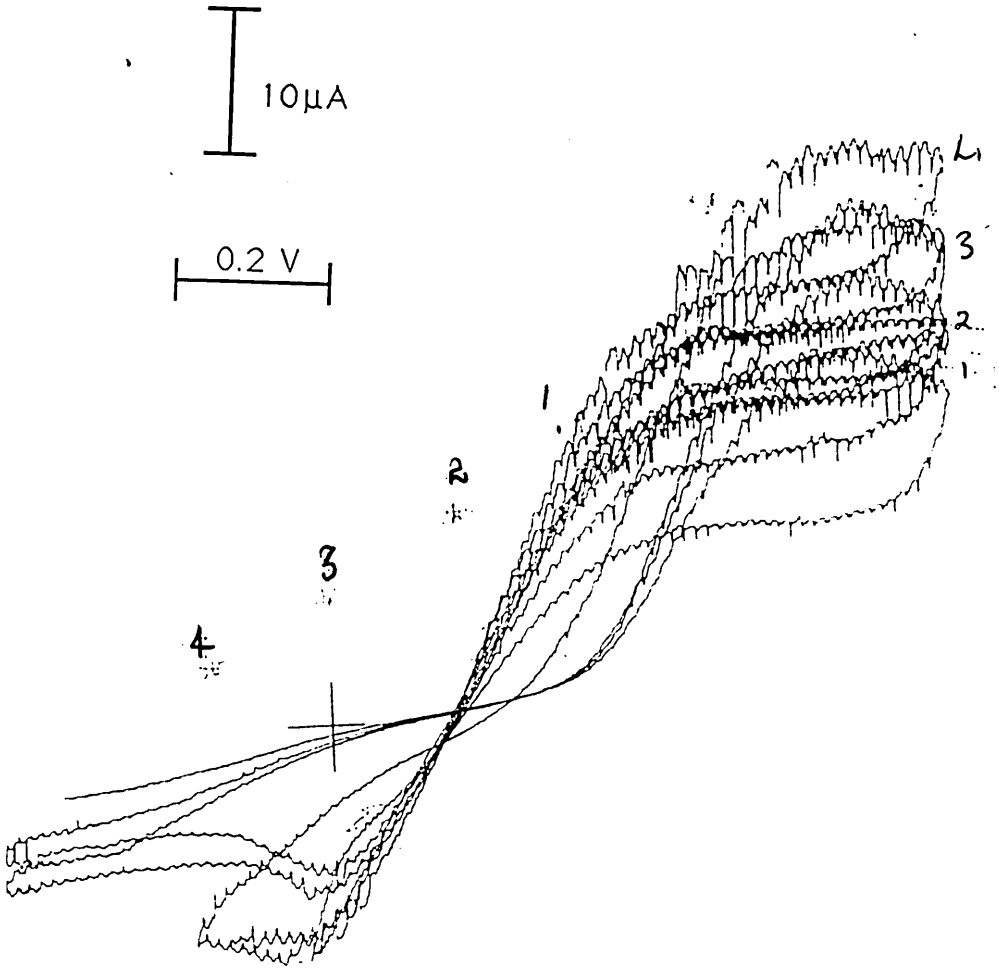

Figure 4.27 Investigating the significance of the cathodic peak. Effect on next forward sweep of stopping reverse sweeps at different points on the cathodic pathway.

attempt was made to reproduce the phenomenon at a gold electrode. On adding glucose to a solution containing glucose oxidase and TTF^+Cl^- no nucleation behaviour was observed. When a glassy carbon electrode was used a catalytic current was observed in the anodic scan, although again nucleation was absent (Figure 4.28). However nucleation was observed at a Pt-ring surrounding an electrosynthesised TTF-TCNQ disk electrode (Figure 4.29).

Since TTF^+Ac^- is the only salt of TTF^+ which is readily soluble, it was decided to examine the effect of the acetate counter-ion on nucleation. A Pt electrode failed to exhibit nucleation when LiAc was used as the background electrolyte. When LiAc was used at a glassy carbon electrode (Figure 4.30), dissolved TTF^+Cl^- gave two peaks at +190 mV and +500 mV, these were attributed to the TTF^o/TTF^+ and TTF^+/TTF^{2+} couples respectively. The magnitude of the current decreased with successive sweeps. On adding GOD, the peaks coalesced to yield a single broad peak/plateau which began ca. +220 mV.

4.4.3.5.5 Effect of Enzymes - at a Pt-electrode

a. FAD

On dissolving $(Na^+)_2FAD$ in buffer an orange solution was obtained. On adding TTF^+Cl^- the solution bacame darker. When glucose was added the colour of the solution lightened but no polarograms were observed (Figure 4.31).

b. Xanthine Oxidase (XOD)

When XOD was cycled at a Pt-electrode polarograms different to those from GOD were obtained. A polarogram showing two anodic peaks at −180 mV and +80 mV and a cathodic peak at −40 mV was obtained. These gradually disappeared with each successive sweep. On adding TTF^+Cl^- the peaks vanished. Addition of hypoxanthine had no effect with no nucleation occurring (Figure 4.32). It is possible that the enzyme was denatured on the electrode surface.

Figure 4.28 Scanning a glassy carbon electrode does not result in nucleation, [GOD] = 100 u/ml, [Glc] = 20mM, TTF⁺Cl⁻ (sat)

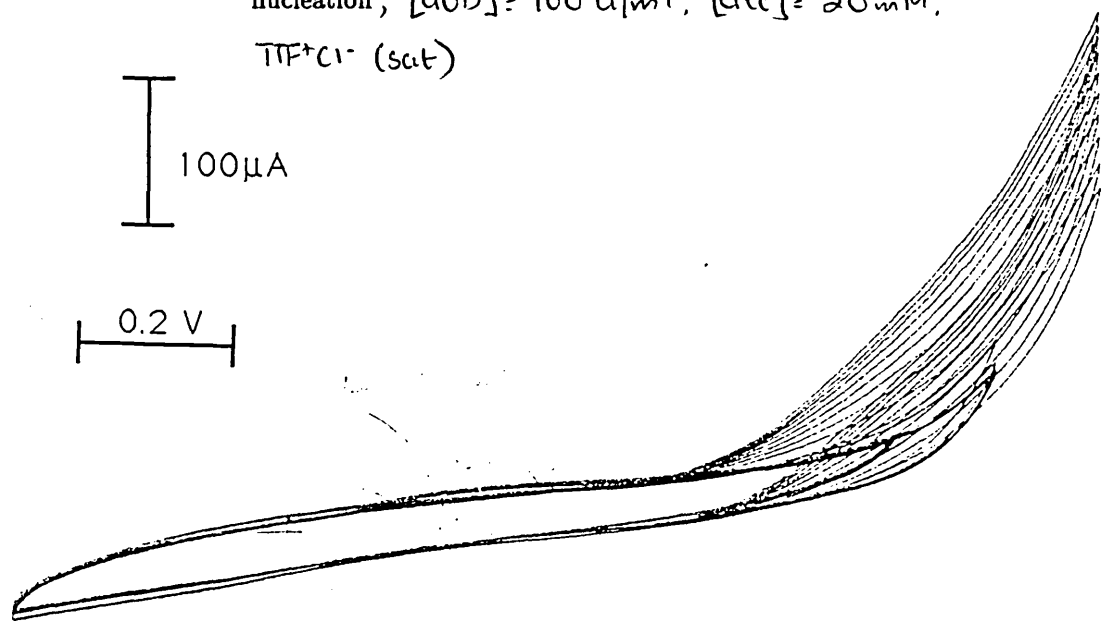

Figure 4.29 Nucleation at an electrosynthesised TTF-TCNQ electrode (7). Conditions as per above expt.

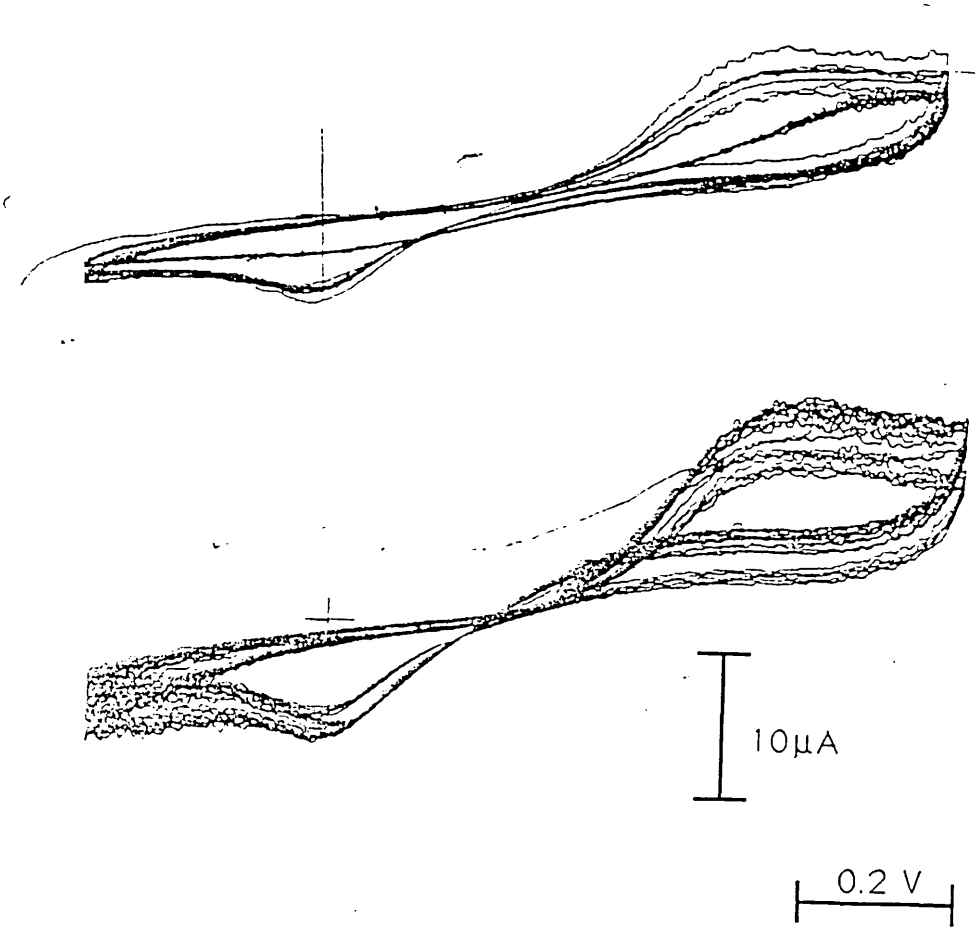

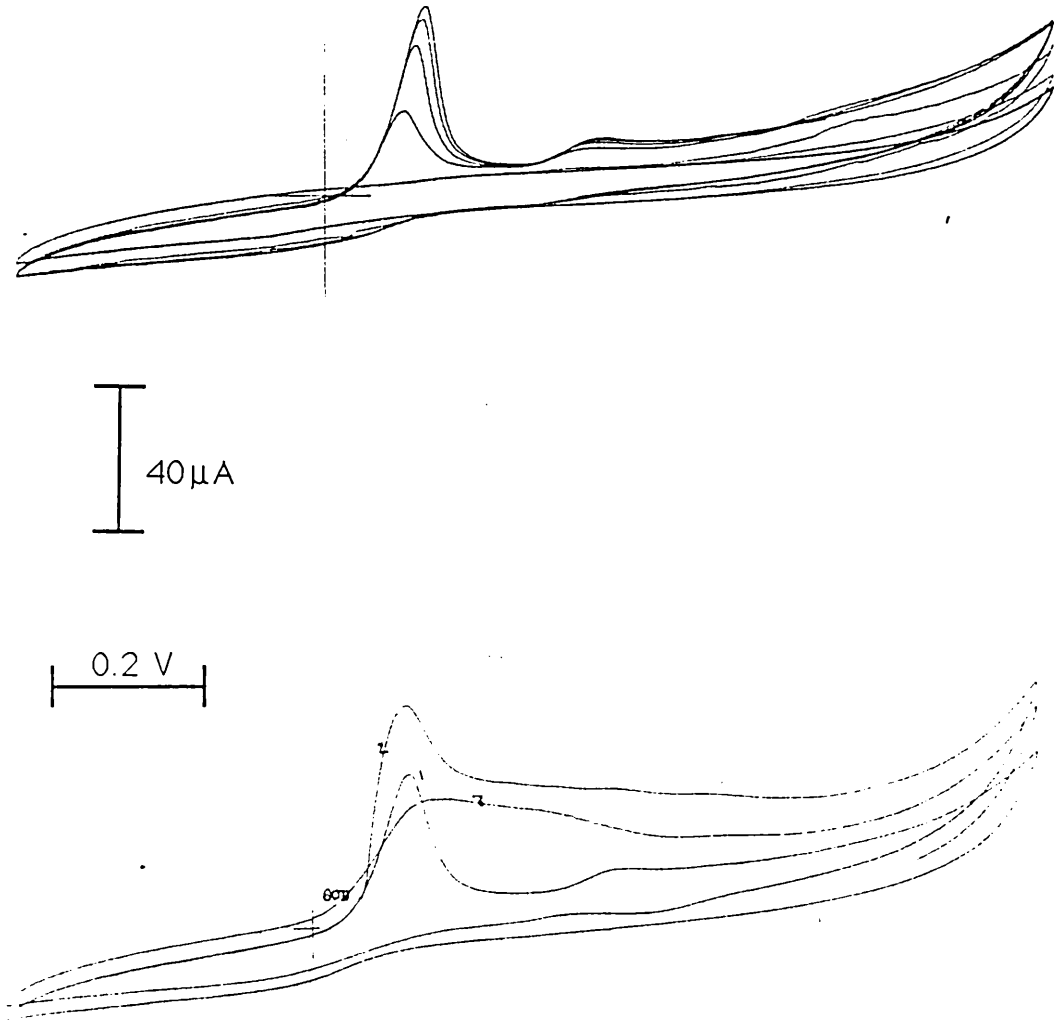

Figure 4.30 Sweeping a glassy carbon electrode using lithium acetate as background electrolyte, [GOD] = 100 U/ml. [glc] = 20 mM

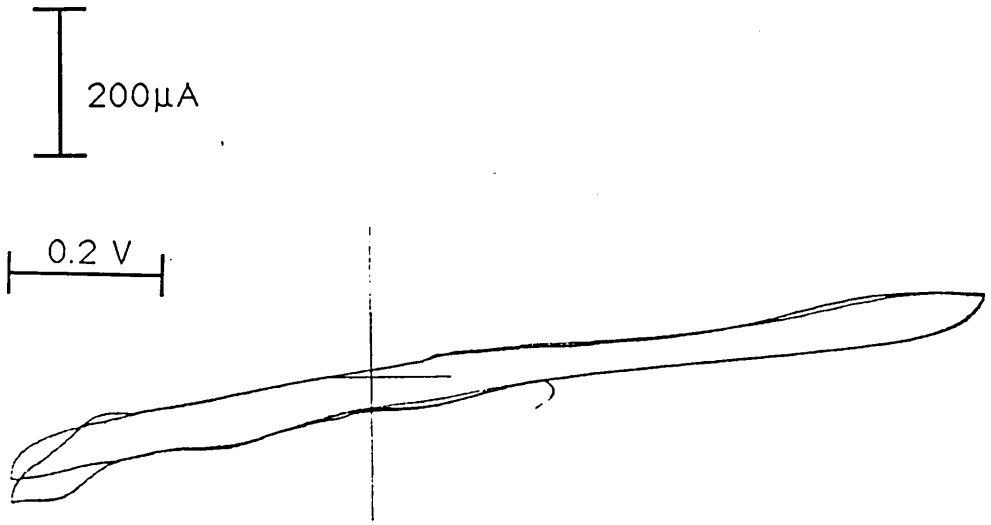

Figure 4.31 Scanning a solution of FAD and $TTF^{+}Cl^{-}$ does not produce nucleation

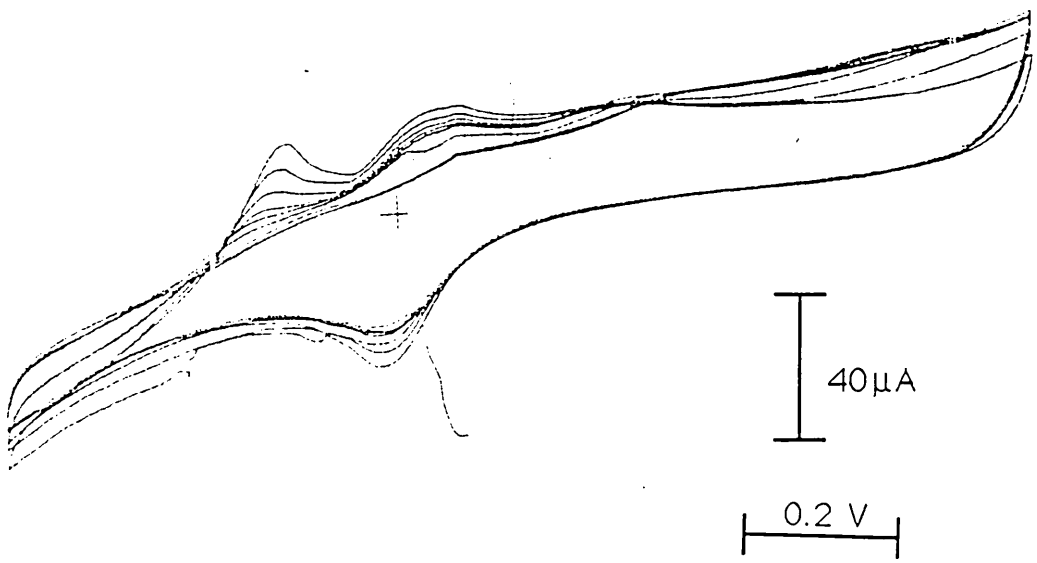

Figure 4.32 Scanning a solution of xanthine oxidase, xanthine and $TTF^{+}Cl^{-}$ does not produce nucleation

c. Choline Oxidase (ChOD)

On addition of TTF^+Cl^- to a solution containing 5 U/ml ChOD, polarograms similar to those from GOD were obtained. Nucleation commenced upon addition of choline (Figure 4.33). A large hysteresis loop was clearly observed. The experiment was carried out at both 1 Hz and a stationary electrode. Nucleation was observed in both cases.

d. Sarcosine Oxidase (SOD)

When sarcosine was added to a solution containing 9.9 U/ml SOD and TTF^+Cl^- nucleation was again detected. However the area of the hysteresis loop was appreciably less than that observed with either GOD or ChOD (Figure 4.34). The area of the anodic loop was far greater than that found with either GOD or ChOD.

e. Alcohol Oxidase (AOD)

When TTF^+Cl^- was added to a solution of AOD no peaks were observed. However nucleation began upon the addition of the substrate, methanol, to the solution. On this occasion, the hysteresis loop was quite large though the anodic loop was small compared to that found with other enzymes. (Figure 4.35). A further modification was attempted with this system. The electrode was poised at -500 mV and placed in a fresh solution of buffer. On resuming sweeping of the electrode, the characteristic polarograms showing nucleation were again observed. However the peak height was reduced by ca. 30 %.

f. Sulfite Oxidase

Sulfite was added to a solution containing sulfite oxidase and TTF^+Cl^-. A simple catalytic current was observed without any hysteresis (Figure 4.36).

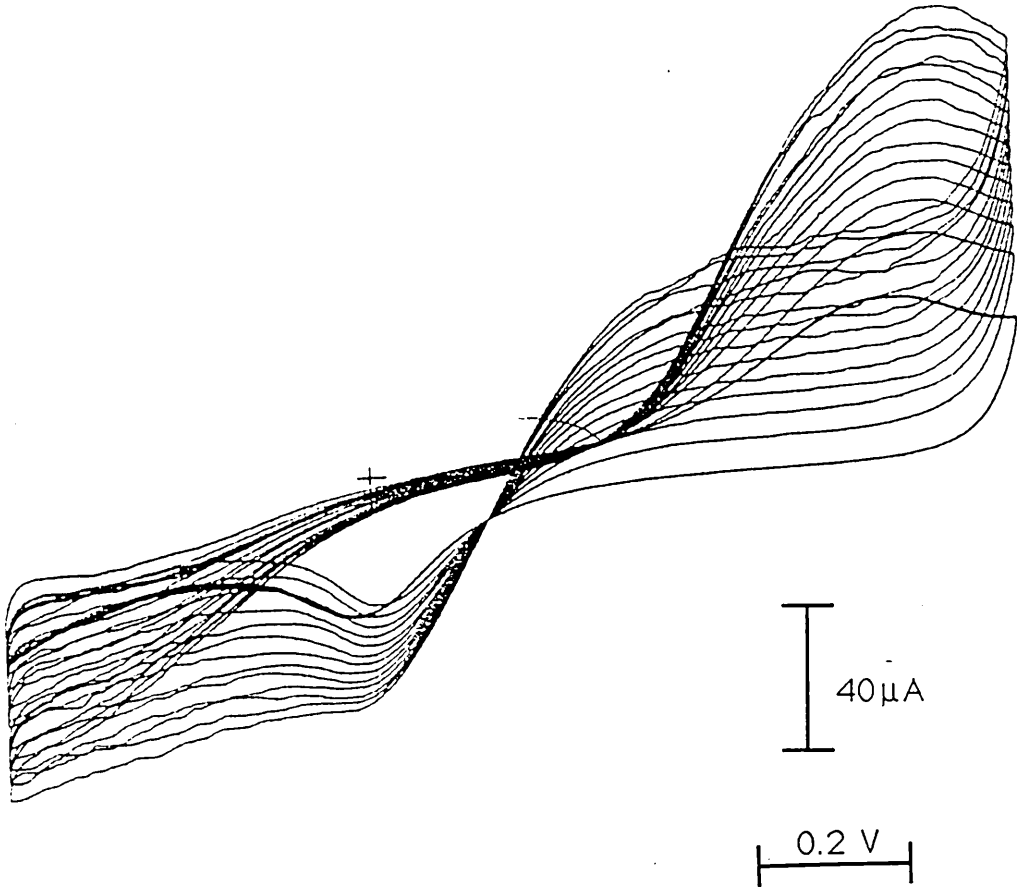

Figure 4.33 Nucleation effect observed on sweeping a solution of choline oxidase, choline and $TTF^{+}Cl^{-}$

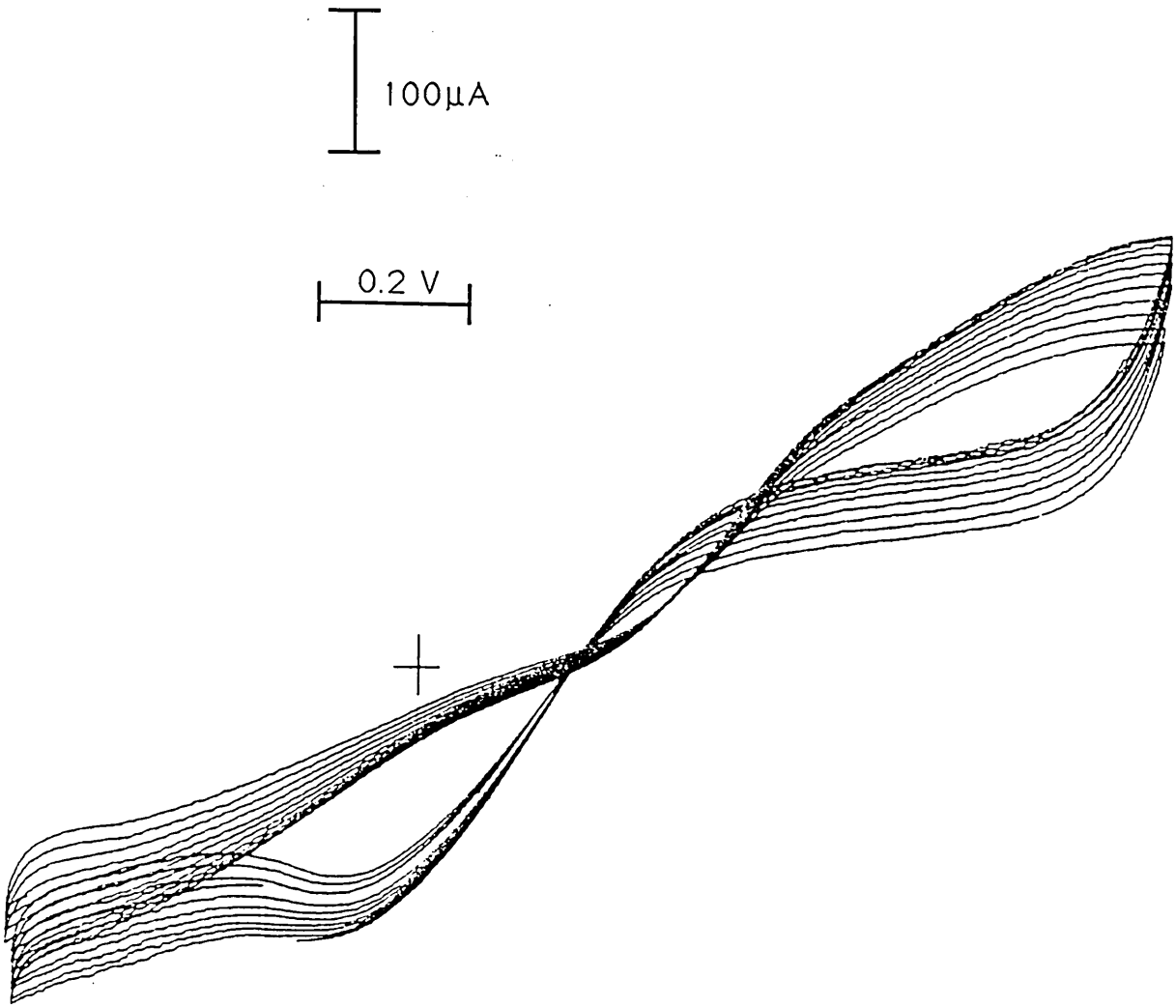

Figure 4.34 Nucleation effect observed on sweeping a solution of sarcosine oxidase, sarcosine and $TTF^{+}Cl^{-}$

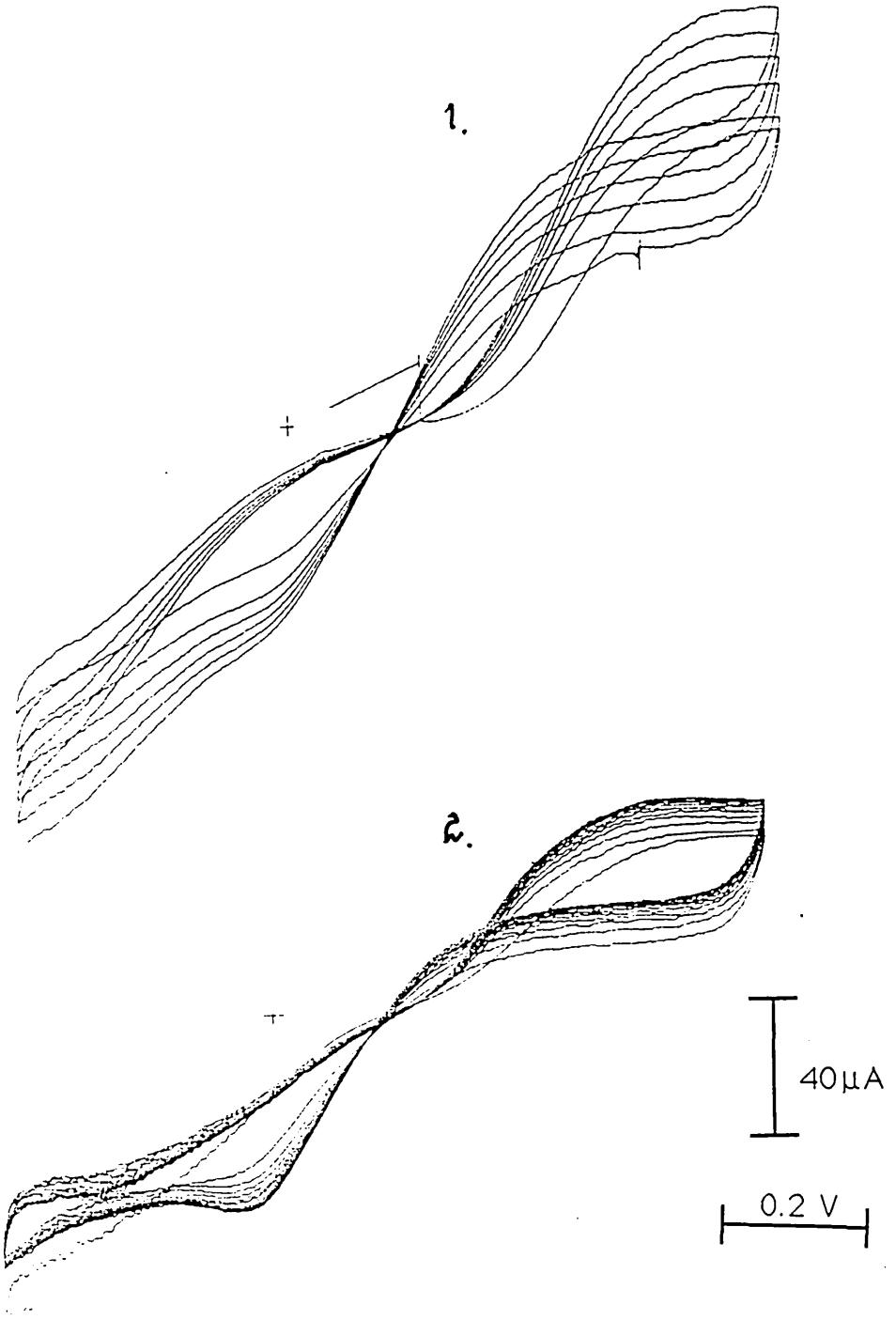

Figure 4.35 Nucleation effect was observed upon sweeping a solution of alcohol oxidase, methanol and $TTF^{+}Cl^{-}$. It was still observed when the electrode was placed in a fresh solution of buffer, [AOD] = 20 U/ml.

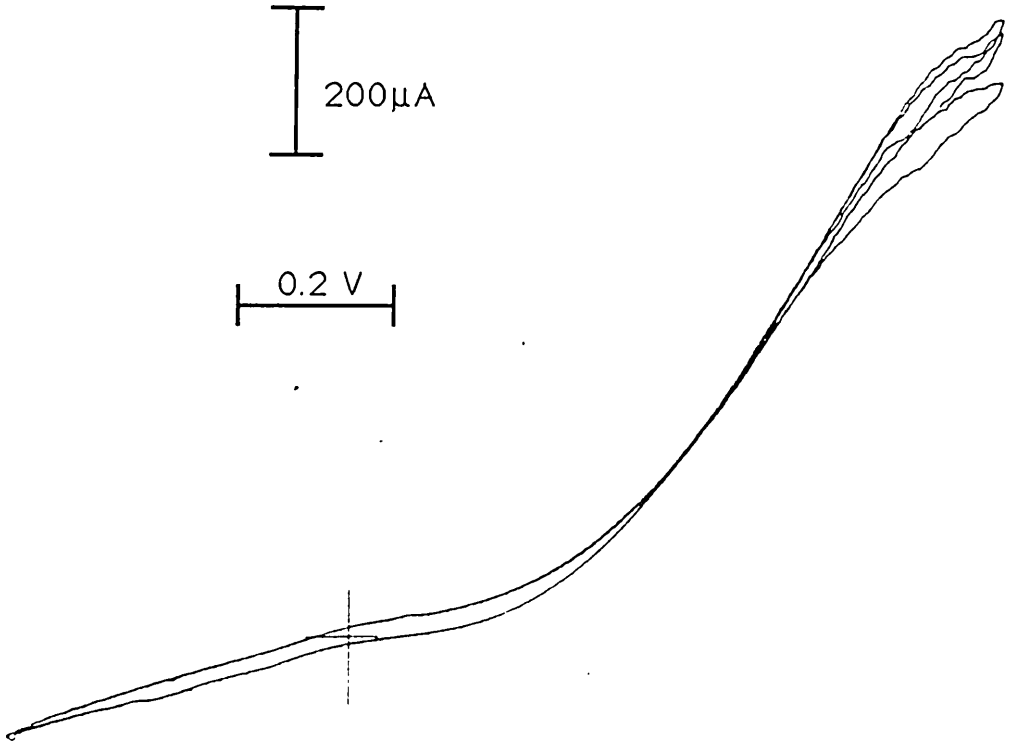

Figure 4.36 Catalytic current obtained on scanning a solution of sulfite oxidase, sulfite and $TTF^{+}Cl^{-}$

4.4.3.5.6 Coulometric Measurements

The charge passed during the four phases of the typical polarogram.

A= Anodic sweep to point of intersection

B= From point of intersection to end of anodic sweep

C= Cathodic sweep to point of intersection

D= From point of intersection to end of cathodic sweep

was measured by integrating the current. A typical plot is shown in Figure 4.37. The charge passed during regions A and D is of the opposite sign to that in regions B and C. Also the sum total charge passed in regions B and C is greater than that passed in zones A and D.

4.4.3.5.7 Effect of Potential Range on GOD/Glucose/TTF^+Cl^-

A 5mM glucose/GOD/TTF^+Cl^- solution was scanned between −200 mV and +400 mV (Figure 4.38). In this potential range no polarograms exhibiting hysteresis were observed. Hysteresis was not observed on extending the positive limit to +600 mV. When the positive limit was further increased to +800 mV then the anodic and cathodic sweeps followed a common pathway between +700 mV and +800 mV. Complete hysteresis was observed on increasing the positive limit to +1 V.

4.4.3.5.8 Behaviour of Glucose and GOD at Pt - Surfaces

Control experiments using TTF^+Cl^- and GOD alone showed that glucose was necessary for nucleation to be observed. On performing control experiments with GOD and glucose, nucleation was observed but the anodic peak was transformed into a much broader plateau which began ca. +600 mV (Figure 4.39). On adding TTF^+Cl^- to the solution the plateau shifted by ca. 100 mV to +700 mV and assumed a more peak-like shape.

Polarographic experiments were repeated, this time using AOD/methanol and

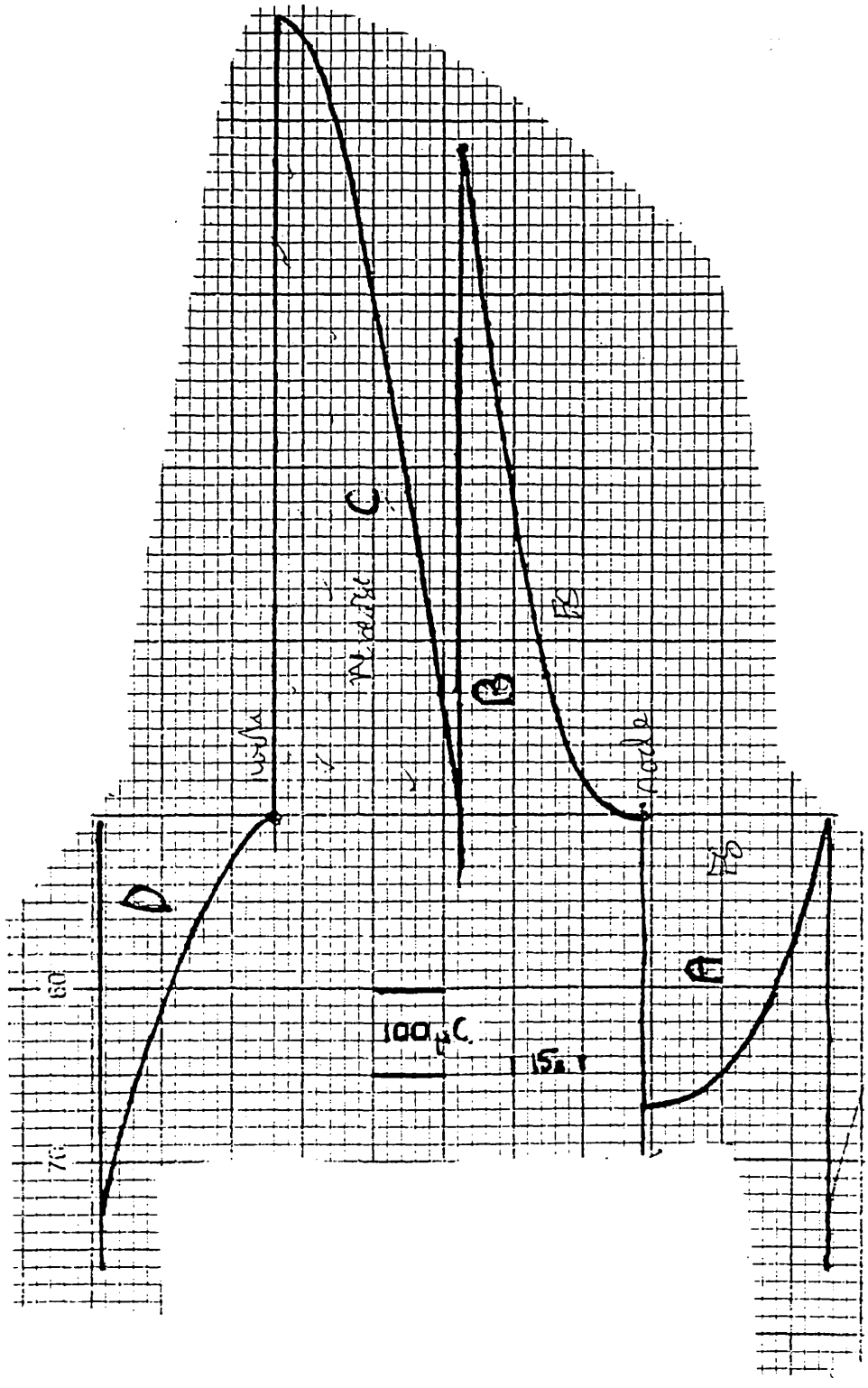

Figure 4.37 Results of coulometric measurements upon the GOD/glucose/TTF^+Cl^- system

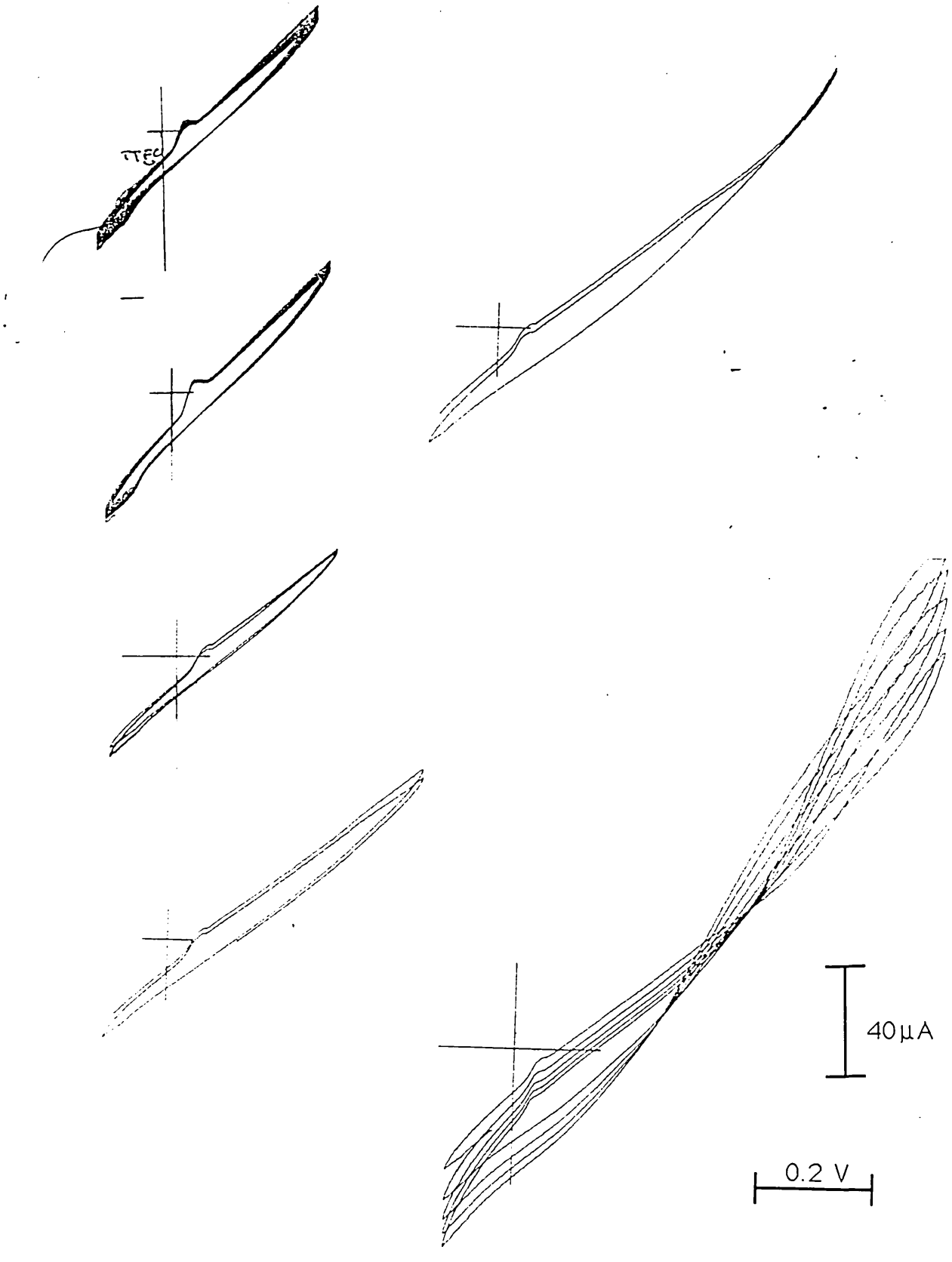

Figure 4.38 Effect of altering the limiting potential upon the nucleation phenomenon. [GOD] = 100 U/ml, [Glc] = 20mM. [TTF⁺Cl⁻] = Sat

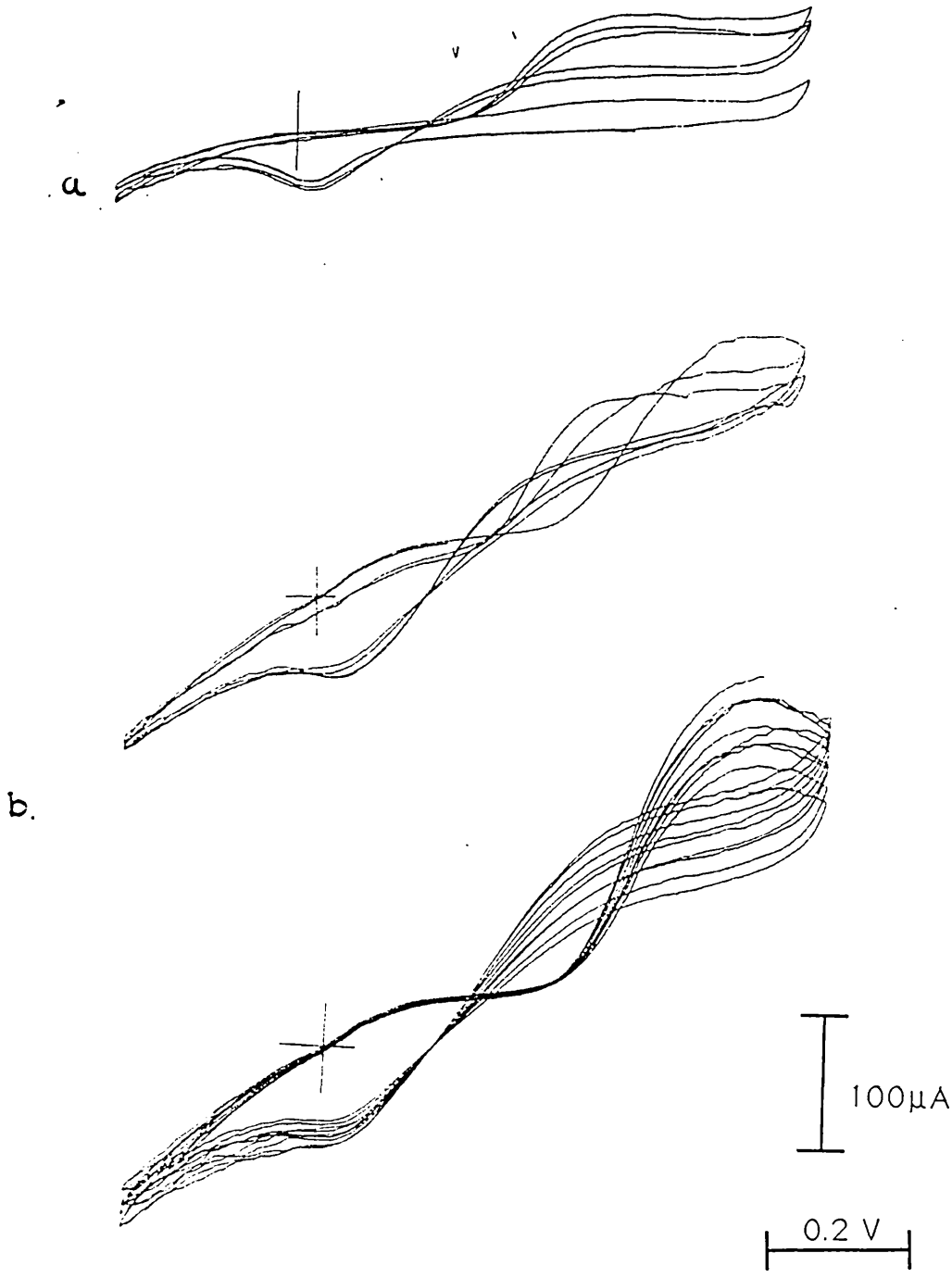

Figure 4.39 a) Nucleation is observed using glucose oxidase and glucose at a Pt-electrode. 100 U(ml GOD), [Cl⁻] = 20 mM

b) Effect of adding TTF^+Cl^- to a GOD/glucose system exhibiting nucleation

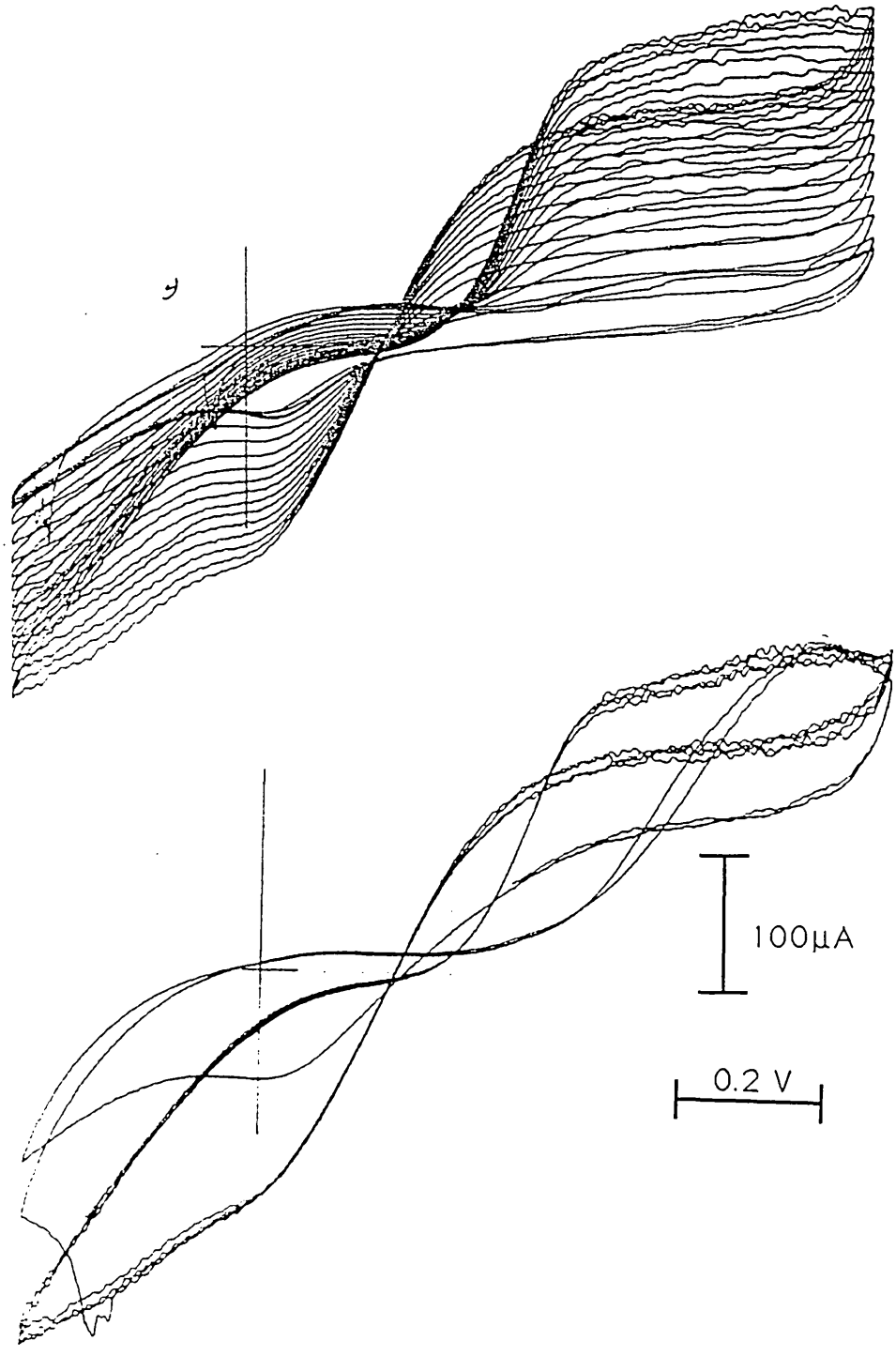

Figure 4.40 a) Nucleation is observed using sarcosine oxidase and sarcosine at a Pt-electrode. 50 U/ml SCD, 10 mM sarcosine

b) Effect of adding TTF^+Cl^- to a sarcosine oxidase/sarcosine system exhibiting nucleation

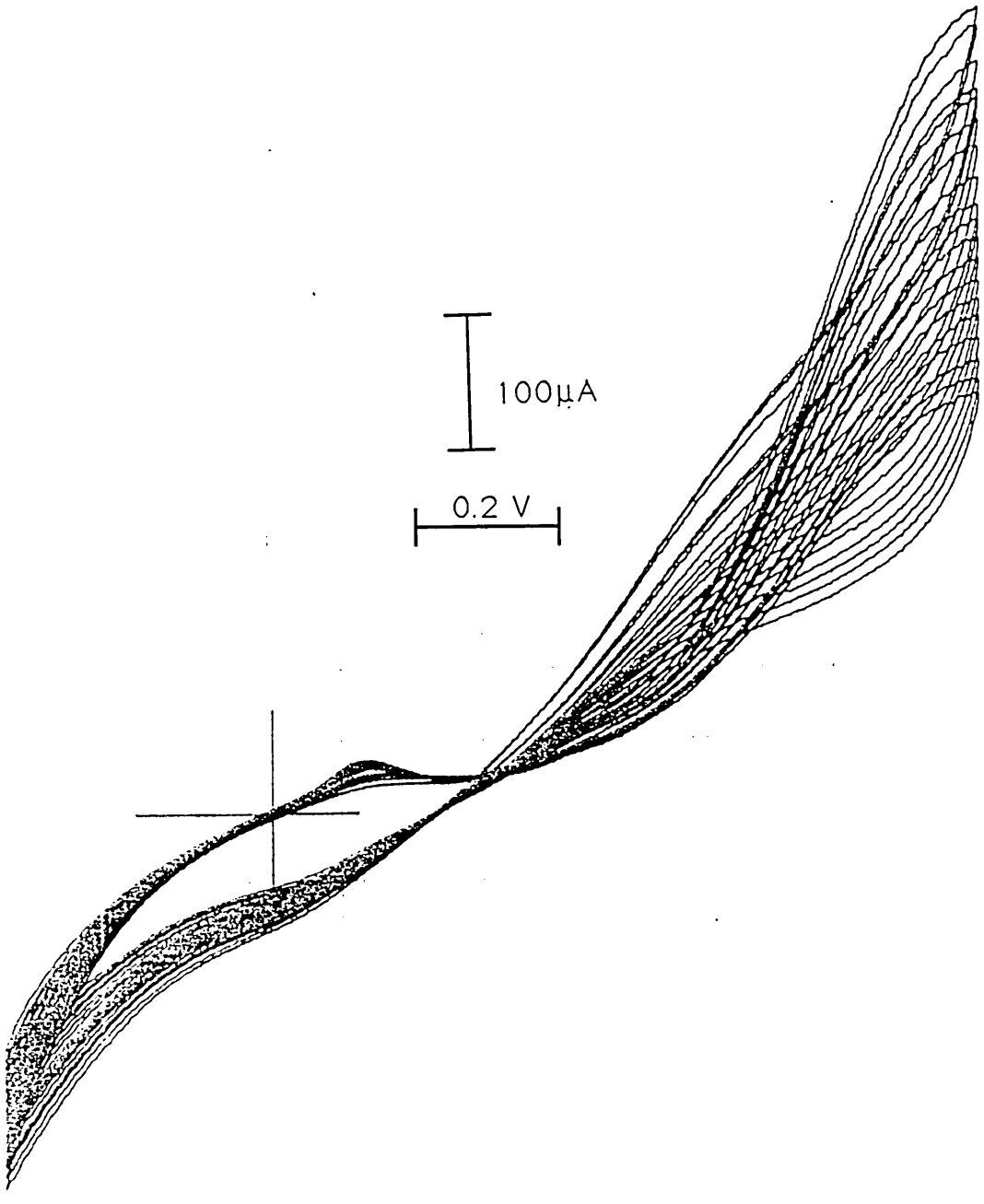

Figure 4.41 Nucleation is observed using alcohol oxidase and methanol

SOD/sarcosine, in the absence of TTF^+Cl^- (Figures 4.40 and 4.41). The latter system behaved in a similar manner to GOD producing a plateau in the anodic region. Alcohol oxidase produced polarograms which were similar to those previously obtained with this enzyme.

4.4.3.5.9 Effect of Scan Rate on Nucleation

All previous experiments had been carried out at a scan rate of 20 mV/s. Hence it was decided to investigate nucleation as a function of sweep rate. Nucleation was initiated at a Pt-disk electrode by scanning a solution of GOD (76 U/ml) and glucose (48mM) at a rate of 20 mV/s (Figure 4.42). The scan rate was then increased to 100 mV/s. The area of the hysteresis loop, and by implication the degree of nucleation, was instantly reduced. On returning to 20 mV/s the original polarogram was restored although the plateau height had increased. On switching to 100 mV/s the hysteresis loop had become almost negligible although there was a superimposition of the anodic and cathodic pathways for ca. 100 mV. As expected a scan rate of 50 mV/s produced intermediate behaviour. At 200 mV/s the anodic and cathodic pathways were clearly separated. Hysteresis was restored on returning to 50 mV/s.

The scan rate dependence of the TTF^+Cl^-/GOD/glucose system was also examined (Figure 4.43). The same pattern of behaviour was observed as in the above system. Hysteresis was present at 20 mV/s, reduced at 50 mV/s and disappeared at 100 mV/s.

4.4.3.5.10 Comparison of the Effects of TTF^+Cl^- and $K_3Fe(CN)_6$

On addition of $Fe(CN)_6^{3-}$ to a solution containing GOD (95 U/ml) and glucose (48 mM) no change was found in the anodic plateau region. However a couple corresponding to $Fe(CN)_6^{3-}/Fe(CN)_6^{4-}$ was observed superimposed upon the usual polarogram (Figure 4.44). This was in stark contrast to the effect of adding TTF^+Cl^- to a GOD/glucose solution. When $Fe(CN)_6^{3-}$ was added to a solution of

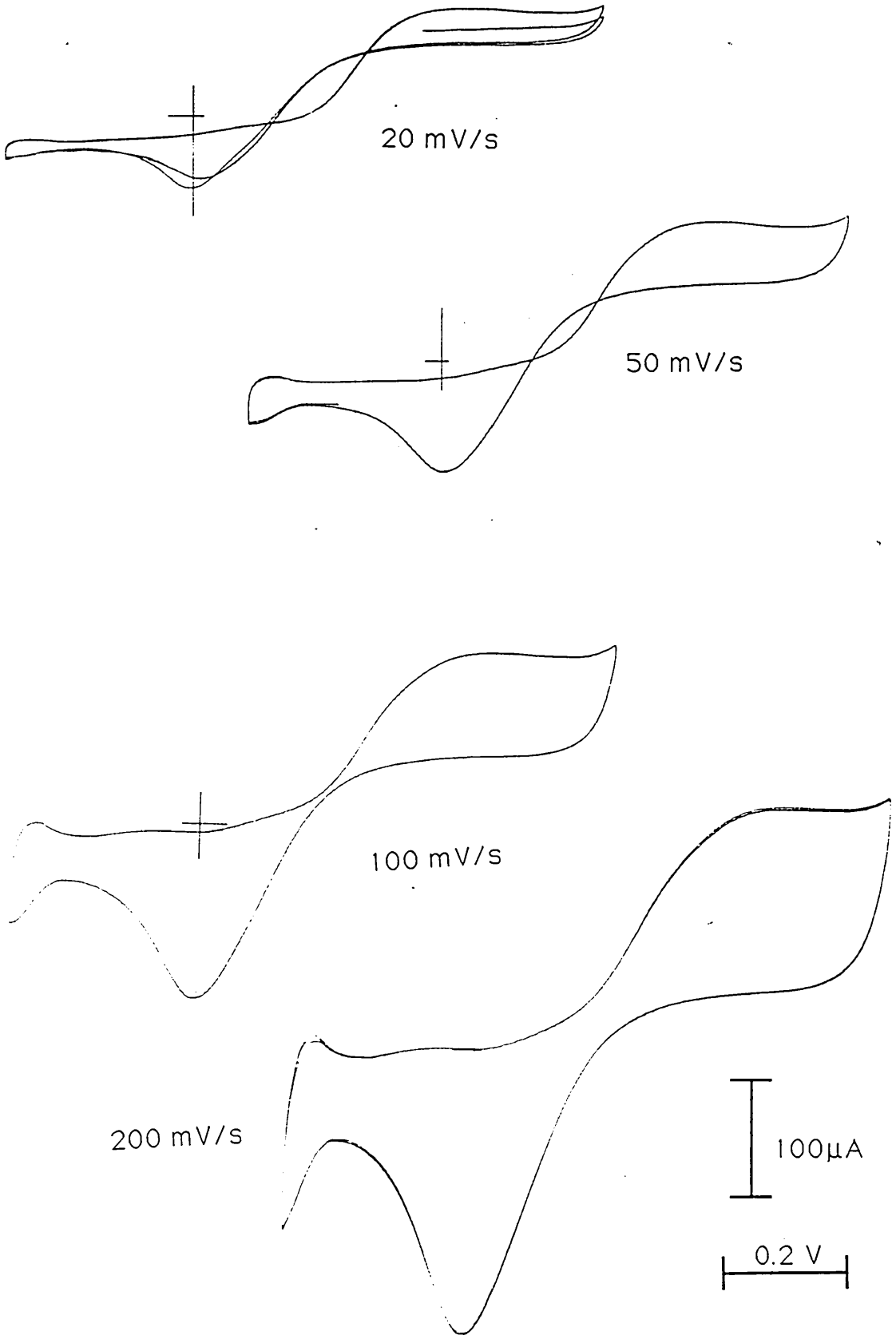

Figure 4.42 Effect of scan rate on nucleation exhibited by a GOD/glucose solution

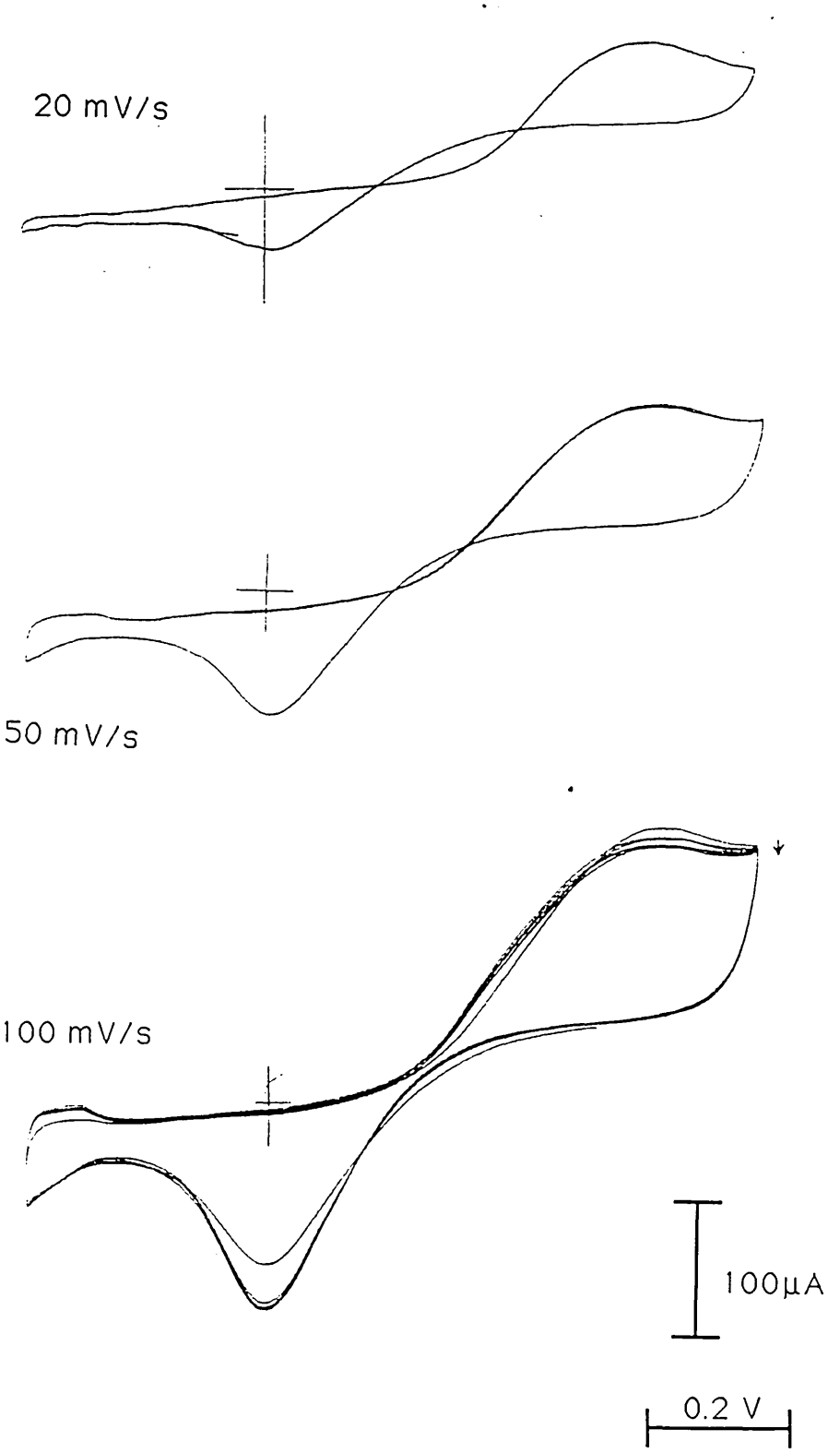

Figure 4.43 Effect of scan rate on nucleation exhibited by a

GOD/glucose/TTF^+Cl^- system. [GOD] = 100 u/ml
[Glc] = 20 mM, $[TTF^+Cl^-]$ = sat

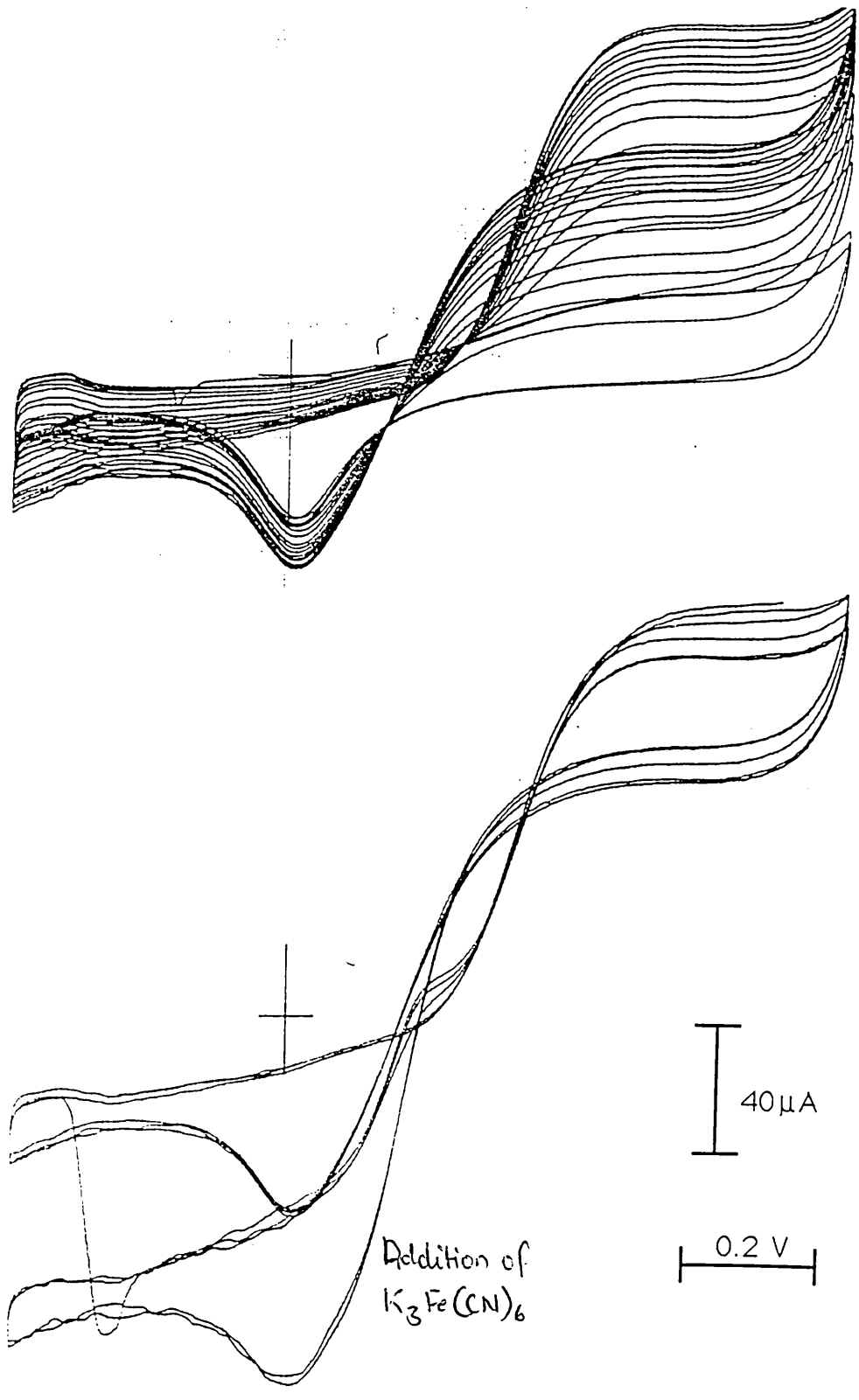

Figure 4.44 Effect of adding $K_3Fe(CN)_6$ to a solution of GOD/glucose exhibiting nucleation

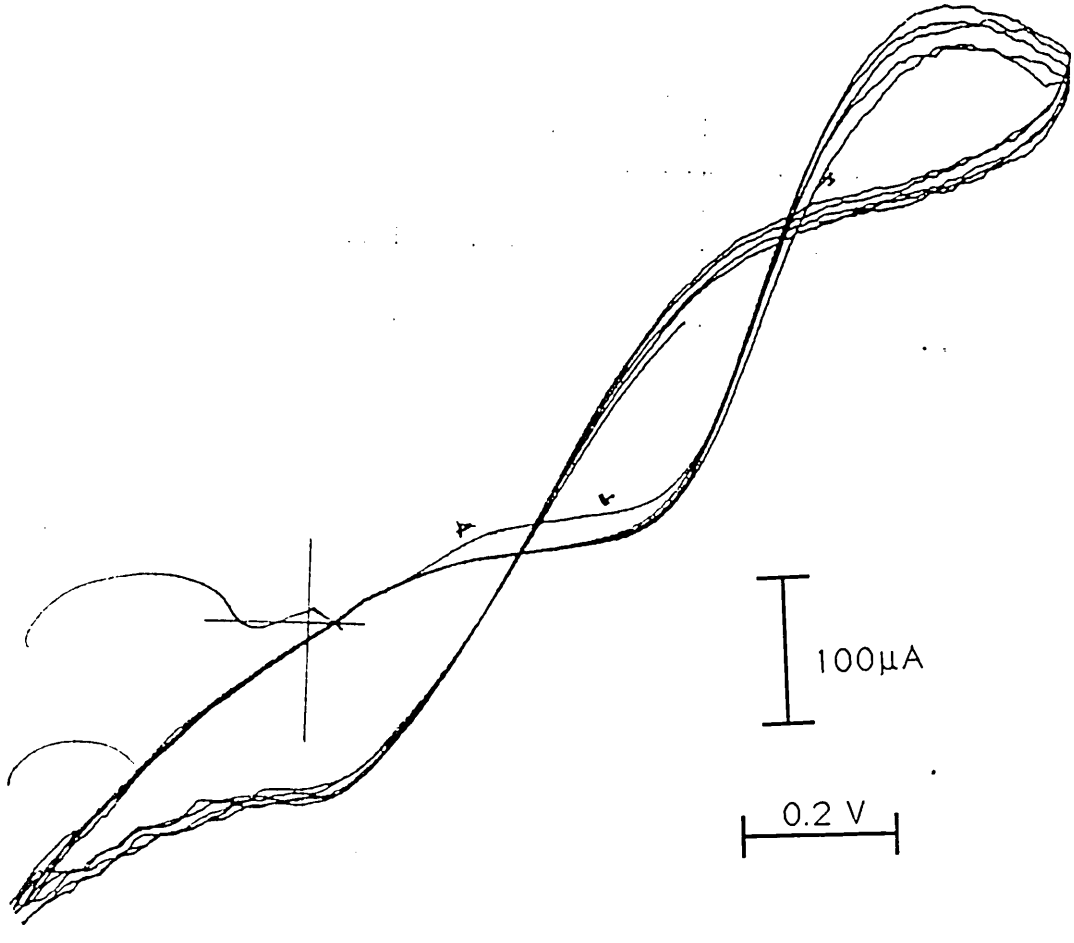

Figure 4.45 Effect of adding $K_3Fe(CN)_6$ to a solution of GOD/glucose/TTF^+Cl^-

TTF^+Cl^-/GOD/glucose a couple due to the mediator was again observed and there was no change in the nature of the anodic peak (Figure 4.45).

4.4.3.5.11 Effect of Poising Electrode at the Anodic Limit

A GOD/glucose system exhibiting hysteresis was held at the positive limit of +950 mV. The current decreased by 80% and on resumption of the cathodic sweep the position of the reverse peak was shifted by ca. 50 mV from +15 mV to -30 mV. The cathodic peak became both larger and sharper (Figure 4.46). TTF^+Cl^- was then added and upon attainment of a new stable anodic state the potential was held at +950 mV. The same effect was observed with the anodic current falling by 85% and the reverse peak shifting by 50 mV.

4.4.3.5.12 Variation of the Anodic Limiting Potential on the GOD/Glucose System

The effect of varying the positive limiting potential was determined using a GOD/glucose system. The initial positive limit was set at +600 mV and nucleation observed (Figure 4.47). Reduction of the positive limit to +400 mV caused the anodic and cathodic sweeps to diverge. Increasing the limit slightly to +450 mV caused a juxtaposition of the forward and reverse pathways from +320 to +370 mV. The anodic limit was then increased to +800 mV.

4.4.3.5.13 Effect of O_2 on Nucleation

All previous experiments had been thoroughly degassed using argon in order to prevent interference by oxygen. Now to accentuate the effect of any residual oxygen, the solution was not degassed. Under these conditions addition of glucose to a solution of GOD again produced hysteresis. However the shape of the polarogram was rather different (Figure 4.48), the cathodic peak became noticeably larger, presumably due to the presence of an increased O_2 reduction/PtO stripping peak. Also with each successive sweep the height of the anodic plateau was reduced as was the degree of hysteresis.

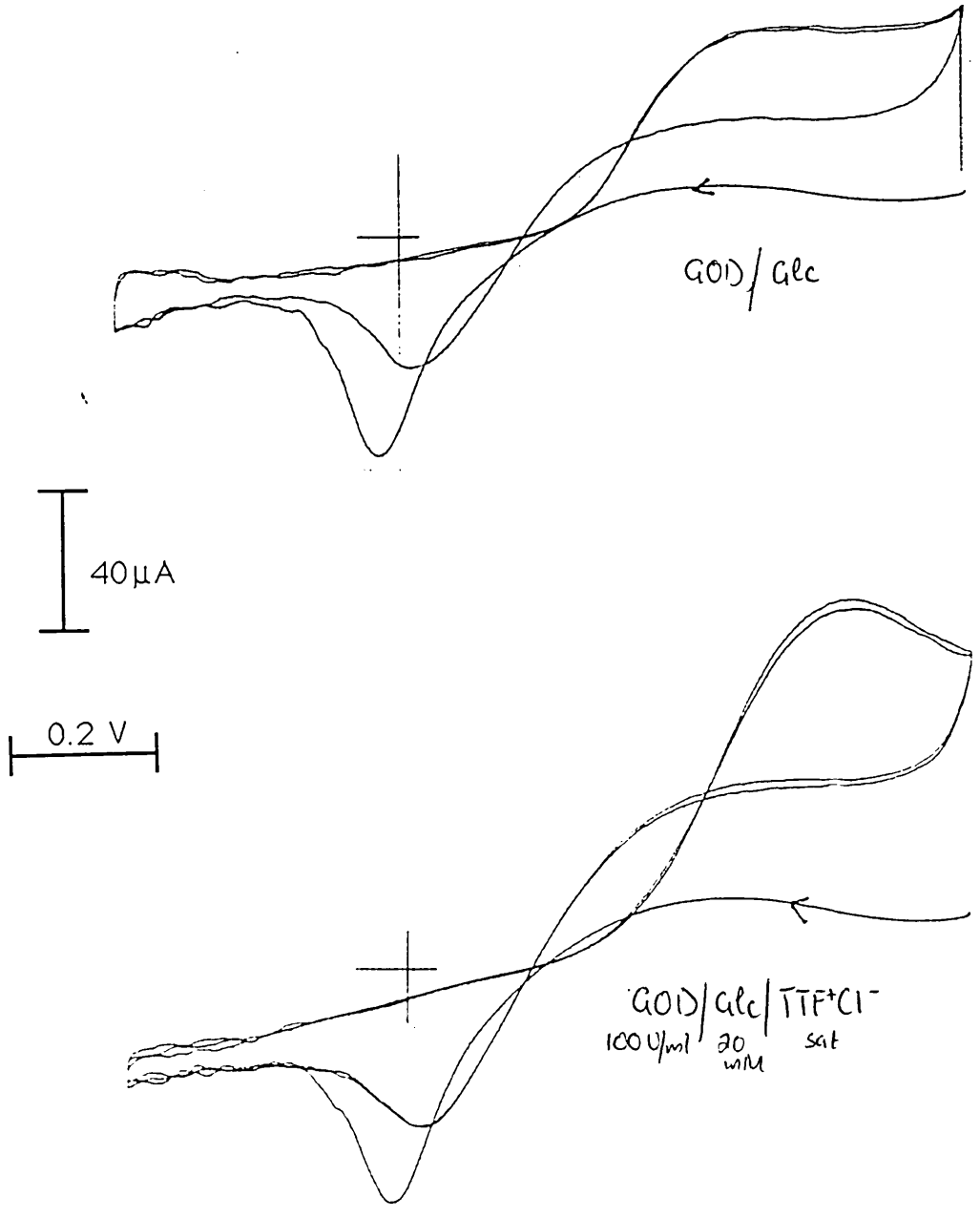

Figure 4.46 Effect of poising the electrode at the anodic limiting potential

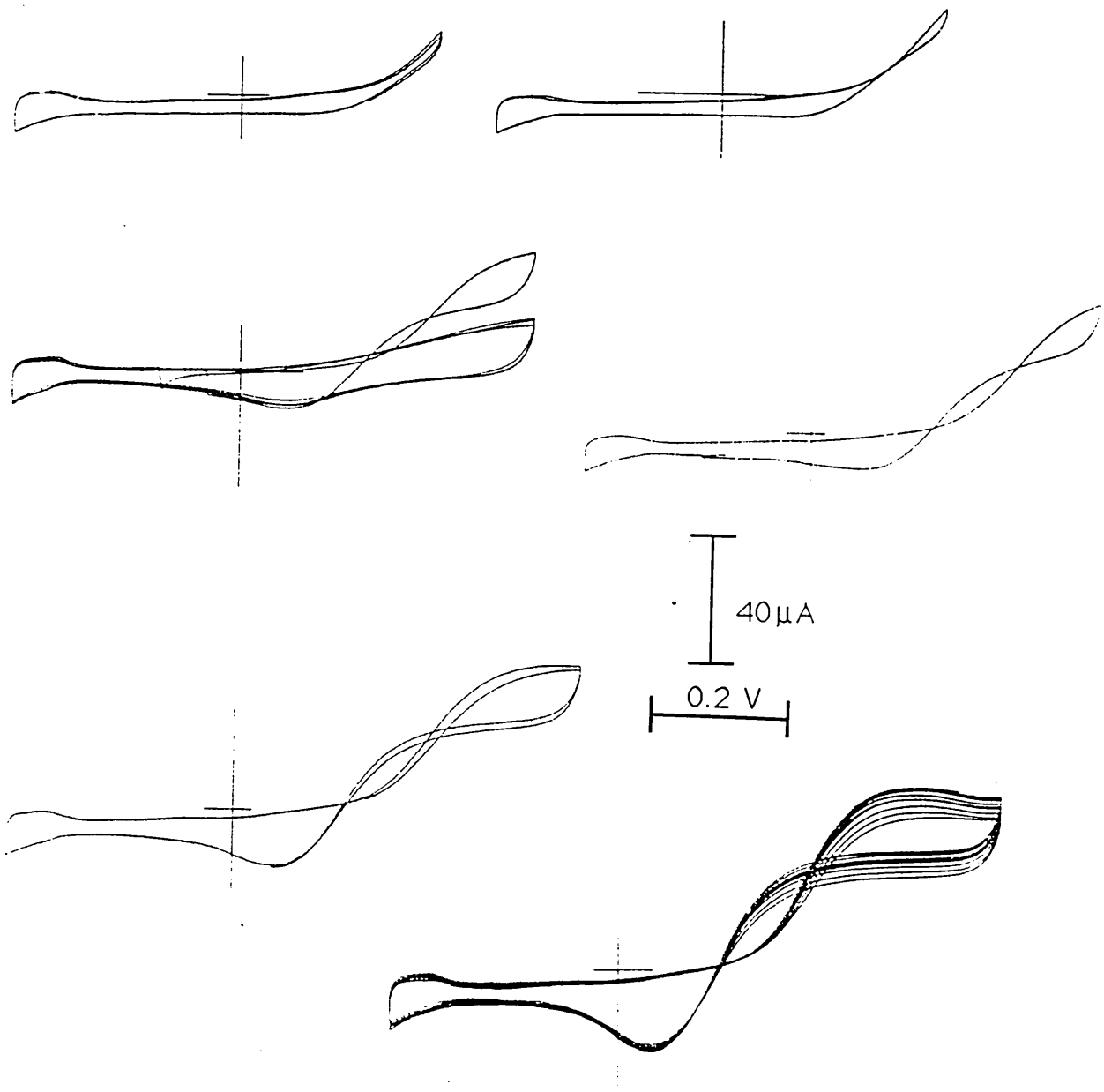

Figure 4.47 Variation of the anodic limiting potential affects the occurrence of nucleation in the GOD/glucose system

[GOD] = 100 u/ml, [Glc] = 20 mM

Eventually the system reached a state where there was no hysteresis and a conventional polarogram was obtained.

4.4.3.5.14 Effect of Altering Pt/PtO on the Surface

All Pt-electrodes were pretreated before use by first polishing with alumina then cycling in 0.2M H_2SO_4. A series of experiments was performed in order to determine whether the degree of O_2 and H_2 adsorption affected subsequent polarograms (Figure 4.49). Thus the cycles in H_2SO_4 were stopped at three particular points.

a. O_2 Adsorption

Poising at +1.8 V on the cathodic sweep ensured that O_2 would be adsorbed onto the electrode surface. Subsequent polarograms exhibited some degree of hysteresis

b. O_2 Stripping

The scan was halted at -200 mV, after the O_2 reduction/ PtO stripping peak. Thus the surface should now be essentially clean. Again polarograms were seen but with reduced hysteresis.

c. H_2 Adsorption

Stopping the scan at -350 mV ensured that a layer of H_2 was adsorbed on the electrode. A hysteresis loop was observed which was larger than those in the above two cases.

4.5 DISCUSSION

4.5.1 Rotating Disk and Ring/Disk Studies

The rotation speed behaviour of pressed pellet, Si-oil and electrodes made using polystyrene binder has been compared and shown to vary with the method of fabrication. This could be due to different rates of corrosion of the electrodes or to the different nature of the surface/enzyme interaction. It has also been shown that Si-oil solubilises TTF-

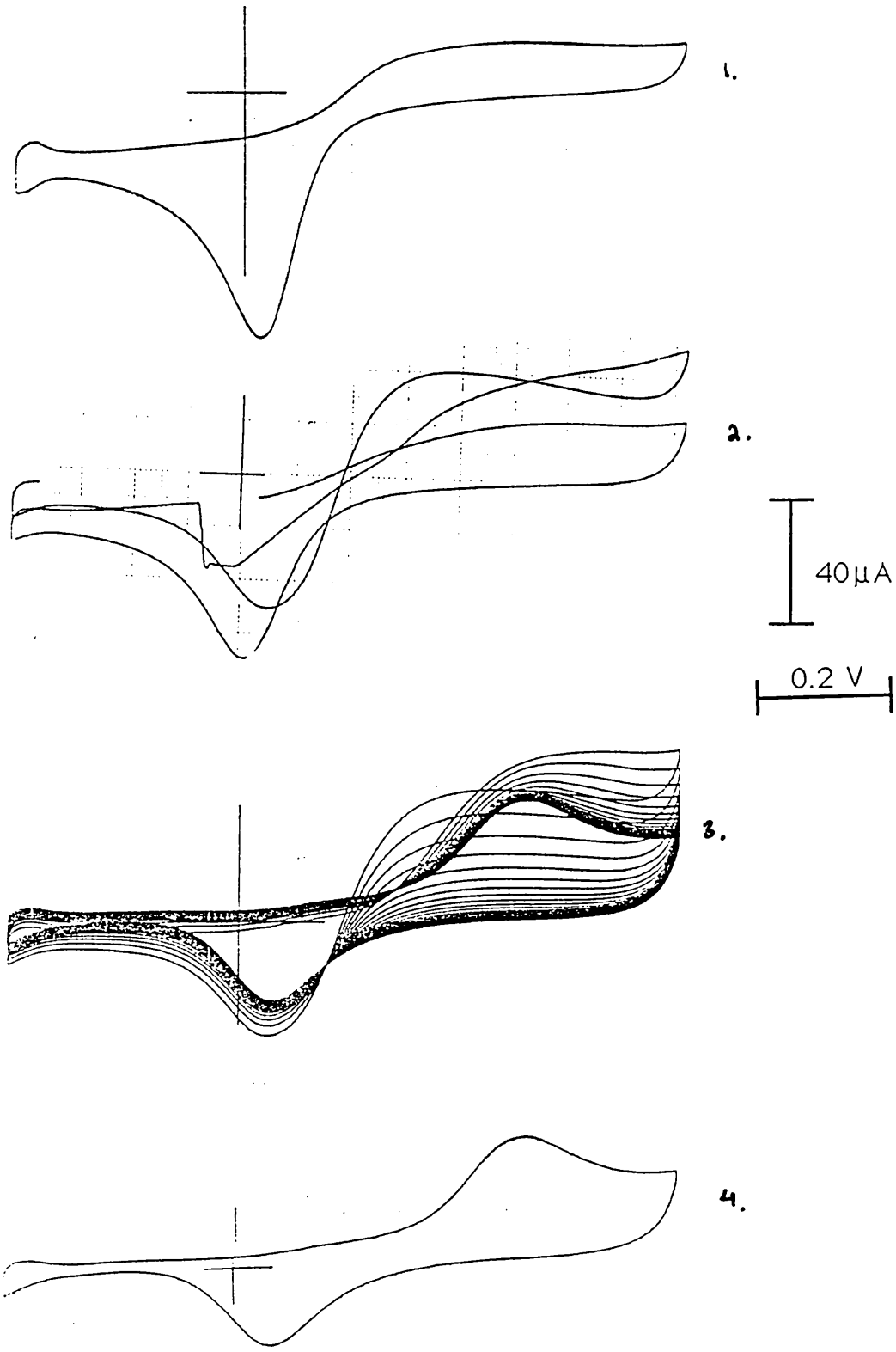

Figure 4.48 Effect of O_2 on nucleation exhibited by GOD/glucose

1-4, increasing time. [GOD] = 100 U/ml.
[Glc] = 20 mM

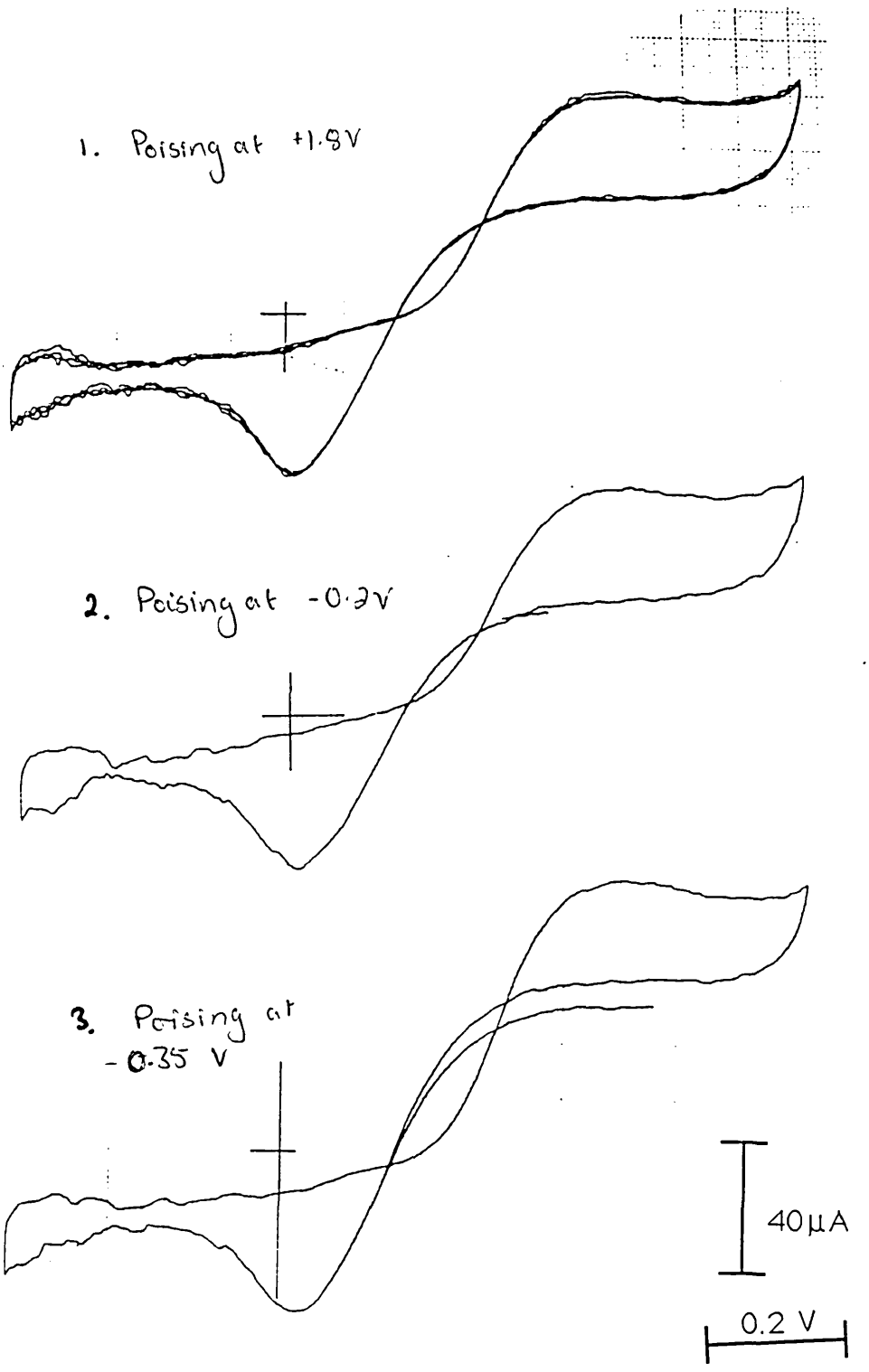

Figure 4.49 Variation of pretreatment procedure has no marked effect on the nucleation behaviour

TCNQ hinting at the involvement of a biphasic system. Modified enzyme has been shown to obey the same rotation speed dependence as its unmodified counterpart. The results obtained using the pressed pellet TTF-TCNQ disk/Pt-ring electrode showed that both the oxidising and reducing ring currents were proportional to the substrate concentration. This weighs heavily against the heterogeneous model. The high collection efficiency observed when the ring was poised at +300mV provided qualitative support for the homogeneous model. However neither theory could account for the inconsistency of the ring current data. The strongest support in favour of the homogeneous model came from experiments using low [glucose]. The collection efficiencies observed were in reasonable quantitative agreement with those predicted by the thin gap thin ring (TGTR) approximation.

The homogeneous mechanism provides a reasonable explanation for the behaviour observed at Si-oil and pressed pellet electrodes (8). However, assuming its validity at PST electodes would imply that the system was in Case V or Case VI at low [glc]. Hence the rate determining processes would involve reactions in the diffusion layer. Thus the magnitude of the observed current should not vary with the nature or area of the elctrode surface. Since this is not the case (§4.4.2.1) a different mechanism must operate at PST electrodes.

4.5.2 Nucleation Phenomena

The nucleation results were initially explained in terms of an enzyme layer being adsorbed on to a film of TTF^+. However as the effect was also observed in the presence of enzyme and substrate alone this suggested the latter was involved, perhaps being destroyed on the surface and effectively forming a modified electrode enabling adsorption of active enzyme. Since TTF^+ alters the nature of the polarogram it is proposed that it can modify either the surface or the enzyme itself since conventional mediators such as $Fe(CN)_6^{3-}$ have no effect.

The adsorption and electro-oxidation of glucose at platinum electrodes has been

investigated in the literature (15). Glucose exists in a dynamic equilibrium in solution

$$G\ (\alpha) \Leftrightarrow G\ (\beta) \Leftrightarrow G\ (\gamma)$$

where α and β are the cyclic hemiacetal forms and γ is the free aldehyde species. There has been considerable debate over the nature of the adsorbed species. However since mass spectrometry (16) revealed the presence of glucono-δ-lactone it was concluded that the hemicacetal (α,β) forms must be involved. Adsorption of phosphate and chloride anions competes with glucose adsoprtion, complicating the picture (14,15). The former is adsorbed via formation of a metal-oxygen bond.

The chemisorption of glucose is accompanied by its dehydrogenation with the observed current being due to the oxidation of hydrogen formed during the dehydrogenation reaction. The overall scheme can be described as

$$G + Pt \Leftrightarrow (R_{ads})Pt + xH^+ + xe^-$$

The terminal oxidation product of any R_{ads} species is CO_2,

$$(R_{ads})Pt + xH_2O \rightarrow CO_2 + nH^+ + ne^- + xPt(H_2O)$$

Thus it is possible that on addition of glucose to a solution of GOD, or GOD/TTF^+Cl^-, it is initially adsorbed and electro-oxidised. By adsorbing onto the electrode surface it facilitates subsequent adsorption by GOD which can then catalytically oxidise glucose present in solution near the metal/solution interface. Since this current will increase with time, tending to a steady state, it explains the continuously increasing currents seen in the polarograms exhibited by these systems.

REFERENCES

1. J. J. Kulys, A. S. Samalius and G. J. S. Svirmickas, FEBS Lett., 114(1), 7, (1980)
2. N. K. Cenas and J. J. Kulys, J. Electroanal. Chem., 128, 103, (1981)
3. J. J. Kulys and A. S. Samalius, J. Electroanal. Chem., 155, 385, (1983)
4. D. H. Craston, Ph. D. Thesis, Univ. of London, (1986)
5. W. J. Albery, P. N. Bartlett and A. E. G. Cass, Phil. Trans. R. Soc., London, B 316, 107, (1987)
6. W. J. Albery, P. N. Bartlett, B. J. Driscoll and R. B. Lennox, to be published
7. B. J. Driscoll, Ph. D. Thesis, Univ. of London, (1988)
8. L. J. Murphy, Ph. D. Thesis, Univ. of London, (1989)
9. P. N. Bartlett, private communication
10. J. Ferraris, D. O. Cowan, V. Walatka and J. H. Perlstein, J. Amer. Chem. Soc., 95, 948, (1973)
11. M. S. Freund and A. Brajter-Toth, Anal. Chem., 61, 1048, (1989)
12. W. J. Albery, unpublished results
13. W. J. Albery, S. Bruckenstein and D. T. Napp, Trans. Faraday Soc., 62, 1932, (1966)
14. Yu. B. Vassilyev, O. A. Khazova and N. N. Nikolaeva, J. Electroanal. Chem., 196, 105 and 127, (1985)
15. M. F. L. de Mele, H. A. Videla and A. J. Arvia, J. Electroanal. Chem., 155, 239, (1983)
16. S. Ernst, J. Heitbaum and C. H. Hamann, J. Electroanal. Chem., 100, 173 (1979)
17. R.S. Nicholson and I. Shain, Anal. Chem., 36, 706, (1964)
18. J. M. Saveant and E. Vianello, Advances in Polarography, Ed. I. S. Longmuir, Vol 1, Pergamon Press, New York, (1960)

CHAPTER 5

MECHANISTIC STUDIES USING A. C. TECHNIQUES

The underlying principle behind a.c. impedance techniques is that of perturbing the system by applying an alternating potential of small magnitude and following the system as it responds to the perturbation (1,2). An advantage of this method of analysis is that the theoretical treatment of the response can be simplified by linearizing the current-potential characteristics.

In the main, the experiments detailed in this chapter were performed at high substrate concentrations. Hence an attempt was made first to fit the data to an a.c. model of Case I of the homogeneous mechanism. Where this proved unsatisfactory, alternative models were developed in order to explain the experimental results.

5.1 A.C. THEORY

5.1.1 AC Treatment of Cases I and II of the homogeneous model (4)

In Case I, a change in potential, ΔE, produces a small change, $m_{*,o}$, in the concentration of the mediator, M, where $\overline{m}$ is the concentration before the change. Thus

$$\frac{m_{*,o}}{\overline{m}} = \frac{\alpha F \Delta E}{RT} \qquad 5.1$$

The observed current has two components. First, the reduced mediator, M', is oxidised at the electrode. Second, the dissolution of the oxidised mediator, M, from the electrode surface can also produce a transfer of charge. Thus assuming that ,

$$M^{+}_{solv} \longrightarrow M^{+}_{aq}$$

contributes to the overall current, then the time variable current, i_*, is given by,

$$i_* = AFD\left[-\left(\frac{\partial m_*}{\partial z}\right)_o + \left(\frac{\partial m'_*}{\partial z}\right)_o\right] \qquad 5.2$$

The negative sign indicates that the concentration gradients for M and M′ lie in opposite directions.

In the Laplace domain, the impedance, Z, is given by

$$Z = \frac{\Delta E}{\bar{si}_*} \quad \text{where } s=i\omega \tag{5.3}$$

The concentration of M can be considered as consisting of a time independent component, m, and a time dependent contribution, $m_{*,o}$, thus

$$m_{tot} = m + m_{*,o} \tag{5.4}$$

In Case I, $m_{*,o}$ is described by the following equation,

$$D\frac{\partial^2 m_{*,o}}{\partial z^2} = km_{*,o} + \frac{\partial m_{*,o}}{\partial t} \tag{5.5}$$

Solving using Laplace transforms gives

$$\bar{m}_* = \frac{m_{*,o}}{s} \exp\left(-\sqrt{\frac{k+s}{D}}\, z\right) \tag{5.6}$$

Differentiating and setting z=0

$$\left(\frac{\partial \bar{m}_*}{\partial z}\right)_o = -\frac{m_{*,o}}{s}\sqrt{\frac{s+k}{D}} \tag{5.7}$$

A similar treatment for the reduced mediator yields,

$$\left(\frac{\partial \bar{m}'_*}{\partial z}\right)_o = \frac{m_{*,o}}{s\sqrt{D}}\left[\sqrt{s+k} - \sqrt{s}\,\right] \tag{5.8}$$

Substituting eqns 5.7 and 5.8 into eqn. 5.2 gives

$$\bar{si}_* = m_{*,o}\, AF\sqrt{D}\left[\,2\sqrt{s+k} - \sqrt{s}\,\right] \tag{5.9}$$

Therefore combining eqns. 5.1, 5.3 and 5.9 gives

$$Z = \frac{RT}{A\sqrt{D}\,F^2\alpha\bar{m}}\left(\frac{1}{2\sqrt{s+k} - \sqrt{s}}\right) \tag{5.10}$$

If

$$\theta = \frac{\omega}{k} \tag{5.11}$$

and

$$Z_o = \frac{RT}{2A\sqrt{Dk}\, F^2 \alpha \overline{m}} \tag{5.12}$$

then

$$\frac{Z_o}{Z} = \sqrt{i\theta + 1} - \tfrac{1}{2}\sqrt{i\theta} \tag{5.13}$$

Thus an a.c. analysis of Case I results in the following expression for the impedance,

$$\frac{Z_o}{Z} = \frac{1}{\sqrt{2}}\left(\left[(1+\theta^2)^{1/2}+1\right]^{1/2} - \frac{\sqrt{\theta}}{2} + i\left\{\left[(1+\theta^2)^{1/2}-1\right]^{1/2} - \frac{\sqrt{\theta}}{2}\right\}\right) \tag{5.14}$$

For small θ, eqn. 5.14 reduces to

$$\frac{Z_o}{Z} = 1 - \frac{\sqrt{\theta}}{2\sqrt{2}} - \frac{i\sqrt{\theta}}{2\sqrt{2}} \tag{5.15}$$

whilst at large θ,

$$\frac{Z_o}{Z} = \frac{\sqrt{\theta}}{2\sqrt{2}} + \frac{i\sqrt{\theta}}{2\sqrt{2}} \tag{5.16}$$

A similar analysis for Case II yields,

$$Z = \frac{RT}{A\sqrt{D}\, F^2 \alpha \overline{m}}\left(\frac{1}{\sqrt{s+k}-\sqrt{s}}\right) \tag{5.17}$$

and

$$\frac{Z_o}{Z} = \frac{1}{\sqrt{2}}\left(\left[(1+\theta^2)^{1/2}+1\right]^{1/2} - \sqrt{\theta} + i\left\{\left[(1+\theta^2)^{1/2}-1\right]^{1/2} - \sqrt{\theta}\right\}\right) \tag{5.18}$$

Now, for small θ,

$$\frac{Z_o}{Z} = 1 - \frac{\sqrt{\theta}}{\sqrt{2}} - \frac{i\sqrt{\theta}}{\sqrt{2}} \tag{5.19}$$

and for large values of θ,

$$\frac{Z_o}{Z} = \frac{1}{\sqrt{2\theta}} - \frac{i}{\sqrt{2\theta}} \tag{5.20}$$

The above analysis shows that at low θ both Cases I and II show similar behaviour (eqns. 5.15 and 5.19). However at large θ they behave very differently and this makes it possible to distinguish between them.

The observed real and imaginary impedances, X' and Y' respectively, were normalised by the following method,

$$X = \frac{X'}{(X')^2 + (Y')^2} \quad \text{and} \quad Y = \frac{-Y'}{(X')^2 + (Y')^2}$$

5.2 EXPERIMENTAL

5.2.1 Chemicals and Solutions

All experiments were carried out using pH 7.4 buffer containing 0.1M phosphate and 0.15M NaCl as in §2.2.1. Glucose oxidase was obtained from Sigma. Modified enzyme was prepared as described in §4.3.2

5.2.2 Electrodes

Electrodes were fabricated as described in §2.1.3 and §4.3.3. Electrodes made with polystyrene (PST) binder were used unless otherwise indicated.

5.2.3 Procedure

The experiments were performed using a frequency response analyser (Solartron Instruments 1250) using standard techniques. A 20mV peak-to-peak a.c. ripple was applied in all the experiments. The electrodes were rotated at 9 Hz unless otherwise indicated. Solutions were degassed using argon. All potentials were measured with respect to a saturated calomel electrode.

An enzyme concentration of approximately 100 U/mL was used unless otherwise indicated. Frequency decreases from origin.

5.3 RESULTS

5.3.1 Impedance Spectrum of GOD/Glc

The complete impedance spectrum for glucose oxidase at 0, +125, +190, +250 and +300 mV and at a series of substrate concentrations, ranging from 250 μM to 200 mM, is shown in Figure 5.1-5.13. Two points are worth noting. First, it is apparent that the real impedance, X', increased with the electrode potential. Second, at a given electrode potential, the imaginary impedance, Y', decreased as the glucose concentration was increased. Also at high [glc] the impedance spectrum began to exhibit "semi-circular behaviour". The effect was most pronounced at the higher electrode potentials, namely 250 and 300 mV. When the electrode was poised at the latter potential, the impedance plots at [glc]$\geq$5mM crossed the X' axis and began forming a second loop. Thus at low frequencies the impedance became inductive. Since the effect was most marked at 300 mV further investigations were carried out at this potential.

5.3.2 Determination of the Low Frequency D.C. Limit

In order to determine whether the low frequency a.c. limit in the inductive region tended towards the d.c. limit, the electrode was held at 289, 300 and 311 mV and its d.c. resistance evaluated. A value of 24.4 kΩ was obtained. This was compared to the impedance at the low frequency limit in an experiment with the electrode poised at 300 mV with a peak-to-peak a.c. ripple of 20 mV. Figure 5.14 shows that the impedance at the low frequency limit does indeed approximate closely to its d.c. equivalent.

A plot of ω/Y' against ω^2 suggested that the system was exhibiting Randles (3) behaviour in the high frequency region. However a confirmatory plot of $1/X'\omega$ against $1/\omega^2$ did not produce a straight line, giving instead a sharp "dog-leg". The first plot gives added weight to the high frequency points whilst the latter is biased to those at the lower end of the frequency spectrum. By plotting $1/Y'\omega$ against $1/\omega^2$, the points at lower frequencies are again given added weighting. This also produced a non-linear plot. Thus it

Figure 5.1 Impedance spectrum : GOD/glc on PST/TTF-TCNQ, 0 mV, 1K-0.1 Hz

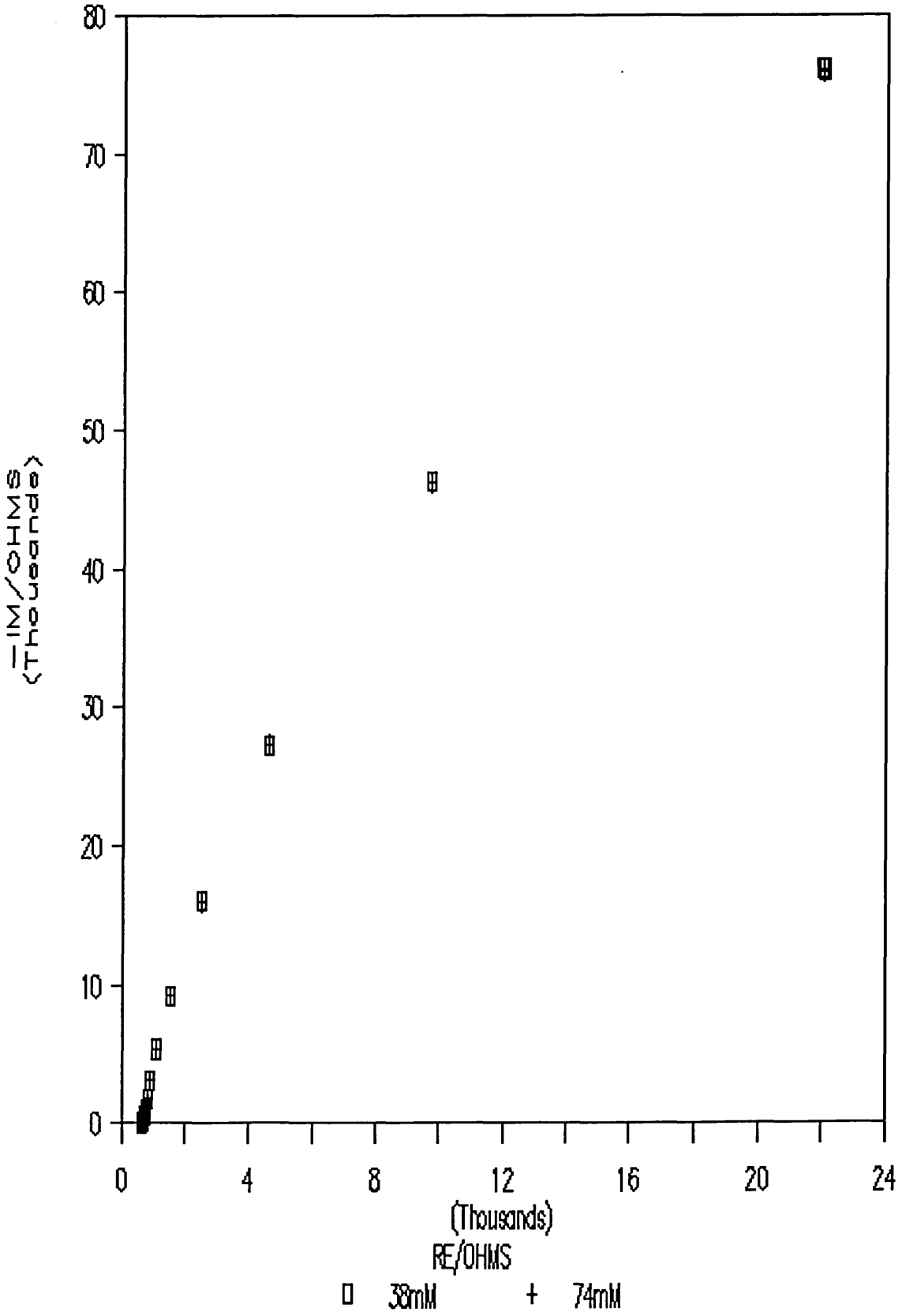

Figure 5.2 Impedance spectrum : GOD/glc on PST/TTF-TCNQ, +125 mV, 1K-0.1 Hz

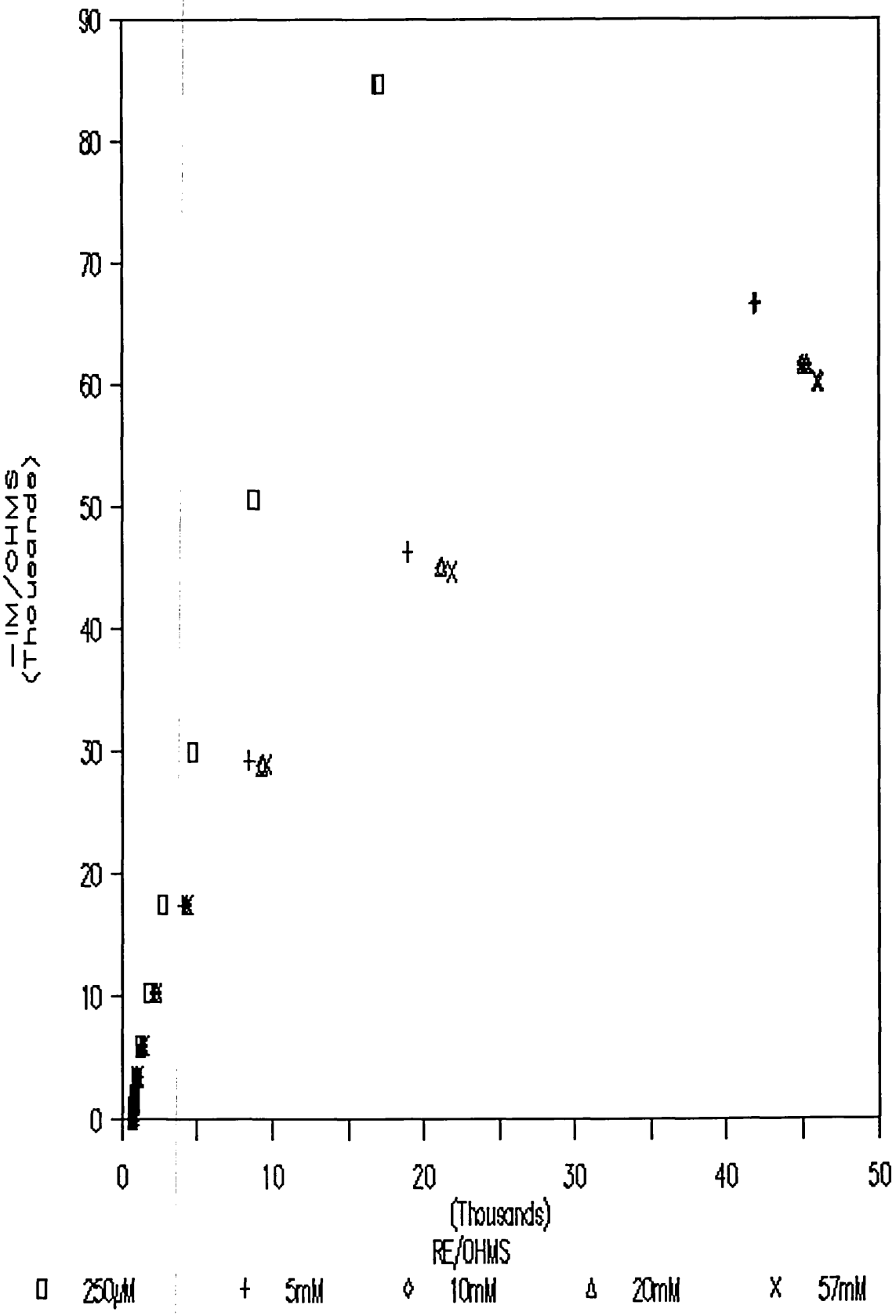

Figure 5.3 Impedance spectrum : GOD/glc on PST/TTF-TCNQ, +190 mV, 1K-0.1Hz

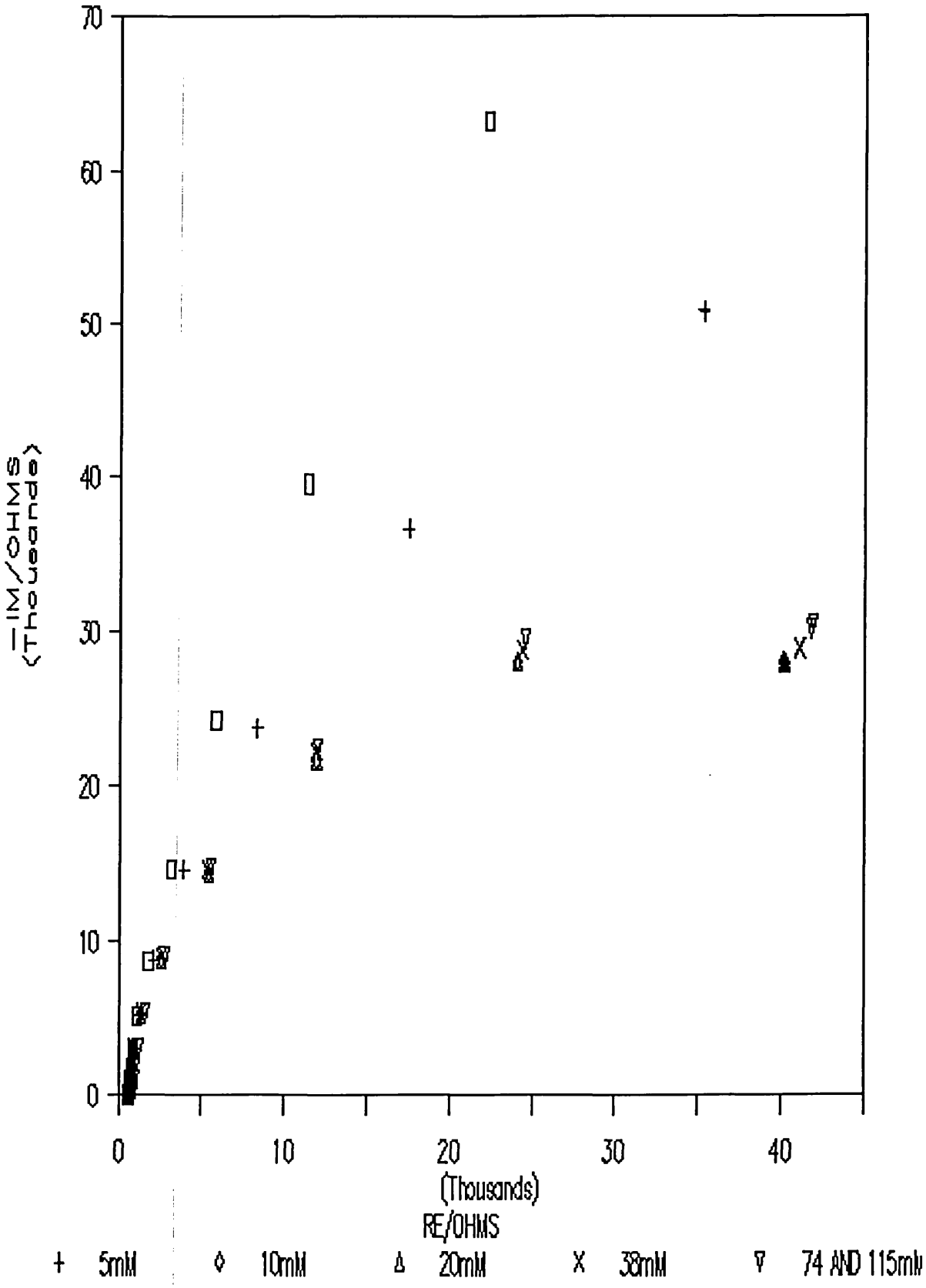

Figure 5.4 Impedance spectrum : GOD/glc on PST/TTF-TCNQ, +250 mV, 1K-0.1 Hz

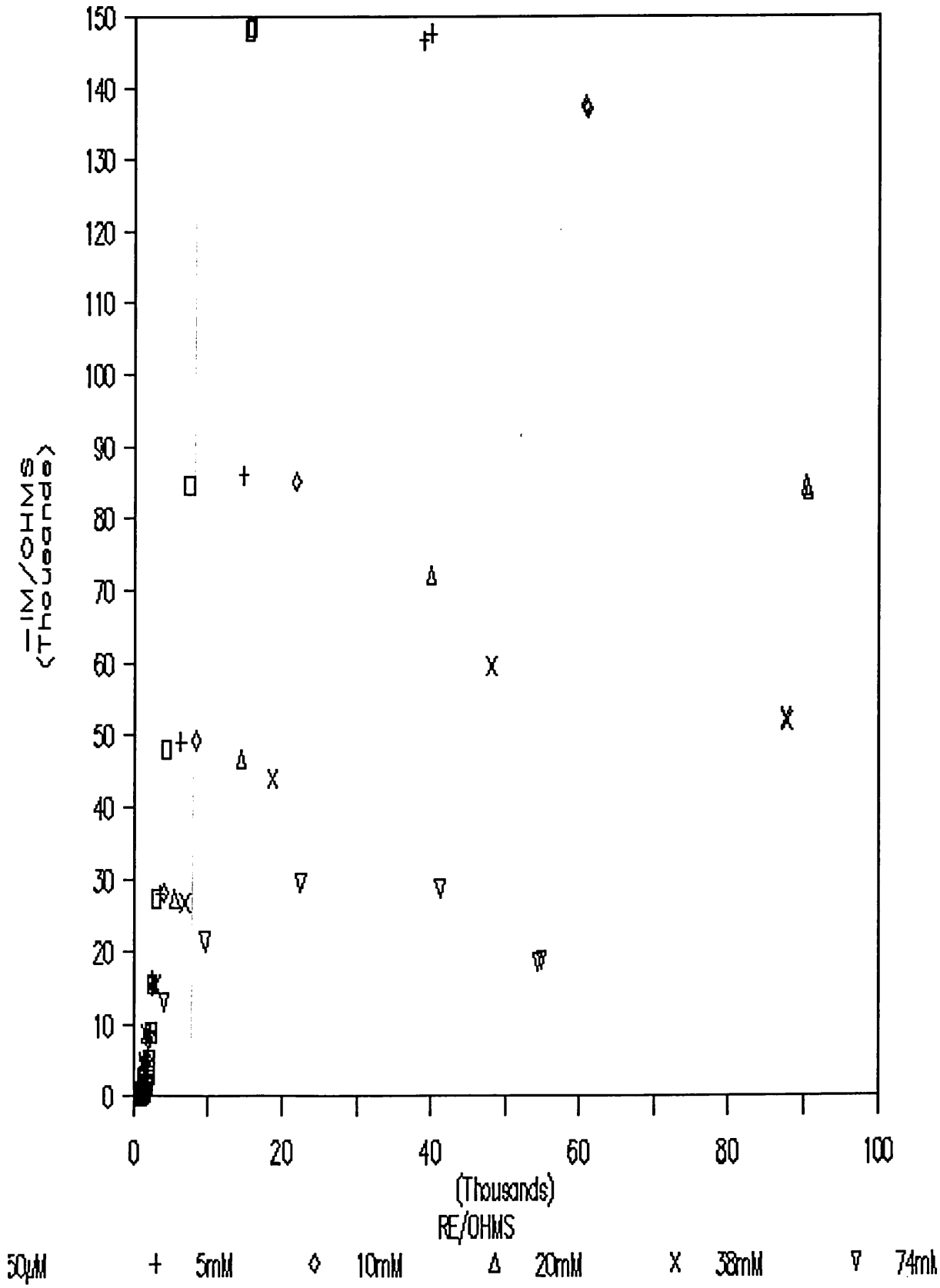

Figure 5.5 Impedance spectrum : GOD/glc on PST/TTF-TCNQ, +300 mV, 1K-0.01 Hz

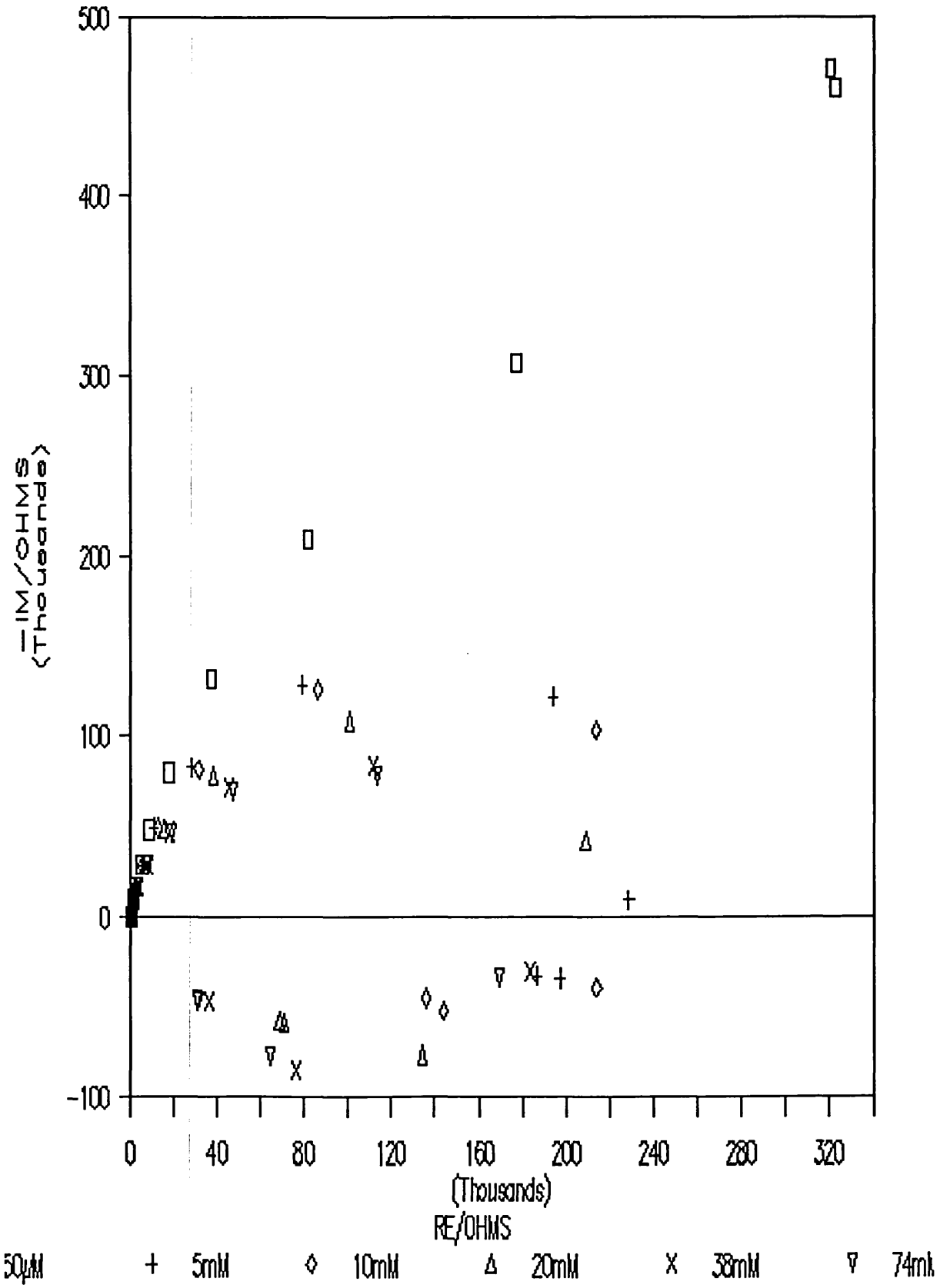

Figure 5.6 GOD/250 μM glc on PST/TTF-TCNQ, +300 mV, 1K-0.01 Hz

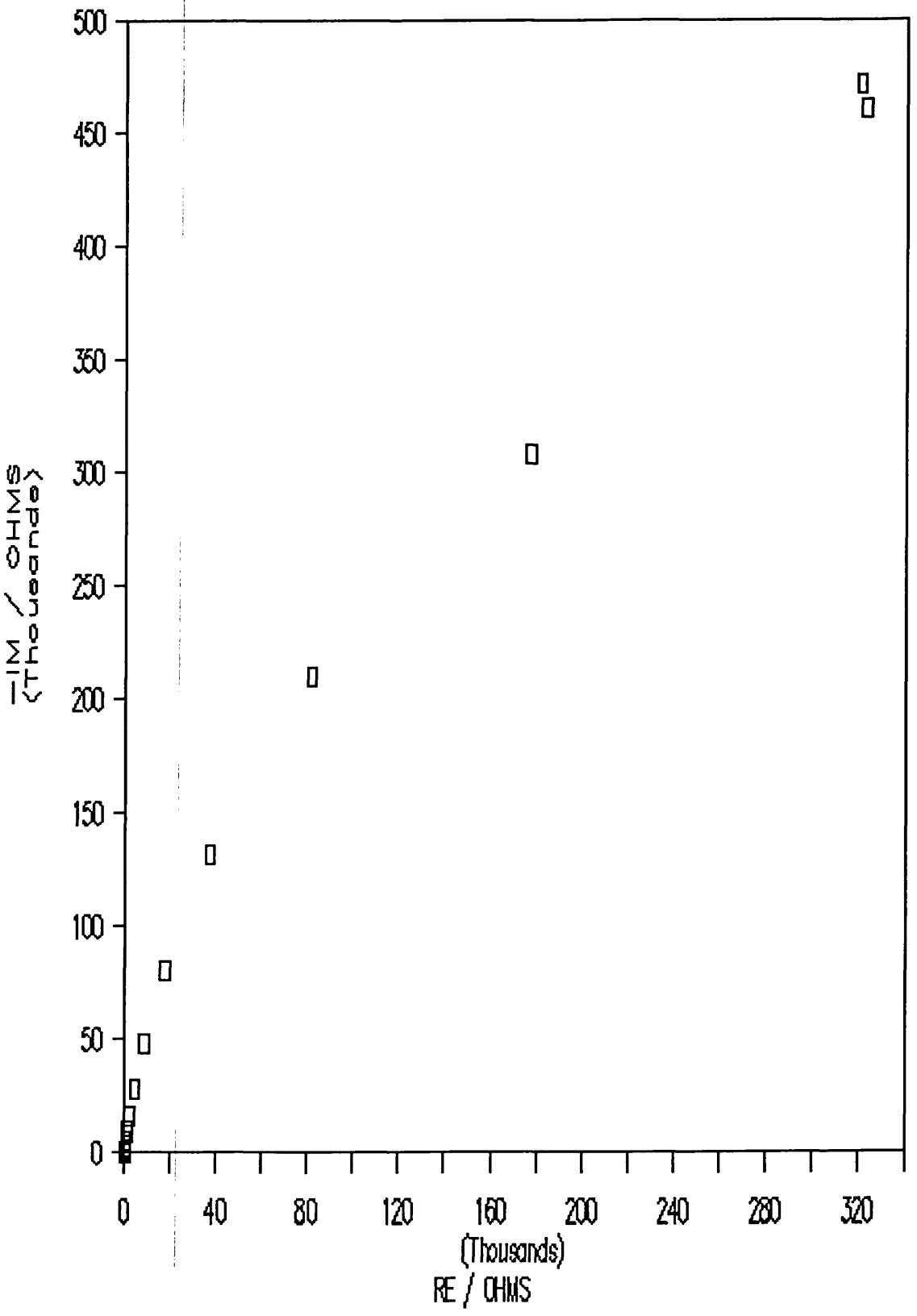

Figure 5.7 GOD/5 mM glc on PST/TTF-TCNQ, +300 mV, 1K-0.01 Hz

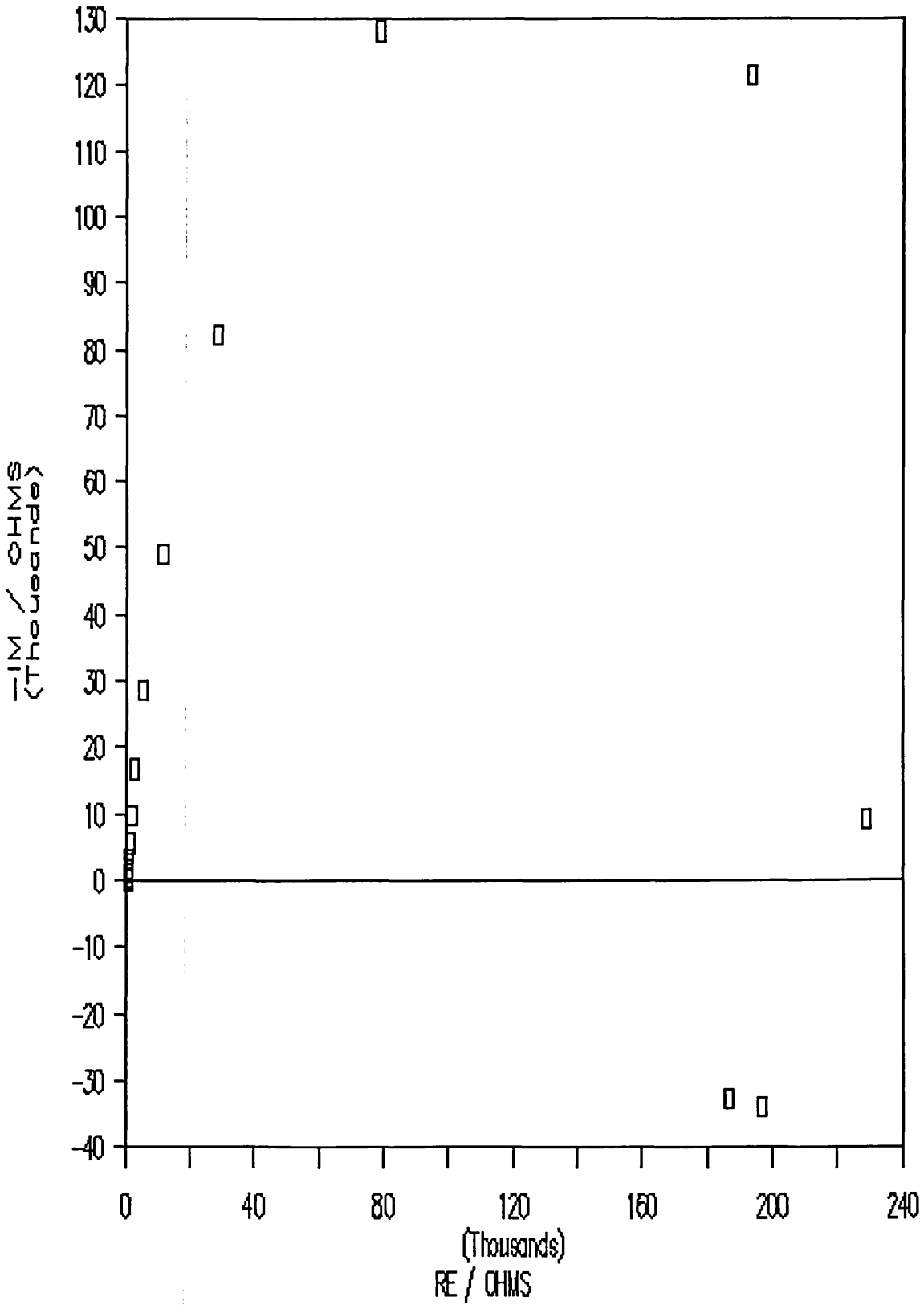

Figure 5.8 GOD/10 mM glc on PST/TTF-TCNQ, +300 mV, 1K-0.01 Hz

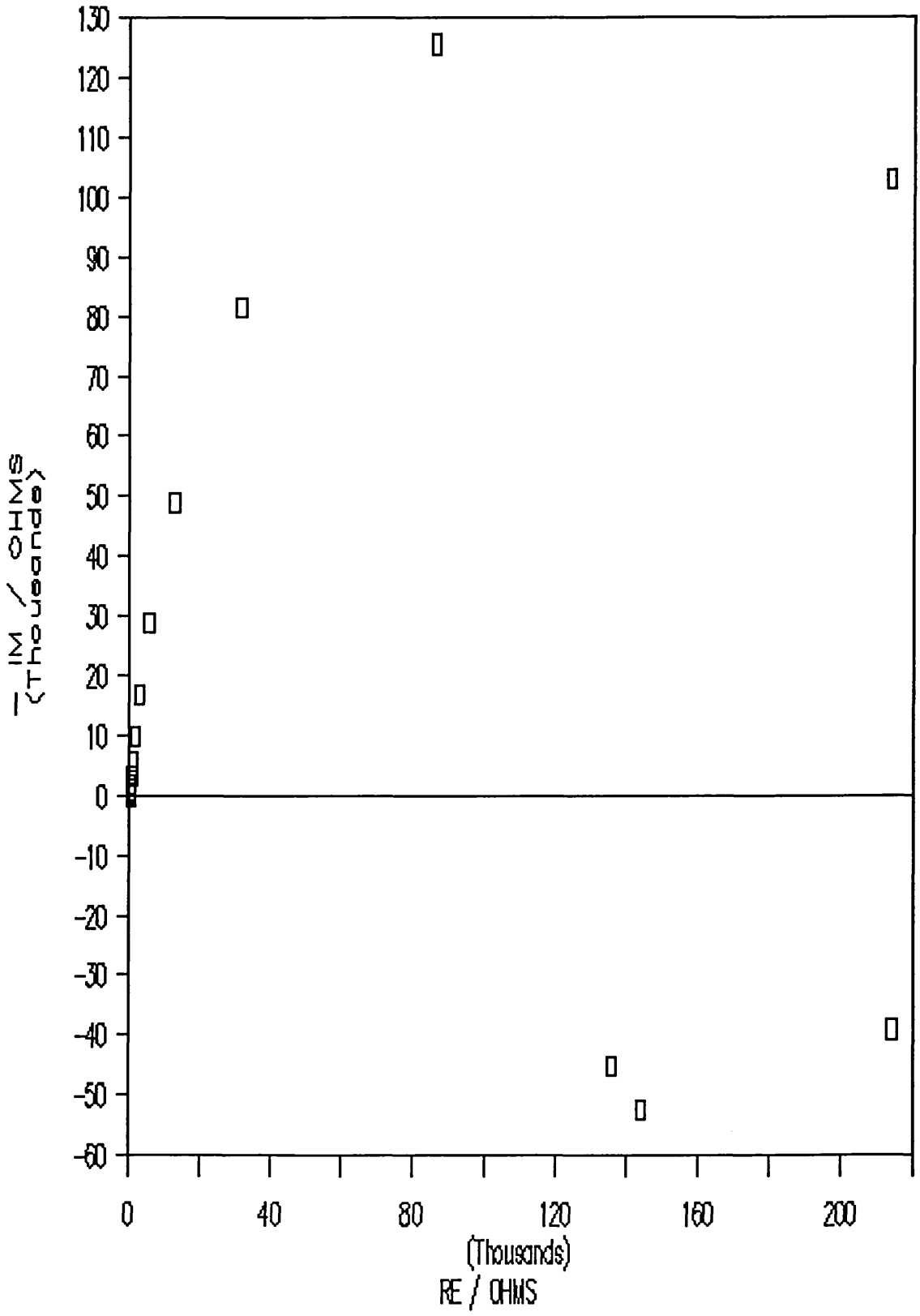

Figure 5.9 GOD/20 mM glc on PST/TTF-TCNQ, +300 mV, 1K-0.01 Hz

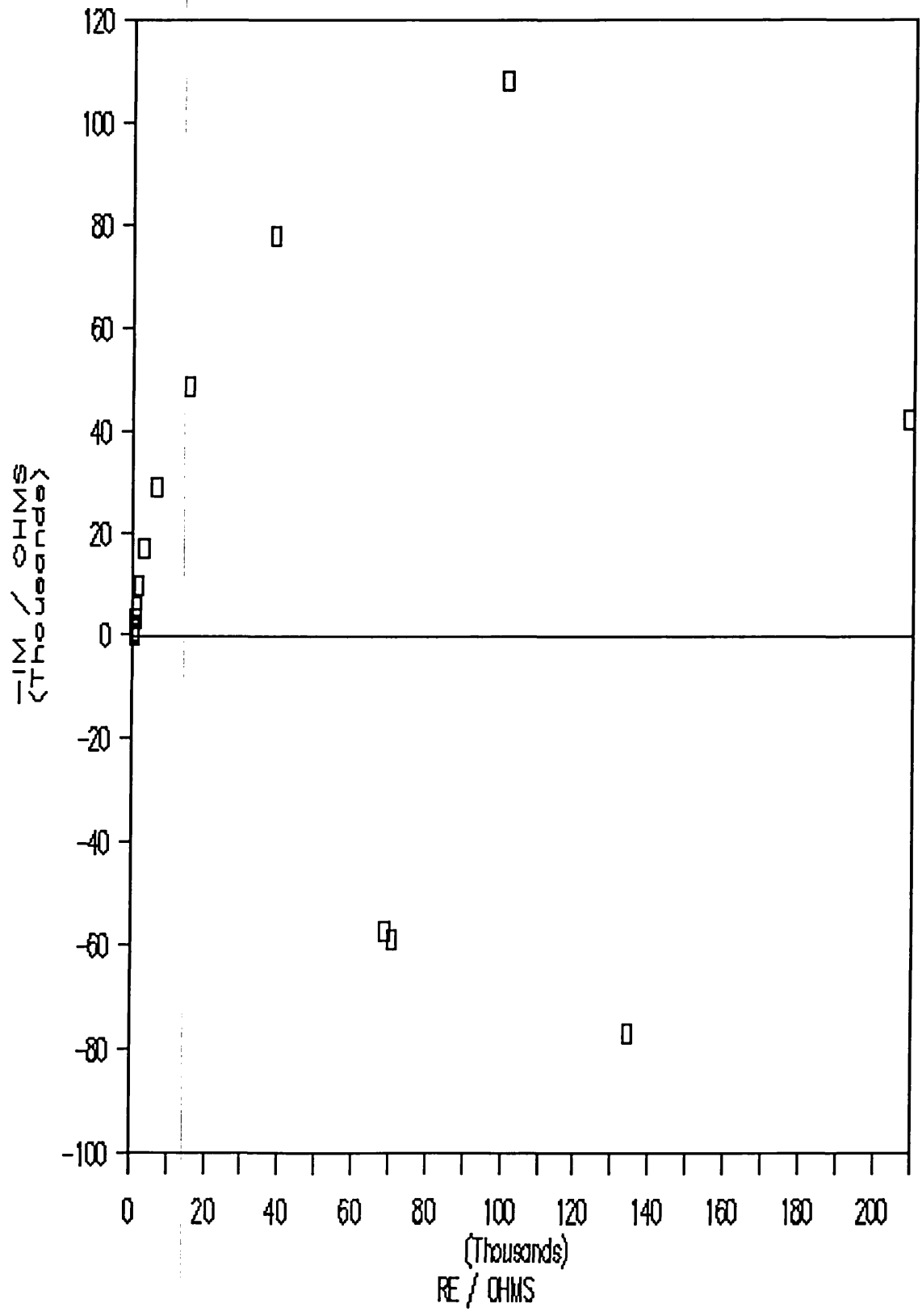

Figure 5.10 GOD/38 mM glc on PST/TTF-TCNQ, +300 mV, 1K-0.01 Hz

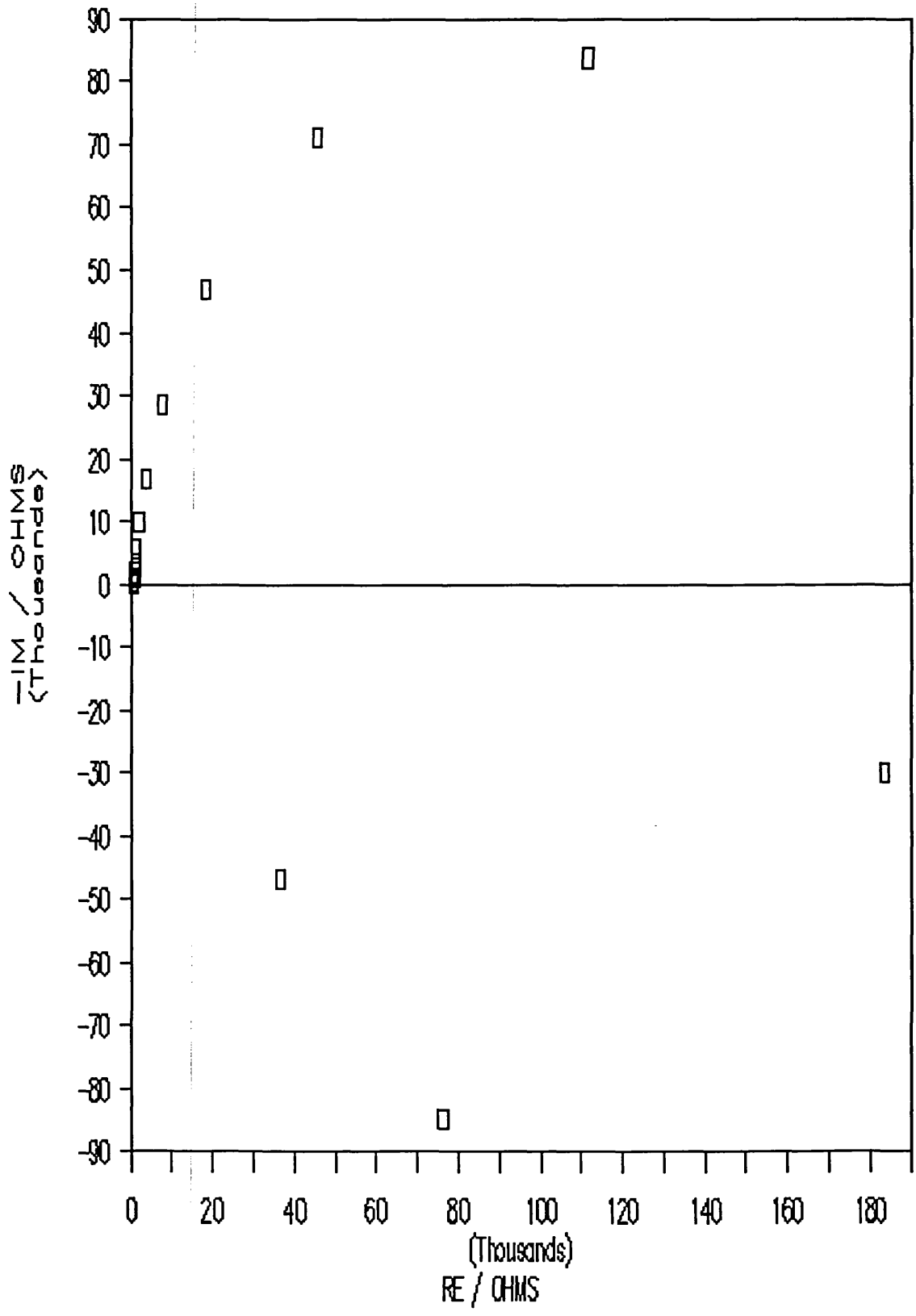

Figure 5.11 GOD/74 mM glc on PST/TTF-TCNQ, +300 mV, 1K-0.01 Hz

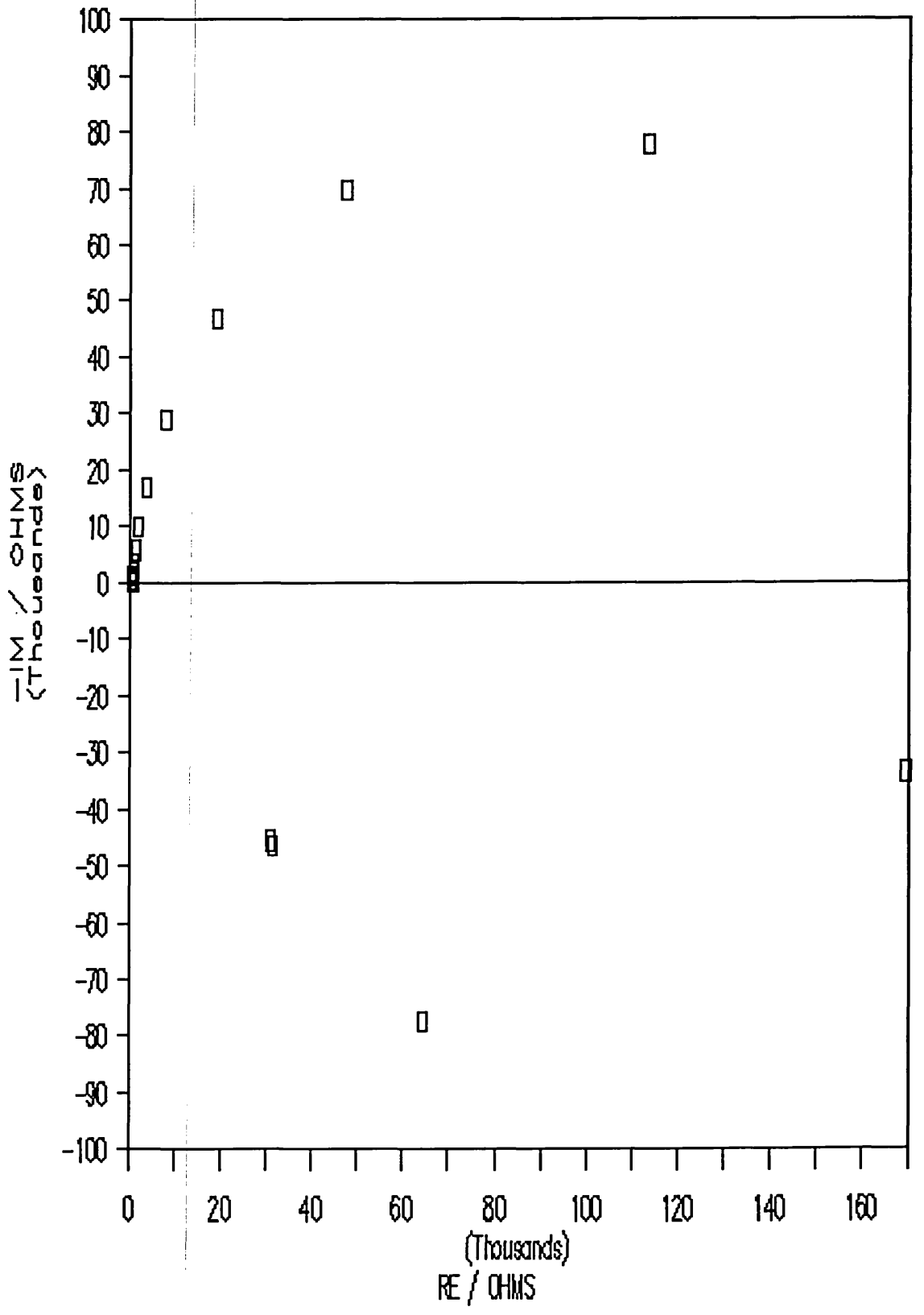

Figure 5.12 GOD/115 mM on PST/TTF-TCNQ, +300 mV, 1K-0.01 Hz

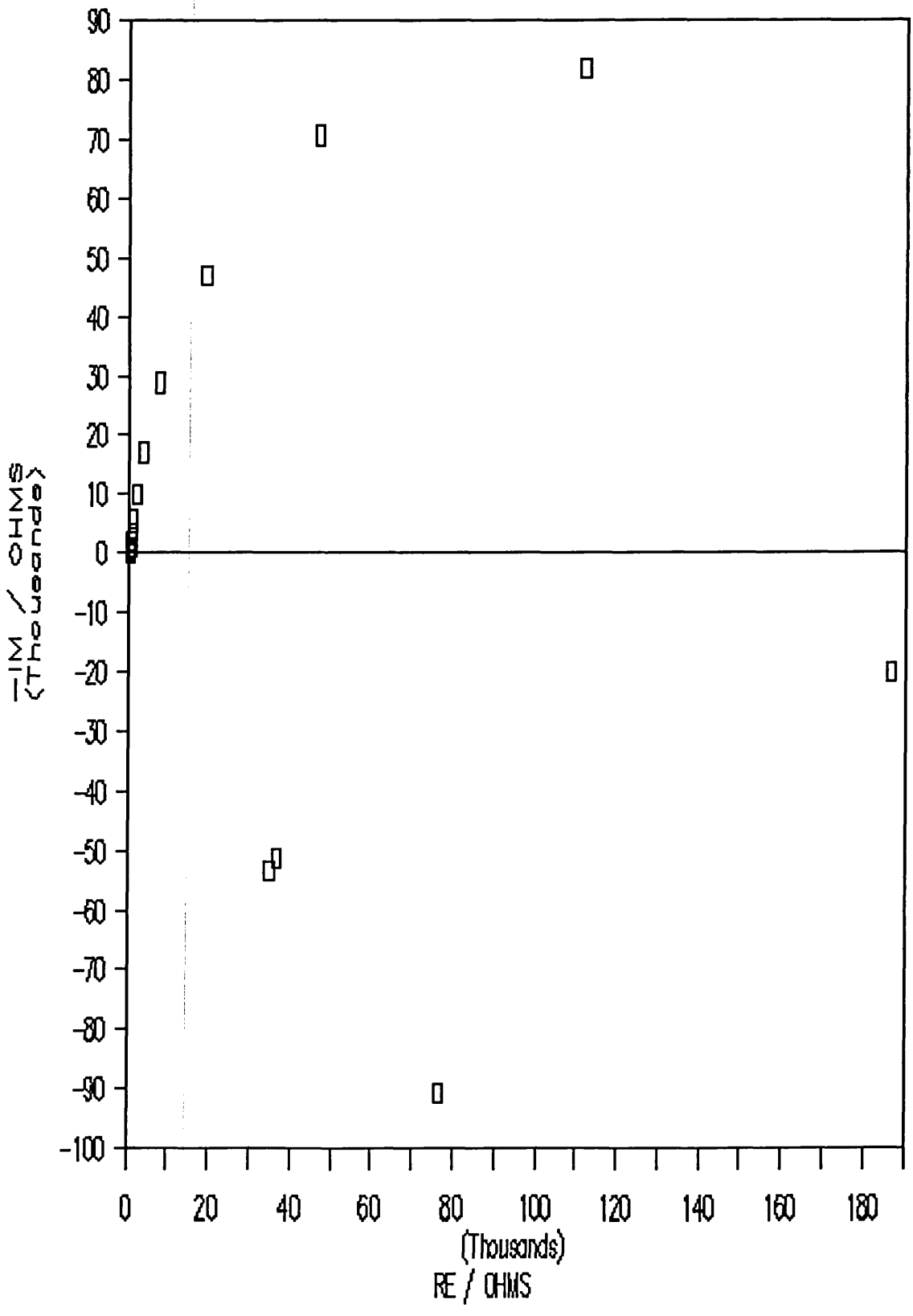

Figure 5.13 GOD/187 mM glc on PST/TTF-TCNQ, +300 mV, 1K-0.01 Hz

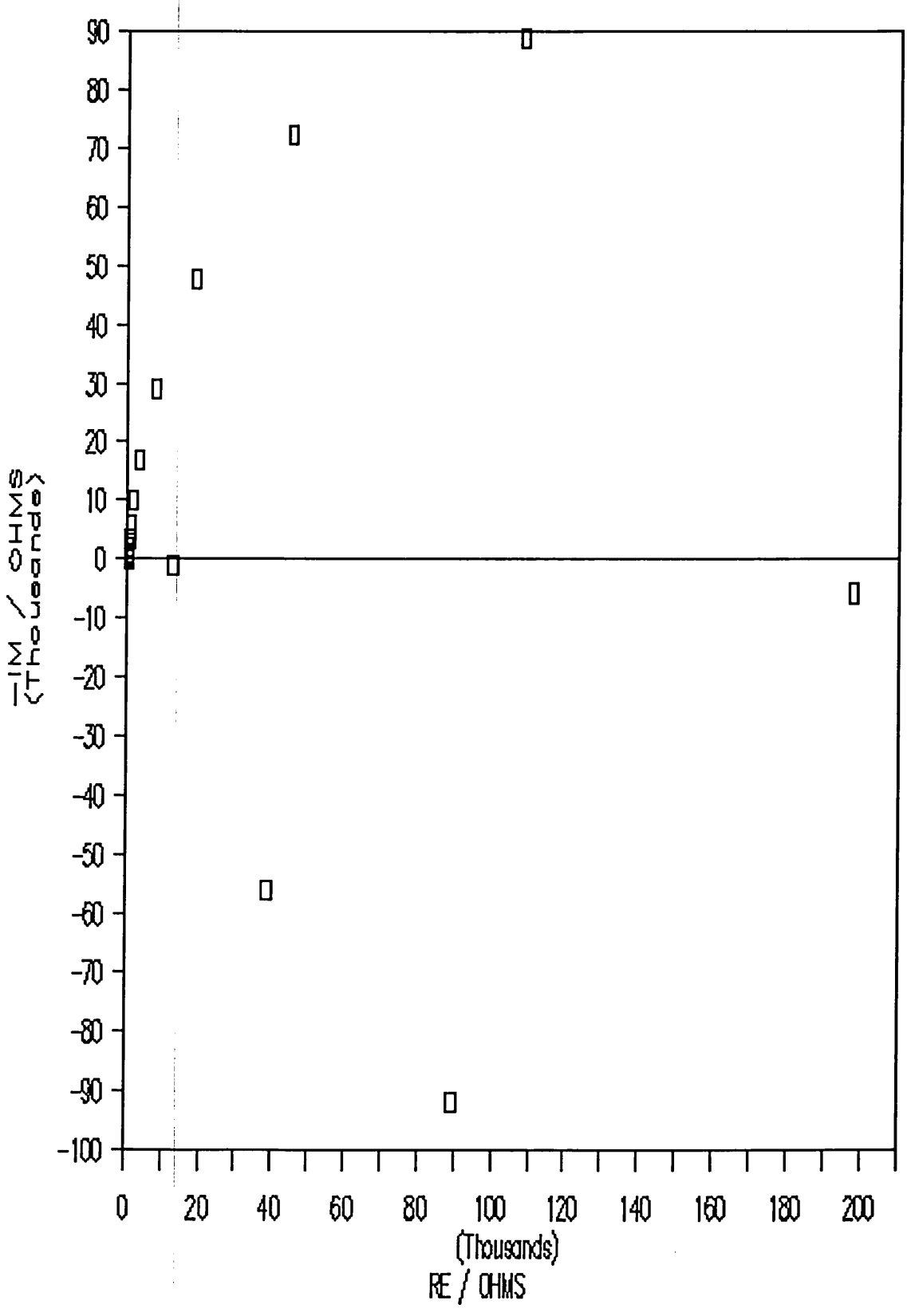

Figure 5.14 Determination of the low frequency D.C. limiting resistance, 187 mM glc, +300 mV, 1K-0.01 Hz

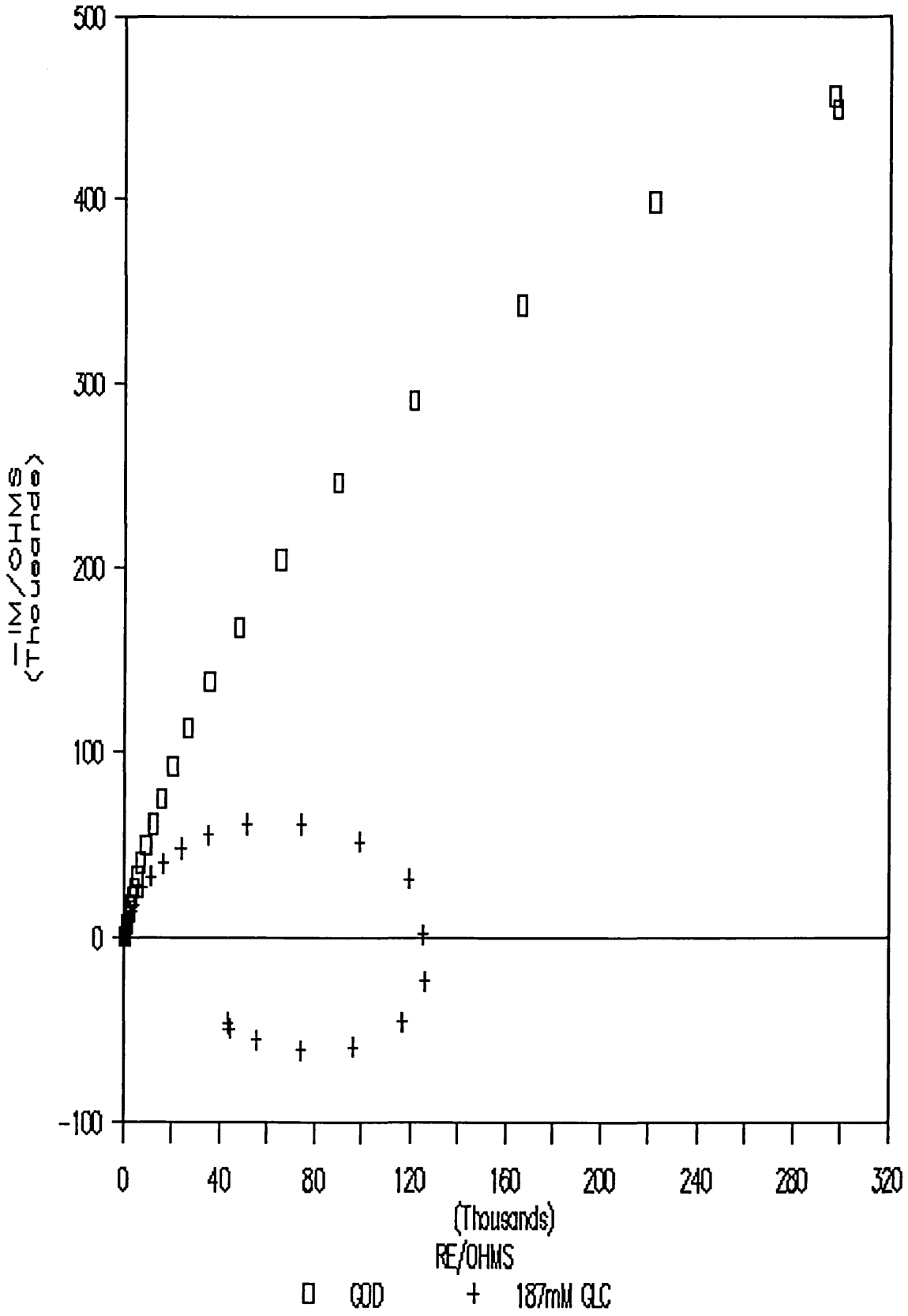

appears that the method of data analysis affects the interpretation of the results.

The Randles model assumes that at high frequencies the Warburg impedance is negligible and the equivalent circuit consists of a resistor in series with a parallel capacitor/resistor combination. However the system in question is more complicated since the inductive element begins to affect the system before Y' passes through its maximum positive value.

5.3.3 A.C. Behaviour using Modified GOD

The impedance behaviour of GOD modified by TTF° was examined at a potential of 300 mV (Figure 5.15). The glucose concentration (187 mM) ensured that the enzyme was saturated. The results were compared with those obtained using unmodified enzyme. Both sets of data produced impedance plots exhibiting inductance loops.

5.3.4 A.C. Behaviour of the Bare Electrode and the Effect of Increasing the Bulk Enzyme Concentration

The impedance spectrum of a newly-made bare TTF-TCNQ electrode made with PST binder was compared with that obtained on adding glucose (200 mM) (Figure 5.16). No noticeable difference was observed. However on adding GOD a cochleated impedance spectrum was obtained. When the concentration of enzyme was increased the radius of the spiral decreased (Figures 5.17).

5.3.5 Effect of Adsorbed Enzyme

Electrodes with preadsorbed GOD were used in order to examine whether the process of enzyme adsorption played a significant role in determining the nature of the impedance spectrum. The impedance plot (Figure 5.18) showed "semi-circular" behaviour on adding glucose to the solution when GOD was not present in solution. When GOD was added to the bulk, Y' became negative and X' decreased in magnitude, the latter being in keeping with the observed increase in current. The response was characteristic of a system possessing an inductive element. As the concentration of GOD was increased the

Figure 5.15 Comparison of the impedance spectra of modified and unmodified GOD, 187 mM, +300 mV, 1K-0.01 Hz

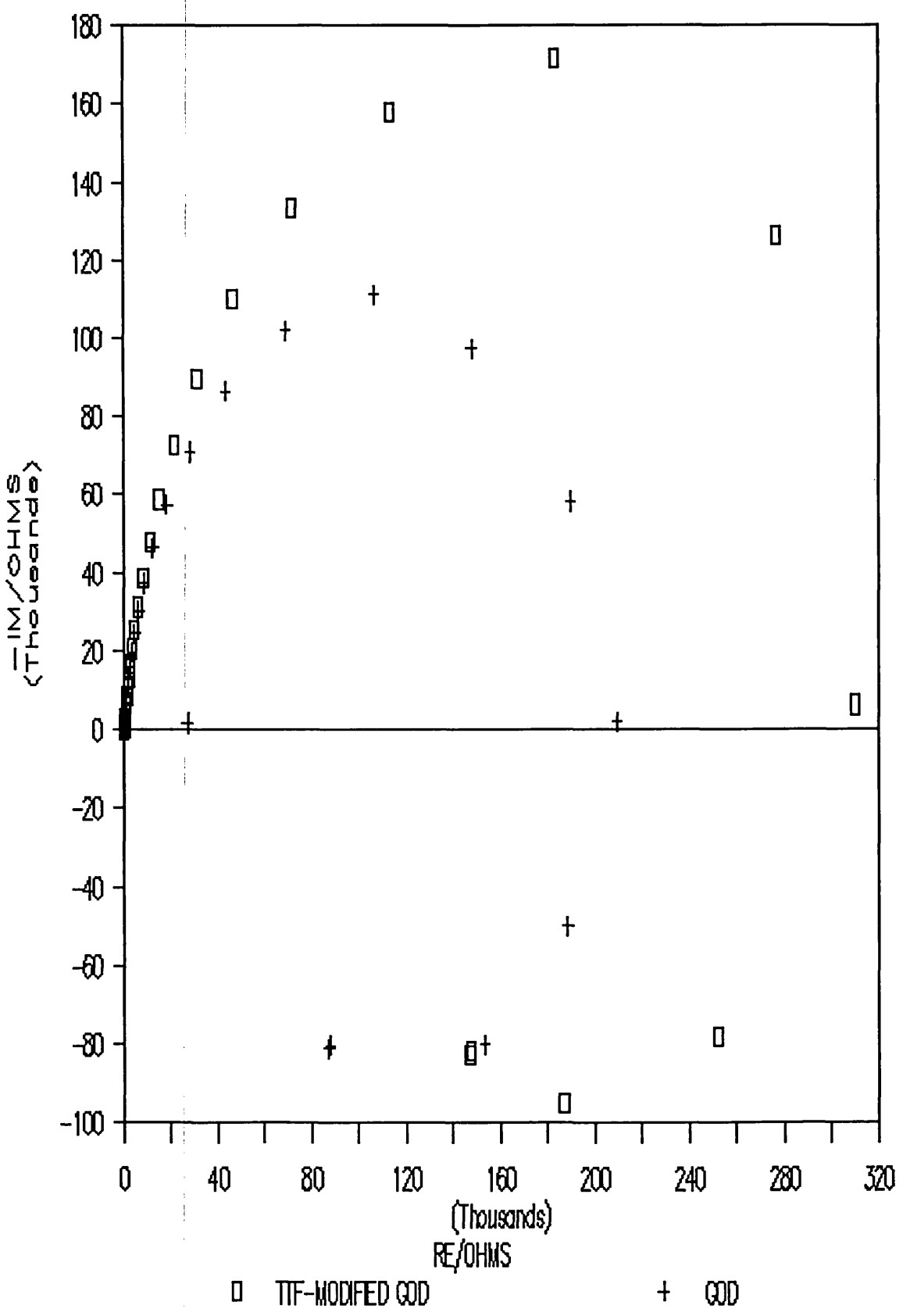

Figure 5.16 Impedance spectrum of glucose on a PST/TTF-TCNQ electrode in the absence of GOD, +300 mV, 1K-0.01 Hz

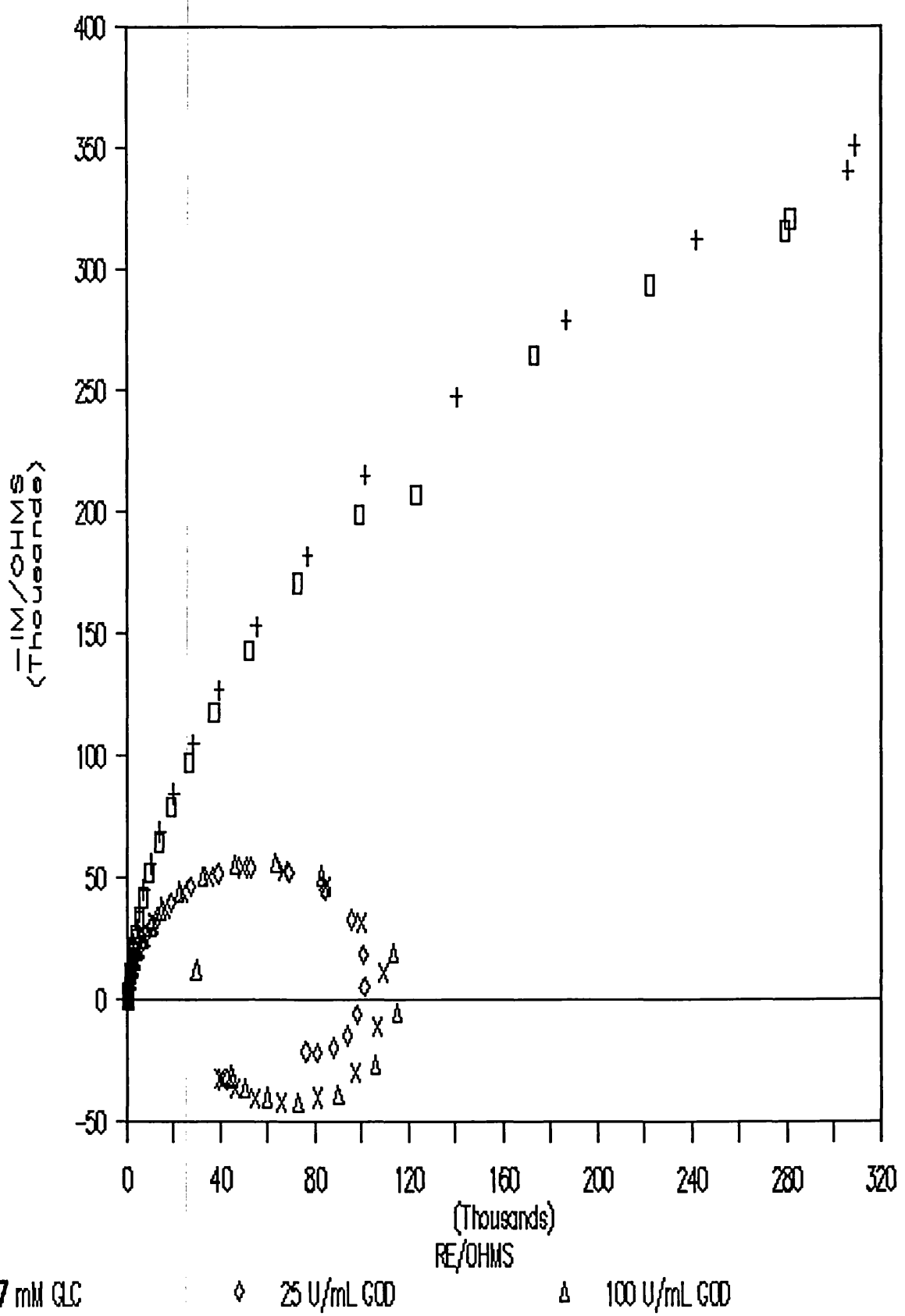

Figure 5.17 Effect of increasing [GOD] on the impedance spectrum,

187 mM glc, +300 mV, 1K-0.01 Hz

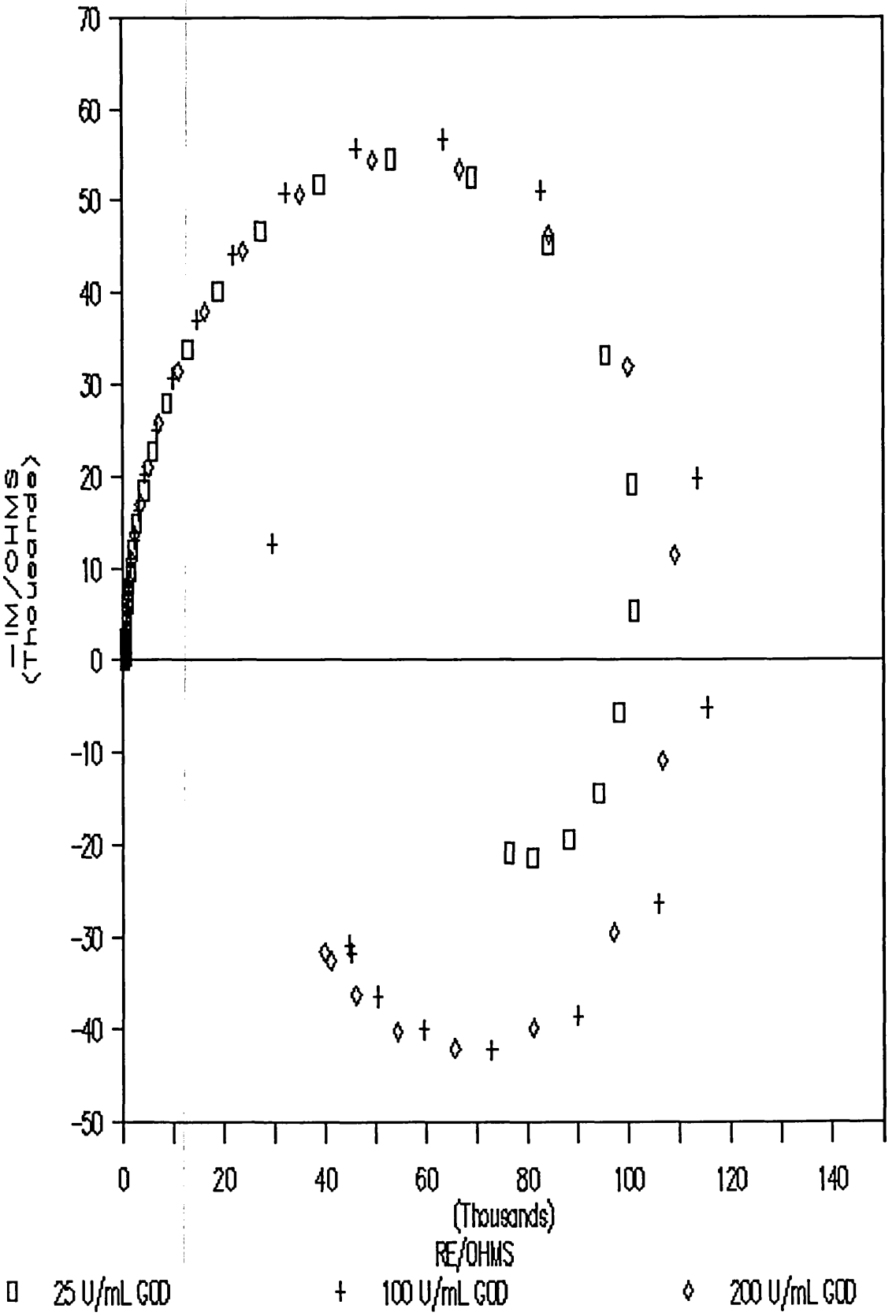

Figure 5.18 Impedance spectra obtained using adsorbed GOD and the effect of adding GOD to the bulk solution, 187 mM glc, +300 mV, 1K-0.01 Hz

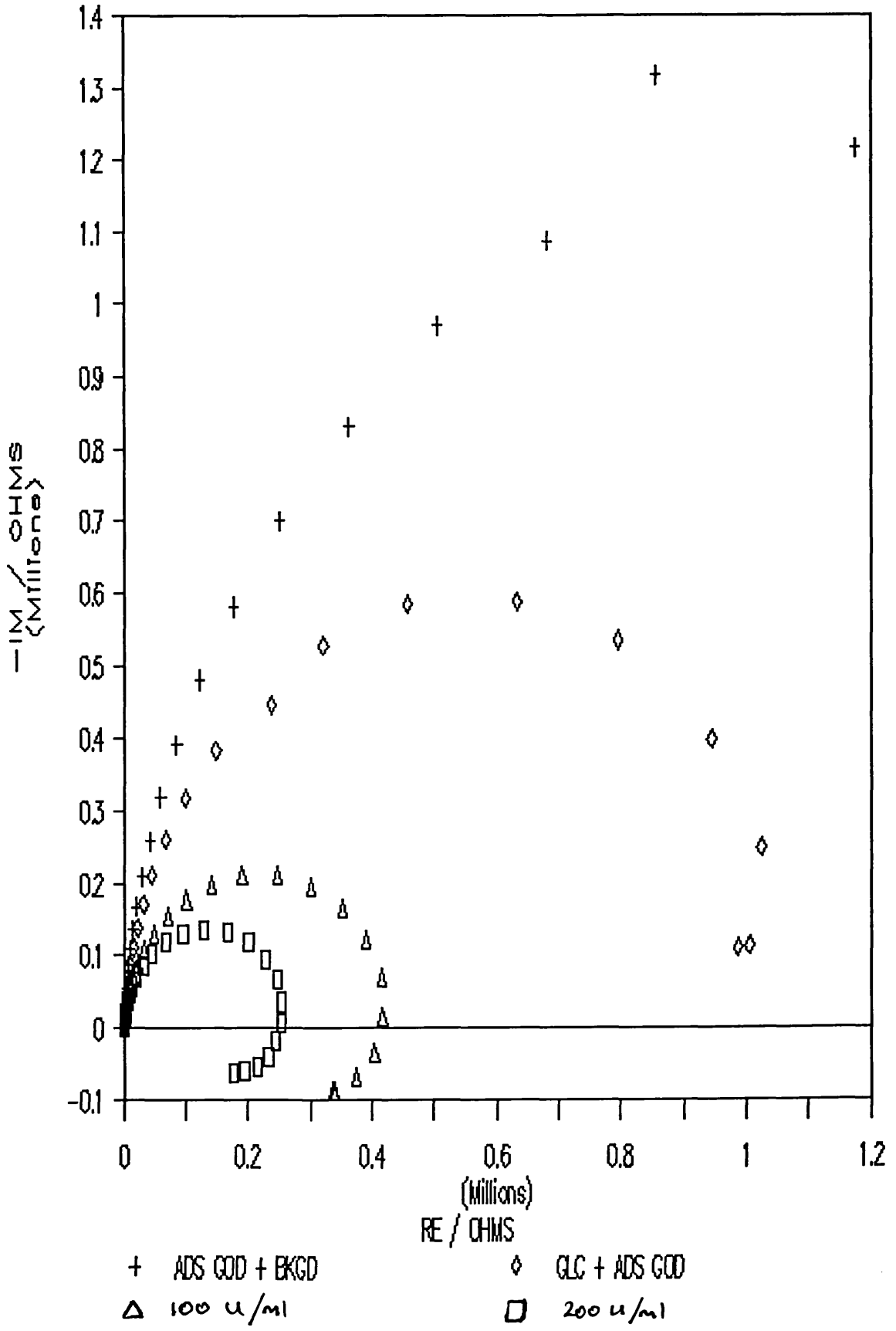

system behaved as in §5.3.4.

5.3.6 A.C. Behaviour at Low Enzyme Concentrations

An experiment was performed using $\simeq$ 8 U/ml GOD (Figure 5.19). This was in contrast to previous experiments at fixed enzyme concentrations which had used $\simeq$ 100 U/ml GOD. The impedance spectra obtained at a bare electrode and at low [glucose] (10 μM) were very similar. On increasing [glucose] the plots began to curve over, however they did not cross the X' axis. Negative values of Y' were only obtained when GOD was added to the bulk, bringing the total enzyme concentration to $\simeq$ 110 U/ml.

5.3.7 A.C Dependence of Rotation Speed Behaviour

The results are shown in Figure 5.20. The experiments were carried out using [GOD]$\simeq$100U/ml and [glc]$\simeq$190mM. Inspection shows that X' decreases with rotation speed at a given substrate concentration. This is equivalent to the current increasing with rotation speed and is in accord with the results of the rotating disk studies described in the previous chapter (§4.4.2.1).

5.3.8 Variation of Rotation Speed at Low Glucose Concentrations

The rotation speed dependence was also investigated at [glc]$\simeq$10 mM and [GOD]$\simeq$110 U/ml (Figure 5.21). On adding substrate the imaginary impedance, Y', exhibited the characteristic curved behaviour. However it did not become negative at low frequencies. As the rotation speed was increased from 1 to 25 Hz, X' was observed to decrease whilst the d.c. current increased.

5.3.9 A.C. Behaviour of Si-Oil Electrodes

Figures 5.22 - 5.24 show the impedance profiles obtained from Si-oil electrodes in the presence of GOD and varying conentrations of glucose. Electrodes fabricated using Si-oil show a much greater impedance on both the real and imaginary axes than those made using PST binder. Inductive behaviour was observed, although to a lesser extent than with PST electrodes.

Figure 5.19 Impedance spectrum using low [GOD], 8 U/ml, +300 mV, 187 mM glc, 1K-0.01 Hz

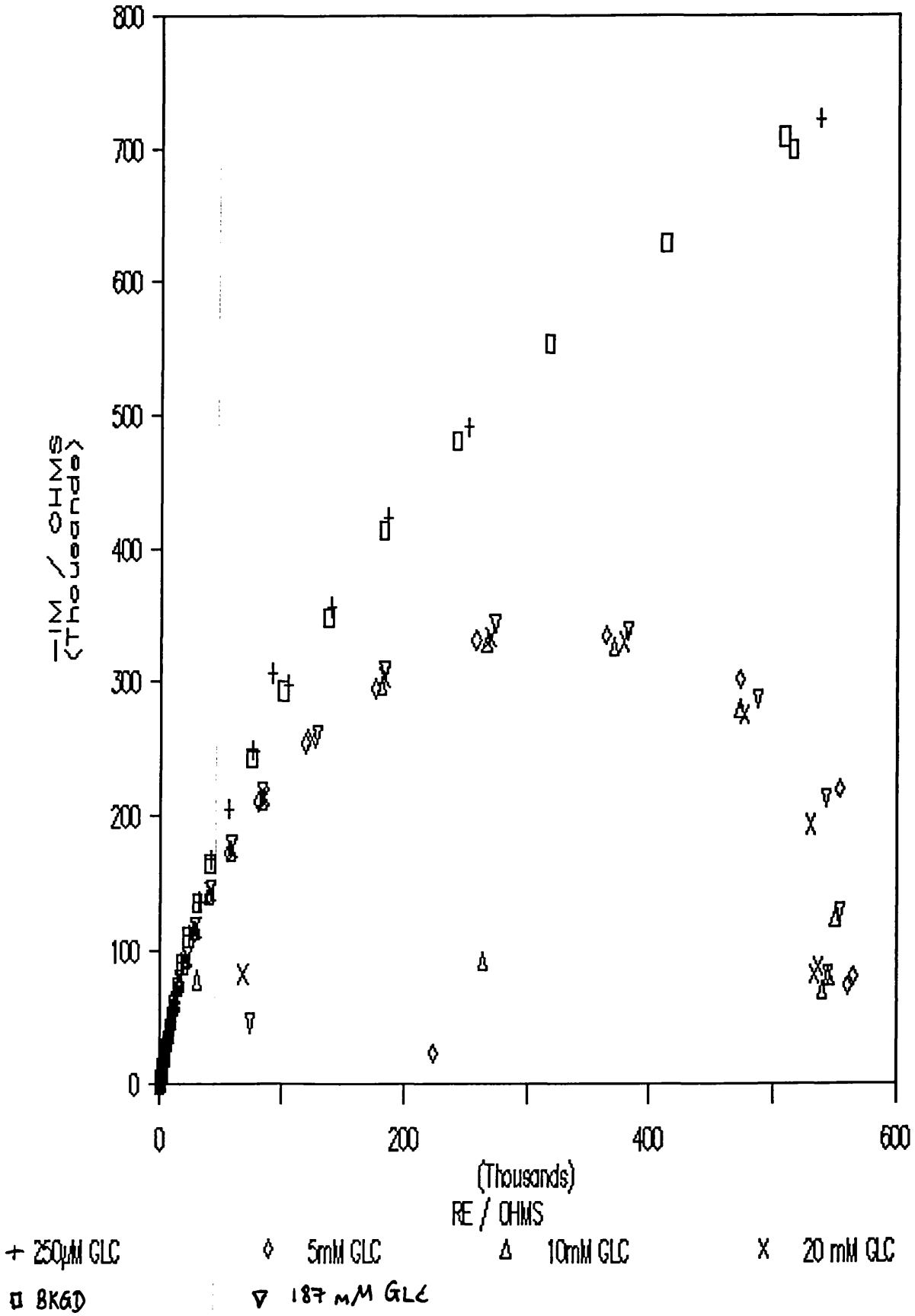

Figure 5.20 Effect of rotation speed on the impedance spectrum,

187 mM glc, +300 mV, 1K-0.01 Hz

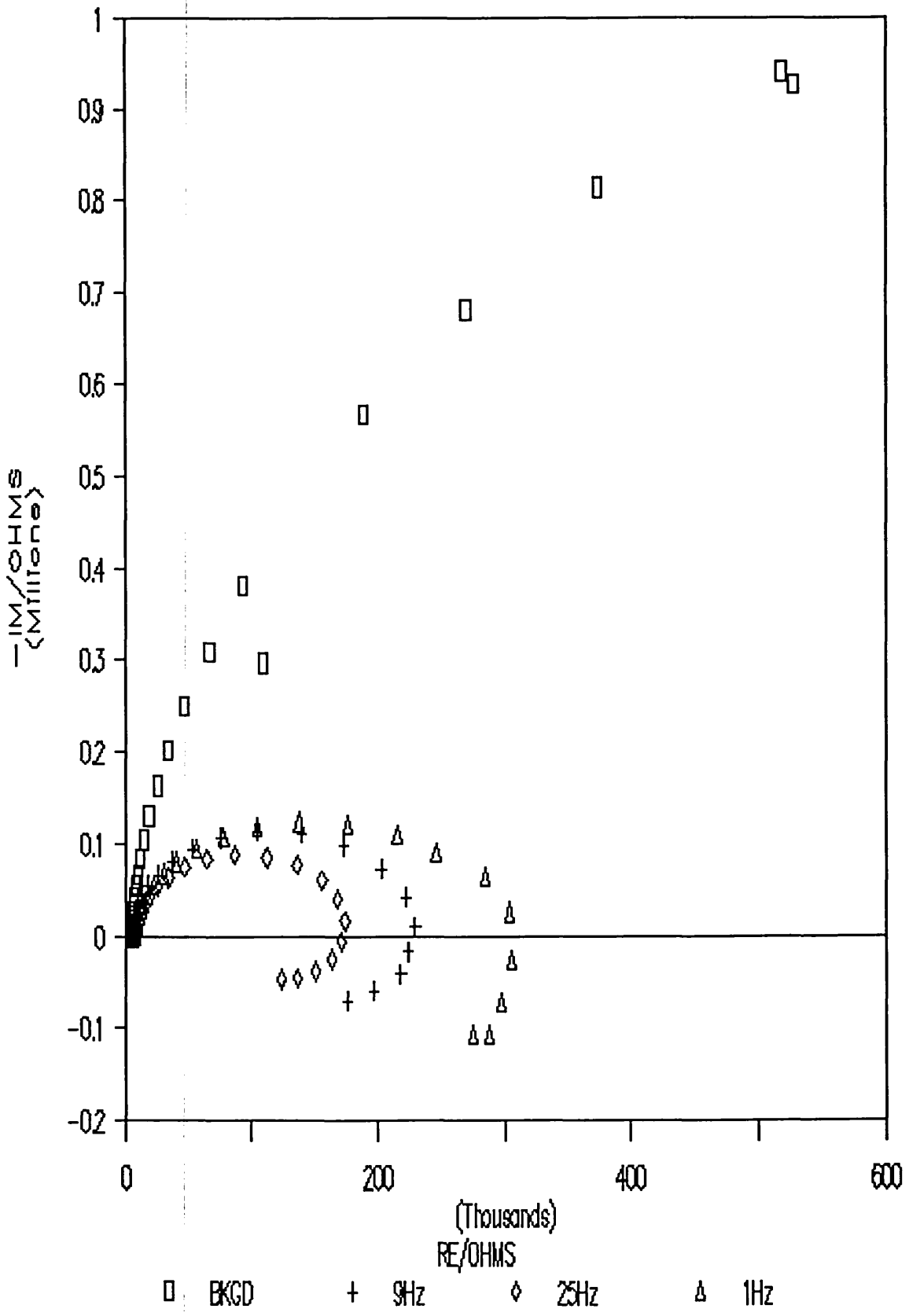

Figure 5.21 Effect of rotation speed on the impedance spectrum at low [glc], 10 mM, +300 mV, 1K-0.01 Hz

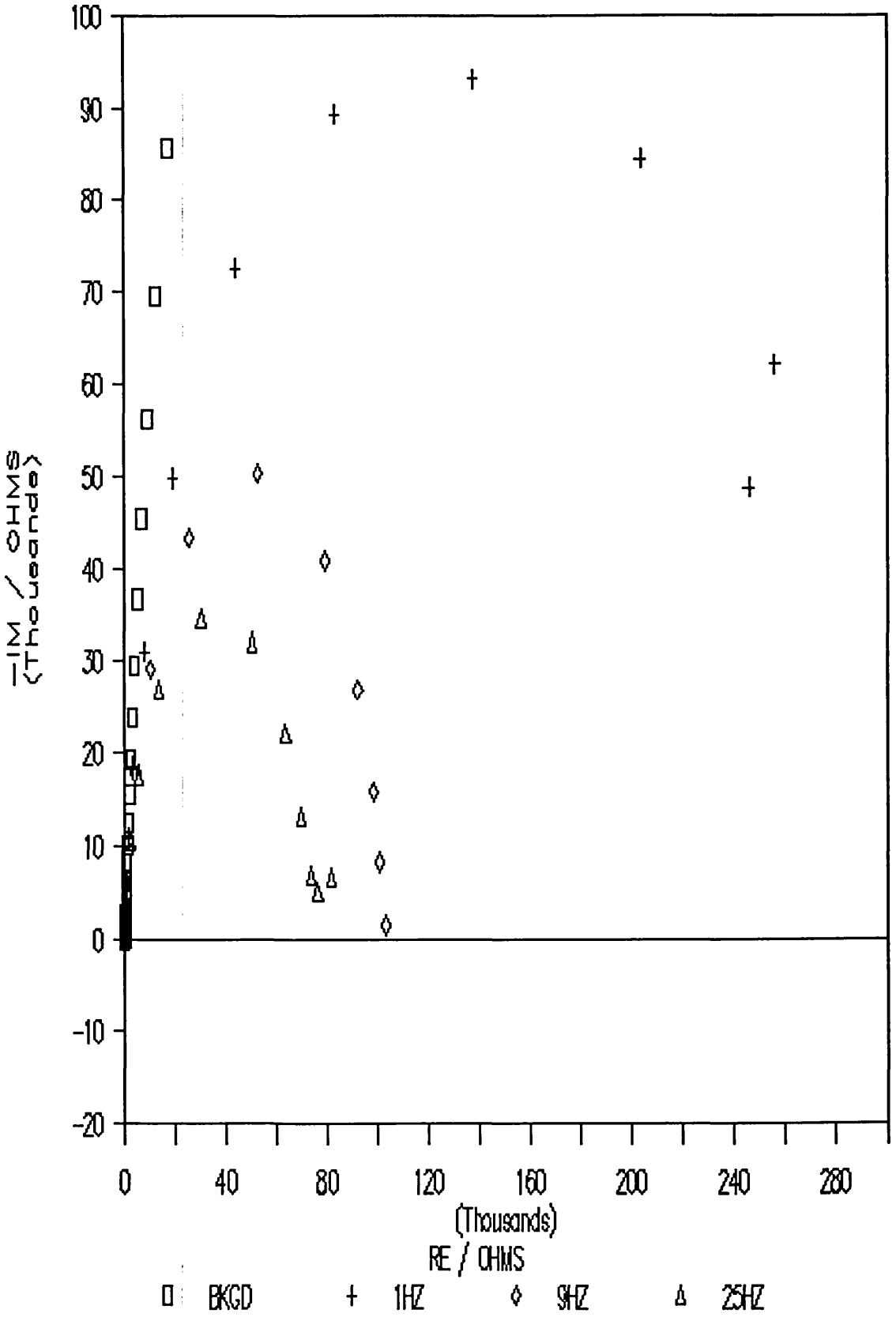

Figure 5.22 GOD/5mM glc on Si-oil/TTF-TCNQ, +300 mV, 1K-0.01 Hz

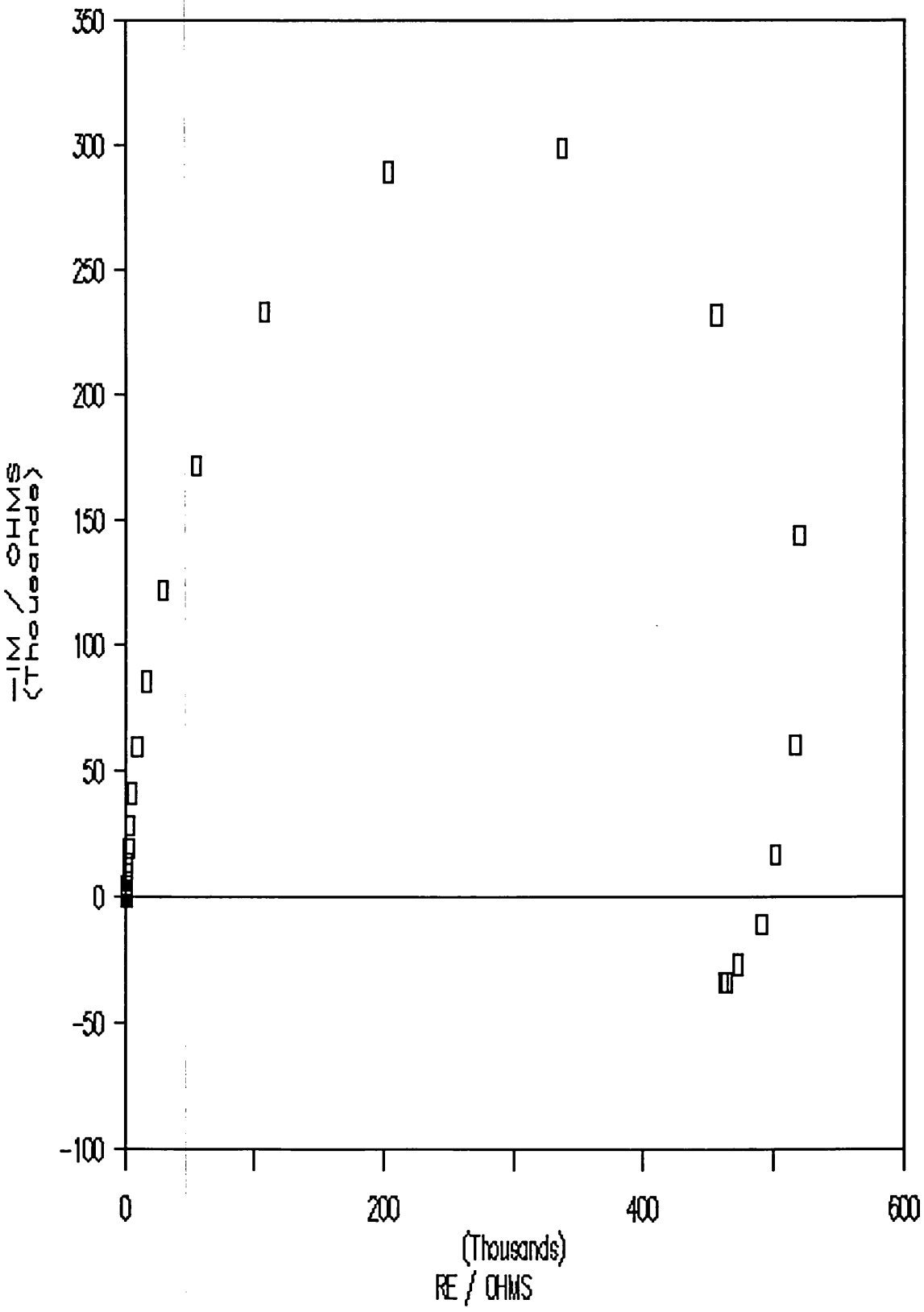

Figure 5.23 GOD/20 mM glc on Si-oil/TTF-TCNQ, +300 mV, 1K-0.01 Hz

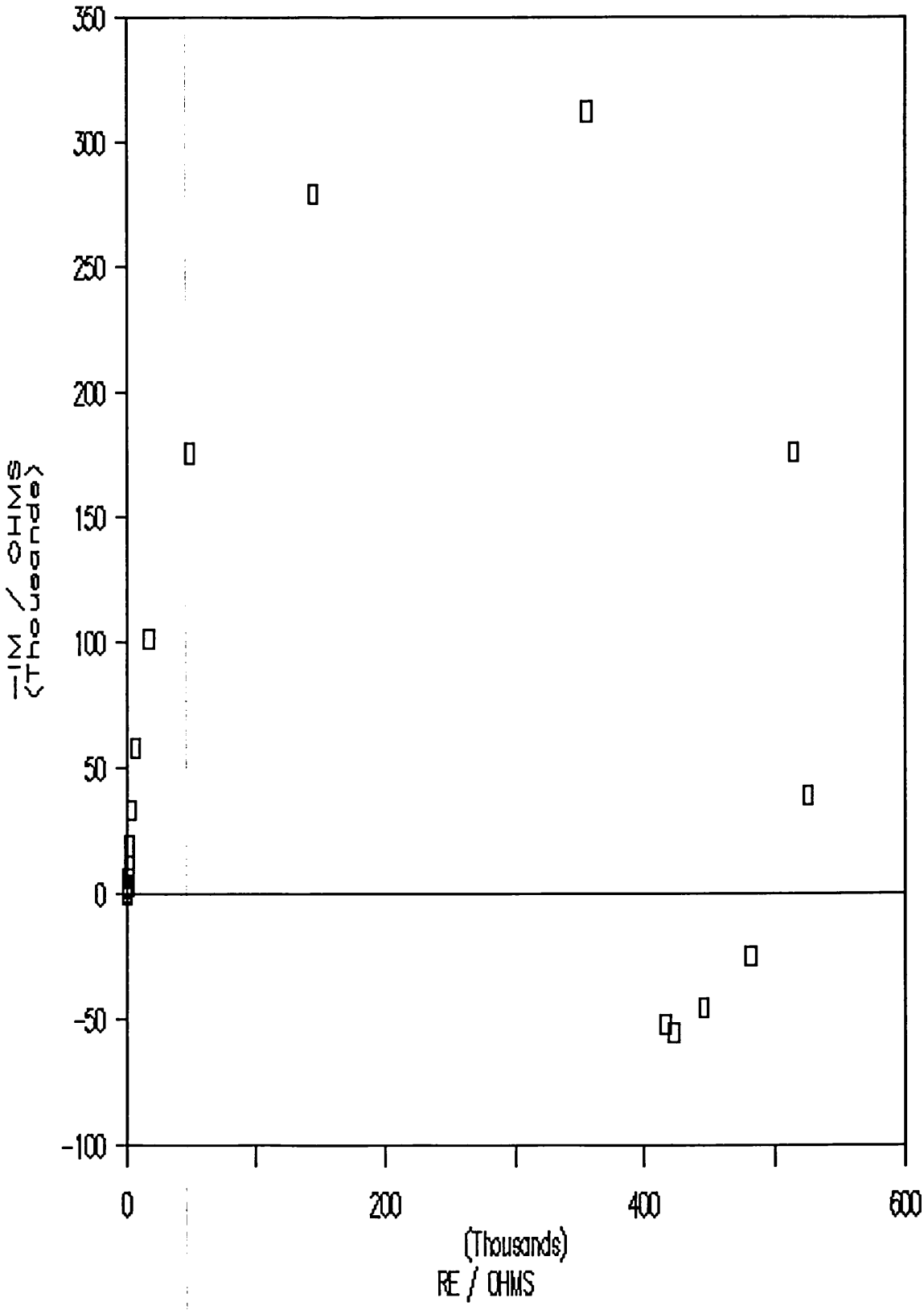

Figure 5.24 GOD/187 mM glc on Si-oil/TTF-TCNQ, +300 mV, 1K-0.01 Hz

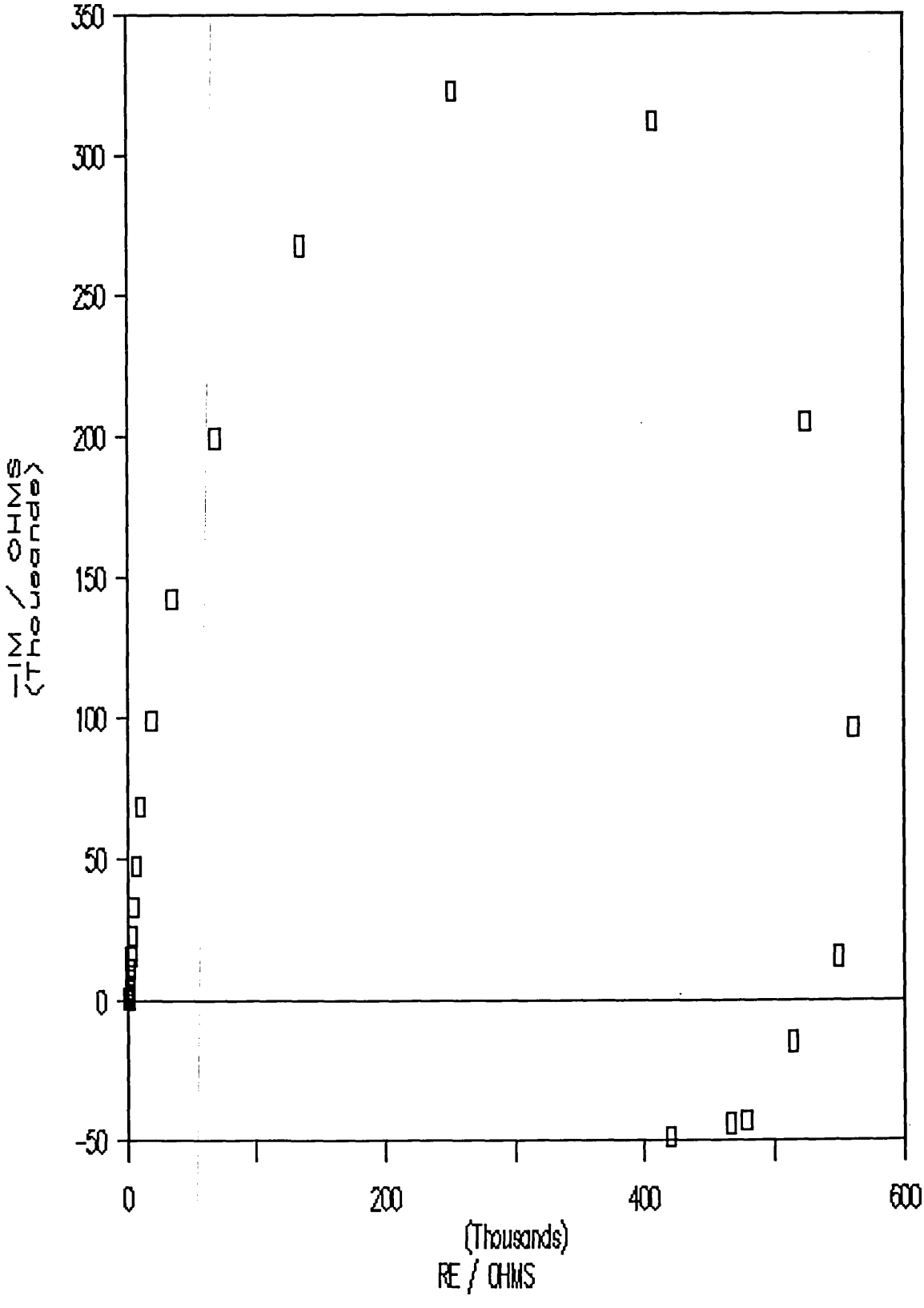

5.4 DISCUSSION

5.4.1 Si-Oil/TTF-TCNQ Results

It was decided to analyse the real impedance data since these did not contain any contributions from the double-layer capacitance $C\omega$. Since the values of X based on the experimental data passed through a minimum (Table 5.1), an attempt was made to fit the results obtained at 187 mM glc to Case I. A plot of X against $\omega^{1/2}$ has a gradient g and gives an intercept X_o, which corresponds to X_o', the value of X' at which $Y'=0$. Thus,

$$X = X_o - g\sqrt{\omega} \qquad 5.21$$

Considering the real part of eqn. 5.14

$$\frac{X}{X_o} = \frac{\left[(1+\theta^2)^{1/2}+1\right]^{1/2}}{\sqrt{2}} - \frac{1}{2}\sqrt{\frac{\omega}{2k}} \qquad 5.22$$

Substitution for g followed by rearrangement gives

$$\left(\frac{X+g\sqrt{\omega}}{X_o}\right)^2 = \frac{(1+\theta^2)^{1/2}+1}{2} \qquad 5.23$$

$$\left[\left(\frac{X+g\sqrt{\omega}}{X_o}\right)^2 - \frac{1}{2}\right]^2 = \frac{1+\theta^2}{4} = y \qquad 5.24$$

Since $\theta = \omega/k$

$$y = \frac{1}{4} + \frac{\omega^2}{4k^2} = \frac{1}{4} + G\omega^2 \qquad 5.25$$

At the low frequency limit,

$$\left(\frac{X+g\sqrt{\omega}}{X_o}\right)^2 \simeq \frac{1}{2} + \frac{\omega}{2k} \qquad 5.26$$

A plot of y against ω^2 at low frequencies, upto 1 Hz, yielded a good straight line, with gradient, G=14, which gave a value of 0.134 s^{-1} for k (Figures 5.25 and 5.26).

TABLE 5.1

Values of 10^6X for Si-oil/TTF-TCNQ, at 5, 20 and 187 mM glc

ω^2/Hz	5mM	20mM	187mM
0.01	2.15	1.86	2.36
0.014	2.14	1.83	2.12
0.021	2.10	1.80	2.07
0.031	2.04	1.76	1.94
0.046	1.99	1.75	1.82
0.068	1.91	1.70	1.73
0.1	–	1.70	1.65
0.14	–	1.73	1.54
0.21	1.66	1.66	1.51
0.31	1.62	1.64	1.49
0.46	1.63	1.63	1.53
0.68	1.69	1.65	1.61
1.0	1.84	1.69	1.82
1.46	2.12	1.82	2.17
2.15	2.52	1.99	2.84
3.16	3.25	2.30	4.00
4.64	4.49	2.87	6.21
6.8	6.64	3.90	10.2
10	10.6	5.85	17.6
14	17.8	9.45	31.1
21.5	31.2	16.3	65.4
31.6	56.4	29.4	97.8
46.4	102.2	54.7	167

A similar plot for moderate frequencies, ie. 1-10 Hz, provided a different value for k, 0.108 s^{-1}.

The above model assumes that one electron is produced for each molecule of mediator entering solution. However in TTF-TCNQ the molecules carry non-integral charges, $TTF^{+0.59}TCNQ^{-0.59}$, thus a further refinement can be introduced by considering the involvement of a fractional charge for the solvation of the mediator species,

$$M^{+}_{surf} \longrightarrow M^{+}_{aq}$$

thus now,

$$X = \frac{X_o}{\sqrt{2}}\left[\left((1 + \theta^2)^{1/2} + 1 \right)^{1/2} - \alpha\sqrt{\theta}\right] \qquad 5.27$$

Then from a plot of X (for the 187 mM glc data, Table 5.1) against $\sqrt{\omega}$, the gradient, g, is given by

$$g = \frac{\alpha X_o}{\sqrt{2k}} \qquad 5.28$$

Thus from the plot g=3.5, $10^5 X_o$=2.55 Ω^{-1}, k=0.134 s^{-1} and α=0.711. Considering the Laplace forms of the original expressions (eqn 5.10)

a. for no generation of charge

$$\sqrt{s + k} - \sqrt{s}$$

b. for full charge transfer

$$2\sqrt{s + k} - \sqrt{s}$$

c. for the intermediate case

$$(1 + \beta)\sqrt{s + k} - \sqrt{s}$$

Assuming α=0.71 then since $\alpha = 1/(1+\beta)$, $\beta \simeq 0.41$.

Figure 5.25 Plot of y against ω^2 for Si-oil/TTF-TCNQ with 187 mM glc, ω up to 1 Hz

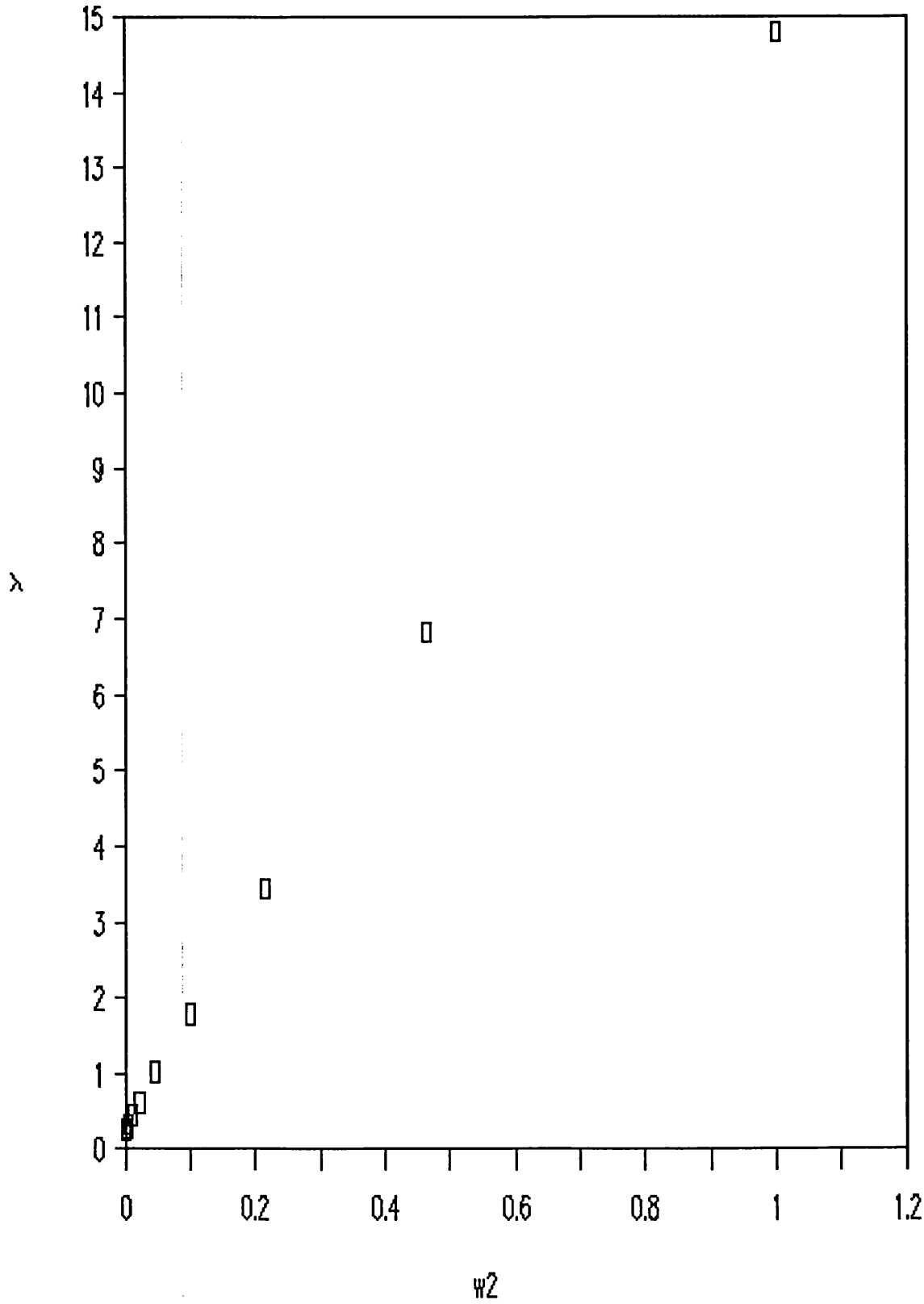

Figure 5.26 Plot of y against ω^2 for Si-oil/TTF-TCNQ with 187 mM glc, ω up to 0.316 Hz

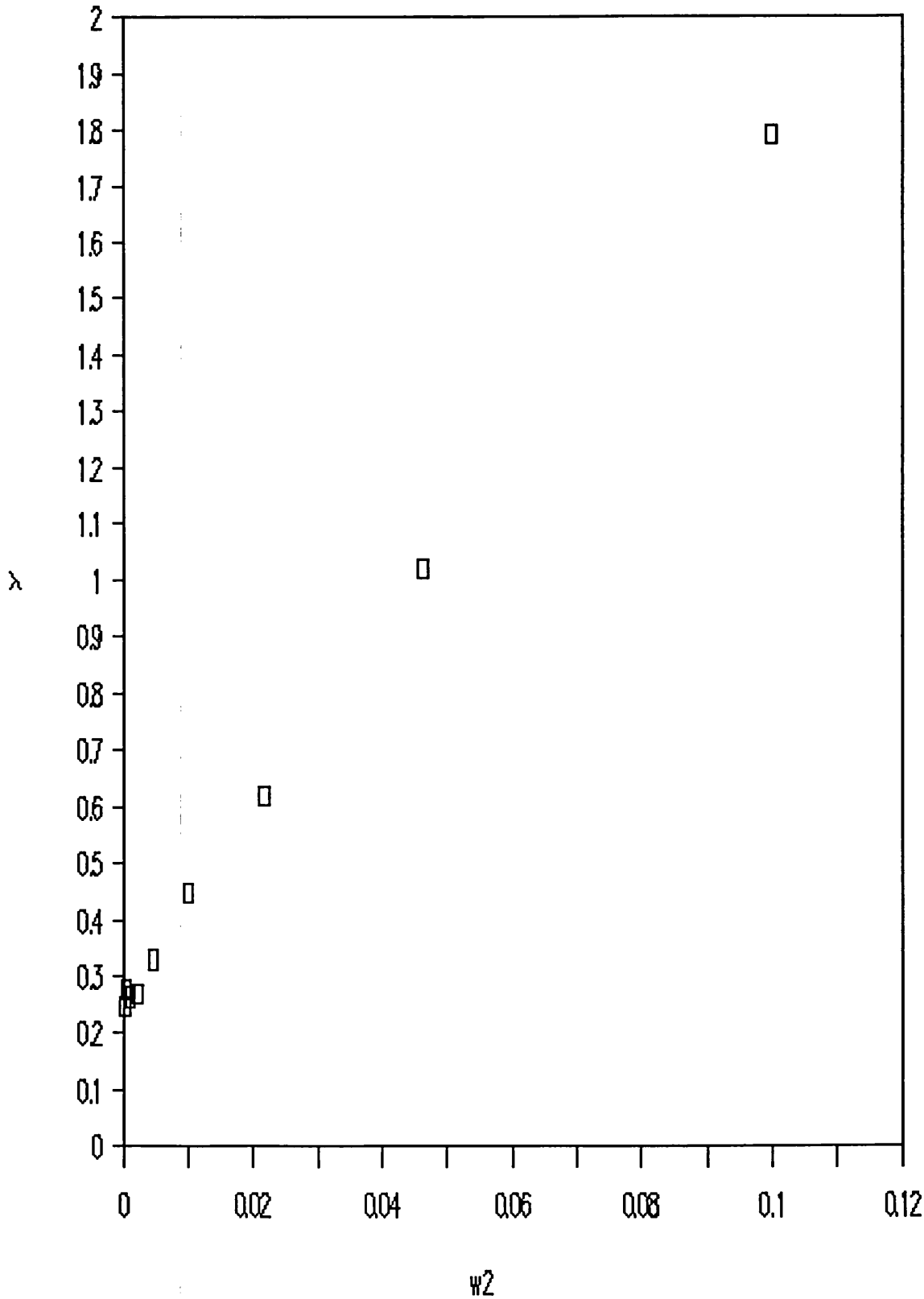

The new expression for y is,

$$y = \left((1 + \theta^2)^{1/2} + 1 \right)^{1/2} - \alpha\sqrt{\theta} \qquad 5.29$$

Let $1 + \theta^2 = \zeta$, then,

$$y = (\zeta^{1/2} + 1)^{1/2} - \alpha(\zeta - 1)^{1/4} \qquad 5.30$$

$$\frac{\partial y}{\partial \zeta} = \frac{1}{4\zeta^{1/2}(\zeta^{1/2} + 1)^{1/2}} - \frac{\alpha}{4(\zeta - 1)^{3/4}}$$

$$(1 - \tfrac{1}{\zeta})^{3/2} = \alpha^2 (1 + \frac{1}{\sqrt{\zeta}}) \qquad 5.31$$

Using α=0.71 the above equality is satisfied with ζ=5, giving a value for k of 0.16 s^{-1}, reasonable agreement.

On comparing X_{calc} with X_{obs} (Table 5.2), good agreement was obtained until $\omega \simeq$2Hz. However after this the model began to breakdown. This occurred because X' lacked a term for the uncompensated solution resistance, R_E.

At high ω,

$$X' = X' - R_E \qquad 5.32$$

therefore,

$$X_{corr} = \frac{X' - R_E}{(X' - R_E)^2 + (Y')^2} \qquad 5.33$$

When this was taken into consideration much better agreement was obtained between the theoretical and observed values. As evidenced by X_{corr} , at high frequencies X $\propto \omega$ and not $\omega^{1/2}$. A similar treatment for values of Y led to reasonably consistent values of 10^3C between 1 Hz and 464 Hz, $\simeq$ 0.0080 F at very high frequencies and $\simeq$ 0.0097 F at moderate frequencies (Table 5.3). Thus the inclusion of R_E corrects the Y values and confirms that X has an extra term and is of the form

$$X = a\omega^{1/2} + b\omega \qquad 5.34$$

TABLE 5.2

Comparison of X_{calc} with X_{obs} for Si-oil/TTF-TCNQ data at 187 mM glc

ω/Hz	$10^5 X_{obs}/\Omega^{-1}$	$10^5 X_{calc}/\Omega^{-1}$
0.01	2.35	2.20
0.015	2.13	2.13
0.021	2.07	2.05
0.0316	1.95	1.95
0.046	1.82	1.83
0.068	1.73	1.71
0.100	1.65	1.60
0.146	1.55	1.50
0.215	1.51	1.44
0.316	1.49	1.44
0.464	1.50	1.49
0.681	1.61	1.60
1.00	1.82	1.77
1.47	2.17	2.01
2.15	2.84	2.32
3.16	4.61	2.72

In order to investigate the behaviour of Y at low ω,

$$Y = \frac{X_o}{\sqrt{2}}\left[\left((1 + \theta^2)^{1/2} - 1 \right)^{1/2} - \alpha\sqrt{\theta} \right] + C\omega \qquad 5.35$$

At very low ω, since $C\omega$ is negligible, $Y \simeq X_o[\,]$, this gives a reasonably constant value of C from $\omega = 0.03$ to 10 Hz proving the validity of the model (Table 5.4).

Considering the data at 5mM (Table 5.5 and 5.6), a very good fit is obtained once the X and Y values are corrected for R_E, $R_E = 810\ \Omega$.

A further point to note is that the frequency, likewise θ, has been measured in Hz. In order to convert to radians,

$$\theta = \frac{\omega}{2\pi k_{fr}} = \frac{\omega}{k/s^{-1}} \text{ where } k = 2\pi k_{fr} \qquad 5.36$$

If $k_{fr} \simeq 0.2\ s^{-1}$ then $k \simeq 1\ s^{-1}$, then the reaction layer thickness is given by

$$\sqrt{\frac{D}{k}} = \sqrt{4 \times 10^{-6}} = 20\mu m$$

TABLE 5.3

Corrected Y values, Y_{corr}, for Si-oil/TTF-TCNQ data at 187 mM glc

ω	$10^3 Y_{corr}/\Omega^{-1}$	$10^3 Y_{corr}/\omega$ (Hz/Ω^{-1})
1000	37	0.037
464	3.58	0.0077
214.5	1.56	0.0072
100	0.76	0.0076
46.4	0.382	0.0082
21.5	0.169	0.0079
10	0.091	0.0091
4.64	0.044	0.0095
1	0.0098	0.0098

TABLE 5.4

Values of C for Si-oil/TTF-TCNQ data at 187 mM glc

ω/Hz	10^6C/F
0.01	1.6
0.0146	3.7
0.0215	5.76
0.0316	8.45
0.0464	7.95
0.0681	8.53
0.100	8.54
0.147	8.63
0.215	8.56
0.316	8.54
0.464	8.53
0.681	8.61
1.00	8.62
4.64	8.86
10	8.67
21.5	7.6
46.4	8.0
100	7.5
215	7.2
464	7.6

TABLE 5.5

Low frequency data for the Si-oil/TTF-TCNQ electrode at 5 mM glc

ω/Hz	$10^6 X_{obs}/\Omega^{-1}$	$10^6 X_{calc}/\Omega^{-1}$	$10^6 C/F$
0.01	2.15	2.20	–
0.015	2.14	2.16	–
0.0215	2.11	2.11	2.8
0.0316	2.04	2.06	4.6
0.0464	1.99	1.99	5.7
0.0681	1.91	1.92	6.0
0.100	1.79	1.83	6.15
0.147	1.74	1.75	6.6
0.215	1.66	1.68	6.7
0.316	1.62	1.64	6.7
0.464			6.7
0.681			6.75
1			6.76
1.46			6.8
2.15			6.3

TABLE 5.6

High frequency data for the Si-oil/TTF-TCNQ electrode at 5mM glc

ω/Hz	$10^3Y/\Omega^{-1}$	$10^4C/F$	$10^3X/\Omega^{-1}$	$10^3X_{calc}/\Omega^{-1}$
681	4.40	0.065	0.76	
464	2.70	0.058	0.553	
316	1.83	0.058	0.376	
215	1.28	0.0595	0.241	
147	0.901	0.0613	0.150	
100	0.636	0.064	0.093	
68	0.447	0.066	0.0569	
46	0.313	0.067	0.0346	
31.6	0.217	0.069	0.0214	
21.5	0.151	0.070	0.0140	
14.6	0.104	0.071	0.0092	
10	0.0724	0.072	0.0064	
6.8	0.0500	0.074	0.0050	0.00381
4.64	0.0346	0.074_5	0.00370	0.00321
3.16	0.0239	0.075_5	0.00287	0.00273
2.15	0.0165	0.076_5	0.00234	0.00235
1.47	0.0113	0.077	0.00203	0.00207
1.00	0.0078	0.078	0.00181	0.00186
0.681	0.0053	0.078	0.00167	0.00172
0.464	0.0036	0.077	0.00162	0.00165

5.4.2 Applying the Homogeneous Model to the PST/TTF-TCNQ Results

An attempt was made to fit the PST electrode data to the homogeneous model proposed for the Si-oil electrode. The X values followed the same general trend giving a shallow minimum and then increasing (Table 5.7). The value of α was again assumed to be 0.71 since if a homogeneous mechanism was indeed operating then α must be the same.

$$X = \frac{X_o}{\sqrt{2}}\left[\left((1 + \theta^2)^{1/2} + 1 \right)^{1/2} - \alpha\sqrt{\theta} \right] + R_E \qquad 5.37$$

The parameters governing the system are X_o, k and α (0.71). It is possible to obtain a value for k and hence θ from the minimum value for the above expression. Rewriting as

$$X = \frac{X_o}{\sqrt{2}} f\left(\theta , \alpha\right) + R_E \qquad 5.38$$

then a plot of X against f gives X_o and R_E (vide infra). Inspection of the X values at 187 mM glucose (Table 5.7) shows that the minimum value lies between 0.0562 and 0.0178 Hz. Thus if,

$$x_1,y_1 = 0.0562 , 0.55$$

$$x_2,y_2 = 0.0316 , 0.505$$

$$x_3,y_3 = 0.0178 , 0.543$$

then,

$$y \simeq y_m + a(x_1 - x_m)^2 \qquad 5.39$$

therefore,

$$y_1 - y_2 = a\left\{(x_1 - x_m)^2 - (x_2 - x_m)^2\right\} = a(x_1 - x_2)(x_1 + x_2 - 2x_m) \qquad 5.40$$

$$y_3 - y_2 = a\left\{(x_3 - x_m)^2 - (x_2 - x_m)^2\right\} = a(x_3 - x_2)(x_3 + x_2 - 2x_m) \qquad 5.41$$

and

TABLE 5.7 $10^5 X/\Omega^{-1}$

X values for the PST/TTF-TCNQ electrode at 0.25, 5, 20, 40 and 187 mM glc

ω/Hz	[Glucose]/mM				
	0.25	5	20	40	187
10	44.4	44.1	43.2	43.1	41.5
5.62	20	20	19.7	19.4	18.4
3.16	8.26	8.26	8.20	8.20	7.75
1.78	3.50	3.56	3.61	3.66	3.51
1.00	1.66	1.70	1.81	1.91	1.83
0.562	0.89	0.94	1.07	1.18	1.15
0.316	0.55	0.61	0.76	0.87	0.86
0.178	0.366	0.448	0.60	0.719	0.70
0.100	0.267	0.373	0.510	0.637	0.62
0.0562	0.200	0.347	0.461	0.571	0.55
0.0316	0.161	0.370	0.461	0.532	0.505
0.0178	0.141	0.437	0.562	0.585	0.543
0.01	0.102	0.521	0.862	1.04	0.781
0.01	0.099	0.493	0.833	1.10	0.83

$$\frac{y_1 - y_2}{x_1 - x_2} \cdot \frac{x_3 - x_2}{y_3 - y_2} = \frac{x_1 + x_2 - 2x_m}{x_3 + x_2 - 2x_m} = -\phi \qquad 5.42$$

thus

$$x_m = \frac{x_1 + x_2 + \phi(x_2 + x_3)}{2(1 + \phi)} \qquad 5.43$$

Hence ϕ=0.664, ω_m=0.0362 Hz and since θ_m=2, k=0.0181 s^{-1}. Thus the value of k is approximately one tenth that of the Si-oil electrode.

A plot of X against f (figure 5.27) gives

$$X_o = 0.933 \times 10^{-5}\ \Omega^{-1}$$

$$(X_o')_{theor} = 1.07 \times 10^5\ \Omega \quad \text{cf. } (X_o')_{obs} = 1.30 \times 10^4\ \Omega$$

Two problems are immediately apparent. First, the value of X_o' from the gradient of the graph does not agree with the measured value; the spiral goes much nearer to the origin than predicted by the homogeneous model. Theoretical calculations show that the homogeneous model is unable to account for spirals which approach the origin so closely (4). Second, the value of k is different at the two types of electrode, a homogeneous pathway would require k to be the same. Also, application of the same type of analysis as in §5.5.1 to obtain values for Y and C does not produce satisfactory results (Table 5.8).

Figure 5.27 Plot of X against f (θ , α) for PST/TTF-TCNQ with 187 mM glc

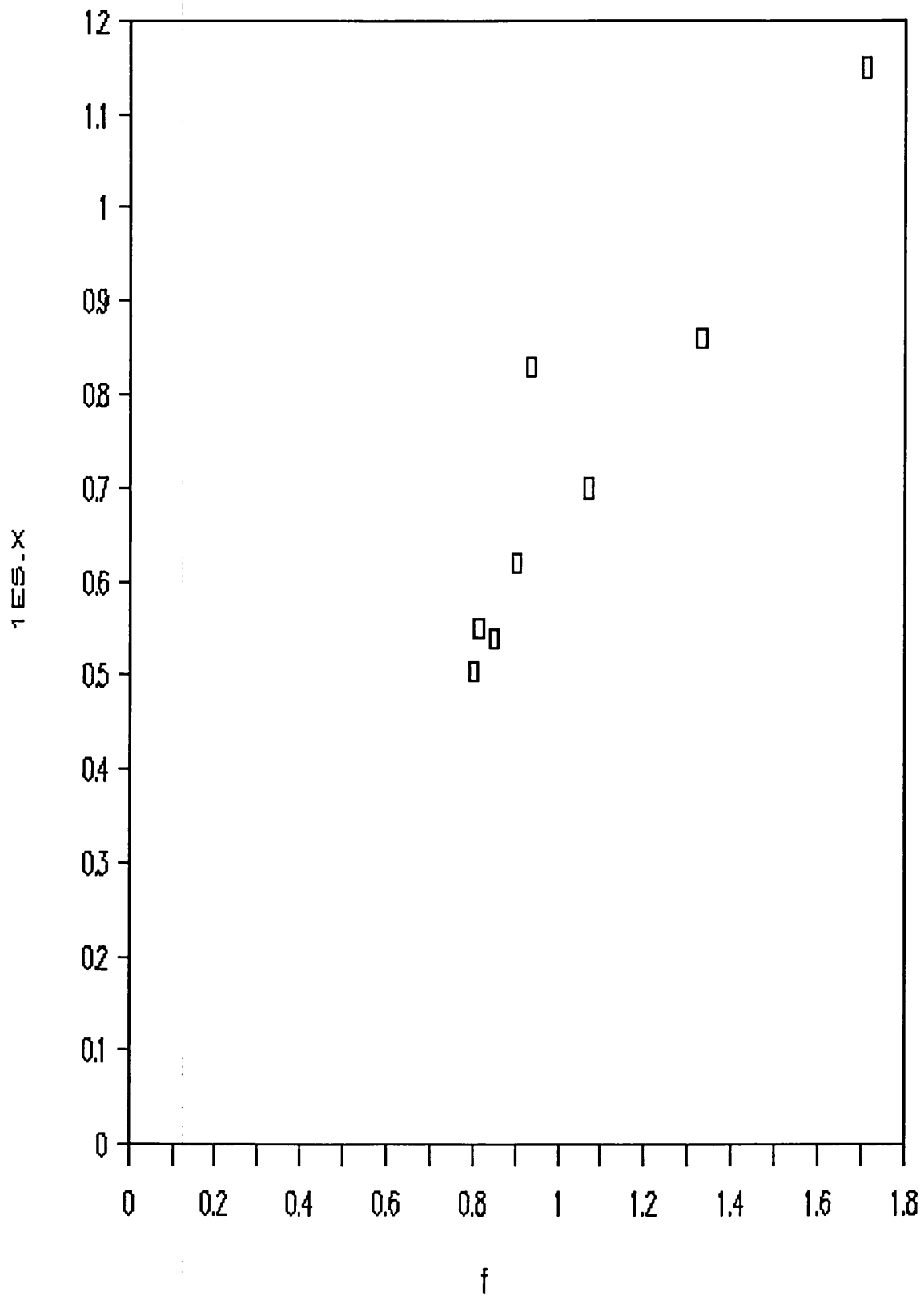

TABLE 5.8

Values of C for the PST/TTF-TCNQ data at 187 mM glc using the homogeneous model

ω/Hz	10^5C/F
0.01	-ve
0.018	-ve
0.032	12.6
0.056	5.1
0.100	6.8
0.178	7.5
0.316	7.9
0.562	8.2

5.4.3 A Combined Model

A number of different models were devised in an attempt to explain the results obtained with the PST/TTF-TCNQ electrode. These included a two step model of the form

$$A \underset{k_{-1}}{\overset{k_1}{\rightleftharpoons}} B \xrightarrow{k_2} C$$

where the first step involved a potential dependent process, perhaps adsorption, followed by a substrate dependent step. Other possible mechanisms included a two state model, a model involving heterogeneous redox catalysis and a combined mechanism coupling some surface process with the two state model (4).

The main conclusion drawn from these proposed mechanisms was that two parallel processes were operating and the observed d.c. flux was the sum of the individual fluxes

$$j_{d.c} = j_{hom} + j_{het}$$

The impedances were related according to the following expression

$$\frac{1}{Z_{obs}} = \frac{1}{Z_{hom}} + \frac{1}{Z_{het}}$$

As the Si-oil data fitted Case 1 of the homogeneous model it was decided to combine this with a mechanism which proceeded via a simple one step heterogeneous process

$$\xrightarrow{k_1} C \xrightarrow{k_2}$$

Then,

$$\frac{\partial c}{\partial t} = k_1 - k_2 c \qquad 5.44$$

and

$$c_o = \frac{k_1}{k_2} \tag{5.45}$$

application of an a.c perturbation gives,

$$\frac{dc_*}{dt} = \alpha k_1 P - \beta k_2 P c_o - k_2 c_* \tag{5.46}$$

Taking Laplace transforms,

$$s\bar{c}_* = \frac{(\alpha - \beta)k_1 P}{s} - k_2 \bar{c}_* \tag{5.47}$$

Rearrangement gives,

$$\bar{c}_* = \frac{(\alpha - \beta)k_1 P}{s(s + k_2)} \tag{5.48}$$

Therefore, assuming β is negligible,

$$\bar{i}_* = \frac{AF\alpha k_1 k_2 P}{s(s + k_2)} \tag{5.49}$$

Thus the heterogeneous impedance is given by,

$$\frac{1}{Z_{het}} = \frac{AF^2 \alpha k_1 k_2}{RT(k_2 + i\omega)} \tag{5.50}$$

$$\frac{1}{Z_{het}} = \frac{AF^2 \alpha k_1 k_2}{RT} \left(\frac{k_2 - i\omega}{k_2^2 + \omega^2} \right) \tag{5.51}$$

$$= \left(\frac{1}{Z_{het}} \right)_o \left(\frac{k_2^2 - i\omega k_2}{k_2^2 + \omega^2} \right) \tag{5.52}$$

where $\left(\frac{1}{Z_{het}} \right)_o = \frac{AF^2 \alpha k_1}{RT}$

The combined model for the PST system, ignoring R_E, is

$$\frac{1}{Z_{obs}} = \left(\frac{1}{Z_{het}}\right)_o \left(\frac{1 - i(\omega/k_{het})}{1 + (\omega/k_{het})^2}\right)$$

$$+ \frac{1}{\sqrt{2}}\left(\frac{1}{Z_{hom}}\right)_o \left(\left[(1+\theta^2)^{1/2} + 1\right]^{1/2} - \alpha\sqrt{\theta} + i\left\{\left[(1+\theta^2)^{1/2} - 1\right]^{1/2} - \alpha\sqrt{\theta}\right\}\right)$$

$$+ iC\omega \qquad 5.53$$

where $\theta = \omega/k_{hom}$. 5.54

Analysing the data at 187 mM [glc] at a PST electrode, a plot of X vs. $\omega^{1/2}$ gives a value of $0.7 \times 10^5\ \Omega^{-1}$ for $(X_o)_{hom}$ with $g \simeq 1.20$. From a plot of y vs. ω^2 (Fig. 5.28), G=154, thus from eqns. 5.25 and 5.26 $k_{fr} \simeq 0.04\ s^{-1}$ and $\alpha = 0.49$. Table 5.9 compares X_{calc} with X_{obs}. Analysis of the Y data gives good values for C from 0.1 to 10 Hz (Table 5.10).

Since $(X_o')_{obs} = 1.3 \times 10^4\ \Omega$ and

$$(X_o)_{obs} = \frac{1}{X_o'} = 7.69 \times 10^{-5}\ \Omega^{-1}$$

then

$$10^5\left[(X_o)_{hom} + (X_o)_{het}\right] = 10^5\,(X_o)_{obs} = 7.69\ \Omega^{-1}$$

since from above $10^5(X_o)_{hom} = 0.7\ \Omega^{-1}$, then, $10^5(X_o)_{het} = 7.0.\ \Omega^{-1}$

Examining the PST data with [glc]=187 mM, the fit for X at $\omega = 0.01$ Hz is evaluated as follows,

$$10^5\,(\,X_{het} + X_{hom}\,) = 0.82\ \Omega^{-1}$$

$$10^5\,X_{hom} = 0.58\ \Omega^{-1}$$

$$10^5\,X_{het} = 0.24\ \Omega^{-1}$$

Figure 5.28 Plot of y against ω^2 for PST/TTF-TCNQ with 187 mM

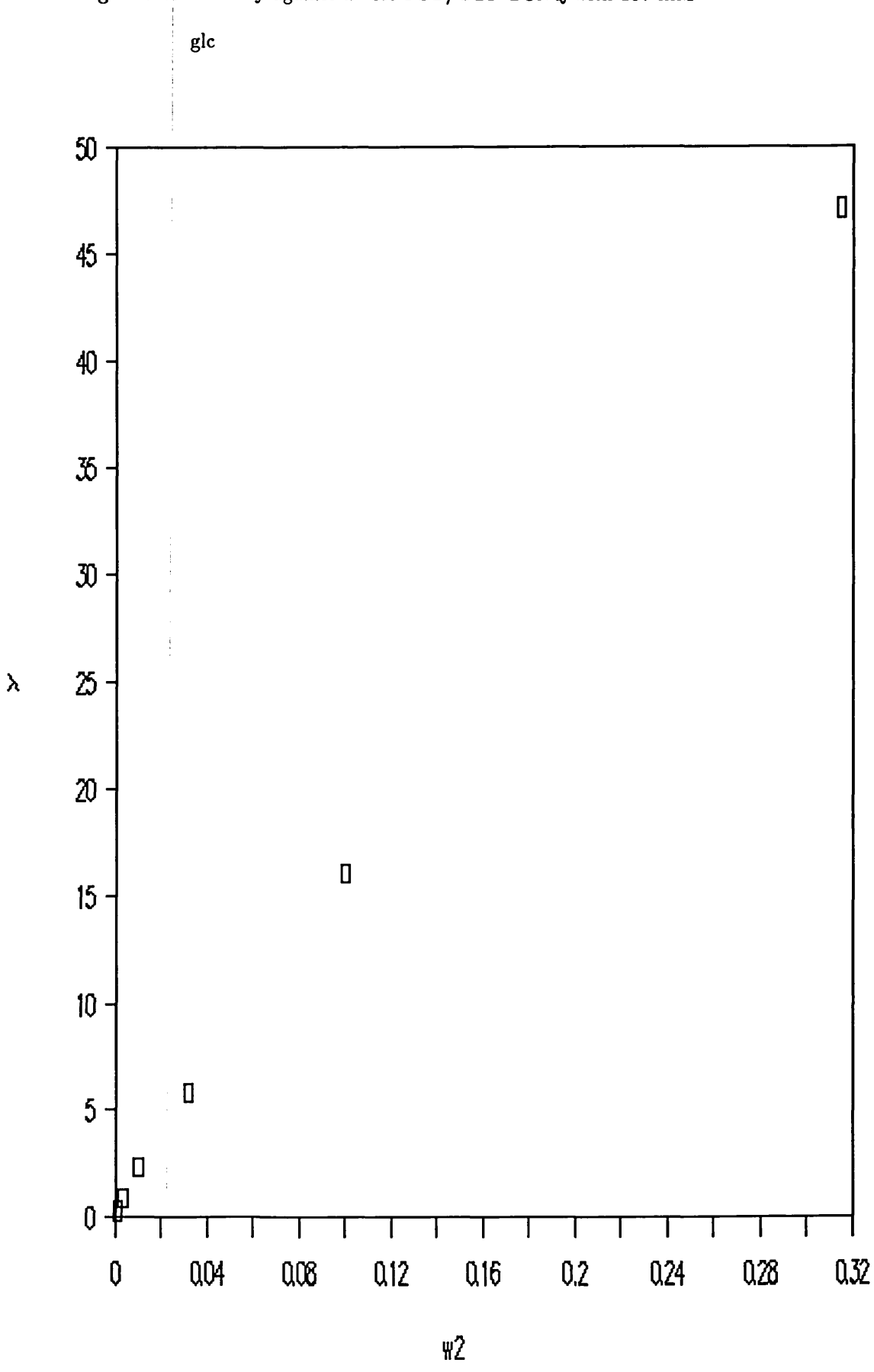

TABLE 5.9

Values of X for PST/TTF-TCNQ data at 187 mM glc using the combined model

ω/Hz	$10^5 X_{obs}/\Omega^{-1}$	$10^5 X_{calc}/\Omega^{-1}$
0.0178	0.544	0.554
0.0316	0.506	0.531
0.0562	0.553	0.530
0.100	0.620	0.570
0.178	0.66	0.69
0.316	0.82	0.80
0.562	0.97-1.04	1.01
1.00	1.26-1.49	1.32
1.78	1.85-2.52	1.73
3.16	2.9-4.9	2.27

TABLE 5.10

Values of C for PST/TTF-TCNQ data at 187 mM glc using the combined model

ω/Hz	10^4C/F
0.0178	2.8
0.316	1.9
0.0562	5.9
0.100	7.6
0.178	7.9
0.316	8.2
0.562	8.6
1.000	8.7
1.780	8.7
3.16	7.8-8.7
5.62	8.3-8.6
10	8.1-8.9

Since $X_{het} \propto 1/Z_{het}$, then

$$X_{het} = \frac{(X_o)_{het}}{1 + (\omega/k_{het})^2} \qquad 5.55$$

Therefore at 0.01 Hz

$$\frac{1}{1 + (\omega/k_{het})^2} = \frac{0.24}{7}$$

thus $\omega/k_{het}=5.3$ and $k_{het} = 2\pi(0.1/5.3) = 1.2\text{x}10^{-2}\ s^{-1}$. At $\omega=0$ Hz, $10^5(X_o)_{het}=7$ Ω^{-1}. At lower frequencies, as k_{het} is more sensitive to changes in frequency and is smaller in magnitude than k_{hom} , X_{het} is reduced more quickly than X_{hom}. Thus 10^5X_{het} falls from 7 to 0.24 Ω^{-1} as ω increases from 0 to 10 mHz.

Considering Y,

$$Y_{het} = \frac{-(X_o)_{het}\omega/k_{het}}{1 + (\omega/k_{het})^2}$$

Therefore at 0.01 Hz,

$$10^5Y = Y_{het} + Y_{hom} + C\omega$$
$$= -1.28 - 0.03 + 0.09$$
$$10^5Y = -1.22\ \Omega^{-1}$$

as compared to the observed value of $-1.21\ \Omega^{-1}$. Table 5.11 gives the theoretical and experimental values of Y and compares the contributions of the homogeneous and heterogeneous pathways for frequencies up to 178 mHz.

The work in this chapter shows that the "spirals" can be fitted by a combination of the heterogeneous one step mechanism and the homogeneous reaction. The full contribution of all three terms to Y is shown in Figure 5.29. At low frequencies $Y_{obs} \simeq Y_{het}$ but as the frequency is increased the contribution of Y_{hom} becomes more significant. The Y_{het} component falls off rapidly and Y_{obs} is soon dominated by Y_{hom}

TABLE 5.11

The contributions of the homogeneous and the heterogeneous pathways to the value of Y. The table shows the good correlation between Y_{calc} and Y_{obs}

ω/mHz	$10^5 Y_{het}$	$10^5 Y_{hom}$	$10^5 C\omega$	$10^5 Y_{calc}$	$10^5 Y_{obs}$	ϕ
17.8	−0.73	−0.01	0.15	−0.59	−0.56	9.4
31.6	−0.42	0.04	0.23	−0.15	−0.015	16.7
56.2	−0.235	0.134	0.49	0.39	0.45	29.6
100	−0.132	0.260	0.87	1.00	1.00	53
178	−0.07	0.422	1.55	1.90	1.83	94.3

Y_{hom} , Y_{het} are in Ω^{-1}

Figure 5.29 Plot comparing Y_{calc} with Y_{obs} for PST/TTF-TCNQ with 187mM glc, showing the contributions of Y_{het}, Y_{hom} and $C\omega$

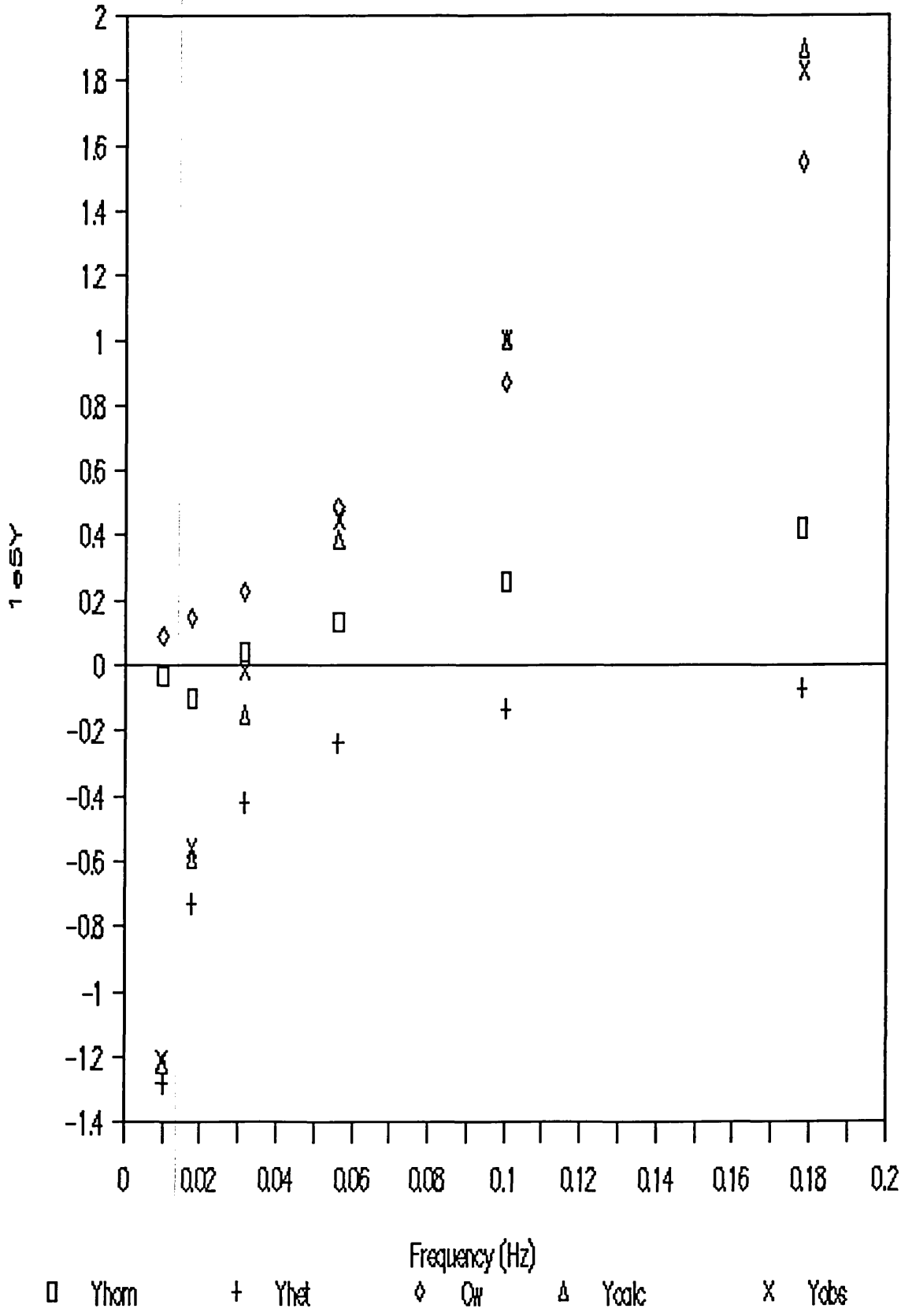

and the double layer capacitance $C\omega$.

The observed d.c. currents can be considered as being observed at ω=0 Hz. Since the value of $(X_o)_{het} \simeq 10(X_o)_{hom}$ and bearing in mind that the theoretical model predicts that the system follows the heterogeneous pathway at low frequencies, as $\omega \rightarrow 0$ Hz, this accounts for the much larger currents seen at PST electrodes as compared to those at Si-oil electrodes which are produced entirely by the homogeneous pathway.

REFERENCES

1. A. J. Bard and L. R. Faulkner, Electrochemical Methods, John Wiley and Sons, Inc., (1980)

2. Southampton Electrochemistry Group, Instrumental Methods in Electrochemistry, Ellis Horwood Limited, Chichester, (1985)

3. J. E. B. Randles, Disc. Faraday Soc., 1, 11, (1947)

4. W. J. Albery, unpublished work

APPENDIX A
THE HOMOGENEOUS MEDIATION MECHANISM

This theory deals with an enzyme electrode where electron transfer from the enzyme to the electrode is achieved by a mediator reacting in solution.

The reactions may be summarised as :

Solution

$$E + S \xrightarrow{k_E} E' + P$$

$$E' + M \xrightarrow{k_M} E + M'$$

Electrode

$$M' \longrightarrow M$$

The enzyme, E, reacts with substrate, S, with a rate constant k_E. Under saturated conditions $k_E = k_{cat}$, whilst if the enzyme is unsaturated

$$k_E = \frac{k_{cat}}{K_M}[S] \qquad \text{A.1}$$

It is assumed that [S] is sufficiently large to ensure that there is no concentration polarisation in the electrode diffusion layer. It is also assumed that all the enzyme in the bulk solution is in the reduced form, E′.

When considering the mediator two different cases can arise. First, as in the case of organic salts, where the electrode is the source of the mediator, the bulk concentrations of both M and M′ are zero. The obvious second case occurs when the mediator is supplied from the bulk where it is present as M′. Since more than one electron may be transferred for the oxidation of an enzyme molecule the treatment below assumes that only the transfer of the first electron is rate limiting. It is also assumed that all M′ reaching the electrode is oxidised and that this step is fast and not rate limiting.

A.1 The Differential Equations and Boundary Conditions

The equations describing the diffusion and kinetics of the four species M, M′, E and E′ within the diffusion layer of thickness Z_D are:

$$D_M \partial^2 m/\partial z^2 - k_M e' m = 0 \qquad \text{A.2}$$

$$D_M \partial^2 m'/\partial z^2 + k_M e' m = 0 \qquad \text{A.3}$$

$$D_E \partial^2 e'/\partial z^2 - k_M e' m + k_E e = 0 \qquad \text{A.4}$$

$$D_E \partial^2 e/\partial z^2 + k_M e' m - k_E e = 0 \qquad \text{A.5}$$

Lower case letters denote the concentrations of the various species and it is assumed that the diffusion coefficient is the same for both oxidised and reduced species.

The boundary conditions are given below:

i. At the electrode surface where z= 0:

$$m = m_o \qquad \text{A.6}$$

$$m' = 0 \qquad \text{A.7}$$

$$\text{and} \quad \left(\frac{\partial e}{\partial z}\right)_o = \left(\frac{\partial e'}{\partial z}\right)_o = 0 \qquad \text{A.8}$$

ii. At the outside edge of the diffusion layer where $z=Z_D$

$$m = m' = 0 \qquad \text{A.9}$$

$$e = 0 \qquad \text{A.10}$$

$$e' = e_\Sigma \qquad \text{A.11}$$

where e_Σ is the total concentration of all enzyme species present.

The flux of electrons, j, from the conversion of M′ to M at the electrode surface, involving n electrons is given by

$$j = nD_M\left(\frac{\partial m'}{\partial z}\right)_o \qquad \text{A.12}$$

Addition of eqns. A.2 and A.3 followed by integration yields an expression linking m and m′

$$m + m' = m_o\left(1 - \frac{z}{Z_D}\right) \qquad \text{A.13}$$

Similarly addition of A.4 and A.5 followed by integration gives

$$e + e' = e_\Sigma \qquad \text{A.14}$$

These equations are now expressed in terms of dimensionless variables. Let $u = m/m_o$, $u' = m'/m_o$, $v = e'/e_\Sigma$, $\chi = z/Z_D$, $\kappa_M = k_M Z_D{}^2 e_\Sigma/D_M$, $\kappa_E = k_E Z_D{}^2/D_E$ and $\gamma = k_M m_o/k_E$. Substitution of eqn. A.14 into eqns. A.2 and A.4 gives

$$\frac{\partial^2 u}{\partial \chi^2} = \kappa_M uv \qquad \text{A.15}$$

$$\frac{\partial^2 v}{\partial \chi^2} = \gamma\kappa_E uv - \kappa_E(1 - v) \qquad \text{A.16}$$

and from eqn. A.13

$$u + u' = 1 - \chi \qquad \text{A.17}$$

The boundary conditions are now:

$$\text{at } \chi = 0\ ,\ u = 1,\ u' = 0 \text{ and } \frac{\partial v}{\partial \chi} = 0 \qquad \text{A.18}$$

$$\text{at } \chi = 1,\ u = u' = 0 \text{ and } v = 1 \qquad \text{A.19}$$

The flux of electrons is given by

$$j = \frac{nD_M m_o}{Z_D}\left(\frac{\partial u'}{\partial \chi}\right)_o \qquad \text{A.20}$$

From eqn. A.20 it is apparent that the dimensionless parameter $(\partial u'/\partial\chi)_o$ needs to be determined in order to obtain a solution for j. Two general relations can be derived for this parameter. Firstly from eqn. A.17

$$\left(\frac{\partial u'}{\partial \chi}\right)_o = -\left(\frac{\partial u}{\partial \chi}\right)_o - 1 \qquad \text{A.21}$$

Alternatively if the uv term is eliminated from eqns. A.15 and A.16 then

$$\beta\frac{\partial^2 v}{\partial \chi^2} - \frac{\partial^2 u}{\partial \chi^2} = -\beta\kappa_E(1 - v)$$

where

$$\beta = \frac{\kappa_M}{\gamma\kappa_E} = \frac{D_E e_\Sigma}{D_M m_o} \qquad \text{A.22}$$

Integration and application of the boundary conditions at $\chi=0$ gives

$$\beta(v - v_o) + 1 - u + \left(\frac{\partial u}{\partial \chi}\right)_o = -\beta\kappa_E \int_0^\chi \int_0^{\chi'} (1 - v) d\chi'' d\chi' \qquad \text{A.23}$$

Applying the boundary condition at $\chi=1$ and using eqn. A.21

$$\left(\frac{\partial u'}{\partial \chi}\right)_o = \beta (1 - v_o) + \beta\kappa_E \int_0^1 \int_0^{\chi'} (1 - v) \, d\chi'' d\chi' \qquad \text{A.24}$$

A.2 The Physical Significance of the Dimensionless Variables

The parameters κ_E and κ_M compare the diffusion layer thickness, Z_D, to a reaction layer thickness. Thus for κ_M the reaction layer thickness is that belonging to M and is given by $(D_M/k_M e_\Sigma)^{1/2}$ whilst in the case of κ_E it is the enzyme reaction reaction layer thickness, $(D_E/ k_E)^{1/2}$. Since a reaction layer thickness is inversely proportional to the rate of reaction,

$$\kappa_M = \frac{\text{diffusion layer thickness}}{\text{reaction layer thickness E+M}} = \frac{\text{rate of reaction E+M}}{\text{rate of diffusion of M}}$$

$$\kappa_E = \frac{\text{diffusion layer thickness}}{\text{reaction layer thickness E+S}} = \frac{\text{rate of reaction E+S}}{\text{rate of diffusion of E}}$$

The parameter κ_M is a measure of the likelihood that the mediator M will react with a molecule of reduced enzyme before it can escape the diffusion layer. Hence if $\kappa_M>1$, i.e. the diffusion layer thickness is greater than the reaction layer thickness then it is more probable that M will react with E′ rather than escape. Conversely if $\kappa_M<1$ then the majority of M escapes from the diffusion layer without reacting.

Similarly the parameter κ_E weighs up the chances of E being converted to E′ in

the diffusion layer. If $\kappa_E > 1$ then most of E will be converted back to E′ before it can escape from the diffusion layer. If $\kappa_E < 1$ then most E will escape from the diffusion layer before being converted to E′.

The parameter γ describes the local steady state between the two enzyme forms at the electrode surface.

$$\gamma = \frac{\text{rate of reaction } E' + M}{\text{rate of reaction } E + S}$$

If $\gamma < 1$, implying $k_M m_o < k_E$, then the predominant form at the electrode surface, E′, is the same as that in the bulk. However if $\gamma > 1$ then, if the kinetics are sufficiently rapid to establish a steady state, the predominant form at the electrode surface will be E. In this case the predominant form of the enzyme switches from being E to E′ somewhere in the diffusion layer.

A.3 Cases I and II

Consider the situation when $\gamma \ll 1$. Since this implies that both u and v are less than unity, the $\gamma\kappa_E uv$ term in eqn. A.16 is negligible compared to κ_E and can be ignored. The differential equation for v and the boundary conditions are then satisfied with $v = 1$. Under these conditions the predominant form of the enzyme is E′. Substitution of $v = 1$ into eqn. A.15 causes the problem to collapse to a simple first order case with a solution,

$$u = \cosh\left(\sqrt{\kappa_M}\,\chi\right) - \sinh\left(\sqrt{\kappa_M}\,\chi\right) \coth\left(\sqrt{\kappa_M}\right) \qquad \text{A.25}$$

From eqns. A.21 and A.25

$$\left(\frac{\partial u'}{\partial \chi}\right)_o = \sqrt{\kappa_M} \coth\left(\sqrt{\kappa_M}\right) - 1 \qquad \text{A.26}$$

When $\kappa_M \gg 1$, $(\partial u'/\partial \chi)_o \simeq \sqrt{\kappa_M}$ and from eqn. A.20

$$j = n(D_M k_M e_\Sigma)^{1/2} m_o \qquad \text{A.27}$$

Under these conditions, Case I, the mediator, M, is consumed by E′ present at its bulk

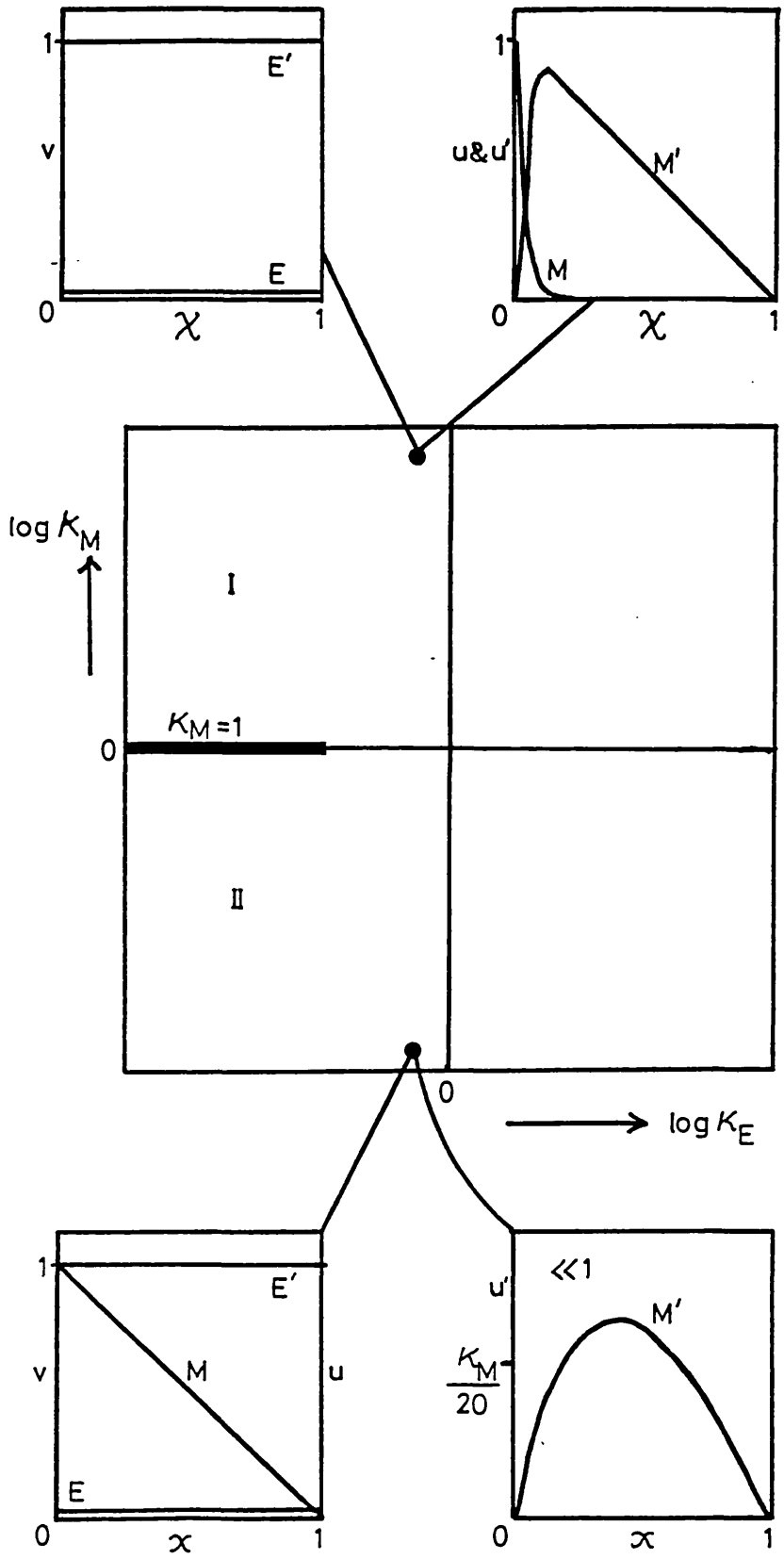

Figure A.1 Constructing the $\gamma > 1$ plane: Cases I and II. The concentration profiles for E, E′, M and M′ are also shown

concentration in a thin reaction layer close to the electrode. On the other hand when $\kappa_M \ll 1$, Case II, expansion of the coth function shows that $(\partial u'/\partial \chi)_o \simeq \kappa_M/3$, and the following expression is obtained,

$$j = \tfrac{1}{3} n k_M m_o e_\Sigma Z_D \qquad \text{A.28}$$

Now most of the mediator escapes across the diffusion layer. There is a leisurely reaction between E′ and M; the concentration of the former is uniform across the diffusion layer whilst that of the latter is linearly decreasing, ranging from m_o at the electrode to zero at Z_D. The rate of formation of M′ in the diffusion layer is $(1/2)k_M m_o e_\Sigma Z_D$, of which two thirds is captured by the electrode and one third lost to the bulk hence accounting for the factor of (1/3) in eqn. A.28. The electrode does better because the concentration of M is greater at the electrode.

If $\gamma \gg 1$, then in eqn. A.16 if $\gamma\kappa_E \ll 1$, this implies that $\kappa_E <<< 1$. Hence all the terms on the right hand side of eqn. A.16 are negligible and $v=1$ throughout the diffusion layer. Thus the same treatment holds and Cases I and II are obtained provided that

$$\kappa_E \ll 1/\gamma \ll 1 \qquad \text{A.29}$$

A.4 Cases II and III

Now consider the region where $\gamma \gg 1$, $\kappa_M \ll 1$, $\kappa_E \ll 1$ and $\gamma\kappa_E \simeq 1$. Since $\kappa_M \ll 1$, eqn. A.15 reduces to zero and the following solution is obtained on applying the boundary conditions

$$u = 1 - \chi = \chi'$$

This implies that M has a linear concentration profile from m_o at the electrode surface to zero at Z_D.

The relative sizes of $\gamma\kappa_E$ and κ_E mean that the $\gamma\kappa_E$ term dominates the right hand side of eqn. A.16. Substitution for u and χ' gives

$$\frac{\partial^2 v}{\partial \chi'^2} = \gamma \kappa_E \chi' v \qquad \text{A.30}$$

The solution of this equation requires the use of Airy functions

$$v = \frac{[\, Bi'(\phi)Ai(\phi\chi') - Ai'(\phi)Bi(\phi\chi') \,]}{[\, Ai(0)Bi'(\phi) - Bi(0)Ai'(\phi) \,]}$$

where

$$\phi = (\, \gamma \kappa_E \,)^{1/3} \qquad \text{A.31}$$

The value of v_o at $\chi' = 1$ ($\chi = 0$) is found and substituted into eqn A.24 to evaluate $(\partial u'/\partial \chi)_o$. In determining v_o, use is made of the Wronskian relation for Airy functions and since $\kappa_E \ll 1$ the integral term in eqn. A.24 can be ignored. Then

$$\left(\frac{\partial u'}{\partial \chi}\right)_o = \beta \left\{ 1 - \frac{1}{\pi[Ai(0)Bi'(\phi) - Bi(0)Ai'(\phi)]} \right\} \qquad \text{A.32}$$

When $\phi < 1$, the Airy functions can be expanded as a series to yield

$$Ai(0)Bi'(\phi) - Bi(0)Ai'(\phi) = \frac{1}{\pi}\left(1 + \frac{\phi^3}{3} + \ldots \right)$$

Substitution in eqn. A.32 together with eqn. A.31 gives

$$\left(\frac{\partial u'}{\partial \chi}\right)_o \simeq \frac{\beta \kappa_E \gamma}{3} = \frac{\kappa_M}{3} \qquad \text{A.33}$$

This result is the same as that obtained from eqn. A.26 for Case II when $\kappa_M \ll 1$.

Case III is found when $\phi > 1$. Now the $Bi'(\phi)$ term in eqn. A.32 $\gg 1$ and hence $(\partial u'/\partial \chi)_o \simeq \beta$. Substitution in eqn. A.20 gives

$$j = \frac{n D_E e_\Sigma}{Z_D} \qquad \text{A.34}$$

This suggests that the rate limiting step is the diffusion of enzyme across the diffusion layer. However since the rate of diffusion of M is fast compared to the rate of reaction between E' and M, the concentration profiles show that E' reacts with M on the outside edge of the diffusion layer and does not significantly penetrate the layer itself. Most of the M' produced is lost to the bulk of the solution rather than diffusing across

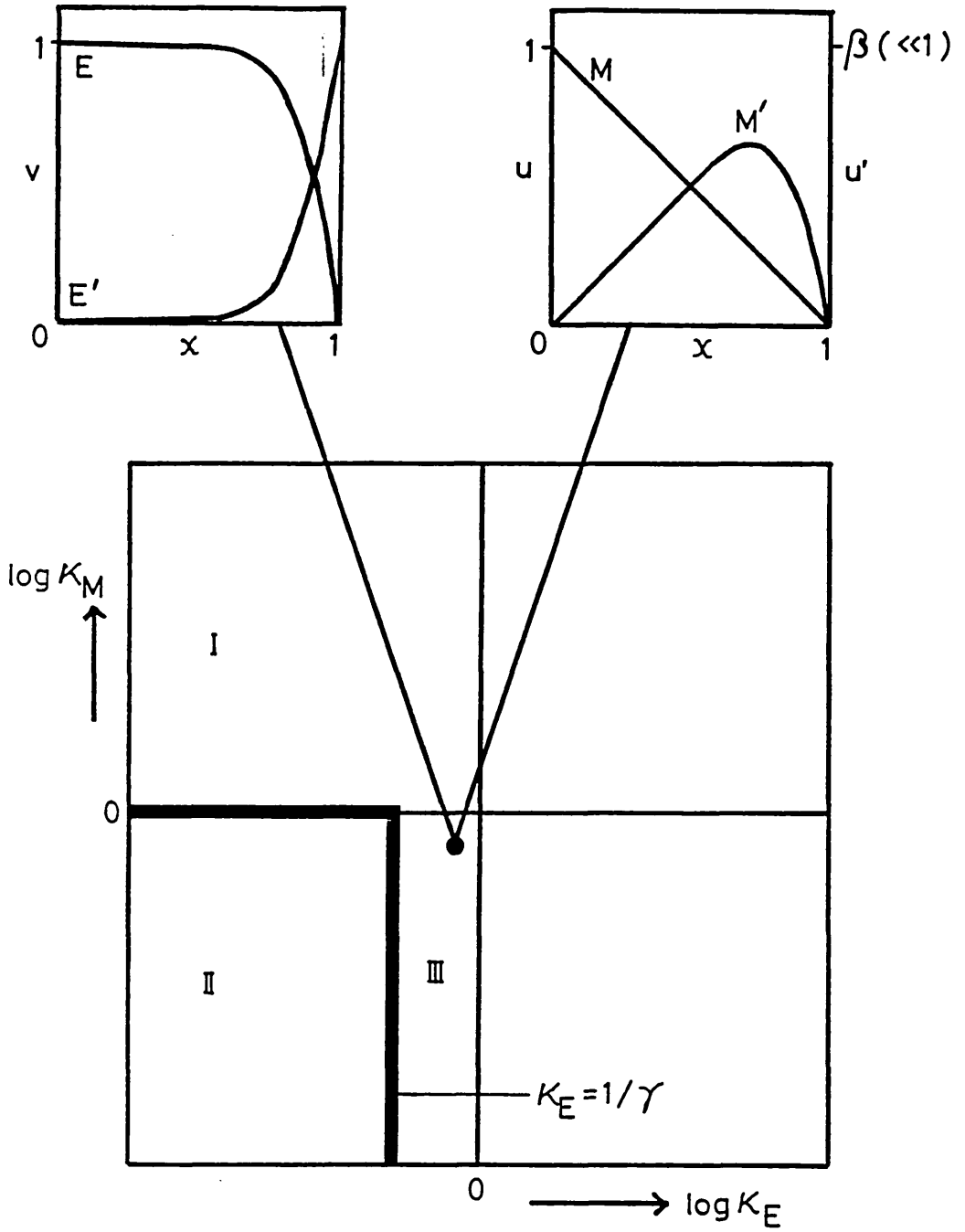

Figure A.2 Constructing the $\gamma > 1$ plane: Cases II and III. The concentration profiles for E, E′, M and M′ are also shown

the diffusion layer to the electrode. Over a small distance Z_* the fluxes of M' diffusing out and E' diffusing in can be matched i.e. $D_M m'_* \simeq D_E e_\Sigma$. Thus the flux of M' reaching the electrode is given by $D_E e_\Sigma / Z_D$. In summary, although it appears from the mathematics that the rate is determined by diffusion of enzyme, the system is physically governed by the transport of reduced mediator across the diffusion layer.

A.5 Cases I and IV

The next region of interest is the Case I boundary in the top left hand of the diagram : what happens when $\kappa_E < 1$ and $\kappa_M > 1$? If in eqn. A.15 it is assumed that over a thin reaction layer close to the electrode $v = v_o$ then,

$$u = \exp\left[-\left(\kappa_M v_o\right)^{1/2} \chi\right] \qquad \text{A.35}$$

Matching the flux of M leaving the electrode surface with that of E' diffusing to the electrode across the reaction layer gives

$$-D_M \left(\frac{\partial m}{\partial z}\right)_o = \frac{D_E(e_\Sigma - e'_o)}{Z_D}$$

Expressing this relation in terms of dimensionless variables and differentiating eqn. A.35 gives

$$-\left(\frac{\partial u}{\partial \chi}\right)_o = \left(\kappa_M v_o\right)^{1/2} = \beta\,(1 - v_o)$$

$$\Rightarrow \beta v_o - \left(\kappa_M v_o\right)^{1/2} - \beta = 0$$

Since M' is made in a thin reaction layer close to the electrode, it is nearly all captured by the electrode, thus $(\partial u'/\partial \chi)_o \simeq -(\partial u/\partial \chi)_o \gg 1$. On solving the above quadratic equation for v_o

$$\left(\frac{\partial u}{\partial \chi}\right)_o = (\kappa_M)^{1/2} \left\{\left(1 + \frac{\kappa_M}{4\beta^2}\right)^{1/2} - \frac{\kappa_M^{1/2}}{2\beta}\right\} \qquad \text{A.36}$$

When $\kappa_M/\beta^2 \ll 1$ eqn. A.36 reduces to $(\partial u'/\partial \chi)_o \simeq (\kappa_M)^{1/2}$. The system is in Case I with M diffusing into the concentration of E'. When $\kappa_M/\beta^2 \gg 1$, then expansion of the

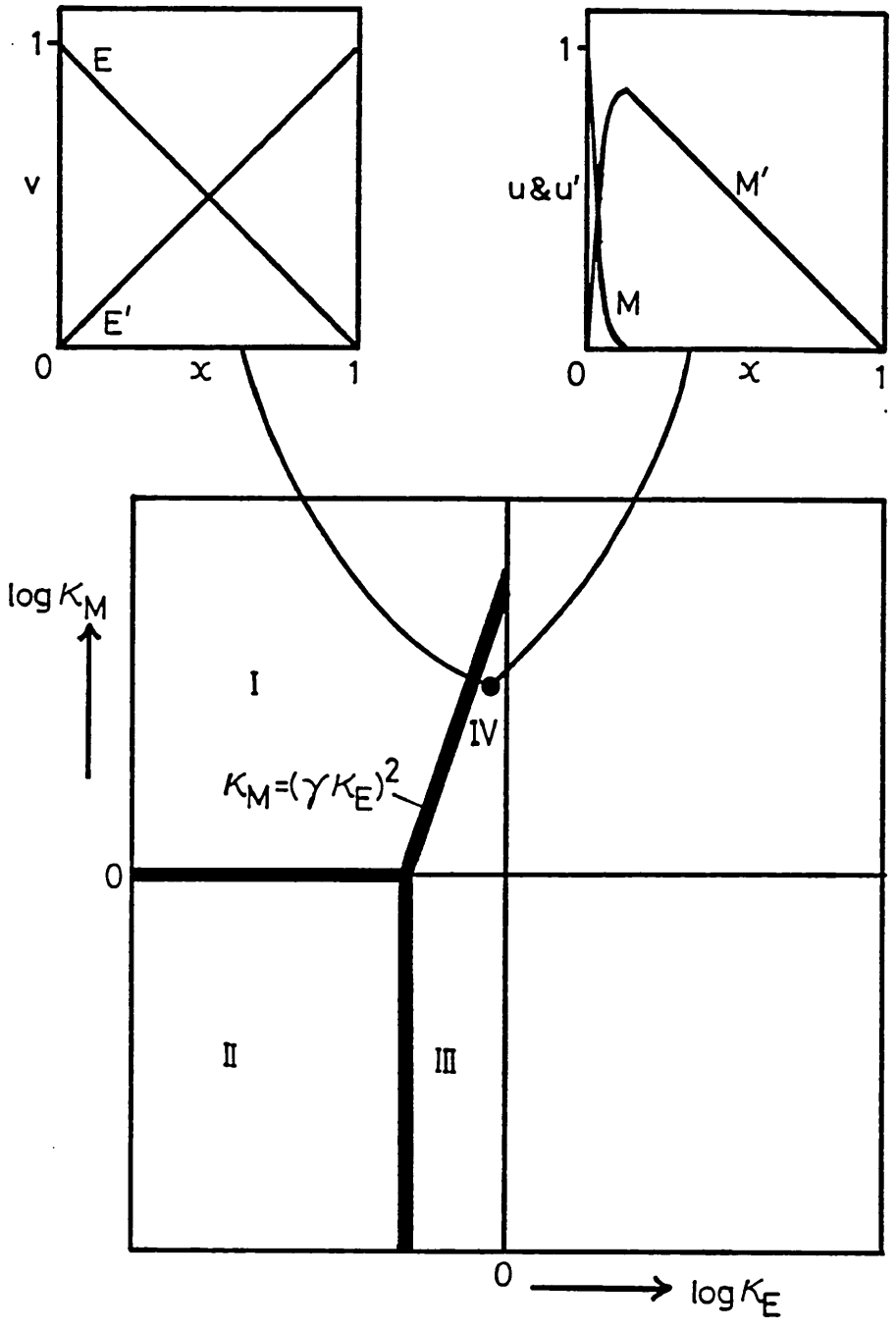

Figure A.3 Constructing the $\gamma > 1$ plane: Cases I and IV. The concentration profiles for E, E′, M and M′ are also shown

root in eqn. A.36 gives $(\partial u'/\partial \chi)_o \simeq \beta$. Now

$$j = \frac{nD_M e_\Sigma}{Z_D} \qquad \text{A.37}$$

This is Case IV where the current is controlled by the diffusion of enzyme across the diffusion layer. The reaction with M means that the surface concentration of E' is significantly lower than that in the bulk. The boundary condition between Cases I and IV is given by $\kappa_M/\beta^2 = 1$. Substitution for β gives the following condition

$$\kappa_M = \gamma^2 \kappa_E{}^2 \qquad \text{A.38}$$

A.6 Cases III and IV

Equations A.34 and A.37 show that j is given by the same expression for cases III and IV. The current appears to be governed by the diffusion of E' across the diffusion layer. Although this is a true representation of proceedings in Case IV, for Case III, E' reacts at the outside edge of the diffusion layer. These results are consistent with eqn. A.24 which shows that when κ_E is small and $v_o \ll 1$, then $(\partial u'/\partial \chi) = \beta$. The boundary between Cases III and IV is found using eqn. A.23. Applying the boundary condition at χ=1 and ignoring the terms in κ_E and v_o gives

$$\left(\frac{\partial u}{\partial \chi}\right)_o = -(1 + \beta) \qquad \text{A.39}$$

On the boundary there will be a reaction zone somewhere in the diffusion layer at χ_*. Since $\kappa_M \gg 1$, the reaction is rapid and so at $\chi = \chi_*$ both u and v are close to zero i.e. $M \simeq E' = 0$. Now substitution of eqn. A.39 into eqn. A.23 gives

$$\chi_* = \frac{1}{1 + \beta} \qquad \text{A.40}$$

When $\beta \ll 1$, reaction is on the outside edge of the diffusion layer. When $\beta \gg 1$, reaction occurs close to the electrode. When β=1 the reaction takes place halfway across the diffusion layer. This is consistent with the definition of the parameter itself, $\beta = D_E e_\Sigma / D_M m_o$.

If $\beta = 1$ then

$$\kappa_M = \gamma\kappa_E \qquad \text{A.41}$$

In Case IV the concentration profile of M has two distinct forms. Close to the I/IV boundary, as M diffuses into a reaction layer, it obeys the exponential form of eqn. A.35. However near to the III/IV boundary, as it diffuses towards the reaction zone in solution devoid of E', M has a linear profile. For $\beta>1$

I/IV $\quad u = \exp(-\beta\chi)$

III/IV $\quad u = 1 - \beta\chi$

The boundary between these two patterns of behaviour occurs when the distance that E' diffuses in the M region close to the electrode before being converted to E, $Z_{E'}$, matches, Z_*, the distance of the reaction zone from the electrode. If $Z_{E'} \ll Z_*$ then E' will never reach the electrode and M will travel a distance Z_* without any reaction thus giving a linear concentration profile. On the other hand if $Z_{E'} \gg Z_*$ then E' will penetrate to the electrode and M will be diffusing in a reaction layer giving rise to an exponential profile. The distance $Z_{E'}$ is given by

$$Z_{E'} = \left(\frac{D_E}{k_M m_o}\right)^{1/2}$$

In terms of dimensionless variables,

$$\chi_{E'} = \frac{Z_{E'}}{Z_D} = (\gamma\kappa_E)^{-1/2} \qquad \text{A.42}$$

Since

$$\chi_* = \frac{1}{\beta} = \frac{\gamma\kappa_E}{\kappa_M}$$

By comparing χ_E with χ_* it can seen that the boundary is given by

$$\kappa_M = (\gamma\kappa_E)^{3/2} \qquad \text{A.43}$$

Above this boundary there is a reaction layer whilst below it titration of M and E' occurs in a narrow reaction zone at the edge of the diffusion layer.

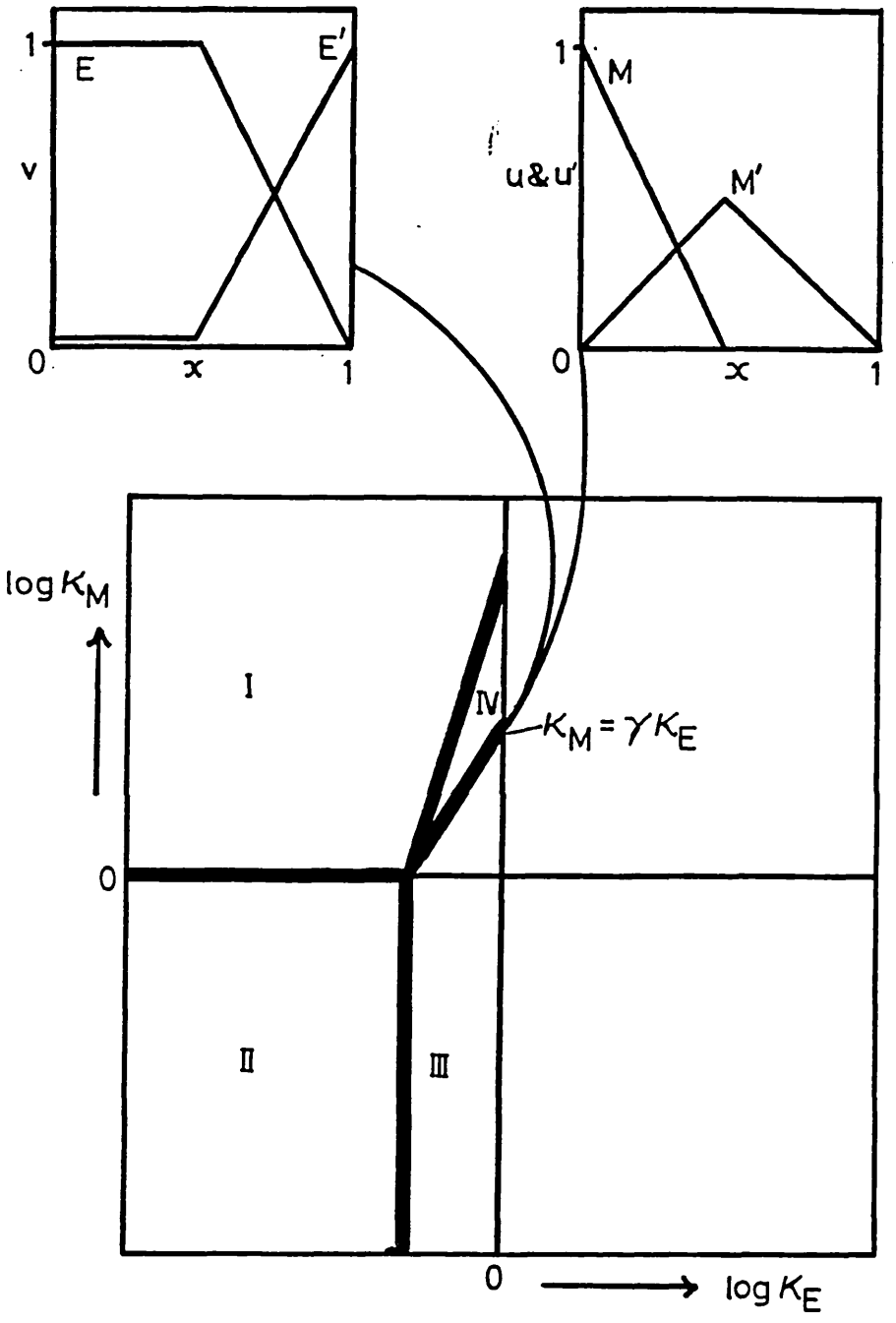

Figure A.4 Constructing the $\gamma > 1$ plane: Cases III and IV. The concentration profiles for E, E′, M and M′ are also shown

A.7 Cases III and V

Now we consider the system as enzyme regeneration in the diffusion layer becomes more significant i.e. κ_E is increasing. Since $\kappa_M \ll 1$ the rate of reaction between $E' +$ M is slow, thus the reaction zone occurs at the outside edge of the diffusion layer. Thus v is small throughout the diffusion layer and the terms in v_o and v in eqn. A.24 can be ignored. Hence

$$\left(\frac{\partial u'}{\partial \chi}\right)_o = \beta \left(1 + \frac{\kappa_E}{2}\right) \qquad \text{A.44}$$

When $\kappa_E \ll 1$ Case III is obtained. However when $\kappa_E \gg 1$ the system enters Case V where $(\partial u'/\partial \chi)_o = \beta \kappa_E/2$, thus

$$j = \frac{n k_E e_\Sigma Z_D}{2} \qquad \text{A.45}$$

Since reaction between E+S is fast there is an abundant supply of E' at the edge of the diffusion layer. As the reaction between E'+M is slow, E' enters the diffusion layer. Now M is diffusing throughout the layer and any E that is regenerated within the layer produces M'. Half of the M' reaches the electrode and half is lost to the bulk solution. This gives rise to a parabolic concentration profile for M'.

A.8 Cases V and VI

Now consider the region where $\kappa_E \gg 1$. Under these conditions the $\partial^2 v/\partial \chi^2$ term in eqn. A.16 can be ignored. Thus

$$v \simeq \frac{1}{1+\gamma u} \qquad \text{A.46}$$

This assumes that the enzyme concentrations are determined by steady state kinetics involving the mediator and enzyme regeneration and that enzyme diffusion is unimportant. Since it is specified that $\gamma \gg 1$ and $u \sim 1$, substitution from eqn. A.46 in eqn. A.15 gives

$$\frac{\partial^2 u}{\partial \chi^2} \simeq \frac{\kappa_M}{\gamma} \qquad \text{A.47}$$

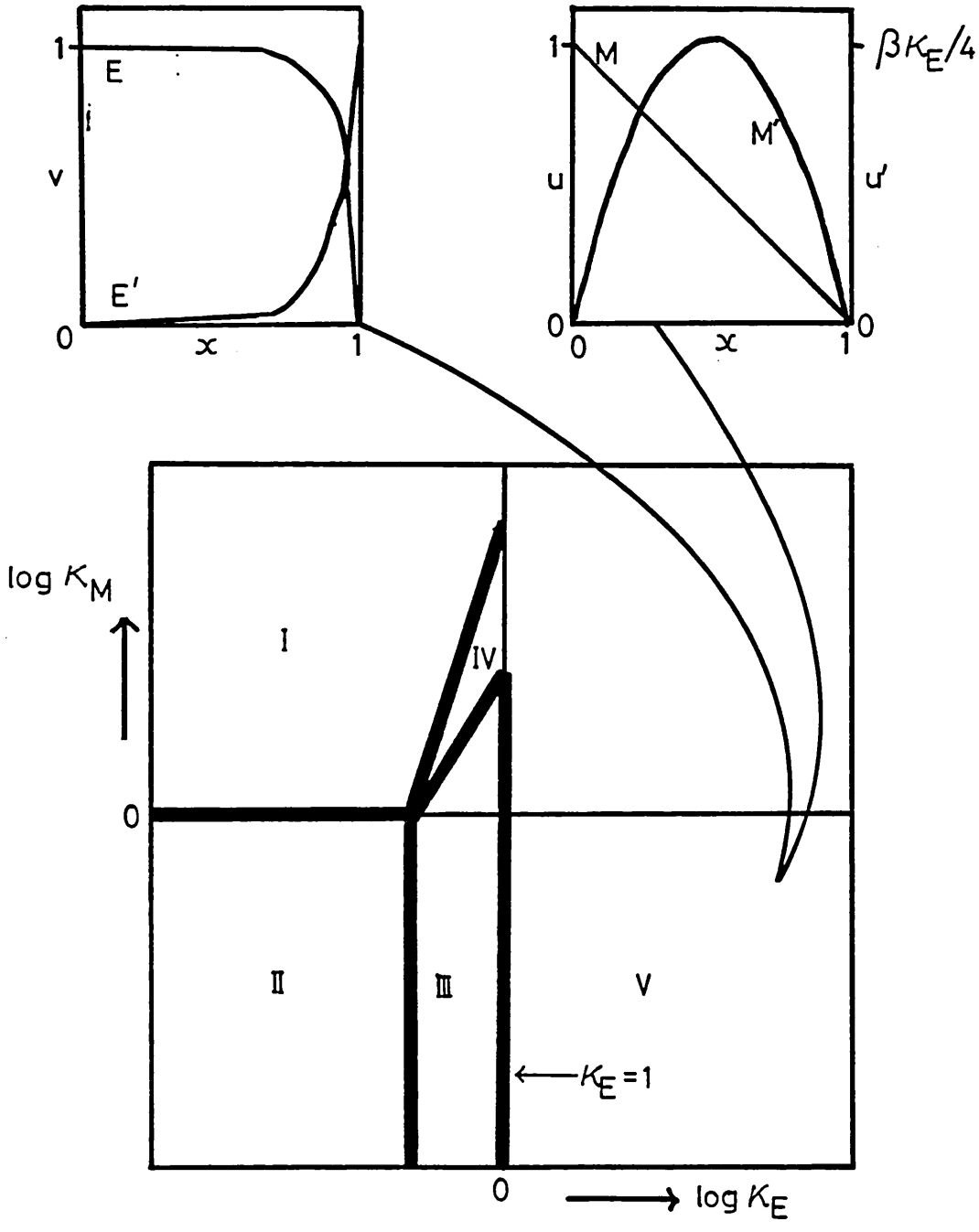

Figure A.5 Constructing the $\gamma > 1$ plane: Cases III and V. The concentration profiles for E, E′, M and M′ are also shown

i.e.

$$D_M \frac{\partial^2 m}{\partial z^2} = k_E e_\Sigma \qquad \text{A.48}$$

This equation describes the diffusion of M in a reaction layer where the rate limiting step for the consumption of M is the generation of E' from E. Since the concentration of E' is markedly lower than its bulk concentration this implies that the concentration of E is approximately equal to e_Σ. This is referred to as a zero-order reaction layer.

Integration of eqn. A.47 yields

$$u = 1 + \chi\left(\frac{\partial u}{\partial \chi}\right)_o + \frac{\kappa_M \chi^2}{2\gamma} \qquad \text{A.49}$$

Under certain conditions in the presence of regenerating enzyme, M only penetrates a distance χ_* across the diffusion layer where χ_* is the reaction layer thickness. At $\chi=\chi_*$ both u and $\partial u/\partial \chi$ are equal to zero. Applying these conditions to eqn. A.49 gives

$$\chi_* = \left(\frac{2\gamma}{\kappa_M}\right)^{1/2} \qquad \text{A.50}$$

and

$$\left(\frac{\partial u}{\partial \chi}\right)_o = -\left(\frac{2\kappa_M}{\gamma}\right)^{1/2} \qquad \text{A.51}$$

Substitution of eqn. A.51 in eqn. A.21 gives

$$\left(\frac{\partial u'}{\partial \chi}\right)_o = \left(\frac{2\kappa_M}{\gamma}\right)^{1/2} - 1 \qquad \text{A.52}$$

From eqn. A.50 it is apparent that M is destroyed in the diffusion layer ($\chi_*<1$) provided that $\kappa_M>2\gamma$. If this holds Case VI is obtained, with its zero order reaction layer. Under these conditions M' has a parabolic profile. However if $\kappa_M<2\gamma$, then M penetrates to the outside edge of the diffusion layer. Returning to eqn. A.49 and applying the boundary condition that $u=0$ at $\chi=1$

$$\left(\frac{\partial u}{\partial \chi}\right)_o = -\left(1 + \frac{\kappa_M}{2\gamma}\right)$$

Substitution in eqn. A.21 gives

$$\left(\frac{\partial u'}{\partial \chi}\right)_o = \frac{\kappa_M}{2\gamma} = \frac{\beta\kappa_E}{2} \qquad \text{A.53}$$

This result is in agreement with that obtained for Case V from eqn. A.44 when $\kappa_E \gg 1$. The boundary between Cases V and VI is

$$\kappa_M = 2\gamma \qquad \text{A.54}$$

From eqn. A.52 the following expression for j is obtained

$$j = n(2D_M k_E e_\Sigma m_o)^{1/2} - \frac{nD_M m_o}{Z_D}$$

When $\kappa_M \gg \gamma$ this reduces to

$$j = n(2D_M k_E e_\Sigma m_o)^{1/2} \qquad \text{A.55}$$

This is the result expected for a zero order reaction layer. This expression can be explained by comparing the regeneration of the enzyme in the reaction layer of thickness Z_* with the diffusion of M into that layer

$$\frac{j}{n} = k_E e_\Sigma Z_* = \frac{2D_M m_o}{Z_*} \qquad \text{A.56}$$

The factor of 2 is due to the parabolic profile for M. If the gradient at the electrode surface were to be extrapolated M would reach zero at $Z_*/2$.

A.9 Cases IV and VII

We now investigate the boundary at $\kappa_E = 1$ between Case I and Case VII. From above, $\chi_* < 1$, and a titration reaction occurs where for $\chi_* < \chi$ there is no E' and for $\chi < \chi_*$ there is no M. To solve for $\chi < \chi_*$ integrate eqn. A.23 with v and v_o set to zero. On applying the boundary condition that $u = 0$ at $\chi = \chi_*$

$$-\left(\frac{\partial u}{\partial \chi}\right)_o = \frac{1}{\chi_*} + \frac{\beta\kappa_E\chi_*}{2} \qquad \text{A.57}$$

Differentiation of eqn. A.23 gives

$$\beta\left(\frac{\partial u}{\partial \chi}\right)_* = -\left(\frac{\partial u}{\partial \chi}\right)_o - \beta\kappa_E\chi_* \qquad \text{A.58}$$

For $\chi > \chi_*$, $u=0$ thus eqn. A.16 reduces to

$$\frac{\partial^2 v}{\partial \chi^2} = -\kappa_E(1 - v)$$

Integration using the boundary conditions that $v=1$ at $\chi=1$ and $v=0$ at $\chi=\chi_* \ll 1$ gives

$$v = 1 - \text{cosech}\,[(\kappa_E)^{1/2}]\,\sinh\,[(\kappa_E)^{1/2}(1-\chi)]$$

and

$$\left(\frac{\partial v}{\partial \chi}\right)_* = (\kappa_E)^{1/2}\coth\,[(\kappa_E)^{1/2}] \qquad \text{A.59}$$

Elimination of $(\partial u/\partial\chi)_o$ between eqns. A.57 and A.58 followed by substitution of $(\partial u/\partial\chi)_*$ by $(\partial v/\partial\chi)_*$ from eqn. A.59, bearing in mind that this is a titration reaction where one molecule of M is used up per molecule of E′, gives

$$\frac{\beta\kappa_E\chi_*^2}{2} + \beta\kappa_E^{1/2}\chi_*\coth\,[(\kappa_E)^{1/2}] - 1 = 0 \qquad \text{A.60}$$

and from eqns. A.58 and A.59

$$-\left(\frac{\partial u}{\partial \chi}\right)_o = \beta\kappa_E{}^{1/2}\coth\,[(\kappa_E)^{1/2}] + \beta\kappa_E\chi_* \qquad \text{A.61}$$

For both these cases $\beta \gg 1$. Under these conditions χ_* is so small that the first term in eqn. A.60 and the last term in eqn. A.61 can both be neglected. The layer represented by χ_* is so thin that there is almost negligible enzyme regeneration occurring in that layer. The error in making this approximation is of the order of $1/\beta$. Thus

$$\left(\frac{\partial u'}{\partial \chi}\right)_o \simeq -\left(\frac{\partial u}{\partial \chi}\right)_o = \frac{1}{\chi_*} = \beta\kappa_E^{1/2}\coth\,[(\kappa_E)^{1/2}] \qquad \text{A.62}$$

It is also assumed that almost all M′ generated close to the electrode is captured by it.

Inspection of eqn. A.62 reveals that if $\kappa_E \ll 1$ then the equation collapses to give

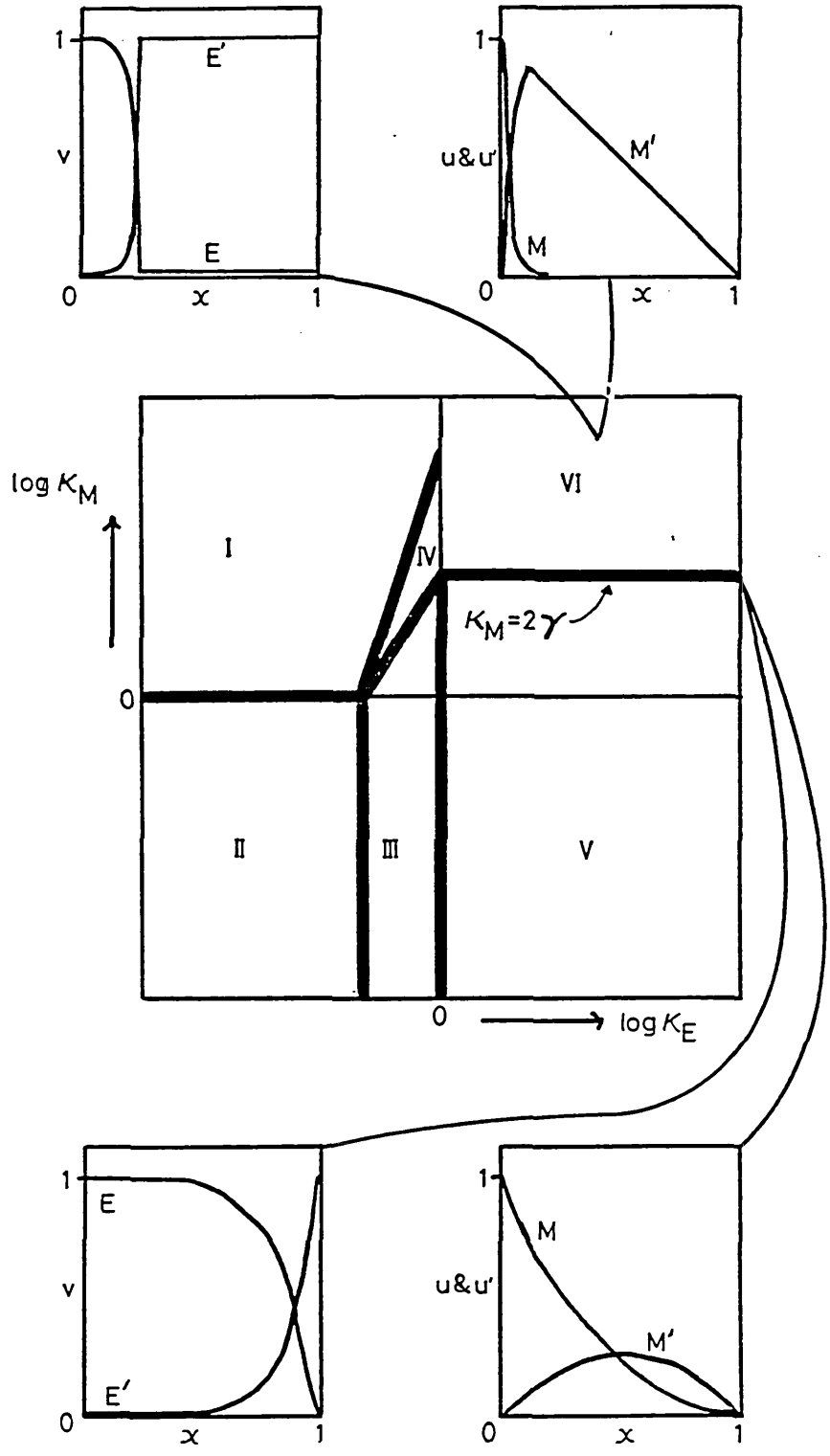

Figure A.6 Constructing the $\gamma > 1$ plane: Cases V and VI. The concentration profiles for E, E′, M and M′ are also shown

the solution for Case IV (eqn. A.36). However when $\kappa_E \gg 1$ then the right hand side becomes $\beta\kappa_E^{1/2}$ thus j for Case VII is given by

$$j = (D_E k_E)^{1/2} e_\Sigma \qquad \text{A.63}$$

The rate limiting process for this Case is the regeneration of the enzyme E′ from E in its own thin reaction layer of thickness $Z_E = (D_E/k_E)^{1/2}$ near to the reaction zone.

A.10 Cases VI and VII

On going from Case V to Case VI the $\kappa_M = 2\gamma$ boundary must be crossed and the line $\kappa_E = 1$ must be traversed on moving from Case IV to Case VII. Thus there must be a boundary between Cases VI and VII where $\kappa_E \gg 1$ and $\kappa_M \gg 2\gamma$. The former condition implies that the $\coth[(\kappa_E)^{1/2}]$ terms in eqns. A.60 and A.61, which govern the IV/VII interface are $\simeq 1$. Thus the resulting quadratic equation in χ_* can be solved to obtain

$$\chi_* = \frac{\left(1 + \frac{2}{\beta}\right)^{1/2} - 1}{\kappa_E^{1/2}} \qquad \text{A.64}$$

Also,

$$\left(\frac{\partial u'}{\partial \chi}\right)_o \simeq -\left(\frac{\partial u}{\partial \chi}\right)_o = \beta\kappa_E^{1/2}\left(1 + \frac{2}{\beta}\right)^{1/2} \qquad \text{A.65}$$

When $\beta \gg 1$ eqn. A.65 collapses to give $\beta\kappa_E^{1/2}$, i.e. yields Case VII. When $\beta \ll 1$,

$$\left(\frac{\partial u'}{\partial \chi}\right)_o = (2\beta\kappa_E)^{1/2} = \left(\frac{2\kappa_M}{\gamma}\right)^{1/2} \qquad \text{A.66}$$

This expression defines Case VI as shown in eqn. A.52. The boundary between Case VI and Case VII is $\beta = 1$ i.e. $\kappa_M = \gamma\kappa_E$. It occurs when the thickness of the zero order reaction layer, Z_*, in eqn. A.56 is equal to the thickness of the enzyme reaction layer, Z_E.

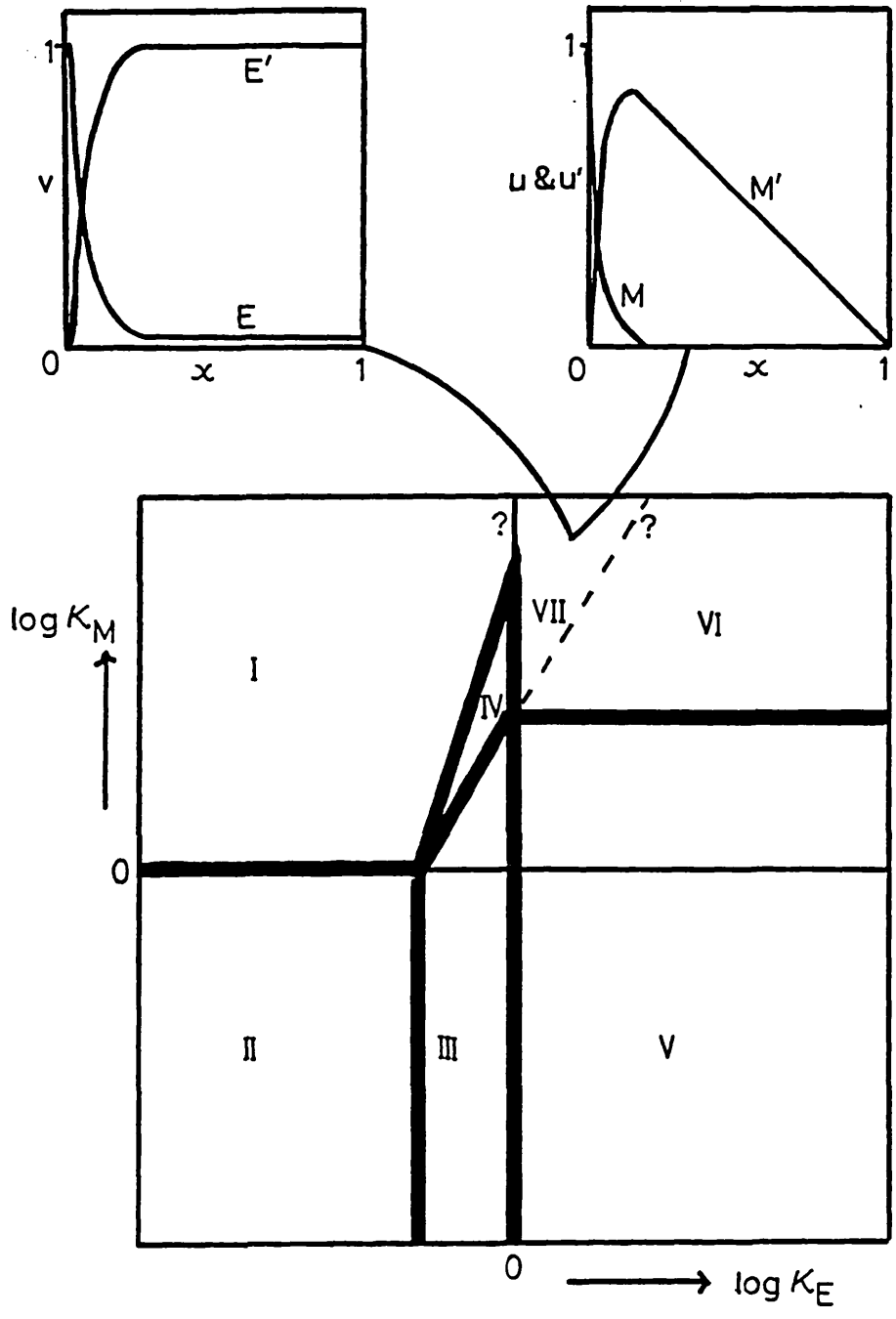

Figure A.7 Constructing the $\gamma > 1$ plane: Cases IV and VII. The concentration profiles for E, E′, M and M′ are also shown.

$$Z_* = \left(\frac{D_M m_o}{k_E e_\Sigma}\right)^{1/2} = Z_E = \left(\frac{D_E}{k_E}\right)^{1/2} \qquad \text{A.67}$$

Eqn. A.67 holds when $\beta=1$. When $\beta \gg 1$, $Z_E > Z_*$, enzyme regeneration in the enzyme reaction layer is dominant and Case VII holds. If $\beta \ll 1$, $Z_* > Z_E$, and enzyme regeneration in the zero order reaction layer is the chief process occurring, the system is in Case VI.

A.11 Cases I and VII

The boundary between Cases I and VII lies in the region where $\kappa_M \gg 1$ and $\kappa_E > 1$. The magnitude of κ_M ensures that M will be diffusing into a reaction layer, thus u will possess a concentration profile of the form

$$u = \exp\left[-(\kappa_M v_o)^{1/2} \chi\right] \qquad \text{A.68}$$

In Case I, $v_o=1$, substituting eqn. A.68 into eqn. A.16 gives a differential equation for v, which can be solved assuming that in the $\gamma\kappa_E uv$ term $v=v_o$ and using the necessary boundary conditions to give

$$v = 1 - \frac{(1-v_o)\left\{(\kappa_E)^{1/2} \exp\left[-(\kappa_M v_o)^{1/2}\chi\right] - (\kappa_M v_o)^{1/2} \exp\left[-(\kappa_E)^{1/2}\chi\right]\right\}}{(\kappa_E)^{1/2} - (\kappa_M v_o)^{1/2}} \qquad \text{A.69}$$

By equating the coefficients of the exp $[-(\kappa_M v_o)^{1/2}\chi]$ term in eqn. A.16 with the second differential of the above expression, eqn. A.69, the following relation for v_o is obtained

$$v_o + \frac{\gamma v_o}{1 + \left(\frac{\kappa_M v_o}{\kappa_E}\right)^{1/2}} = 1 \qquad \text{A.70}$$

If one assumes that on the I/VII interface $\kappa_M \gg \gamma\kappa_E$, it can be shown that $\kappa_M v_o \gg \kappa_E$. Then the resulting quadratic,

$$v_o + \left(\frac{\gamma^2\kappa_E}{\kappa_M}\right)^{1/2} v_o^{1/2} - 1 = 0$$

can be solved to give

$$v_o^{1/2} = \left(1 + \frac{\gamma^2\kappa_E}{4\kappa_M}\right)^{1/2} - \left(\frac{\gamma^2\kappa_E}{4\kappa_M}\right)^{1/2} \qquad \text{A.71}$$

From eqns. A.68 and A.70 it can be shown that

$$\left(\frac{\partial u'}{\partial \chi}\right)_o = -\left(\frac{\partial u}{\partial \chi}\right)_o \simeq (\kappa_M v_o)^{1/2} = \left(\kappa_M + \frac{\gamma^2\kappa_E}{4}\right)^{1/2} - \frac{\gamma}{2}(\kappa_E)^{1/2} \qquad \text{A.72}$$

When $\kappa_M \gg \gamma^2\kappa_E$ eqn. A.72 reduces to $\kappa_M^{1/2}$ i.e. gives Case I. If the converse is true, $\kappa_M \ll \gamma^2\kappa_E$ then the expression simplifies to give $\kappa_M/[\gamma(\kappa_E)^{1/2}] = \beta\kappa_E^{1/2}$, this being Case VII.

As in Case IV there is a dichotomy in the concentration profile for M. In Case VII the rate limiting step is regeneration of E' in an enzyme reaction layer, but close to the I/VII interface M diffuses into a reaction layer with an exponential profile predicted by eqn. A.68. However near the VI/VII interface there is a reaction zone to which M diffuses in the absence of E'. The internal boundary between these two patterns of behaviour can be determined by comparing χ_E with χ_*. The former is given in eqn. A.42 and the latter obtained by expanding eqn. A.64 binomially

$$\chi_E = (\gamma\kappa_E)^{-1/2}$$

$$\chi_* = (\kappa_E)^{-1/2}[\,(1+2/\beta\,)^{1/2} - 1\,] \simeq \frac{1}{\beta\kappa_E^{1/2}} = \frac{\gamma\kappa_E^{1/2}}{\kappa_M} \qquad \text{A.73}$$

Matching fluxes

$$\kappa_M = \gamma^{3/2}\kappa_E \qquad \text{A.74}$$

Above this boundary there exists a reaction layer in which M has an exponential profile whilst below it is a reaction zone where M has a linear profile.

A.12 Cases II and V

For these $\kappa_M \ll 1$ and $\kappa_E \gg 1$. The former condition implies that M will have a linear profile

$$u = 1 - \chi = \chi'$$

As $\kappa_E \gg 1$, the $\partial^2 v/\partial \chi^2$ term in eqn. A.16 can be ignored, thus

$$v \simeq \frac{1}{1+\gamma u} = \frac{1}{1+\gamma \chi'}$$

Substituting these two equations into eqn. A.15 gives

$$\frac{\partial^2 u'}{\partial \chi^2} = \frac{\partial^2 u'}{\partial \chi'^2} = -\kappa_M uv = -\frac{\kappa_M \chi'}{1+\gamma\chi'} \qquad \text{A.75}$$

Integration using the boundary conditions $u'=0$ at $\chi'=0$ gives

$$\frac{\partial u'}{\partial \chi'} = \left(\frac{\partial u'}{\partial \chi'}\right)_{\chi'=o} - \frac{\kappa_M \chi'}{\gamma} + \frac{\kappa_M}{\gamma^2} \ln(1+\gamma\chi') \qquad \text{A.76}$$

and

$$u' = \chi' \left(\frac{\partial u'}{\partial \chi'}\right)_{\chi'=o} - \frac{\kappa_M}{\gamma^3}\left((1+\gamma\chi')\ln(1+\gamma\chi') - \gamma\chi' - \frac{(\gamma\chi')^2}{2}\right) \qquad \text{A.77}$$

Application of the boundary condition that $u'=0$ at $\chi'=1$ ($\chi=0$) enables $(\partial u'/\partial \chi')_{\chi'=o}$ to be found from eqn. A.77. Substitution of this into eqn. A.76 permits $(\partial u'/\partial \chi)_o$ to be determined

$$\left(\frac{\partial u'}{\partial \chi}\right)_o = -\left(\frac{\partial u'}{\partial \chi'}\right)_{\chi'=1} = \frac{\kappa_M}{\gamma}\left(\frac{1}{2} - \frac{1}{\gamma} + \frac{1}{\gamma^2}\ln(1+\gamma)\right) \qquad \text{A.78}$$

If $\gamma \gg 1$ this expression reduces to

$$\left(\frac{\partial u'}{\partial \chi}\right)_o = \frac{\kappa_M}{2\gamma} = \frac{\beta\kappa_E}{2} \qquad \text{A.79}$$

This implies that the system is in Case V. On the other hand when $\gamma \ll 1$, expansion of the ln term gives $(\partial u'/\partial \chi)_o = \kappa_M/3$, i.e. now the system has entered Case I. Therefore eqn. A.78 connects Cases II and V in the region of $\gamma \simeq 1$.

A.13 Cases I and VI

At the boundary between Cases I and VI both κ_M and $\kappa_E \gg 1$. Following the procedure for Case VI, eqn. A.46 is substituted into eqn. A.15 to give

$$\frac{\partial^2 u}{\partial \chi^2} = \frac{\kappa_M u}{1+\gamma u} \qquad \text{A.80}$$

Multiplying through by $(\partial u/\partial \chi)$ and integrating gives

$$\left(\frac{\partial u}{\partial \chi}\right)^2 = \frac{2\kappa_M}{\gamma}\left(u - \frac{1}{\gamma} \ln (1+ \gamma u) \right) \qquad \text{A.81}$$

As $\kappa_M \gg 1$ it is assumed that both u and $(\partial u/\partial \chi)$ go to zero at some point in the diffusion layer and eqn. A.81 obeys this condition. Substituting eqn. A.81 into eqn. A.21 and remembering that u=1 at χ=0 gives

$$\left(\frac{\partial u'}{\partial \chi}\right)_o = \left\{ \frac{2\kappa_M}{\gamma}\left(1 - \frac{1}{\gamma} \ln (1+ \gamma) \right) \right\}^{1/2} - 1 \qquad \text{A.82}$$

When $\gamma \gg 1$ the ln term is negligible and the expression simplifies to eqn. A.52 which implies Case VI. When $\gamma \ll 1$ expansion of the ln term gives $(\partial u'/\partial \chi)_o$ to be $\sqrt{\kappa_M}$ which is consistent with Case I behaviour. Thus eqn. A.82 describes the behaviour at the I/VI interface in the region of $\gamma \simeq 1$.

A.14 The Complete Case Diagram

The seven cases can be divided into three categories. In Cases I and II the rate is governed by reaction between E′ and M either in a first order reaction layer or in the diffusion layer respectively. In cases III and IV the rate limiting process is transport of M′ or E′ across the diffusion layer. In the remaining Cases, V, VI, and VII the rate is controlled by regeneration of E′ from E in the diffusion layer, the zero-order reaction layer or the enzyme reaction layer respectively.

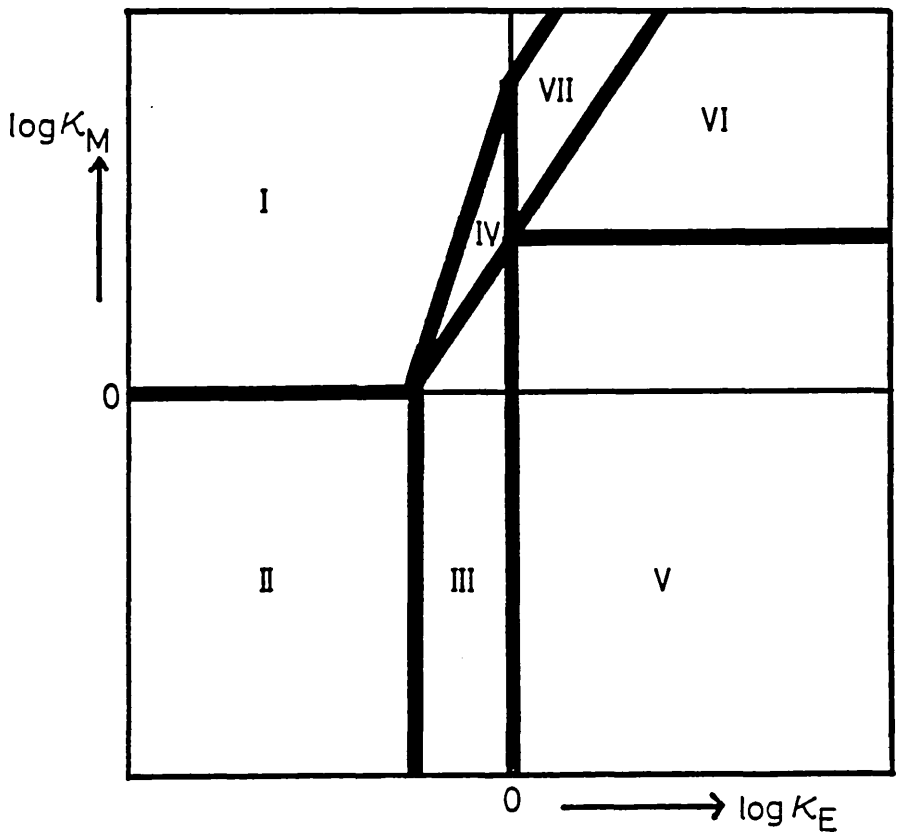

Figure A.8 The complete case diagram for the $\gamma > 1$ plane

In Case I, although reaction between E' and M is faster than that between E and S, the concentration of E' at the electrode surface is equal to that in the bulk since its rate of diffusion is sufficiently rapid to ensure that there is ample E' present to mop up M in a reaction layer close to the electrode surface. In Case II the rate of reaction between E' and M is slow enough to ensure that the concentration of E' is not altered from that in the bulk.

In the remaining cases the concentration of E' at the electrode surface is much lower than that in the bulk and there is a change in the nature of the dominant enzyme species somewhere in the diffusion layer. In Case III the rate of diffusion of M is such that it meets E' at the edge of the diffusion layer and the changeover described above occurs at this point since the rate of reaction between E' and M is sufficiently rapid. In Case V the switchover also occurs at the edge of the diffusion layer. Since κ_M is small there is only a thin diffusion layer hence there is sufficient M available to mop up any E'. In Case VI $\kappa_M \gg 1$, implying that $Z_D^{VI} > Z_D^{V}$, thus there is insufficient M at the edge of the diffusion layer. Now therefore the reaction occurs inside the diffusion layer. Since reaction between E' and M is very quick there is a titration reaction with almost instant annihilation of both species in a zero-order reaction zone independent of Z_D. In Case VII the rate of reaction between M and E' is again very fast and the rate is governed by regeneration of the latter in an enzyme reaction layer close to the electrode surface.

In summary, in Cases II, III and V $\kappa_M \ll 1$, thus the kinetics of reaction between E' and M are sluggish and [M] is greater than [M′] in the diffusion layer. In the remaining cases $\kappa_M \gg 1$ and M is destroyed before it escapes the diffusion layer.

The system is a function of the following experimental variables m_o , e_Σ, k_E, k_M and Z_D. Table A.1 shows the dependence of the dimensionless parameters κ_E, κ_M and γ on the experimental variables mentioned above.

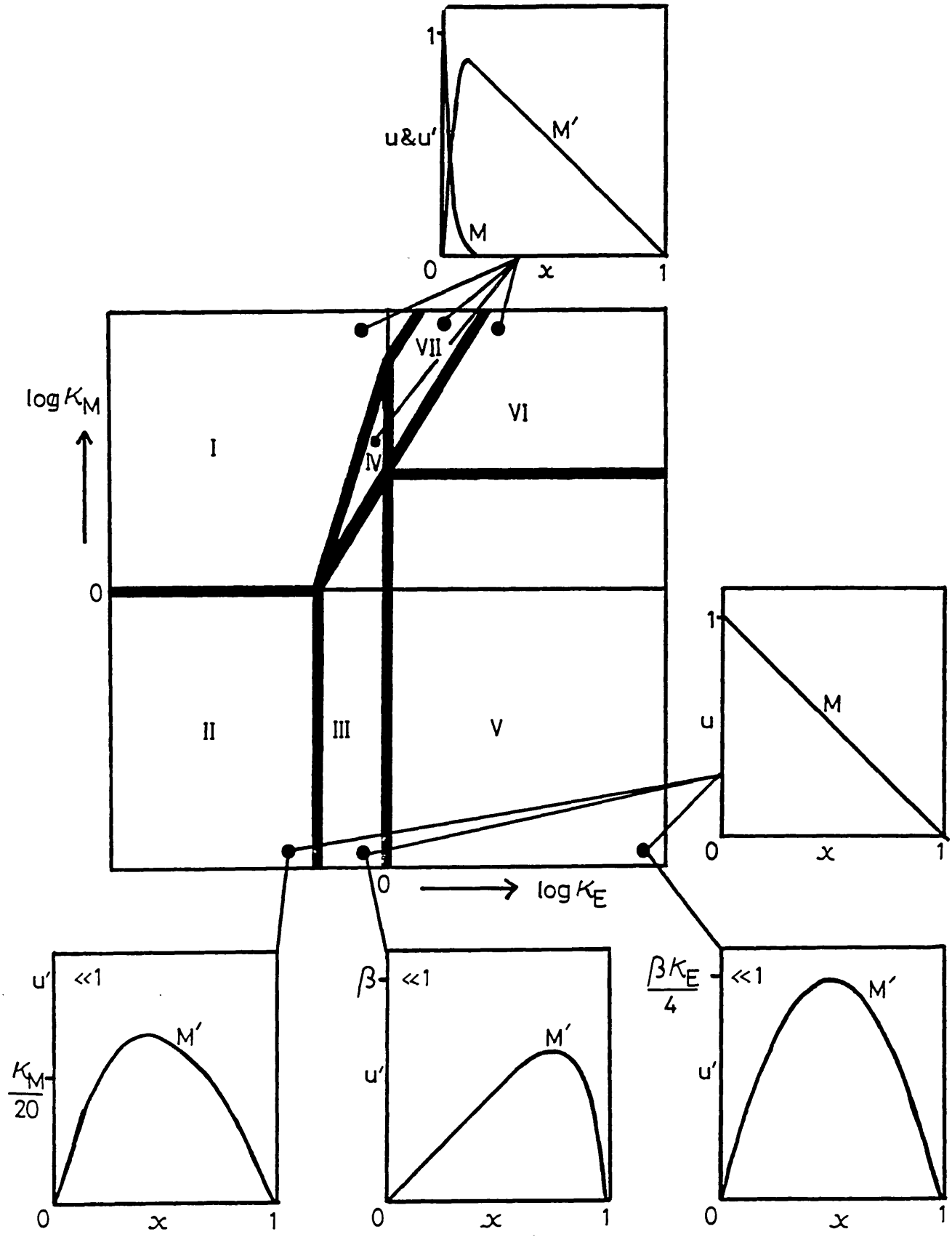

Figure A.9 The concentration profiles for M and M' for each case in the $\gamma > 1$ plane

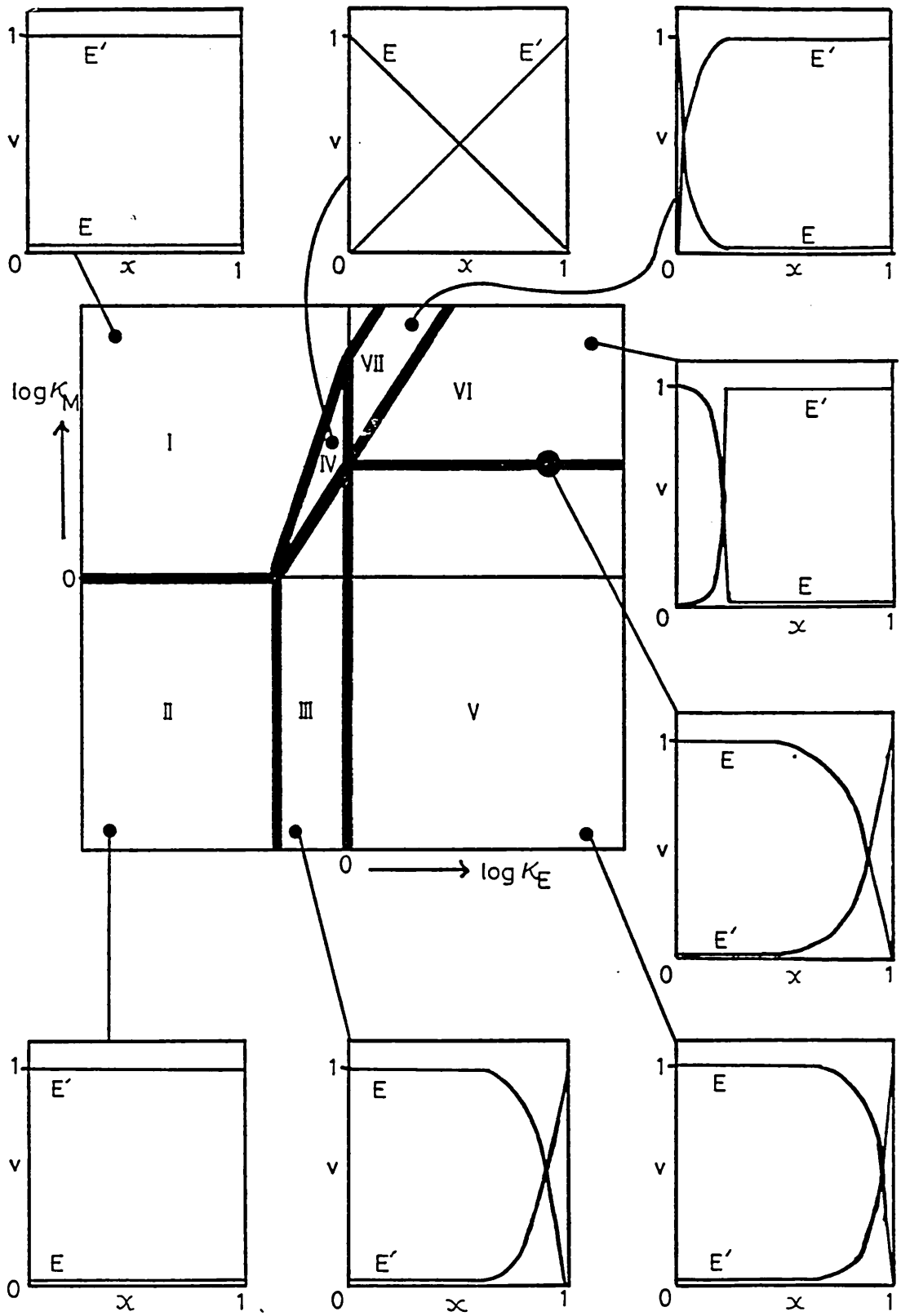

Figure A.10 The concentration profiles for E and E′ for each case in the $\gamma > 1$ plane

TABLE A.1

Summary of the planes to be used for each experimental variable

Experimental Variable	Dimensionless Variables			Plane(s)
	γ	κ_M	κ_E	
m_o	✓	X	X	$\gamma\kappa_E$ or $\gamma\kappa_M$
e_Σ	X	✓	X	$\gamma\kappa_E$ or $\gamma\kappa_M$
k_E	✓	X	✓	$\gamma\kappa_E$
k_M	✓	✓	X	$\gamma\kappa_M$
Z_D	X	✓	✓	$\kappa_M\kappa_E$

APPENDIX B
THE HETEROGENEOUS REDOX CATALYSIS MODEL

This model proposes that electron transfer occurs via a surface mediated process since the insolubility of the mediator species precludes a homogeneous pathway. It assumes the presence of a labile equilibrium on the electrode surface between the salt A^+B^- and the energetic species A° and B°.

$$A^+B^- \underset{}{\overset{K_1}{\rightleftharpoons}} A^\circ + B^\circ$$

It is assumed that A° is readily oxidised to A^+ with a first order rate constant, k_2,

$$A^\circ \xrightarrow{k_2} A^+ + e^-$$

It is also assumed that E' is oxidised by B° with a second order rate constant, k_3

$$E' + B^\circ \xrightarrow{k_3} E + B^-$$

Although it is possible that two equivalents of B° may be required to oxidise E', it is assumed that only removal of the first electron can be rate limiting. Recombination of A^+ and B^- to form the original salt is assumed to be fast,

$$A^+ + B^- \xrightarrow{\text{fast}} A^+B^-$$

In order to account for the observed inverse rotation speed behaviour it is necessary to incorporate into the model the possibility that A° can be lost by corrosion into the solution

$$A^\circ \overset{K_S}{\rightleftharpoons} A^\circ_{aq} \xrightarrow{k_D}$$

K_S/cm = solubility of A°

k_D/cm s^{-1} = mass transfer rate constant $= \frac{D_A}{Z_D}$ B.1

D_A is the diffusion coefficient of A and Z_D is the thickness of the diffusion layer. In the steady state the flux of A° dissolving in the solution must be matched by an equal flux of B^- leaving the electrode surface.

In solution E reacts with S to generate E' and product P

$$E + S \xrightarrow{k_E} E' + P$$

The first order rate constant k_E is given by

$$k_E = \frac{k_{cat}}{1 + K_M/[S]} \qquad \text{B.2}$$

It is also assumed that [S] is sufficiently large to ensure there is no concentration polarisation.

B.1 Surface Kinetics

Under steady state conditions

$$K_1 = ab \qquad \text{B.3}$$

$$j_e = k_2 a \qquad \text{B.4}$$

$$j_E = k_3 e'_o b \qquad \text{B.5}$$

where a, b and e'_o denote the surface concentrations of A°, B° and E'. Under steady state conditions the fluxes of A° and B° can be matched

$$(k_2 + K_S k_D) a = n k_3 e'_o b \qquad \text{B.6}$$

From eqns. B.4-B.6 the following expression relating the enzyme flux, j_E, and the electron flux, j_e, is obtained

$$j_e = \frac{n j_E}{1 + \theta} \qquad \text{B.7}$$

θ is a dimensionless parameter which describes the partition of A° between corroding into

the solution and being oxidised to A^+.

$$\theta = \frac{K_S k_D}{k_2} \qquad \text{B.8}$$

By eliminating a from eqns. B.3-B.6 and substituting for b in eqn. B.5 the following expression for j_E is obtained

$$j_E = \left(\frac{K_1 k_2 k_3 (1 + \theta) e_o'}{n} \right)^{1/2} \qquad \text{B.9}$$

B.2 Enzyme Kinetics

The following differential equation relates the diffusion and enzyme kinetics

$$D_E \frac{\partial^2 e'}{\partial z^2} = - k_E e \qquad \text{B.10}$$

where e is the concentration of E. Assuming that E and E′ have the same diffusion coefficient and

$$e + e' = e_\Sigma \qquad \text{B.11}$$

where e_Σ is the concentration of enzyme species. The first boundary condition for the system is that at $z = Z_D$, $e=0$ and

$$e' = e_\Sigma \qquad \text{B.12}$$

The second boundary condition is that at the electrode surface

$$D_E \left(\frac{\partial e'}{\partial z} \right)_o = j_E \qquad \text{B.13}$$

As in the homogeneous mediation model the variables are now converted into dimensionless parameters $v=e'/e_\Sigma$, $\kappa_E=k_E Z_D^2/D_E$ and $\chi=z/Z_D$. Substitution of eqn. B.11 into B.10 gives

$$\frac{\partial^2 v}{\partial \chi^2} = -\kappa_E (1 - v) \qquad \text{B.14}$$

with the boundary conditions that at $\chi=1$, $v=1$ and that at $\chi=0$

$$j_E = \frac{D_E e_\Sigma}{Z_D}\left(\frac{\partial v}{\partial \chi}\right)_o \qquad \text{B.15}$$

Integration of eqn. B.14 gives

$$1 - v = (1 - v_o)\,[\,\cosh(\kappa_E^{1/2}\chi) - \sinh(\kappa_E^{1/2}\chi)\coth(\kappa_E^{1/2}\chi)\,] \qquad \text{B.16}$$

Differentiation of this gives

$$\left(\frac{\partial v}{\partial \chi}\right)_o = (1 - v_o)\,\kappa_E^{1/2}\coth(\kappa_E^{1/2}) \qquad \text{B.17}$$

B.3 The Flux of Electrons

The dimensionless parameter, f, describes the flux of electrons

$$j_e = \frac{fnD_E e_\Sigma}{Z_D} \qquad \text{B.18}$$

From eqns. B.7, B.15 and B.18

$$\left(\frac{\partial v}{\partial \chi}\right)_o = f\,(\,1 + \theta\,) \qquad \text{B.19}$$

Defining a dimensionless parameter ρ,

$$\rho = \frac{ne_\Sigma}{K_1 k_2 k_3}\left(\frac{D_E}{Z_D}\right)^2 \qquad \text{B.20}$$

Combining eqns. B.9, B.15, B.19 and B.20

$$v_o = (\,1 + \theta\,)\rho f^2 \qquad \text{B.21}$$

Substitution from eqns. B.19 and B.21 into eqn. B.17 gives a quadratic equation in f

$$\rho f^2 + f\,\frac{\tanh(\kappa_E^{1/2})}{\kappa_E^{1/2}} - \frac{1}{1 + \theta} = 0 \qquad \text{B.22}$$

This is solved to give

$$f = \frac{1}{2\rho}\left\{\left(\frac{\tanh^2(\kappa_E^{1/2})}{\kappa_E} + \frac{4\rho}{1+\theta}\right)^{1/2} - \frac{\tanh(\kappa_E^{1/2})}{\kappa_E^{1/2}}\right\} \qquad \text{B.23}$$

This equation shows that the system is described by three parameters. The parameter κ_E is the same as that in the homogeneous mediation mechanism. If $\kappa_E >> 1$ then enzyme regeneration is rapid and nearly all E is converted to E′ in a thin reaction layer of thickness $(D_E/k_E)^{1/2}$ with very little E escaping from the diffusion layer. If the converse is true and $\kappa_E \ll 1$ then regeneration of E′ is inefficient. The parameter θ is a measure of the propensity of A° to corrode away into the solution rather than undergo reoxidation to A^+. The parameter ρ reflects the balance between the surface kinetics and mass transport. If $\rho \gg 1$ then the surface kinetics are slow and govern the overall rate. However when $\rho \ll 1$ then the surface kinetics are fast and the flux will be controlled by either the enzyme kinetics or mass transport.

The solution given in eqn. B.23 can be reduced to three simpler cases depending on the nature of the rate limiting process. Firstly if

$$\frac{\rho}{1+\theta} \gg \frac{\tanh^2(\kappa_E^{1/2})}{\kappa_E} \qquad \text{B.24}$$

then eqn. (B.23) is dominated by the ρ term and collapses to give,

$$f \simeq \frac{1}{\sqrt{\rho(1+\theta)}} \qquad \text{B.25}$$

Substitution of eqn. B.25 into eqn. B.16 gives the electron flux

$$j_e = \left(\frac{nK_1k_2k_3e_\Sigma}{1+\theta}\right)^{1/2} \qquad \text{B.26}$$

In this situation the rate is governed by the surface kinetics.

If the inequality in eqn. B.24 is reversed then the square root term in eqn. B.23

can be expanded to give

$$f \simeq \frac{\kappa_E^{1/2}\coth(\kappa_E^{1/2})}{1+\theta} \qquad \text{B.27}$$

This expression can be further simplified depending on whether κ_E is larger or smaller than unity. If $\kappa_E \ll 1$ then

$$f \simeq \frac{1}{1+\theta} \qquad \text{B.28}$$

and j_e is given by

$$j_e = \frac{nD_E e_\Sigma}{Z_D(1+\theta)} \qquad \text{B.29}$$

The surface kinetics are fast and the rate limiting process is the transport of E' across the diffusion layer.

The third case occurs when $\kappa_E \gg 1$ and enzyme regeneration is efficient, then

$$f \simeq \frac{\kappa_E^{1/2}}{1+\theta} \qquad \text{B.30}$$

giving

$$j_e = \frac{n(D_E k_E)^{1/2} e_\Sigma}{1+\theta} \qquad \text{B.31}$$

In this situation the rate is governed by regeneration of the enzyme.

The $(1+\theta)$ term is common to eqns. B.25-27 since the partition between dissolution of A° and B^- and reoxidation occurs regardless of the rate-limting process.

B.4 The Complete Case Diagram

Three parameters ρ, κ_E and θ are used to describe the system. Hence a three

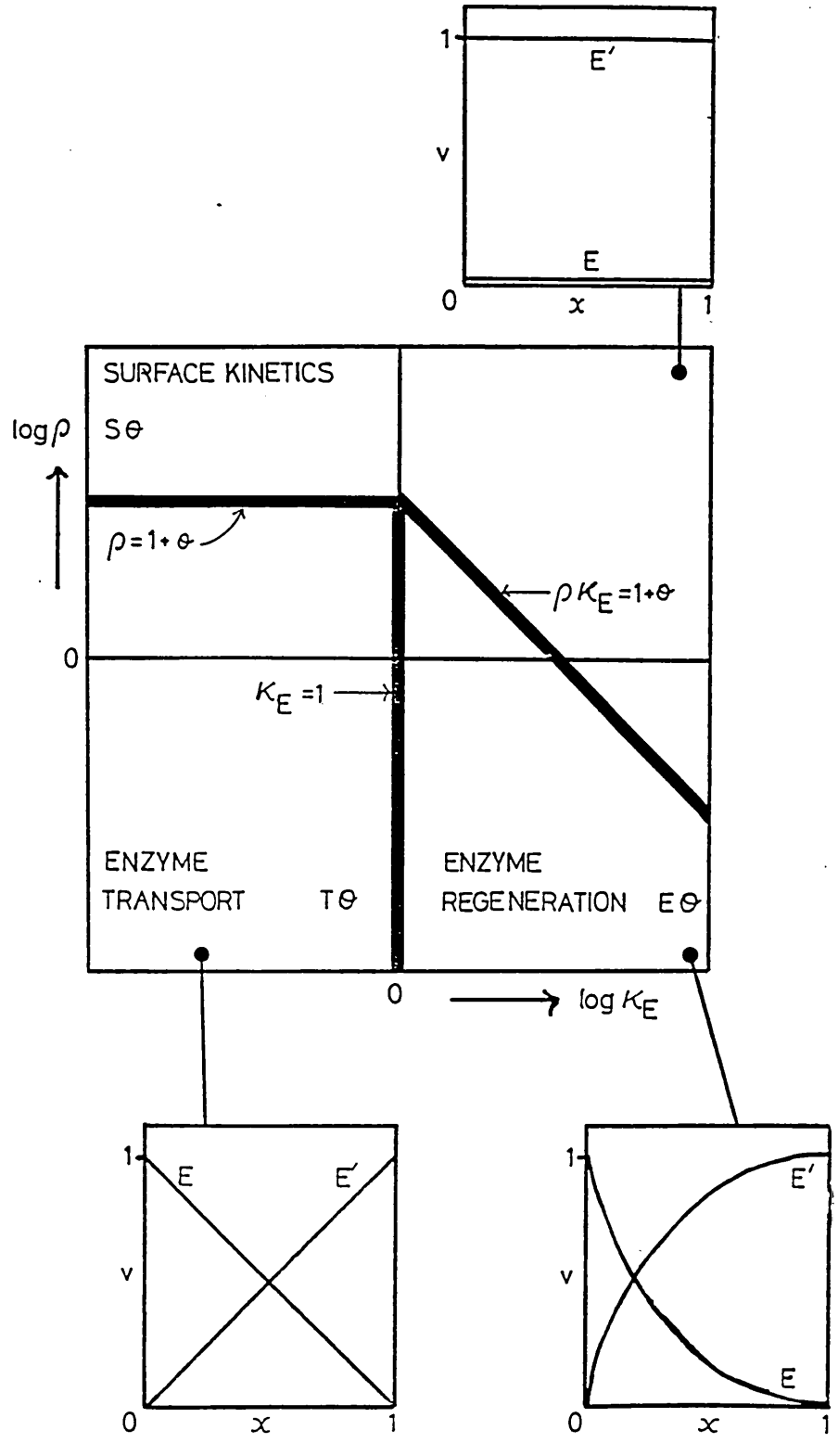

Figure B.1 The $\theta > 1$ plane. The concentration profiles for E and E′ are shown for each case

dimensional case diagram can be constructed. Considering the system when $\theta \gg 1$, then at low values of ρ the rate controlling process is either the enzyme kinetics (E) or enzyme transport (T) depending on whether κ_E is greater or smaller than unity. At large ρ both these cases are bounded by surface kinetic control (S). Cases when $\theta \gg 1$ have an added θ label to distinguish them from those when $\theta \ll 1$.

The system is governed by the following experimental variables : e_Σ, k_E, $K_1k_2k_3$, K_S/k_2 and Z_D. Since θ is independent of e_Σ and k_E, variation of these parameters can be shown on a $\rho\kappa_E$ plane. Increasing e_Σ entails a vertical translation parallel to the ρ-axis. Increasing [S] and hence k_E, involves a horizontal translation parallel to the κ_E-axis. The surface kinetic parameters $K_1k_2k_3$ and K_Sk_D/k_2 are examined on $\theta\rho$ plane. Increasing K_1k_3 implies a translation parallel to the ρ-axis whilst increasing k_2 implies a decrease in both ρ and θ hence it is equivalent to a translation in a SW-direction. In order to investigate the effect of varying the diffusion layer thickness Z_D it is necessary to introduce a new variable ξ, where

$$\xi = \rho\kappa_E = \frac{ne_\Sigma D_E k_E}{K_1k_2k_3} \qquad \text{B.32}$$

It compares the rate of enzyme regeneration with the rate of surface kinetics and is independent of Z_D. Thus Z_D is investigated using a $\theta\kappa_E$ plane at constant ξ.

APPENDIX C

THE MODIFIED ENZYME MECHANISM

In order to enhance electron transfer it is possible that the enzyme E undergoes some form of modification, possibly incorporating electron relays such as TTF^+ or $TCNQ^o$ upon coming into contact with the electrode surface. Thus assuming that E is modified with a rate constant k'

$$E_\infty \underset{\longleftarrow}{\overset{k_E}{\longrightarrow}} E_o \longrightarrow E'_o$$

If the rate constant for adsorption is k_E where

$$k_E = \frac{D_E}{Z_{D_E}} \qquad \text{C.1}$$

and the total enzyme concentration e_∞ is given by

$$e + e' = e_\infty \qquad \text{C.2}$$

then

$$k_E(e_\infty - e_o) = k' e_o \qquad \text{C.3}$$

therefore the concentration of unmodified enzyme adsorbed on the electrode surface is given by

$$e_o = \frac{e_\infty}{1 + k'/k_E} \qquad \text{C.4}$$

and that of modified adsorbed enzyme is given by

$$e'_o = \frac{k' e_\infty}{k_E + k'} \qquad \text{C.5}$$

Thus e'_o is inversely proportional to rotation speed which is in accord with experimental observations at Si-oil and pressed pellet electrodes.

C.1 Combining Heterogeneous Redox Catalysis with the Modified Enzyme Model

A system of simultaneous equations can be constructed

$$j = k_1 - k_{-1}ab \qquad C.6$$

$$= k_A a \qquad C.7$$

$$= k_B b e'_R \qquad C.8$$

$$= k_S s_o e'_{OX} \qquad C.9$$

Also

$$e'_R + e'_{OX} = \kappa\, e'_o = \frac{\kappa e_\infty k'}{k_E + k'} \qquad C.10$$

From eqn. C.9

$$e'_{OX} = \frac{j}{k_S s_o} \qquad C.11$$

and from eqns C.10 and C.11

$$e'_R = \kappa e'_o - \frac{j}{k_S s_o} \qquad C.12$$

From eqn. C.7

$$a = \frac{j}{k_A} \qquad C.13$$

and using eqns. C.8 and C.12

$$b = \frac{j}{k_B(\kappa e'_o - j/k_S s_o)} \qquad C.14$$

Following substitution of eqns. C.13 and C.14 into eqn. C.6 and making the assumption that $k_{-1} \gg k_A k_B / k_S s_o$ subsequent rearrangement gives

$$\kappa k_1 k_A k_B e'_o = j k_A k_B \left(\kappa e'_o + \frac{k_1}{k_S s_o} \right) + j^2 k_{-1} \qquad C.15$$